Selectivity in Host-Guest Compounds

A project submitted to the
University of Cape Town
in fulfilment of the requirements for the
Doctoral degree in Chemistry

Nicole M. Sykes

Supervised by Professor Luigi R. Nassimbeni and Professor Susan A. Bourne

Journey to a PhD…

DECLARATION

I, Nicole Margaret Sykes, declare that the contents of this thesis represent my own unaided work, and that the thesis has not been previously submitted for academic examination towards any qualification. Furthermore, it represents my own opinions and not necessarily those of the University of Cape Town.

I confirm that I have been granted permission by the University of Cape Town's Doctoral Degrees Board to include the following publications in my thesis, and my co-authors have agreed that I may include the publications:

1. N. M. Sykes, H. Su, E. Weber, S. A. Bourne and L. R. Nassimbeni, Selective Enclathration of Methyl- and Dimethylpiperidines by Fluorenol Hosts, *Cryst. Growth Des.*, 2017, **17**, 819–826.

2. N. M. Sykes, H. Su, E. Weber, S. A. Bourne and L. R. Nassimbeni, Selectivity of aliphatic alcohols by host–guest chemistry, *CrystEngComm*, 2017, **19**, 3682–3688.

3. N. M. Sykes, H. Su, E. Weber, S. A. Bourne and L. R. Nassimbeni, Crystallisation temperature control of stoichiometry and selectivity in host–guest compounds, *CrystEngComm*, 2017, **19**, 5892–5896.

4. N. M. Sykes, H. Su, S. A. Bourne and L. R. Nassimbeni, Enclathration by Werner Hosts: Selectivity and Polymorphism, *Cryst. Growth Des.*, 2020, **20**, 274–280.

5. N. M. Sykes, H. Su, S. A. Bourne and L. R. Nassimbeni, Enclathration by a Halogenated Host: Structures, Polymorphism, Kinetics, and Guest Exchange, *Cryst. Growth Des.*, 2021, **21**, 6465–6472.

Signed …… Date ……

ACKNOWLEDGEMENTS

I am thankful to all who have been part of my journey over the past six years, including:

My parents, for their unfailing interest, support, and encouragement.

My supervisor, **Prof. Luigi Nassimbeni** for initially taking me on as a vac student in my final year as an undergraduate, ensuring I stayed on as an honours student, and teaching me everything I know about this supramolecular business. I will fondly remember all our chats, spanning topics such as European and science histories, geography, the proper spelling of the word *desiccator*, what SPQR stands for, my attempts at converting you to an Oxford comma adherent, and your attempts at convincing me to learn French and Italian – *piano piano*. I will remember to work hard, but also enjoy *la dolce vita*.

My co-supervisor, **Prof. Susan Bourne**–the first woman head of the UCT Chemistry department–for being an inspirational role model, and improving every article with her perceptive comments and eagle-eyed corrections.

My co-author, **Dr Hong Su**–our crystallography expert – for always managing to find suitable single crystals when I could not, and help refining many disordered structures.

My co-author, **Dr Edwin Weber**, who provided two of the compounds used in this research and was always kind when writing to me. May he rest in peace.

Prof. Neil Ravenscroft–for so much NMR help, dark chocolate treats, teasing (blue & yellow slides, gumboots!), and showing me around Zurich one lovely Lindt and gelato filled summer afternoon.

Dr Cessarina 'Ces' Edmonds-Smith–for determining guest concentrations by GC as reported in chapters 3 and 4. I've enjoyed so much being your tutor for CEM1009H over the last three years, especially dropping in for many chats, and occasional kitten cuddles.

Dr Roxanne Mohunlal–for the most special friend, with the kindest heart. I've valued so much being able to hop across the passage and have a chat, or gossip over a few (or sometimes more) of our favourite *pastéis de nata*. I'm looking forward to more laughter and good times.

Dr Savannah Zacharias–for all your guidance, chats, and the friendship that grew over our write-up-area plants.

Dr Dyanne Cruickshank–who checked in and regularly offered to help me as a new student–be it with finding a reference or teaching me to do cell checks on the old Nonius diffractometer.

Dr Merrill Wight–for sharing her knowledge of making images pretty through the programme, Mercury, and for being a receptive listener off which to bounce ideas.

Dr Terrence Noonan–for many helpful discussions on differential scanning calorimetry, and always being willing to listen to my current experimental problems, and subsequently offering solutions.

My desk-mate–**Dr Richard Payne**–for much help when I was new to the lab, including running many NMRs for me. I remember with affection that you took me to my first cricket test, and the fun we had together watching the 2019 rugby world cup.

My classmate–**Alex Vicatos**–for enduring my and Luigi's teasing (the Greek Trojan horse!), all our discussions, and sharing the stress of tutoring 3rd year. I particularly enjoyed the organ recitals at Baxter theatre, and the revival of the Cape Town Carillion bells–your energy and excellence in so many areas is admirable.

Ruth Amoore–the first student I 'looked after' in the lab–for the fun we had together during your vac work; I appreciate the friendship that has further developed through social media and our games of (not very good) tennis.

Emma Tiffin–the first student I mentored for an Honours and MSc project, for teaching me much about the supervising process. I enjoyed so much your infectious laughter, and your legendary stories ('the dog is gone').

All other members of the CSCR lab I have known- I appreciate each smile, each encouraging 'you can do it', each heartfelt 'congrats' when things went well, and all the sympathetic noises when they did not. Thank you for the memories.

The administrative staff, especially **Joanne Polzin** with her funny, cheery emails, **Karin Badenhorst** who we miss so much**,** and **Deidre Brooks** - who mothers us all.

And lastly, thank you to **Dyl**, my love and comfort through it all.

ABSTRACT

It isn't easy to separate structurally similar guests by conventional methods such as distillation if the mixture components have similar functional groups and boiling points. This thesis aimed to investigate the relationship between the internal structures of host-guest compounds and the selectivity shown by the host molecule when presented with a guest mixture.

Four host compounds were used to prepare 29 new inclusion compounds. Two of these hosts were similar bulky diols and were synthesised by Weber (**H1** and **H2**). The other two, a Ni-based Werner-type host (**H3**) and a brominated host (**H4**), were synthesised by known methods. In addition, two new structures of the host, **H1**, alone are reported.

Inclusion compounds were prepared by recrystallising the host from liquid guests or exposing the powdered host to guest vapours. The internal structure of the resulting compounds was determined by single crystal X-ray diffraction (XRD), and the secondary interactions between host and guest were carefully studied. The thermal stability of compounds was measured using differential scanning calorimetry, and thermal gravimetry – the latter of which also confirmed the ratio of host to guest within compounds.

The preference of a host for one guest over another was determined by exposing the host to mixtures of guests, waiting for crystals to form, and then subjecting these crystals to ^{1}H nuclear magnetic resonance (NMR) spectroscopy or gas chromatography (if guest molecules were indistinguishable by NMR). In some cases, the kinetics of host-guest compound formation and guest exchange was monitored by powder XRD, using an in-house custom-built sample holder. These techniques allowed for the measurement of the relative proportions of guests in the crystals, which was then compared to the ratio of guests from which the host was initially recrystallised.

In some cases, it was found that the thermal stability of host-guest compounds correlates with the guest preference of the host. I.e., the guest that formed the most thermally stable host-guest compound is the guest the host prefers. However, it was not always possible to assign structural reasons why this should be the case. In one example, the selectivity of a host was dependent on the temperature of recrystallisation. In another system, the inclusion compound crystallised from a guest mixture had a different structure than when crystallised from either individual guest. In addition, this host's selectivity decreased with time and increasing guest concentration, with concomitant structural changes.

While much progress has been made in predicting the structures of single-component crystals, it is still not possible to predict the structures of crystals with multiple components. With the view to predicting the required conditions to grow materials with desired properties, such as being highly selective, more studies on polymorphic inclusion compounds formed under different crystallisation methods are needed.

ABBREVIATIONS AND SYMBOLS

m.p.	melting point
b.p.	boiling point
$K_{A/B}$	Selectivity coefficient
X_A	Mole fraction of guest A in the mother liquor
X_B	Mole fraction of guest B in the mother liquor
Z_A	Mole fraction of guest A in the crystal
X_B	Mole fraction of guest B in the crystal
E_a	activation energy
PXRD	Powder X-Ray Diffraction
SCXD	Single Crystal X-Ray Diffraction
2θ	θ is the glancing angle between the incident ray and the scattering planes
Å	Angstrom, a metric unit of length equal to 10^{-10} m
a,b,c	unit cell axes
α	angle between b and c unit cell axes
β	angle between a and c unit cell axes
γ	angle between a and b unit cell axes
V	unit cell volume
Z	number of formula units per cell
TGA	Thermogravimetric Analysis
TG	Thermal Gravimetry
DSC	Differential Scanning Calorimetry
^{1}H NMR	Proton Nuclear Magnetic Resonance
D_6-DMSO	Deuterated dimethyl sulfoxide (contains six deuterium atoms)
$CDCl_3$	Deuterated chloroform (contains one deuterium atom)
GC	Gas Chromatography
CSD	Cambridge Structural Database
FID	Flame Ionisation Detection
UV-VIS	ultraviolet-visible

TABLE OF CONTENTS

Chapter 6. Enclathration by Werner Hosts: Selectivity and Polymorphism

Chapter 7. Enclathration By A Halogenated Host: Structures, Polymorphism, Kinetics And Guest Exchange

Chapter 8. Summary, Conclusion, and further work

CHAPTER 1: Introduction

In 2014 I was in my 3rd year as an undergraduate when I applied to Prof. Nassimbeni for a position during the June vacation. I was invited for an interview, and duly given "the grand tour". We made arrangements that I would begin work after I'd written my last mid-year exam.
I remember emailing to ask what time he would expect me - his reply required the assistance of Google Translate: "Vieni a lavorare verso le nove di mattin -LRN". I was amused at the language choice, but not bemused - during the lab tour I had noted that most labels in his section were written in Italian. I arrived at the advised time excited to work in a research laboratory. I was met with a reserved desk and my very own research project: the xylene isomers...

(a) Prof Nassimbeni's Labelled lab drawers. (b) December 2014, BSc Chemistry and Mathematics graduation. (c) UCT Chemistry honours class of 2015 (Note Alexios top left). (d) July 2015, photo taken so my research over vac could be featured in Prof Nassimbeni's presentation at the 15th International Seminar on Inclusion Compounds (Warsaw); my green hair was much remarked upon. (e) June 2016, BSc(Hons) Chemistry graduation.

1.1 ISOMER SEPARATION: A CHALLENGE

"One can state, without exaggeration, that the observation of and the search for similarities and differences are the basis of all human knowledge"

Alfred Nobel[1.1]

Such incredible diversity is present on Earth, from all manner of plants, animals, fungi, and other living creatures to everyday items made of metals, glass, and plastics, to entities like rivers, oceans, mountains, and minerals. All commonly observed matter is made of electrons, and up and down quarks – the latter which combine to form protons and neutrons. Together, protons, neutrons, and electrons make atoms – the building blocks of our lives. How wonderful it is all the different ways that these particles come together to make up the world around us. Even when we limit matter to just one type of atom, it is still possible to produce incredibly varied materials. A well-known example is carbon – the atoms of which are able to bond in different arrangements – one form being sparkly diamond, while another the soft and grey graphite of pencils. It is remarkable that materials exist comprising the exact same type and number of atoms – arranged in such ways as to produce matter with vastly different properties.

While distinct forms of the same element are named *allotropes*, molecules or polyatomic ions with identical atomic compositions are termed *isomers* – from the Greek' iso' meaning same and 'meros' meaning parts. Isomers can be classified into various types (Figure 1.1), and isomers that are more structurally alike are more likely to exhibit similar properties.[1.2] For example, molecules that are mirror images of each other (termed enantiomers) have identical chemical and physical properties in achiral environments (except that they react differently to plane polarised light). In contrast, isomer pairs with noticeable structural differences also tend to have more disparate properties. For example, the solvents n-butanol and diethyl ether (functional group isomers) have the molecular formula $C_4H_{10}O_1$, but the alcohol's normal boiling point is 117.7 °C compared with the ether which boils at the much lower temperature of 34.6 °C.[1.3]

By exploiting the more than 80-degree difference in the boiling points between n-butanol and diethyl ether, a chemist could easily separate a mixture of these solvents by fractional distillation. However, many such classic physical separation techniques are often not applicable when tasked with separating more similarly structured isomers. For example, many isomers have homogeneous phases and similar solubilities that thwart separation by filtration and liquid-liquid extraction. Many isomers do have varied melting points, but separation by fractional crystallisation is often unsuccessful due to the formation of a eutectic mixture[†]. The most common isomer separation method is fractional distillation, used in petroleum refineries, petrochemical and chemical plants, natural gas processing and cryogenic air separation plants.[1.4] However, fractional distillation is efficient only if the isomer's boiling points are not too close.[1.5]

[†] a homogenous mixture that behaves as a single entity that melts/ freezes at a single temperature, which is lower than the melting point of both entities[1.6].

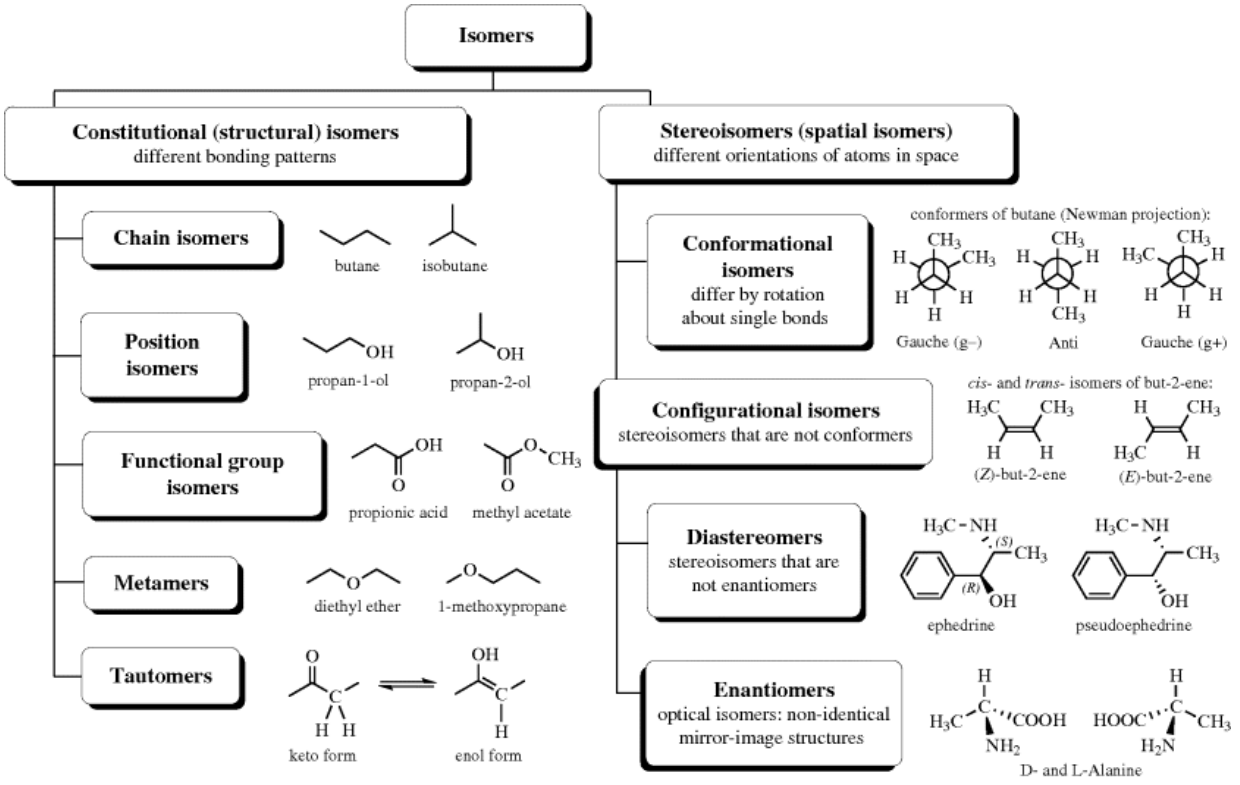

Figure 1.1. Types of isomers.[1.7]

The quintessential, well-researched example of structurally similar isomers is that of dimethylbenzene, or xylene (Figure 1.2). Xylene – from the Greek' xylo' meaning wood, was so named by Cahours,[1.8] a French chemist researching the light oils obtained by distilling wood in 1850. In modern times, approximately 90% of xylene is obtained by the catalytic reforming of naphtha distilled from crude oil.[1.9] This process results in a mixture that consists of approximately 40% meta-xylene, 24% ortho-xylene, and 19% para-xylene (as well as 17% ethylbenzene)[1.10]. Efficient separation of this mixture is a critical focus,[1.11] particularly the recovery of pure para-xylene, which is reacted with ethylene glycol to produce polyethylene terephthalate (PET). PET, also known as polyester, is the world's 4th most produced polymer - it is mainly used in synthetic textiles, and to make bottles and packaging for food and drink.[1.12]

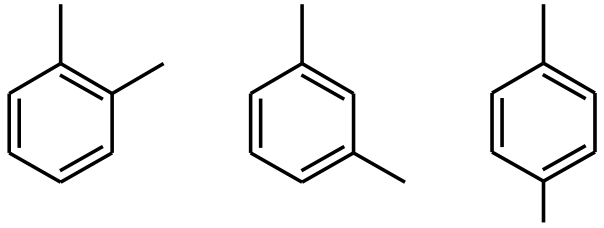

ortho-xylene	meta-xylene	para-xylene
b.p. 144.4 °C	b.p. 139.1 °C	b.p. 138.3 °C
m.p. -25.2 °C	m.p. -47.9 °C	m.p. +13.4 °C

Figure 1.2. Skeletal structure and normal boiling and melting points of the xylene isomers.[1.3]

Unfortunately, due to the xylene's very close boiling points, especially that of meta- and para-xylene, which differ by less than one degree (139.1 °C and 138.3 °C), separating a mix of these isomers by distillation would require a large number of theoretical plates and create high energy costs.[1.13] Para-xylene *can* be separated from the ortho and meta isomers by fractional crystallisation due to its higher melting point, but this process uses large amounts of energy by operating at either a low temperature or high pressure.[1.14] In addition, the crystallisation process is inefficient because the mixture composition at the eutectic point retains large amounts of para-xylene[1.15] and so is used industrially only when the feedstock is already much enriched in para-xylene.[1.14] ǂ

There are many other mixtures where the constituents, like the xylenes, have similar physico-chemical properties and so are difficult to separate into their individual and useful components. Clearly it is important that improved separation methods are studied that do not rely as heavily on high temperatures and pressures, so that carbon dioxide emissions and other production costs associated with the purification of chemicals can be reduced.

Table 1.1. Eutectic points and eutectic mixtures of xylene isomers[1.15]

System	Eutectic Point (°C)	Composition at Eutectic Point (mol. %)			
		p-Xylene	*o*-Xylene	*m*-Xylene	Ethylbenzene
p-Xylene—*o*-Xylene	−35.3	24.3	75.7		
p-Xylene—*m*-Xylene	−52.8	13.0		87.0	
o-Xylene—*m*-Xylene	−61.9		33.1	66.9	
p-Xylene—Ethylbenzene	−95.5	1.8			98.2
o-Xylene—Ethylbenzene	−97.4		8.1		91.9
m-Xylene—Ethylbenzene	−100.3			17.2	82.8
p-Xylene—*o*-Xylene—*m*-Xylene	−64.5	8.1	30.2	61.7	
p-Xylene—*o*-Xylene—Ethylbenzene	−97.8	1.6	8.0		90.4
p-Xylene—*m*-Xylene—Ethylbenzene	−100.7	1.4		17.0	81.7
o-Xylene—*m*-Xylene—Ethylbenzene	−102.1		6.5	16.0	77.5
p-Xylene—*o*-Xylene—*m*-Xylene—Ethylbenzene	−102.4	1.2	6.4	15.8	76.7

ǂ if for e.g., 80 mol p-xylene and 20 mol m-xylene were slowly cooled to -53 °C then 77 mol of p-xylene would crystallise from solution. After the last p-xylene crystal is removed the leftover 3 mol of p-xylene and 20 mol m-xylene form a solid "mixture" – this is the eutectic composition. The ratio of 3 mol p-xylene to 20 mol m-xylene is the same as the ratio 13:87 (see Table 1.1).

1.2 HOST-GUEST CHEMISTRY: AN INTODUCTION

"the least obtrusive graphic device for concealing the unavoidable ignorance".
H.M. Powell describing the middle dot used to denote a 'Host ¶Guest' complex[1.16]

Many everyday items are mixtures - consider the air we breathe, the toothpaste used twice each day, a 925-silver piece of jewellery, or a cup of tea near at hand? I think I'd be safe in saying that most *things* encountered in our day-to-day lives are not pure substances, but mixtures in some way (how many counterexamples can you think of offhand?). In laboratories around the world, synthetic chemists labour to create new covalent bonds between atoms, and in so doing create new *molecules*. Also hard at work are supramolecular chemists, who create new mixtures and study the weaker bonds *between* the molecules in these multi-component systems.

Supramolecular chemistry can be thought of as a receptor 'host' molecule that binds one or more other molecules, ion or ion pairs - the acceptor 'guest' - to form a host ¶guest complex.[1.17] This host-guest complex behaves as a single unit, with a unique structural relationship between host and guest and with properties different from the host and guest by themselves. For example, many chemistry students would have encountered the iodine test for starch, where a piece of bread squirted with a yellow/ brown iodine solution proceeds to turn a dark blue/ black colour. This happens because amylose, a polysaccharide in starch, has a helical structure that creates space in which I_2 molecules fit and bind to the sugar.[1.18] The result is the amylose ¶I_2 complex which has a characteristic blue colour, and so provides a way to test for the presence of starch.

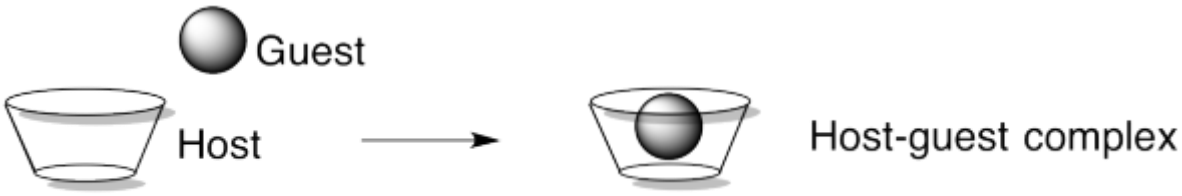

Scheme 1.1. Host ¶Guest complex.[1.19]

A timeline of supramolecular history is listed in Appendix A. This timeline was reproduced from the manuscript, 'Inclusion Compounds: Structure, Kinetics and Selectivity.' by L. R. Nassimbeni and N. M. Sykes, which is currently in review at the journal, Crystallography Reviews.

The origins of our knowledge on the structure of host-guest materials came about due to the ability of many complexes to form crystalline solids which have an ordered internal structure. von Laue discovered that crystals act as three-dimensional diffraction gratings for X-ray radiation (1914 Nobel Prize in Physics).[1.20] Shortly afterward, the Bragg father/ son duo developed an equation that related a crystal's diffraction pattern to its internal structure (1915 Nobel prize in Physics).[1.21] Owing to much of the work of Powell and Pauling, the latter who used X-ray diffraction to measure the distances and angles between atoms in crystal structures (1954 Nobel Prize in Chemistry),[1.22] we now know that the binding or 'glue' that holds a host and guest together results from the sum of multiple non-covalent (secondary) interactions.

In covalently bonded atoms electrons are shared and atoms are relatively closer together than atoms with secondary or non-covalent bonds between them. Non-covalent interactions were first taken into consideration by Johannes Diderik van der Waals who, in 1873,[1.23] helped revise the equation of state for real gases, considering that all matter containing electrons can interact with each other through weak interactions, which we now call *van der Waals* forces. They are the dominant force in nonpolar molecules like oils and gases (e.g., O_2, He) and have energy less than 5 kJ mol^{-1}. Conversely, the strongest type of secondary interactions (100-350 kJ mol^{-1}) occurs between positively and negatively charged ions like Na^+ and Cl^-, as found in regular table salt. Some molecules have a partially positive end and a partially negative end, and so display attractive interactions with ions and other so-called polar molecules through "ion-dipole" or "dipole-dipole" interactions which are of the order of 50–200 and 5–50 kJ mol^{-1}, respectively.

Molecules with O-H, N-H, and F-H bonds, like those found in water, sugars, and amino acids, are particularly important in supramolecular chemistry and biology as they can form hydrogen bonds, which are strong dipole-dipole interactions of the order of 4–120 kJ mol^{-1}. For example, the hydrogen bonding interaction between the two chains of DNA are responsible for its double helix configuration (Figure 1.3a), a discovery made possible by an X-ray diffraction photograph (Figure 1.3b) taken by Raymond Gosling of crystals grown by Rosalind Franklin. The 1962 Nobel prize in Physiology or Medicine was awarded for the structure of DNA to Watson, Crick, and Wilkins.[1.24]

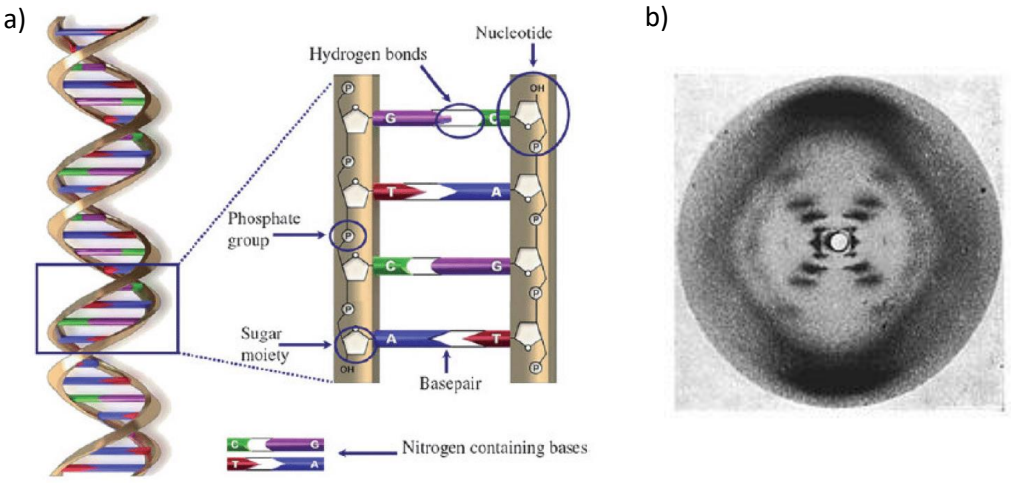

Figure 1.3. (a) DNA double helix is held in place by hydrogen bonds (b) An X-ray photo of a gel of polycrystalline DNA.

The strength of secondary bonds is reflected in the amount of energy required to break them, in water. For example, H_2O molecules form hydrogen bonds to each other, with water only boiling at 100 °C at 1 atm of pressure. While substances made of only one type of atom, like helium (boils at -267 °C at 1 atm of pressure), have only weak van der Waals interactions occurring between atoms and so are gasses at low temperatures. The strengths of some intermolecular interactions have been given in Table 1.2.

Table 1.2. Examples of and strengths of some non-covalent interactions[1.25]

Interaction	Bond energy (kJ mol^{-1})	Example
Ion-ion	100–350	Na^+ Cl^-
Ion-dipole	50–200	Na^+ and H_2O
Halogen Bonding	10–200	Halogen atoms can act as electron acceptors, as with Br_2 and 1,4-dioxane
Dipole-dipole	5–50	Intermolecular interactions between molecules of HCl, where the Cl region is electron rich and the H region electron deficient.
Hydrogen bonding	4–120	A type of dipole-dipole interaction e.g., interactions between molecules of H_2O.
Cation-π	5–80	Benzene is rich in π electrons above and below the ring, and these faces can interact with a cation, e.g. Na^+
π-π	8–40	Interactions between aromatic rings, two benzene rings can interact where one if flat and the other side on, in an 'edge -to -face' orientation, or by being parallel to each other, but offset.
Van der Waals	<5, but varies depending on surface area	Exhibited by every atom and molecule, and is the dominant force in nonpolar molecules like oils. The strength of the interaction increases with increasing molecular surface area, and with molecular size (due to increased electrons)

1.3 HOST-GUEST CHEMISTRY: A SEPARATION METHOD

"A round man cannot be expected to fit into a square hole…"
Mark Twain[1.26] in *Following the Equator* (ch. 68, 1897)

For a host to bind with a guest and form a new complex, both Host and guest molecules should have sites that attract each other without creating strong repulsive forces. Then one could assume that for a host to bind *selectively* with one guest over another, the winning host-guest complex should have a lower net energy than the other potential complexes. This is a highly relevant question; for example, our bodies digest sugar in the small intestine with help from the enzyme sucrase (the 'host'), which only binds to the sugar sucrose (the 'guest'), forming a sucrase-sucrose complex. This complex stresses the bond between sucrose's constituent parts: glucose and fructose. Once the bond is broken, the separated sugars can be absorbed and used as a source of energy (Scheme 1.2a). While similar synthetic sugars, like sucralose (made by chlorinating three hydroxy groups of sucrose), can bind to our taste receptors, but are mostly unable to be absorbed in the gut – making them effective non-nutritional sweeteners.

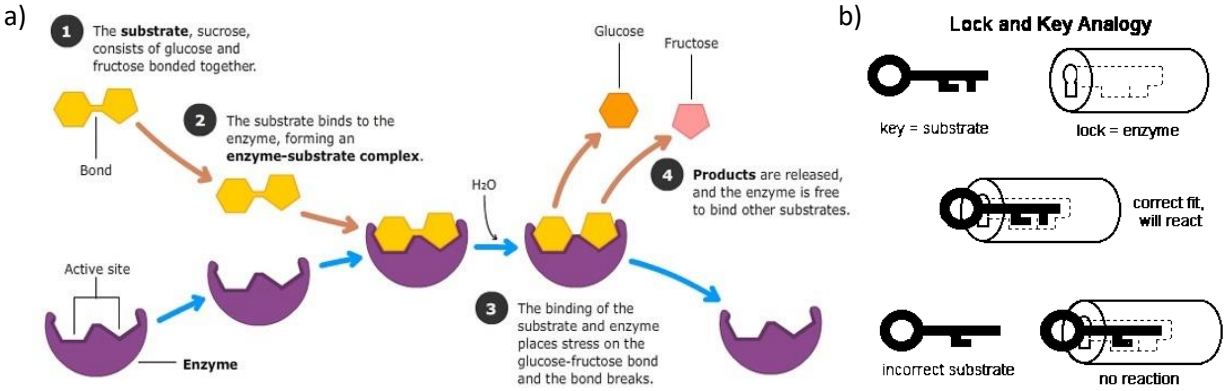

Scheme 1.2. (a) Example of model of action of an enzyme- here sucrase- which acts on sucrose to break it down into glucose and fructose.[1.27] (b) Fischer thought enzyme and substrate had complementary shapes and fit together like a lock and key.[1.28]

In 1894, Fischer[1.29] studied this ability of enzymes to discriminate between similar molecules. He proposed that the selective binding between the active site on an enzyme and the receptor site on a substrate occurs because these molecules possess a complementary geometric shape that allows them to perfectly fit into one another, where the binding will be stronger if the "fit" is better. To quote Fischer, "I should say that the enzyme and substrate must fit each other like a lock and key" (Scheme 1.2.b). In other words, the host and guest binding sites need to be similar in size and shape as well as electronically stabilising.

The reversible reaction of enzyme and substrate to an enzyme ¶substrate complex, or more generally, host and guest to a host ¶guest complex can be represented by the equation (1.1),

$$\text{Host}_{(aq)} + n(\text{guest})_{(aq)} \underset{k_r}{\overset{k_f}{\rightleftarrows}} \text{host ¶}n(\text{guest})_{(aq)} \qquad (1.1)$$

where n is the number of guest molecules, k_f is the rate constant for the forward reaction, and k_r is the rate constant for the reverse reaction.

The extent to which the host and guest bind can be represented by the constant K_c, defined as the ratio between the concentration of the complex and the concentrations of host and guest at equilibrium (when rate of forward reaction = rate of reverse reaction), given in equation (1.2) where [ ] denotes the concentration in mol/dm^3.

$$K_c = {[\text{host-(guest)}_n]}/{[\text{host}][\text{guest}]^n} \qquad (1.2)$$

From (1.2), large K_c values would indicate a higher concentration of the host-guest complex at equilibrium, implying a stronger binding between host and guest, and resulting in a more stable complex.

Fischer and those who first studied enzymes thought that the molecular recognition between enzyme and substrate (or host and guest) is absolutely selective or *specific,* i.e., that enzymes would react with one and only one substrate. But this is not always the case. Other digestive enzymes, like pepsin, can bind to most types of protein, allowing us to absorb and use almost all most proteins consumed in meat, dairy, nuts, beans, and legumes.

To what extent the host is selective for one guest over another can be simply expressed as the ratio of the binding constants of the different guests as written in Eq. 1.3.

$$\text{Preference of Host for guest A over guest B} = K_{A/B} = {K_{\text{Guest A}}}/{K_{\text{Guest B}}} \qquad (1.3)$$

Scheme 1.3 shows an example where the Host (H) can bind both guest A and guest B, but binds guest B to a greater extent. And so, when host, guest A, and guest B are mixed, the host acts selectively towards guest B and more H-B complex is formed than H-A.

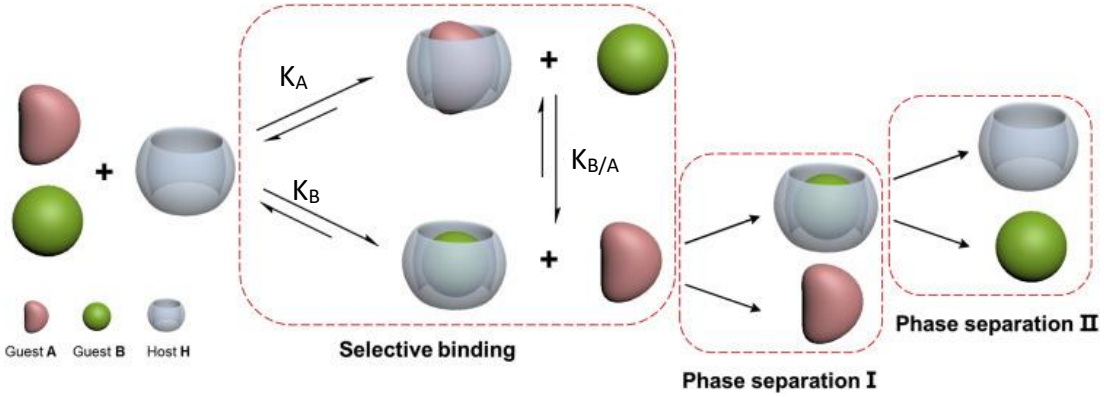

Scheme 1.3. Example of the selective separation process of guest B from guest A[1.30] by the host H, which has a stronger binding affinity for guest B.

Please note that all equilibrium constants should be pure numbers as it is not possible to take the log of units of measurement. To get around this, a standard state is declared, which would be 1 mol/dm^3 for equilibria in solution. K_c is then defined as before, but with the concentration of each species being divided by the standard state. The units of concentration will cancel out, leaving K_c as a pure number.

The earliest work in selective binding began in 1967 when Pedersen[1.31] synthesised doughnut-shaped molecules that could mimic the action of ion channels[ǂ] by binding preferentially to Na^+ and K^+ (see Figure 1.4). Pedersen's cyclic polyethers, named crown ethers, form complexes with alkali metal ions held inside their central cavity by ion-dipole interactions between the metal cation and the partial negative charge on the oxygen atoms surrounding it (Figure 1.4a).

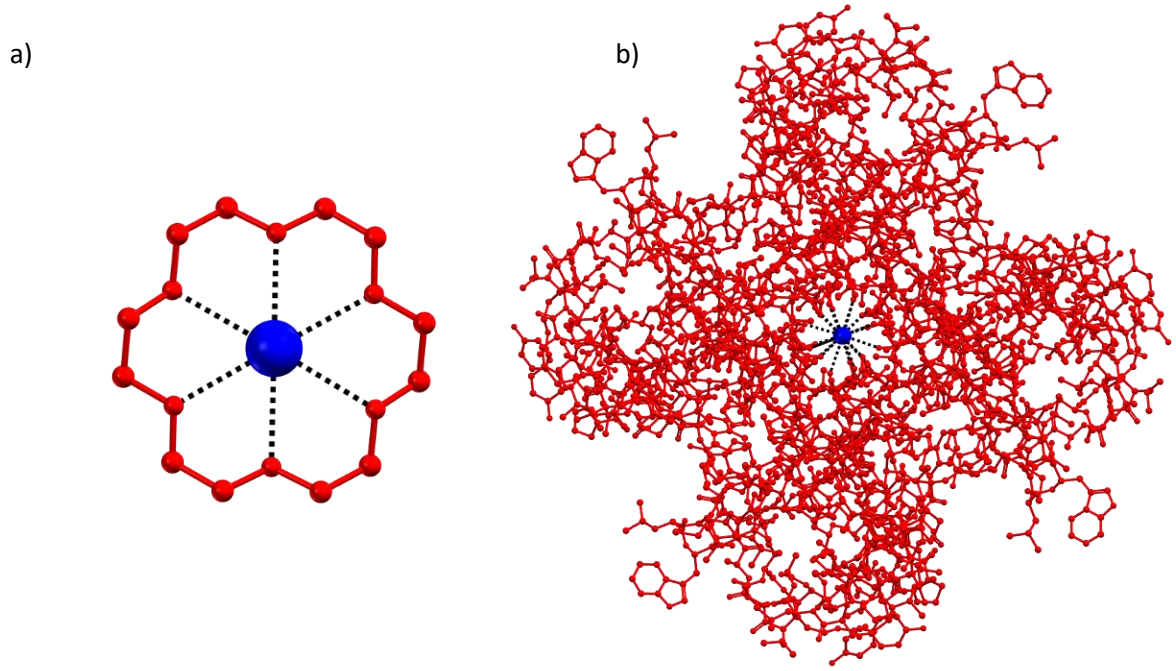

Figure 1.4. K^+ ions (blue) are bound within (a) [18]-crown-6, and (b) the much larger potassium channel of a soil bacterium,[1.32] comprising of 2824 atoms and weighing 41,130 g/mol. Ion-dipole interactions between K^+ and oxygen atoms shown as black dotted lines.

The largest binding constants (K) were obtained when the diameter of the crown ether ring matched that of the metal cation. For example, the diameter of a sodium ion is 1.90 Å, and the diameter of a potassium ion is 2.66 Å; [18]-crown-6 (cavity of diameter 2.6–3.2 Å) gives a binding constant with sodium, $K_{Na^+} = 10^4\ M^{-1}$, while with potassium, the binding constant is much large (K_{K^+} is of the order of $10^6\ M^{-1}$). Then, given that the selectivity of the crown ether is the ratio of its binding constants with different cations, we can say that [18]-crown-6 has a 100 times ($10^6\ M^{-1}/10^4\ M^{-1}$) greater preference for K^+ than Na^+.

[ǂ] ion channels transport sodium (Na^+) or potassium (K^+) ions across cell membranes. The rapid change in concentrations of the different charged particles create propagating electrical signals, responsible for e.g., making our muscles move, and helping us feel sensations like heat and pain. Potassium channels select K^+ over Na^+ by a ratio of ~1000:1, whereas sodium channels select Na^+/K^+ in a ratio higher than 500:1.[1.33 - 1.35]

Lehn and Cram furthered Pedersen's work, synthesising molecules with more complex shapes – resembling cages, baskets, or vases. In 1969 Lehn presented the synthesis of cage-like bicyclic crown ethers, called cryptands, many of which exhibit higher selectivity than natural macrocycles. For example, the K^+ complex with the cryptate in Figure 1.5a has a binding constant about 10 000 times greater than the K^+ complex with valinomycin (Figure 1.5b), which is bound 100,000 times more strongly than the sodium-valinomycin complex.[1.36]

In 1979 Cram[1.37] designed hosts called spherands and augmented them over several years until creating cryptahemispherands that exhibited extremely high selectivity, one of which had a 420 000-times-stronger preference to bind sodium ions than lithium. Lehn and Cram coined the terms 'host-guest' and 'supramolecular' chemistry, and together Pedersen, Lehn, and Cram won the 1987 Nobel Prize in Chemistry for their efforts in the "development and use of molecules with structure-specific interactions of high selectivity".

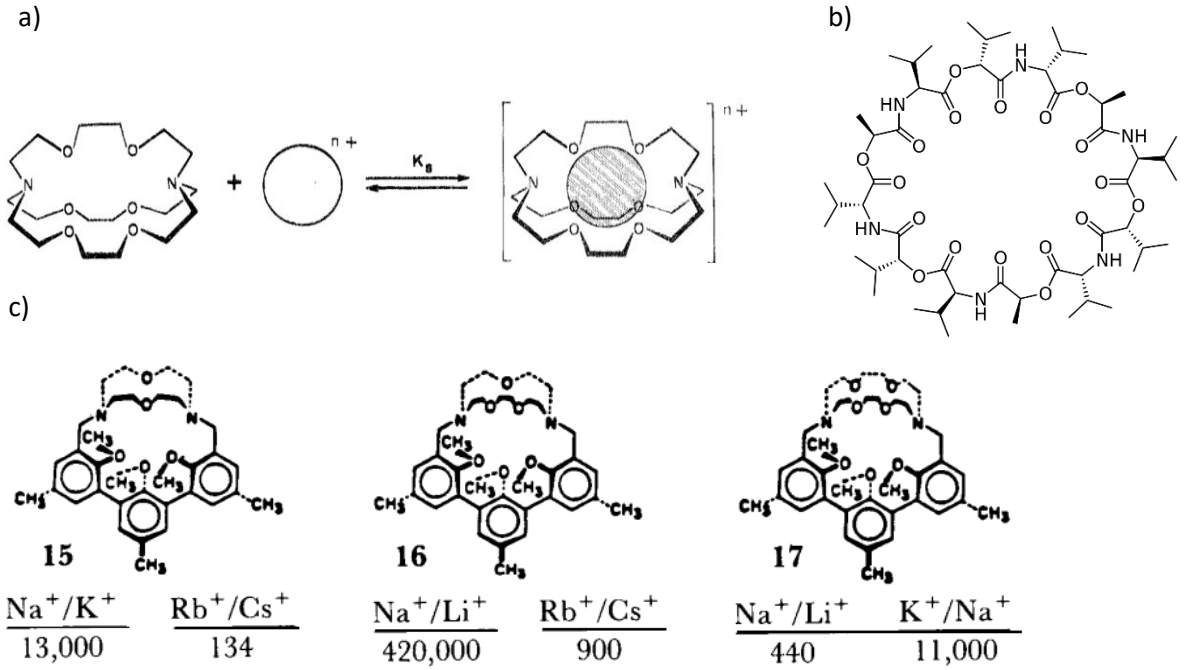

Figure 1.5. (a) a cryptand binding a cationic guest (b) valinomyacin[1.36] (c) structural recognition of cryptahemispherand hosts as measured by $K_{A/B}$ values where a and b are alkali ions.[1.37]

1.4 INCLUSION CHEMISTRY: AN INTRODUCTION

CLATHRATUS. *Closed or protected by crossbars of trellis (clathri)…*
CLATHRI. *A trellis or grating of wood or metal employed to cover over and protect an aperture, such as a door or window, or to enclose anything generally…*
A dictionary of Roman and Greek Antiquities[1.38]

Inclusion chemistry, in particular, is defined as the chemistry of host-guest complexes that are stable in the *solid* state and dissociate when dissolved.[1.39] Although amorphous materials do exist, they are rarely the most stable solid form,[1.40] and so many molecular compounds tend to be crystalline in the solid state. Crystalline materials contain long-range order (see Figure 1.6a), where atoms form arrangements that repeat in three dimensions (quasicrystals are the exception). The unit cell is the smallest arrangement of atoms, and is repeated over and over again to form the crystal (Figure 1.6b).

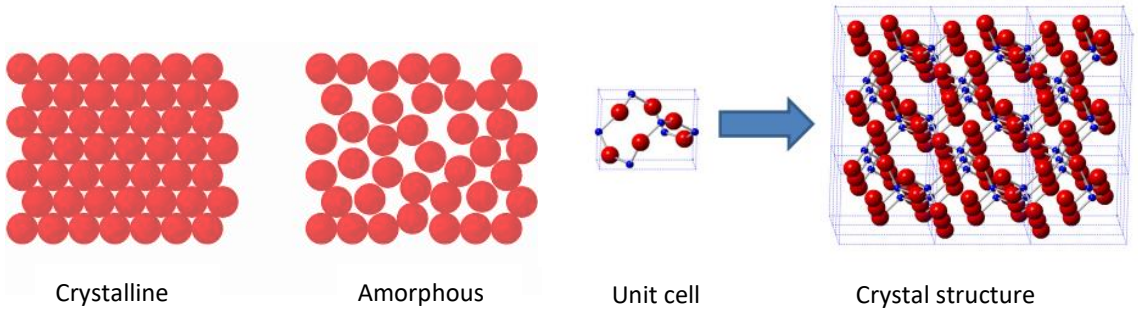

Figure 1.6. (a) crystalline (left) vs amorphous (right) solid[1.41] (b) when a particular arrangement of molecules called the unit cell (left) is repeated in all directions to make a crystal with a particular structure.[1.42]

The history of crystalline host-guest complexes[1.43] dates to 1823 when Faraday reported a chlorine clathrate hydrate that corresponds to the formula Cl_2 ¶10H_2O. Although only in 1952 was the term 'Inclusion compound' (from the German Einschlußverbindungen) introduced by Cramer, who presented the first inclusion compounds with cyclodextrin hosts.[1.44]

We can represent the formation of an inclusion compound by the equation:

$$H_{(s,\alpha)} + n\ G_{(l\ or\ g)} \rightleftarrows H\ ¶G_{(s,\beta)} \qquad (1.4)$$

where α represents the non-porous phase of the pure host, the apohost, and β is the host–guest inclusion compound with a guest/host ratio equal to n. The ratio of host to guests does not have to be a whole number; for example, "fire ice" (CH_4 ¶.75H_2O) forms when methane gas becomes trapped within a cage of water at high pressures and low temperatures on the ocean floor (Figure 1.7a).[1.45] This could create a knock-on effect as rising global temperatures cause the release of CO_2 into the atmosphere via methane-clathrates.

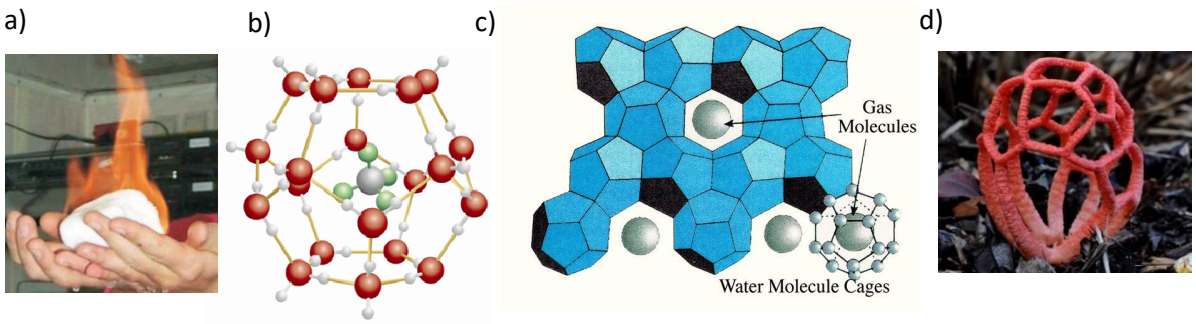

Figure 1.7. (a) as a methane clathrate melts the released guest can feed a flame while the framework drips apart as liquid water [1.45] (b) one methane molecule surrounded by a cage of water molecules[1.46] (c) showing the packing of many units in the structure[1.47] (d) *Clathrus ruber*[1.48] or *"red lattice" mushroom,* so named by Micheli[1.49] in 1729.

Inclusion compounds are defined as a *molecular inclusion* if the host contains a cavity within itself wherein the guest is located, like the crown ethers and cryptates made by Pedersen, Cram, and Lehn. But if, instead, the host molecules arrange to form a lattice containing spaces wherein the guests reside, the compound is termed a crystal lattice inclusion or *clathrate* (see Scheme 1.4). The term 'clathrate'[§] was initially introduced in 1948 by Powell[1.52] when studying the crystal structure of an organic inclusion compound with β-quinol. Note the similarity between the structure of methane clathrate (Figure 1.7b) and the *Clathrus ruber* mushroom in Figure 1.7d.

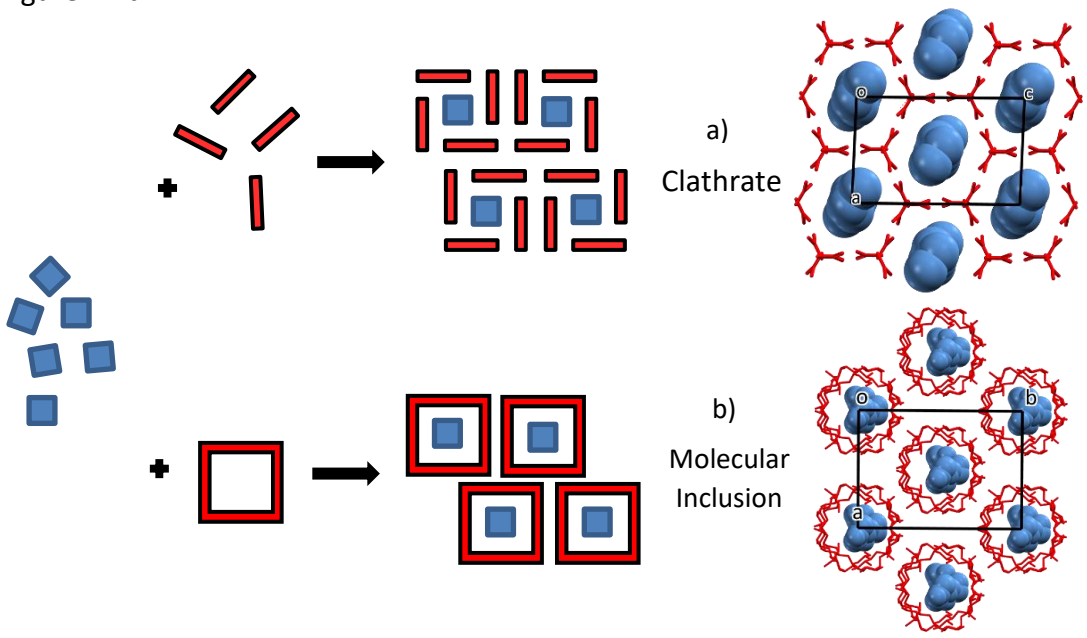

Scheme 1.4. Types of inclusion compounds. Molecules in blue are guests, and in red are hosts (a) clathrate: hosts arrange to form a framework that traps the guest, example given is urea guests enclathrated by dichlorohexane hosts (CSD code: WOMGIO). (b) molecular inclusion: the host naturally contains a cavity which accommodate a guest e.g., β-cyclodextrin hosts with methylparaben guests (CSD code: AJUVEG).

[§] 'clathrate' comes from 'klethra', the Greek name for the alder tree and is derived from 'kleio', meaning 'I close' or 'I confine'. Kleio originates from the Aeneid, a Latin epic (Virgil ~20 BC) wherein the mythical Heliades sisters were transformed into alder thickets about the shores of a river island, there confining the remains of their deceased brother, Phaëton.[1.50, 1.51]

Clathrates have been further classified by Weber[1.53] as either true clathrates or coordinatoclathrates. Coordinatoclathrates have specific interactions between host and guest, like hydrogen bonding. In contrast, genuine clathrates contain specific host-host interactions, but with the guest held in place by weak non-specific van der Waals forces (see Figure 1.8).

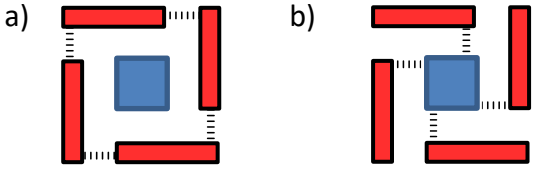

Figure 1.8. In this schematic diagram, the bars represent hosts and the square is symbolic of a guest molecule. The broken lines indicate secondary interactions e.g., hydrogen bonds. (a) true clathrate (b) coordinato clathrate.

Nassimbeni[1.54] described the formation and possible decomposition routes of an inclusion compound (Figure 1.9) as taking place in two steps: (a) the host molecules are dissolved in a guest solvent and (b) a host-guest complex is formed upon crystallisation. Once removed from solution the inclusion complex may either stay intact or decompose. The latter could (c) decompose to yield the original host excluding the guest molecules, (d) partially decompose to produce a new phase of the complex or (e) lose the guest molecules to yield an empty host structure.

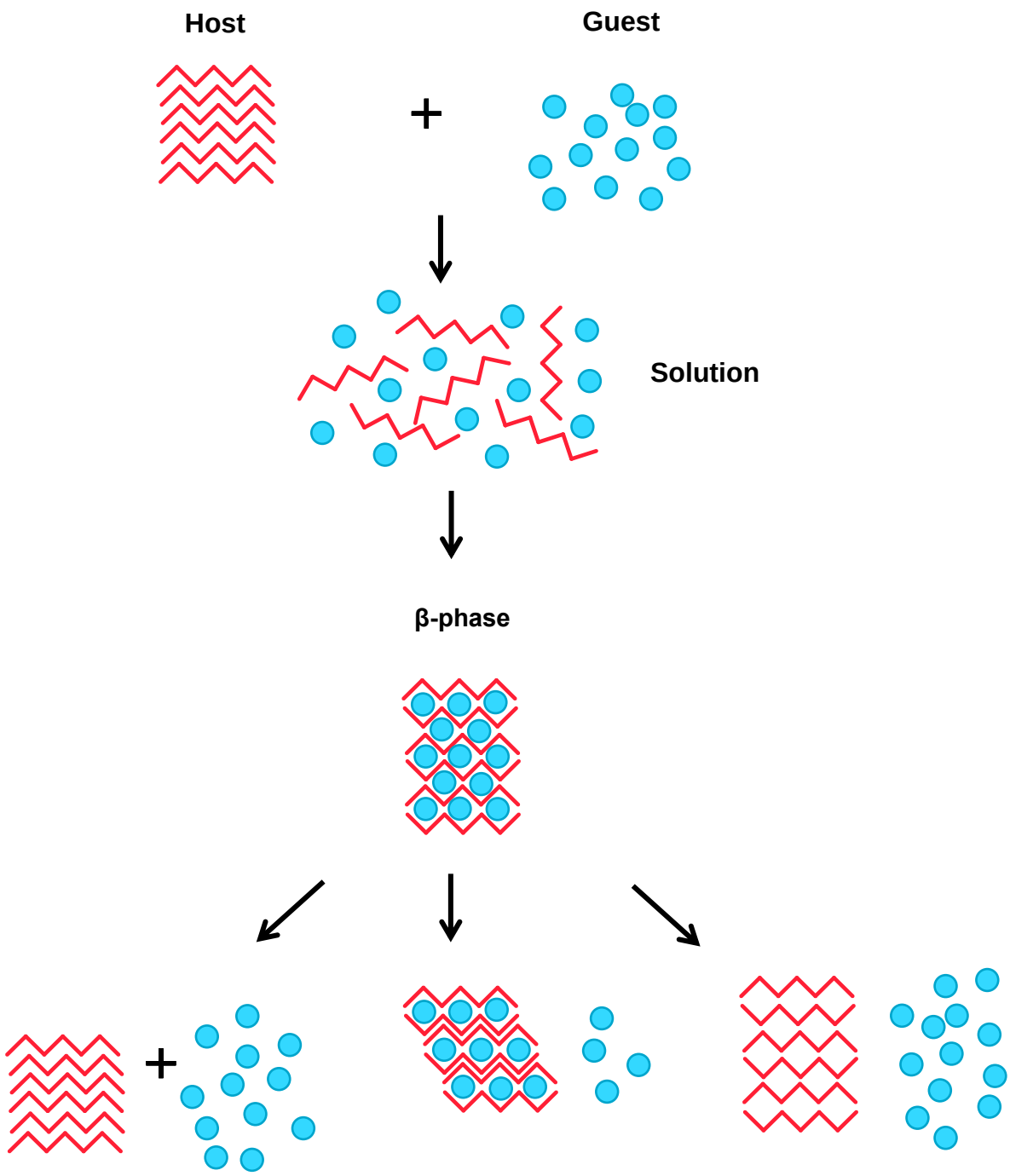

Figure 1.9. The formation and possible decomposition routes of an inclusion compound where guests are shown in blue and host molecules in red.

1.5 SOME FACTORS AFFECTING INCLUSION COMPOUND STRUCTURE:

"It has long been an axiom of mine that the little things are infinitely the most important"
-Sir Arthur Conan Doyle in the 1981 novel, 'A Case of Identity'

Via simulations, Boothroyd has shown that the primary criterion for inclusion compound formation is that the host–guest affinity must be sufficient to overwhelm the host–host and guest–guest affinities. A strong host-guest affinity is not a sufficient condition; host molecules with even a weak affinity for a guest can form inclusion compounds provided if the self-affinities of the host and the guest are relatively weaker.[1.55]

Furthermore, the growth of crystalline inclusion compounds is sensitive to several factors, affecting their composition, structure, colour, and shape, in much the same way that an egg prepared using diverse methods can produce widely different outcomes (See Figure 1.10).

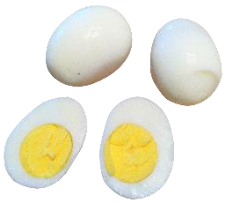

hard-boiled[1.56]

• submerge whole egg in water at 100 °C for 1 min
•87 °C for 6 minutes

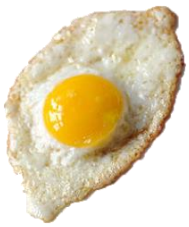

fried sunny side up[1.57]

•crack egg into oiled pan at 150 °C
•3 minutes, spoon oil on top

omelette[1.58]

• whisk 3 eggs together
• pour into oiled pan at 120 °C for 5 minutes

chick[1.59]

•keep freshly laid, fertilized egg at 37 °C for 21 days

Figure 1.10. Starting materials (eggs) can become different products depending on the cooking method used.

1.5.1 Temperature.

By crystallising inclusion compounds at various temperatures, Ibragimov[1.60 - 1.62] discovered that low temperatures resulted in inclusion compounds with a high proportion of guest relative to the host. As the crystallisation temperature increases, the guest/ host ratio decreases. This continues until the crystallisation temperature reaches the guest's boiling point, when the resulting material has a guest/host ratio equal to zero and is not an inclusion compound (as only apohost remains). Ibragimov also noted that this proportion change is reflected in the arrangement of the guests in the crystal lattice. Low temperatures cause the guests to reside in layers within the host framework, while increasing the temperature results in guests that reside in channels, and eventually in isolated cages (Figure 1.11).

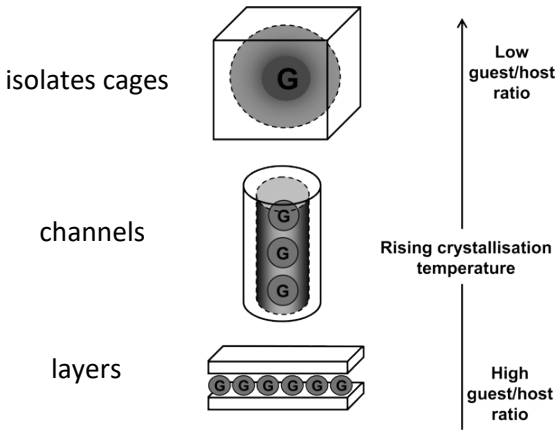

Figure 1.11. Changes in the host-guest topology with changing crystallisation temperature.[1.54]

1.5.2 Solvent.

Sometimes guests are solids at ambient temperature and pressure, or cannot dissolve the host. In these cases, it is either impossible or impractical to recrystallise an inclusion compound from a solution of host and guest, and a solvent (also called co-solvent) is required to facilitate complexation. However, because a solvent can interact with both host and guest, it may compete with guest molecules for host binding sites. In this way, solvents can be unintentionally included[1.63] or can produce inclusion compounds with different host: guest ratios.[1.64] For example, Moorthy and co-workers report a tetraarylpyrene host (TP) that forms a 1:1 inclusion compound when recrystallised from dicyclopentadiene (Figure 1.12, top right). But, when this host is recrystallised from a mix of guest and chloroform, the resultant compound has an H: G ratio equal to 1:3.

Similarly, to how isomers are molecules with the same number and type of atoms, but arranged differently, it is also possible to produce inclusion compounds with the same ratio of host and guest components, but arranged differently in space. The same host TP forms a 1:2 host: guest inclusion compound with toluene as guest (Figure 1.11). But when the host and guest crystallise in the presence of chloroform, the TP·2(toluene) compound that forms has a different packing (Figure 1.12 lower left).[1.64] Such crystalline structures with the same ratio of components, but with different internal structures are termed polymorphs, from the Greek' poly' meaning many and 'morphe' meaning form.

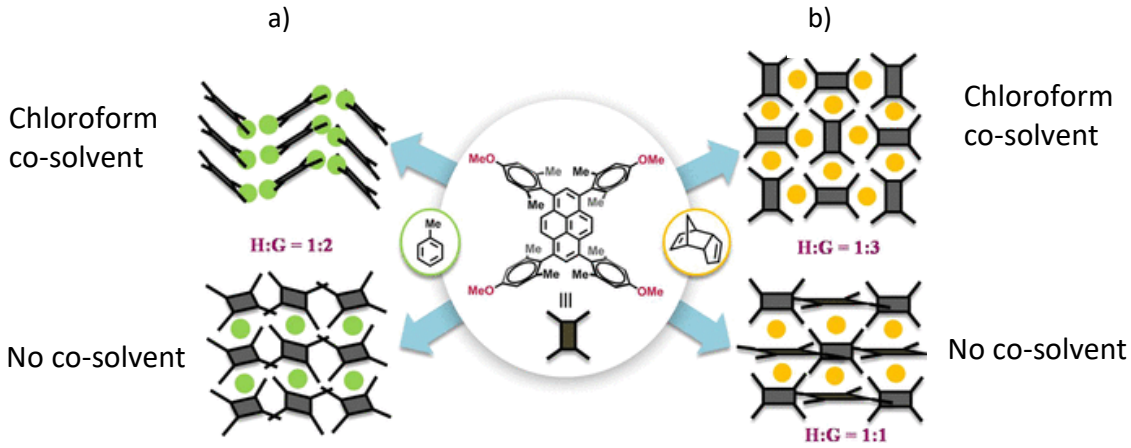

Figure 1.12. Packing of host with (a) toluene (left, green), giving two polymorphs with H:G ratio = 1:2 where top packing was recrystallized from a mix of guest and chloroform, and (b) dicyclopentadiene (right, yellow) recrystallized from a mix of guest and chloroform (top, H:G = 1:3) or guest alone (bottom, H:G = 1:1).[1.64]

The concentration of guest can also influence which inclusion compound crystallises. For example, Tanaka found that when recrystallised from a low concentration of the guest, 2-methyl naphthalene, a nickel-based host forms an inclusion compound with only methyl cellosolve – the co-solvent. However, when guest concentrations of greater than 1.5 mol/L were exposed to the host, an inclusion compound formed having a Host: Guest (or H: G) ratio of 1:2, with 2-methyl naphthalene as guest.[1.63]

In the same way that adding a co-solvent can change the resulting structure of the inclusion compound, so can using different co-solvents produce different inclusion compounds. Jacobs et al. reported solvent manipulation of N-methyl acetamide inclusion compounds formed from a xanthenol host. Figure 1.13 below shows the resulting packing and accompanying H: G ratios resulting from using N, N-dimethylacetamide, 1,4-dioxane, or aniline as a solvent.[1.65]

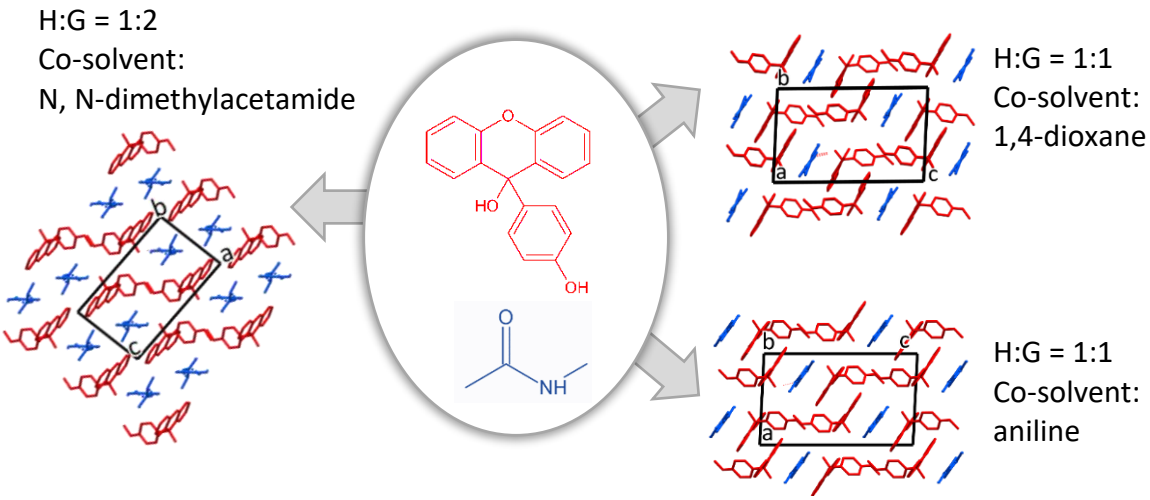

Figure 1.13. Packing of the crystal structures formed with a xanthenol host and N-methylacetamide as guest. The compound were grown using the co-solvents: N,N-dimethylacetamide (left), 1,4-dioxane (top right), and aniline (bottom right).

1.5.3 Crystallisation Method.

Aristotle summarised his observations by concluding, "Corpora non agunt nisi fluida", meaning "No reaction occurs in the absence of solvent" in Latin. Such philosophies had a significant influence on the evolution of the modern sciences in Europe, and this provides one historical reason most organic reactions have been studied in solution. Nevertheless, it has been found that many reactions proceed efficiently without the components needing to be in solution.[1.66]

An example of the effect of the crystallisation method on the resultant inclusion compound structure was reported by Ripmeester et al., who made five polymorphic inclusion compounds (H: G ratio = 2:1), using the host tris(5-acetyl-3-thienyl) methane with 1,3-dichloropropane as guest. The first and third forms were prepared (as a mixture) by slow cooling. Pure form 2 was prepared separately by two different techniques, fast cooling and annealing at 50 °C. The 4th and 5th forms 4 and 5 were prepared by slow evaporation.[1.67]

Sometimes reactions can even be more efficient without a solvent. Barbour and Lusi[1.68] reported that an inclusion compound does not form when a Werner host is dissolved in hot DMSO and layered with toluene (while the same method produces inclusion compounds with the similarly structured guests, benzene, and ortho- and meta-xylene). Two polymorphic toluene inclusion compounds were grown by slow evaporation from solutions of host, guest, and methanol as co-solvent, but only as minor components. However, one of these forms is obtained within minutes using the solvent-free method of exposing the polycrystalline host to the vapour of toluene.

1.5.4 Kinetics vs Thermodynamics.

As mentioned previously, the general assumption is that inclusion compounds form because they are more stable, and have lower free energy than the host and guest alone. As represented in Figure 1.14, inclusion compound formation proceeds from the separate host and guest mixture - the starting materials (SM) - to the lowest energy host-guest compound – the thermodynamic product (P2) - via the transition state (TS2), which is reached by the input of activation energy (E_A2). However, the crucial stage in crystal growth is determined by the rate of crystal nucleation, which is a kinetic factor. Therefore, the first compound formed (P1) will be the one that nucleates quickest, due to the lower activation energy (E_A1) required to reach the transition state (TS1). In this way a metastable form, which is not the lowest energy inclusion compound, is formed. This form can subsequently be converted into the more thermodynamically stable compound by solution or solid state-mediated phase transformation. This successive phase change was identified and proposed as the *Law of States* by Ostwald.[1.69]

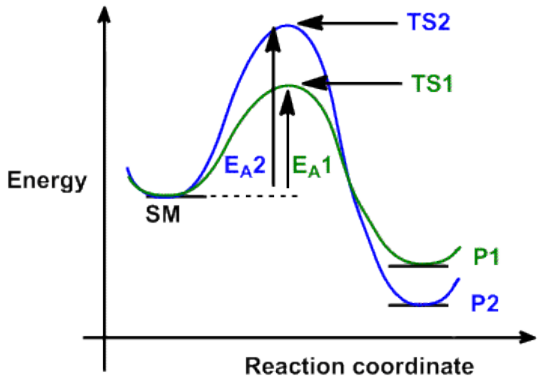

Figure 1.14. The starting materials (SM, host and guest molecules) can react to form products, P1 or P2, where P2 is the more stable product, having the lowest free energy).[1.70]

Although the kinetic control of host-guest systems is rare,[1.71 - 1.75] Toda et al. have extensively studied the isolation of different meta-stable inclusion compounds.[1.76 - 1.78]
An example was reported by Sashuk et al. where a macrocyclic host cucurbit[6]uril (CB6) initially forms a meta-stable 1:1 host-guest compound with adrenaline (Figure 1.15), but when left in solution the needle-like crystals slowly dissolve and recrystallise to form the thermodynamic inclusion compound with a 1:2 host: guest ratio.[1.79]

A special case of metastable and stable crystal forms occurs when the inclusion compound crystal structures have a different packing arrangement, but have the same ratio of host to guest. As mentioned previously, these types of structures are called polymorphs, and are a type of supramolecular isomer.[1.80] Many historical examples of polymorphs are presented in Bernstein's book "*Polymorphism in Molecular Crystals*".[1.81]

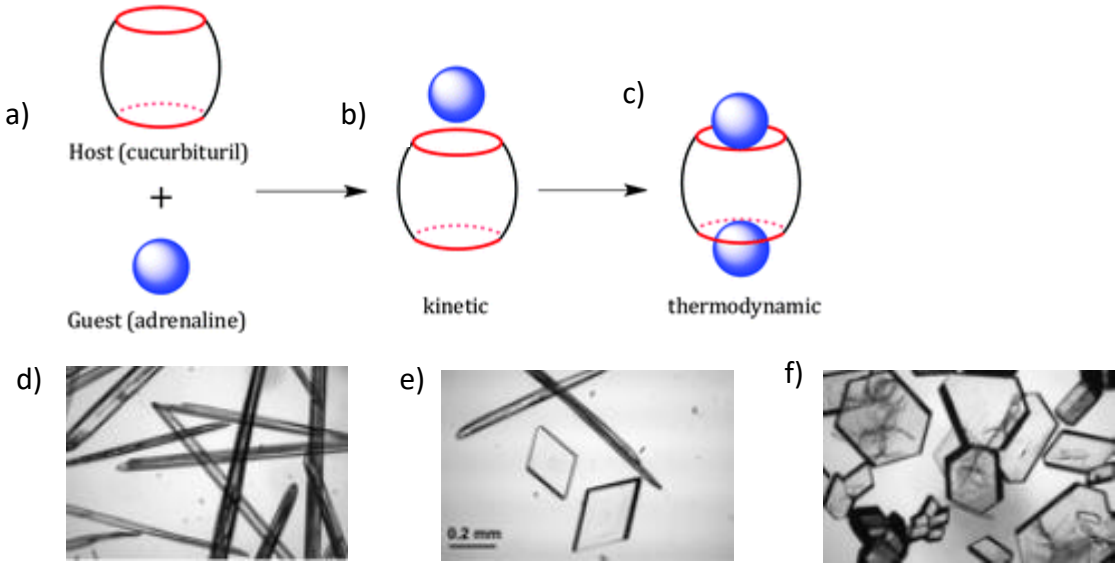

Figure 1.15. (a) The CB6 host and adrenaline as guest form two host-guest compounds (b) 1:1 kinetic product (c) 1:2 thermodynamic product. Photographs of crystals of the CB6 and adrenaline compounds after (d) 1 hour – forming the needle-like 1:1 kinetic product, (e) 2 days – a mixture of both compounds is observed (f) 1 week – only the 1:2 thermodynamic product remains.

1.6 INCLUSION CHEMISTRY: A SEPARATION TECHNIQUE

When a suitable host compound is exposed to a mixture of guests, it can selectively bind with a particular guest to form an inclusion compound. The crystallised material can be filtered from the remaining solution, the guest desorbed by warming, and the host recycled.[1.82] This process may be represented by Scheme 1.5 and Eq. 5,

$$H_{\alpha\text{-phase (s)}} + G_A + G_B \rightarrow H \P G_{A\ \beta\text{-phase (s)}} + G_B \qquad (5)$$

where generally the Host, H (α-phase, non-porous), is a solid that dissolves in the liquid guest mixture, G_A and G_B, to yield an inclusion compound (β-phase) with a Guest/ Host ratio = n.

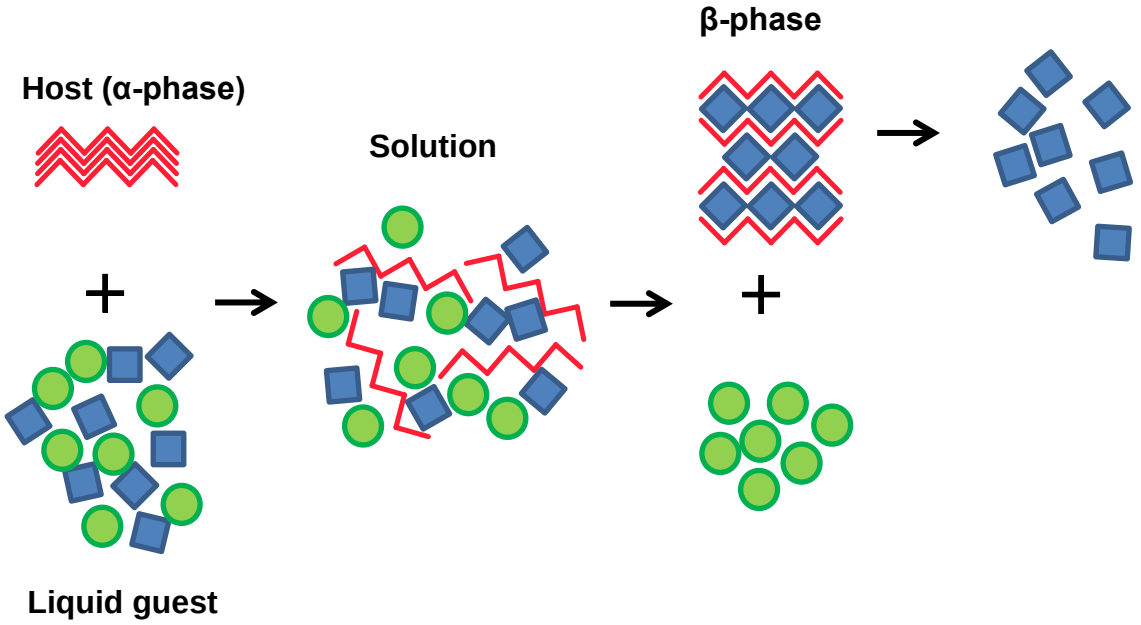

Scheme 1.5. In this schematic diagram, an example of liquid recrystallisation, the darker blue square guests are selected over the lighter blue circular guests because the former have a "better fit" in the cavities of the host's β – phase.[1.82]

However, depending on the molecular recognition between host and guest, the desorbed liquid may not be 100% pure. In this case, it may take several cycles of crystallising the host from the increasingly concentrated guest mixture before a selectivity > 99% is achieved.[1.83]

Ward et al. defined the selectivity coefficient (Eq. 6) as a way to measure the extent of the selectivity of a host towards a mixture of two guests.

$$K_{A:B} = (K_{B:A})^{-1} = \frac{Z_A X_B}{Z_B X_A} \qquad (X_A + X_B = 1) \qquad (6)$$

Where X_A and X_B are the mole fractions of two guests, A and B, in the mother liquor while Z_A and Z_B represent the mole fractions of the respective guests in the resultant crystals. A $K_{A:B}$ value equal to 1 means that the host displays no selectivity towards a mixture of A and B under those particular conditions. However, if $K_{A:B}$ is greater than 1, then A is preferred by the host, while if $K_{A:B} < 1$, then guest B is preferred.[1.84]

Pairwise competition experiments can be used to map the inclusion selectivity of one guest (A) relative to another (B), as shown in Figure 1.16a. The mole fractions of guests in the inclusion compound (Y_A or Y_B) are plotted as a function of the mole fraction of guests in the original solution mixture (X_A or X_B). The selectivity coefficient, $K_{A:B}$ (or $K_{B:A}$) can be calculated at any point on the curve. Larger selectivity coefficients correspond to a greater enrichment of guest A in the inclusion compound, as shown in Figure 1.16a.

The isomers, 2,6- and 2,7-dimethyl naphthalene (DMN), are the most difficult to separate using conventional methods due to their close normal boiling points (262 and 265 °C, respectively). Ward et al.[1.84] demonstrated that a guanidinium organodisulfonate host could be used to obtain 2,6-DMN in greater than 94% purity within three successive crystallisation steps from an initial mixture that contains only 20% 2,6-DMN (Figure 16b).

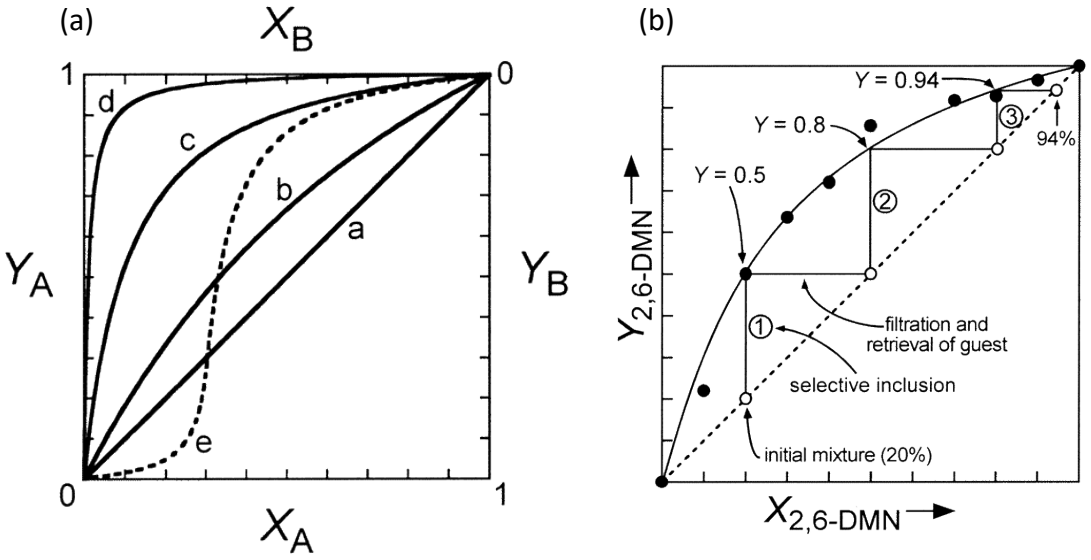

Figure 1.16. (a) Selectivity curves showing various possible host preferences: (a) $K_{A:B} = 1$ (no selectivity), (b) $K_{A:B} = (K_{B:A})^{-1} = 2$, (c) $K_{A:B} = (K_{B:A})^{-1} = 10$, (d) $K_{A:B} = (K_{B:A})^{-1} = 100$. (e) $K_{A:B}$ is concentration dependent. Under conditions of low X_A ($0 < X_A < 0.3$) guest B is preferentially included ($K_{A:B} < 1$). At larger X_A ($0.3 > X_A > 1$) the selectivity is inverted ($K_{A:B} > 1$) and guest A is included. (b) sample of 2,6-DMN (94% pure) can be obtained in only three crystallisation and filtration steps from an initial mixture containing only 20% 2,6-DMN and 80% 2,7-DMN.

An example of exclusive selectivity was observed by Barbour et al., who reported a dinuclear Cu-based metallocycle host that removes p-xylene impurities from commercially pure o-xylene liquid (≥99%).[1.85] Crystallographic studies showed that the selectivity observed is due to the size and shape of the guest, in combination with the flexibility of the host. Therefore, we can calculate $K_{p:o}$ as:

$$K_{p\text{-}:o\text{-}} = \frac{Z_1 X_{0.99}}{Z_0 X_{0.01}} \approx 99 \text{ (very large)}$$

Research reported by Ward et al. revealed that isomer selectivity is most pronounced when the structures of corresponding inclusion compounds are significantly different, i.e., when the isomeric guests template different architectural isomers of the host. Furthermore, selectivity appears to be a consequence of size and shape compatibility between the host and the guest.[1.84]

Kitaigorodskii determined that the packing of molecular solids was governed mainly by considerations of size and shape, the so-called principle of close-packing, which invokes geometrical arguments[1.86] Nassimbeni et al. has reported that this packing factor, which represents the occupied *vs* available space by the guest in the crystal structures, correlates with the measured selectivities.[1.87]

Many factors can influence the composition of guests in the resulting inclusion compound, including:

1.6.1 Temperature.

Ibragimov and Weber et al. reported a carboxylic acid-based host that forms three different types of structures with the xylene isomers, and with different corresponding stabilities as measured by thermal analysis. From a solution of host and an equimolar mix of the three xylenes, it was found that temperatures of -10 to +10 °C yielded H ¶-xylene crystals only. Room temperature saw a mix of o- and p-xylene inclusion compounds, while +40 to +60 °C yielded H ¶-xylene only.[1.88]

1.6.2 Solvent effect.

Coleman et al. reported the effect of the co-solvent isopropanol on the selectivity of the host beta-cyclodextrin for an equimolar mix of the two terpenes – cineole and eugenol. As shown in Figure 1.17, the host shows no selectivity when recrystallised from an aqueous solution of guests, but when more than 20% of water is replaced with isopropanol, the resulting crystals contain only cineole.[1.89]

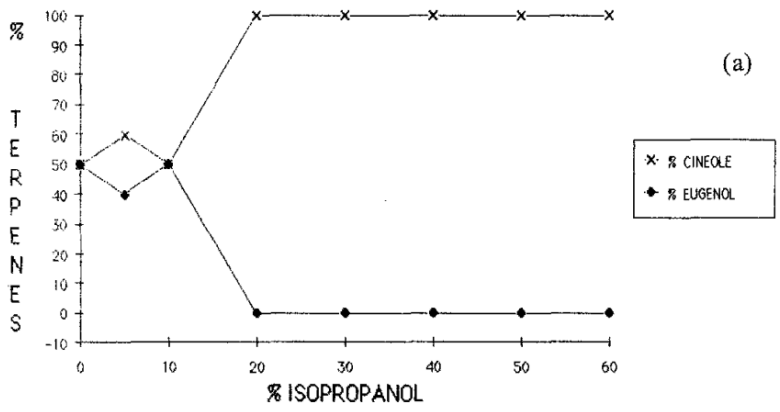

Figure 1.17. Ratio of cineole and eugenol in inclusion compounds crystallised from solution comprising varying percentages of isopropanol in water.

Nassimbeni et al.[1.90] reported the solvent-induced enhanced selectivity by an organic diol host. When the host is recrystallised from mixtures of 3- and 4-picoline (boils at 144 and 145 °C, respectively) in competition experiments with methanol as a co-solvent, the resulting selectivity curve is very similar to that achieved with no co-solvent. However, when benzene is used as a co-solvent, the selectivity curve is enhanced toward the 4-picoline dramatically, with $K_{4\text{-pic:3-pic}}$ increasing from 7.5 to 61.1. This result is attributed to the fact that benzene is not a "neutral" solvent but is incorporated into the crystal structure with the 4-picoline, but not with 3-picoline.

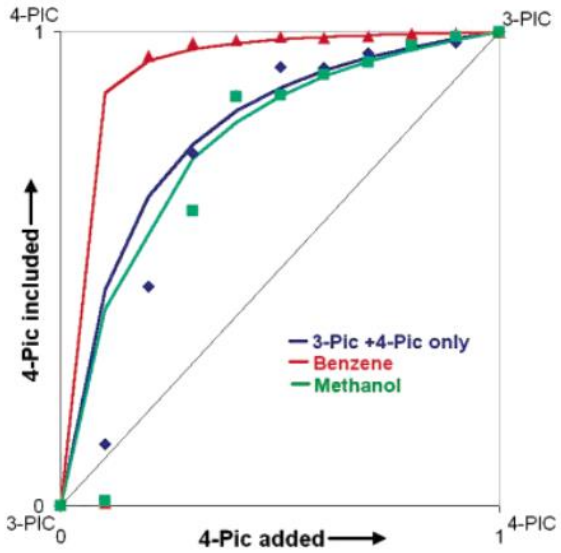

Figure 1.18. Benzene used as a co-solvent enhances selectivity of a diol host for 4-picoline over 3-picoline.

1.6.3 Method.

Yang and Wu[1.91] found a macrocyclic host with a different selectivity preference for equimolar mixtures of chlorobenzene and chlorocyclohexane (with similar normal boiling points of 132 and 142 °C, respectively), depending on whether liquid or vapour diffusion was used to prepare the inclusion compounds. The host can crystallise in two different apohost forms; the α form has a dense packing that preferentially absorbs chlorocyclohexane (97.2%) upon immersion in an equimolar solution of the two guests. However, the β form of the host has intrinsic pores, and when exposed to an equimolar mix of the guest vapours, shows the opposite selectivity preference, with the resulting guest included comprising 88% chlorobenzene.

In addition, the authors show that the chlorobenzene inclusion compound exchanges guest molecules for chlorocyclohexane upon soaking the material in an equimolar mix of guests. In this way, you can separate both guests consecutively, by first exposing the host to a mixture of guest vapour, and subsequently by exposure to a mixture of the liquid guests.

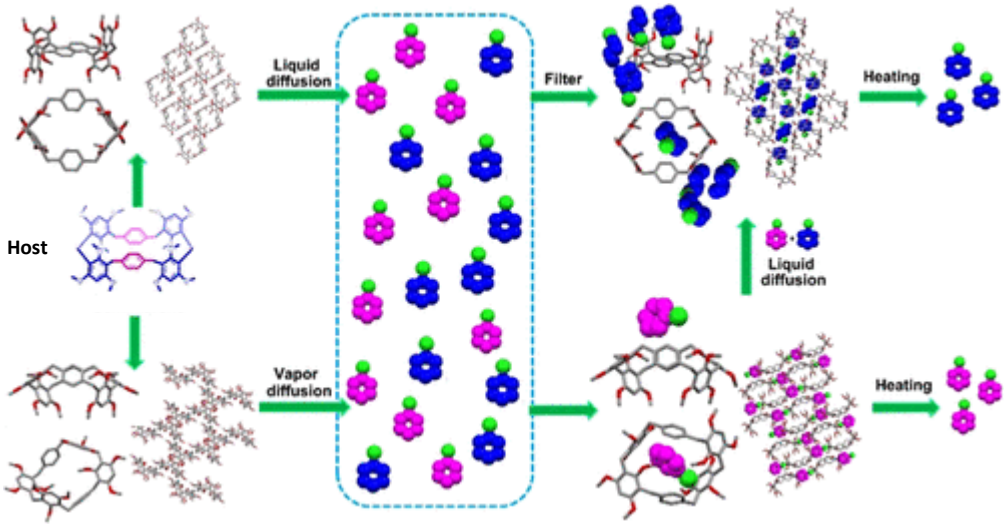

Figure 1.19. The α and β forms of a cyclic host molecule show different selectivity preferences towards an equimolar mixture of chlorobenzene (pink) and chlorocyclohexane (blue) dependent on the method of inclusion compound preparation.

1.6.4 Guest exchange.

The mechanism of guest exchange can be zeolitic, where the guest framework remains mostly unchanged during the exchange process. Or, the exchange can be more akin to recrystallisation, where the original guest is desorbed, leaving the apohost only, which then absorbs the incoming guest to form a new inclusion compound (Figure 1.20a). However, Nassimbeni et al. recently reported an inclusion compound formed from a halogenated host and dichloroethane (DCE) that exchanged guest for iodomethane (MeI) via an enlarged cell which quadrupled in volume (Figure 1.20b).[1.92]

Guest exchange can be used to prepare inclusion compounds that do not form when the host is exposed to the guest. For example, Gorbatchuk et al. reported that 1-propanol and propionitrile could not replace water in a saturated β-cyclodextrin hydrate. As shown in Figure 1.21, these two guests can, however, replace an inclusion compound of the host with benzene, ethanol, and acetonitrile as guest.[1.93]

However, if the incoming guest does not replace the starting guest, this result can be used as a selectivity mechanism. For example, Bacchi et al. reported that the guest in an inclusion compound formed from a 'wheel-and-axle' metallorganic host and tetrahydrofuran could be exchanged with p-xylene by vapour uptake. However, exposing the THF inclusion compound to the vapours of other aromatic guests such as benzene, toluene, and o-and m-xylene only yield partial exchanges, while p-cymene did not exchange at all.[1.94]

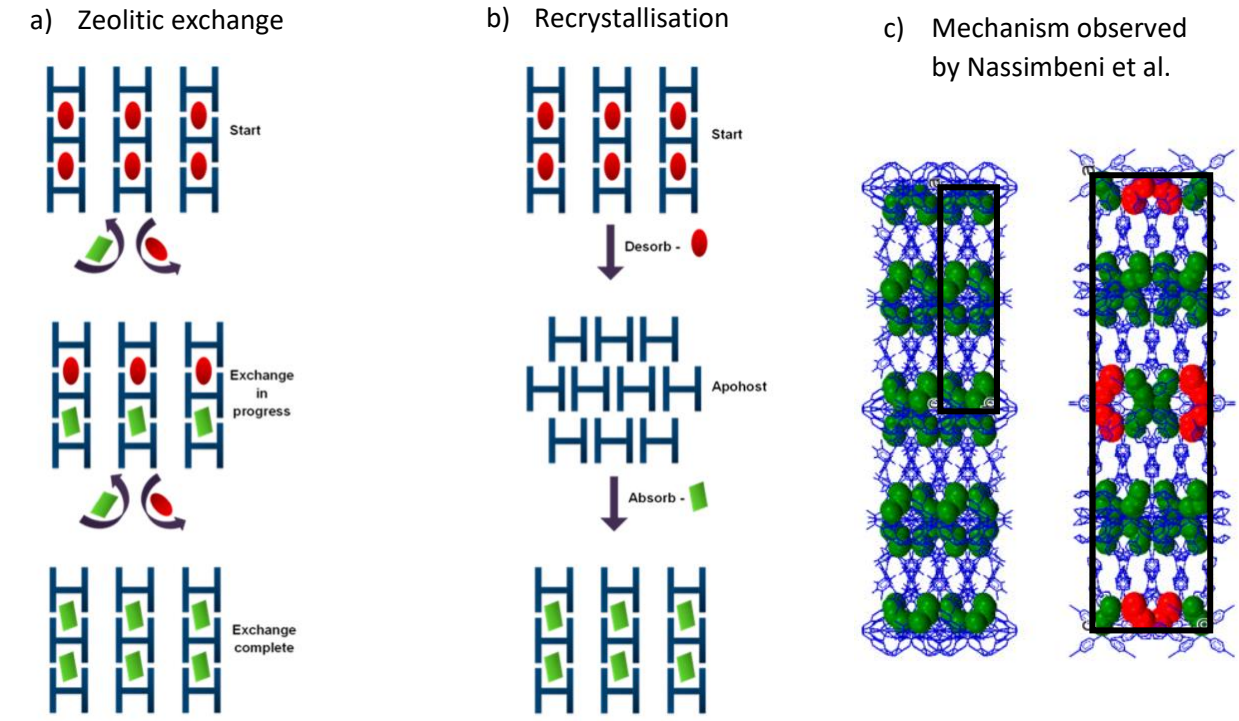

Figure 1.20. Guest exchange mechanisms[1.92] a) zeolitic b) recrystallisation, c) mechanism observed by Nassimbeni et al., left shows four unit cells of the starting inclusion compound, 1.5H ¶DCE, and right shows one unit cell of the intermediate exchange product, 6H ¶DCE ¶MEI after exposure to MeI vapor.

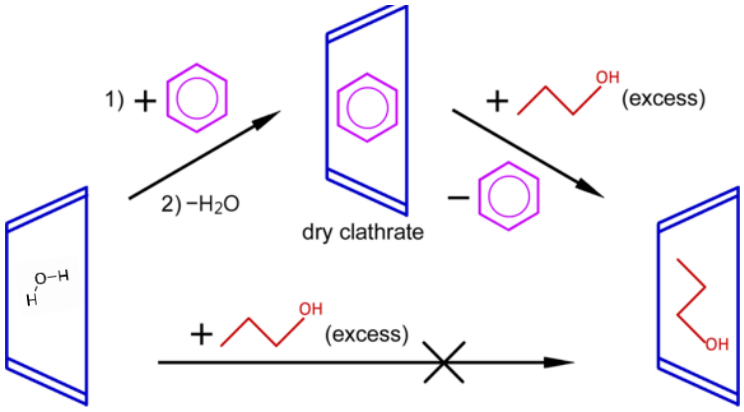

Figure 1.21. An inclusion compound with β-Cyclodextrin and 1-propanol can be prepared by guest exchange from the benzene clathrate, but not the hydrate.

1.7 CRYSTAL ENGINEERNG

"One of the continuing scandals in the physical sciences is that it remains in general impossible to predict the structure of even the simplest crystalline solids from a knowledge of their chemical compositions."

-John Maddox, 1988[1.95]

Crystal engineering began with observing a material's property, and then associating the property with a crystal structure, which was then associated with a particular intermolecular interaction.[1.96] Intermolecular interactions were then linked to structural patterns in crystals, called supramolecular synthons. For example, Etter identified the hydrogen bond as being both directional and strong and a determining factor of crystal structures.[1.97] By understanding the patterns of intermolecular interactions that appear in crystal structures, crystal engineers can work backwards to determine the appropriate starting materials and conditions to prepare compounds with similar patterns. This approach has been summarised by Desiraju [1.98] and used successfully by Zaworotko, [1.99, 1.100] Metrangolo,[1.101] Braga,[1.102] and Aakeröy.[1.103 - 1.105]

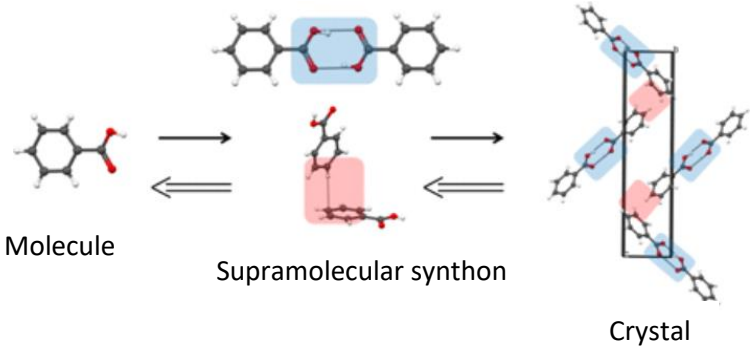

Figure 1.19. Benzoic acid can form a hydrogen bond to another benzoic acid molecule, and commonly appears as acid dimer synthon in crystal structures, with two hydrogen bonds between the molecules.[1.98]

The ultimate form of crystal engineering would be to predict crystal structures. However, this is a challenging problem. In the 1990s Sally Price stated that "There is still a long way to go",[1.106] while Gavezzotti, [1.107] when asked "Are crystal structures predictable?", bluntly answered, "No".

Six blind tests have been conducted since 1999, occurring every three years; the 7th is currently underway and will conclude in June 2022.[1.108] In these tests, participants are given a list of molecules and over nine months run their computations, after which they submit their computer-generated crystal structures. These predicted structures are then compared with experimental outcomes of crystallisations (which had been held in confidence), and the results published.[1.109]

The results of the 6th test[1.110] show that whilst the stable structure prediction of a given single-component compound is close,[1.109] the situation is still difficult for inclusion compounds in which the asymmetric unit is made up of two or more separate molecular entities. In addition, it remains unanswered why some compounds are polymorphic or which of the predicted forms can be realised experimentally and how.

1.8 THESIS AIMS AND OBJECTIVES

The general aim of this thesis was to investigate the selectivity of different host molecules to various guests with similar structural and physical characteristics. This aim was achieved via the following objectives:

choose appropriate host and guest compounds, and crystallisation conditions by surveying the literature

synthesise new inclusion compounds, elucidate their crystal structures, and measure their thermal stability.

measure the selectivity preference of host compounds by recrystallising the host from mixtures of guests, and using analytical methods to determine the composition of guests in the resulting inclusion compounds. An alternative approach to investigating the separation abilities of a host was by means of guest exchange studies, where inclusion compounds are exposed to the vapours of different guests.

compare the packing and interactions of the crystal structures with the compound's thermal stability, and the selectivity preference exhibited by the host.

Gain further insights into the secondary interactions and the concomitant packing of the host-guest structures by analysing their kinetics of decomposition and/or vapour sorption.

1.9 HOSTS AND GUESTS STUDIED

1.9.1 Diol hosts and H-bond donor/acceptor guests

Weber[1.111] showed that hosts with a bulky skeleton and functional groups capable of strong secondary interactions (like hydrogen bonding) can create clathrate-typical lattice cavities in which guests are bound. The similarly structured diol hosts, **H1** and **H2**, were synthesised by Weber,[1.112] also proved these hosts capable of forming inclusion compounds with alcohols and amines, in which guests form hydrogen bonds with the host hydroxyl (OH) moiety. Both hosts were used as received without further purification. The structures and names of H1 and H2 are displayed in Scheme 1.6, as are the structures and normal boiling points of the guests used in chapters 3, 4, and 5.

Chapter 3 concerns the study of the inclusion compounds formed with **H1** and **H2** and the guests, methyl- and dimethylpiperidines, namely, 2-methylpiperidine (**2MP**), 3-methylpiperidine (**3MP**), 4-methylpiperidine (**4MP**), 2,6-dimethylpiperidine (**2,6DMP**), and 3,5-dimethylpiperidine (**3,5DMP**). The selectivity preferences of the two hosts were compared, and the preference of **H1** for these methylpiperidines compared to the structurally similar methylpyridines, reported previously by Nassimbeni et al.[1.113]

In chapters 4 and 5, **H1** was the only host used. Chapter 4 concerns the selectivity of the host towards 1-butanol (**1BUT**) and three isomers of pentanol, 3-methyl-2-butanol (**3MBUT**), 2-pentanol (**2PENT**), and 3-pentanol (**3PENT**). Chapter 5 presents the inclusion compounds formed from **H1** with the guests, tertiary butanol (**t-BUT**) and 2-propnaol (**2-PROP**), at various temperatures of crystallisation.

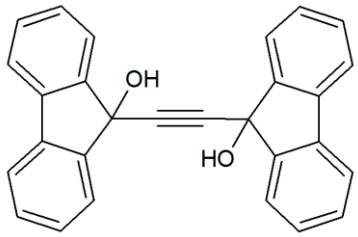

H1 = 9,9'-(ethyne-1,2-diyl)-bis(fluoren-9-ol)

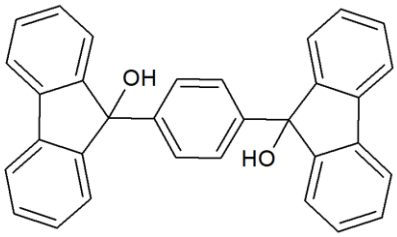

H2 = 9,9'-(1,4-phenylene)-bis(fluoren-9-ol)

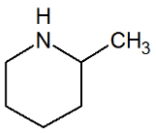

2MP

118–119 °C

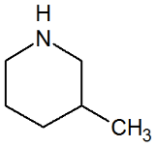

3MP

125–126 °C

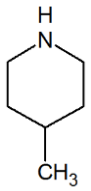

4MP

124 °C

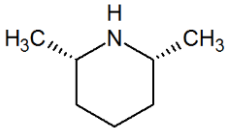

2,6DMP

127–128 °C

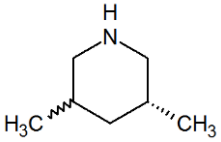

3,5DMP

144 °C

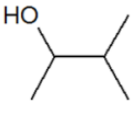

3MBUT

114 °C

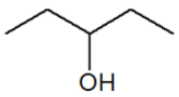

3PENT

115 °C

1BUT

118 °C

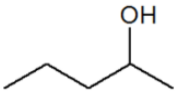

2PENT

119 °C

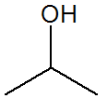

2-PROP

82.6 °C

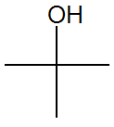

t-BUT

82.2 °C

Scheme 1.6. The molecular structure of the 'dumbbell'-type Weber hosts, **H1** and **H2**, and the guests used in chapters 3, 4, and 5, which are labelled with their respective abbreviations and normal boiling points.

1.9.2 Werner host and methylnaphthalene guests.

The modern theory of coordination chemistry is based largely on the work of Werner (1913 Nobel Prize in Chemistry[1.114]), who proposed the correct structures for coordination compounds, a central transition metal atom surrounded by neutral or anionic ligands.

Hosts named for Werner have the general formula MX_2L_4, where M is a divalent transition metal cation, e.g., Ni^{2+}, X is an anionic ligand, e.g., NCS^-, and L is an electrically neutral substituted pyridine, e.g., 4-methylpyridine. The Werner host, $Ni(NCS)_2(4\text{-}MePy)_4$, was once used by the Union Oil Company[1.115] to separate para-xylene, which it preferred, from a mixture with meta-xylene. Tanaka et al. discovered that this host forms various inclusion compounds with 1-methyl and 2-methylnaphthalene (**1-MN** and **2-MN**) at different concentrations of guest (see section 1.5.2), and explained the host's dynamic selectivity preference.

In chapter 6, the similar host **H3** was studied in conjunction with **1-MN** and **2-MN** guests. This host is synthesised by a known method using the ligand, 4-phenyl pyridine, instead of 4-methylpyridine. This involved making nickel(II)thiocyanate ($Ni(SCN)_2$) by mixing ethanoic solutions of nickel chloride hexahydrate, $NiCl_2$ ¶(H_2O), with ammonium thiocyanate (NH_4SCN). The resulting precipitate, ammonium chloride (NH_4Cl), was filtered from the solution, and an ethanolic solution of 4-phenyl pyridine was added to the filtrate, causing the powdered **H3** to precipitate.

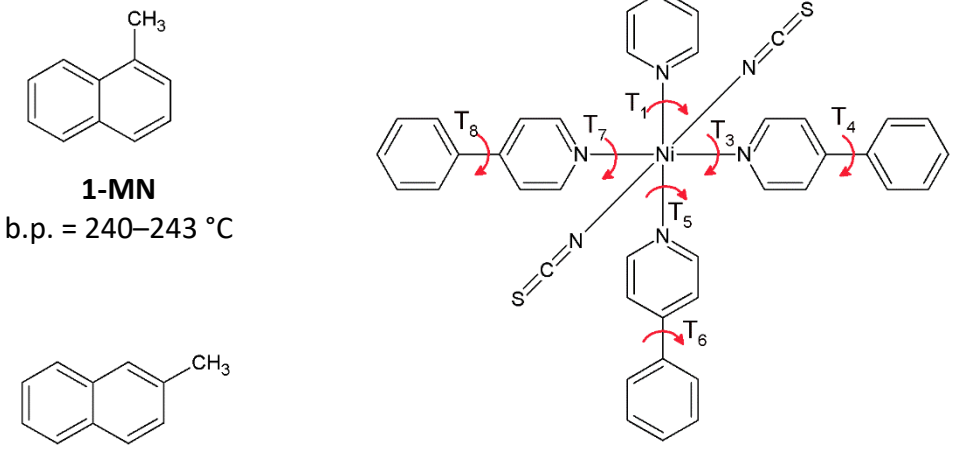

1-MN
b.p. = 240–243 °C

2-MN
b.p. = 241–243 °C

H3 = $Ni(NCS)_2(4\text{-}PhPy)_4$
4-PhPy = 4-phenylpyridine

Scheme 1.7. Structures of the host **H3** and guest compounds, 1- and 2- methylnaphthalene with their respective normal boiling points.

1.9.3 Brominated host and oxygen-containing guests.

Chapter 7 deals with the inclusion compounds formed by the Host, **H4**, tetra(p-bromophenyl)ethylene, and guests having some structural similarities, inclusion all containing an oxygen atom. This host has successfully been used by Nassimbeni et al. to study guest exchange reactions, and an example was reported where the exchange proceeded by the formation of an intermediate structure with an enlarged unit cell.

H4 was synthesised according to a known method, which involved exposing the starting material, tetraphenylethylene, to bromine vapour for one day. The product obtained was dissolved in a minimum volume of hot chloroform, and **H4** was precipitated by the addition of cold ethanol.

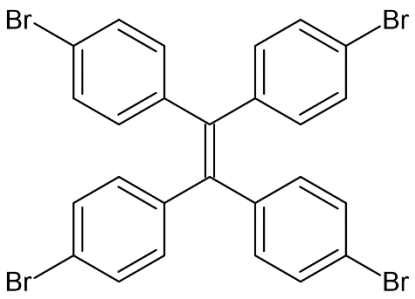

H4 = tetra(p-bromophenyl)ethylene

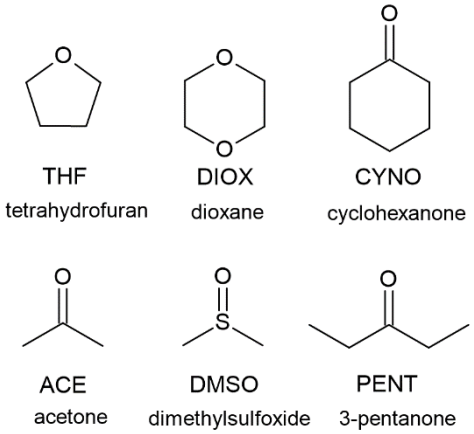

Scheme 1.8. Structures of the host, **H4** (left) and guests under study (right).

1.10 THESIS LAYOUT

This introductory chapter provides an overview of host-guest chemistry, lists some of the factors that affect a host's selectivity preference, outlines the aim of this thesis, and presents the host and guest compounds used.

The following chapter (chapter 2) provides detailed explanations of all experimental methods used.

Chapters 3, 4, 6, and 7 are articles, and chapter 5 is a communication, all of which have been published in international peer-reviewed journals. Each publication is a separate body of work. In all cases the text has been reproduced exactly as it appears in the published manuscripts, and the same figures and tables have been inserted. However, the following changes were made:

Figures and tables have been renumbered and their styles reformatted to maintain consistency throughout the thesis.

References are listed at the end of each chapter in the form x.y, where x is the chapter number and y the reference number. Due to this style, some references are repeated between chapters. All references have been formatted to the Royal Society of Chemistry style to maintain consistency throughout the thesis.

Supplementary data for chapters 3–7 have been moved to appendices at the end of the thesis.

All new crystal structures presented in this thesis have been deposited into the Cambridge Structural Database, and their codes have been added to the relevant tables of crystallographic information.

Each of the chapters 3–7 begins with an additional synopsis of the enclosed manuscript, serving as an extended abstract.

Lastly, Chapter 8 provides a summary of the outcomes of this work and concluding remarks, and suggestions are made regarding future work in the field of inclusion compounds.

1.11 REFERENCES

1.1. Alfred Nobel – Life and Philosophy, https://www.nobelprize.org/alfred-nobel/alfred-nobel-life-and-philosophy/, (accessed 24 October 2021).

1.2. P. Willett, The Calculation of Molecular Structural Similarity: Principles and Practice, *Mol. Inform.*, 2014, **33**, 403–413.

1.3. W. M. Haynes, Ed., *CRC handbook of chemistry and physics: a ready-reference book of chemical and physical data*, CRC Press, Boca Raton, Fla., 94. ed., 2013.

1.4. R. H. Perry and D. W. Green, *Perry's Chemical Engineers' Handbook*, McGraw-Hill, 1998.

1.5. H. Z. Kister, *Distillation design*, McGraw Hill, 1992.

1.6. I. Grout, in *Digital Systems Design with FPGAs and CPLDs*, ed. I. Grout, Newnes, Burlington, 2008, pp. 123–176.

1.7. V. Andrushko and N. Andrushko, in *Stereoselective Synthesis of Drugs and Natural Products*, American Cancer Society, 2013, pp. 1–42.

1.8. A. Cahours Recherches sur les huiles légéres obtenues dans la distillation du bois (Investigations of light oils obtained by the distillation of wood), *Compte rendus*, 30 : 319-323, 1850

1.9. U.S. Environmental Protection Agency. *Locating and estimating air emissions from sources of xylene*. Emission Inventory Branch, Technical Support Division, Office of Air Quality Planning and Standards, Research Triangle Park, NC, March 1994. EPA-454/R-93-048:

1.10. E. G. Hancock, Ed., *Toluene, the xylenes, and their industrial derivatives*, Elsevier, Amsterdam ; New York, 1982.

1.11. D. S. Sholl and R. P. Lively, Seven chemical separations to change the world, *Nature*, 2016, 532, 435–437

1.12. E. F. Aransiola, M. O. Daramola, T. V. Ojumu, in *Xylenes: synthesis, characterisation and physicochemical properties*, ed. M. O. Daramola, Nova Publishers, New York, 2013, ch. 1.

1.13. Y. Yang, P. Bai and X. Guo, Separation of Xylene Isomers: A Review of Recent Advances in Materials, *Ind. Eng. Chem. Res.*, 2017, **56**, 14725–14753.

1.14. G. Zhang, A.-H. Emwas, U. F. Shahul Hameed, S. T. Arold, P. Yang, A. Chen, J.-F. Xiang and N. M. Khashab, Shape-Induced Selective Separation of Ortho-substituted Benzene Isomers Enabled by Cucurbit[7]uril Host Macrocycles, *Chem*, 2020, **6**, 1082–1096.

1.15. T. Amemiya, E. Tsunetomi, E. Nakamura, T. Nakazawa, R. Hatta, T. Iwasaki and M. Shimizu, Production of *p*-Xylene from Xylene Mixture by Recycle Process, *J. Japan Pet. Inst.*, 1959, 1, 78–84.

1.16. J. E. D. Davies, W. Kemula, H. M. Powell and N. O. Smith, Inclusion compounds —Past, present, and future, *J. Incl. Phenom.*, 1983, **1**, 3–44.

1.17. L. Nassimbeni, Physicochemical Studies of Separation of Isomers by Supramolecular Systems. In *Separations and Reactions in Organic Supramolecular Chemistry: Perspectives in Supramolecular Chemistry*, ed. F. Toda, and R. Bishop, John Wiley & Sons Ltd, England, 2004; ch. 8, p. 123.

1.18. J. Holló and J. Szejtli, The mechanism of starch-iodine reaction, *Period. Polytech. Chem. Eng.*, 1957, **1**, 141–145.

1.19. Structure & Reactivity: Macromolecules, https://employees.csbsju.edu/cschaller/Principles%20Chem/macromolecules/MMsupramolecular.htm, (accessed 12 January 2022).
1.20. The Nobel Prize in Physics 1914, https://www.nobelprize.org/prizes/physics/1914/laue/lecture/, (accessed 12 January 2022).
1.21. The Nobel Prize in Physics 1914, https://www.nobelprize.org/prizes/physics/1914/laue/lecture/, (accessed 12 January 2022).
1.22. The Nobel Prize in Chemistry 1954, https://www.nobelprize.org/prizes/chemistry/1954/pauling/lecture/, (accessed 12 January 2022).
1.23. M. J. Klein, The historical origins of the Van der Waals equation, *Physica*, 1974, **73**, 28–47.
1.24. The Nobel Prize in Physiology or Medicine 1962, https://www.nobelprize.org/prizes/medicine/1962/summary/, (accessed 12 January 2022).
1.25. D. J. Berry and J. W. Steed, Pharmaceutical cocrystals, salts and multicomponent systems; intermolecular interactions and property based design, *Adv. Drug Deliv. Rev.*, 2017, **117**, 3–24.
1.26. M. Twain, *Following the equator; a journey around the world*, Hartford, Conn. : American Pub. Co., 1897.
1.27. Action of sucrase on sucrose, https://www.sciencelearn.org.nz/images/2260-action-of-sucrase-on-sucrose, (accessed 12 November 2021).
1.28. L. Poshyvailo-Strube, Modelling and simulations of enzyme-catalysed reactions, MSc thesis at the Kyiv-Mohyla Academy, 2015.
1.29. E. Fischer, *Berichte der deutschen chemischen Gesellschaft*, 1894, **27**, 2985–2993.
1.30. G. Zhang, Y. Ding, A. Hashem, A. Fakim and N. M. Khashab, Xylene isomer separations by intrinsically porous molecular materials, *Cell Rep. Phys. Sci.*, 2021, **2**, 100470.
1.31. C. J. Pedersen and H. K. Frensdorff, Macrocyclic Polyethers and Their Complexes, *Angew. Chem. Int. Ed.*, 1972, **11**, 16–25.
1.32. D. A. Doyle, J. M. Cabral, R. A. Pfuetzner, A. Kuo, J. M. Gulbis, S. L. Cohen, B. T. Chait and R. MacKinnon, The Structure of the Potassium Channel: Molecular Basis of K+ Conduction and Selectivity, *Science*, 1998, **280**, 69–77.
1.33. T. Dudev and C. Lim, Factors Governing the Na+ vs K+ Selectivity in Sodium Ion Channels, *J. Am. Chem. Soc.*, 2010, **132**, 2321–2332.
1.34. L. G. Palmer, Ion selectivity of the apical membrane Na channel in the toad urinary bladder, *J. Membr. Biol.*, 1982, **67**, 91–98.
1.35. B. Hille, *Ionic Channels of Excitable Membranes*, Oxford University Press, Incorporated, 1992.
1.36. M. C. Rose and R. W. Henkens, Stability of sodium and potassium complexes of valinomycin, *Biochimica et Biophysica Acta (BBA) - General Subjects*, 1974, **372**, 426–435.
1.37. E. P. Kyba, R. C. Helgeson, K. Madan, G. W. Gokel, T. L. Tarnowski, S. S. Moore and D. J. Cram, Host-guest complexation. 1. Concept and illustration, *J. Am. Chem. Soc.*, 1977, **99**, 2564–2571.

1.38. W. Smith, W. Wayte and G. E. Marindin, *A dictionary of Greek and Roman antiquities.*, J. Murray, London, 1890.
1.39. J. W. Steed and J. L. Atwood, *Supramolecular Chemistry*, John Wiley & Sons, 2022.
1.40. K. M. Steed and J. W. Steed, Packing Problems: High Z' Crystal Structures and Their Relationship to Cocrystals, Inclusion Compounds, and Polymorphism, *Chem. Rev.*, 2015, **115**, 2895–2933.
1.41. P. Flowers, K. H. Theopold, R. Langley and W. R. Robinson, *Chemistry 2e*, OpenStax, 2019.
1.42. Lattice Structure of Crystals - Course Hero, https://www.coursehero.com/sg/general-chemistry/lattice-structure-of-crystals/, (accessed 12 January 2022).
1.43. M. Faraday and H. Davy, XIV. On fluid chlorine, *Philos. Trans. R. Soc.*, 1823, **113**, 160–165.
1.44. F. Cramer, Einschlußverbindungen der Cyclodextrine, *Angew. Chem*., 1952, **64**, 136–136.
1.45. W. L. Mao, C. A. Koh and E. D. Sloan, Clathrate hydrates under pressure, *Phys. Today*, 2007, **60**, 42–47.
1.46. J. Lee, B.-J. Ryu, T. Yun, J. Lee and G.-C. Cho, Review on the Gas Hydrate Development and Production as a New Energy Resource, *KSCE J. Civ. Eng.*, 2011, **15**, 689–696.
1.47. OC/GEO 103 - Deep Ocean Currents, http://dusk.geo.orst.edu/oceans/deep_currents.html, (accessed 20 November 2021).
1.48. lovecraftsgarden, Lovecraft's Garden, https://lovecraftsgarden.tumblr.com/post/166691624909/clathrus-ruber-latticed-stinkhorn-basket, (accessed 13 January 2022).
1.49. P. A. Micheli, *Nova plantarum genera juxta Tournefortii methodum disposita Plantarum Genera Juxta Tournefortii Methodum Disposita*, Bernardi Paperini, Florentiae, 1729.
1.50. A. San-Miguel and P. Toulemonde, High-pressure properties of group IV clathrates, *High Press. Res.*, 2005, **25**, 159–185
1.51. R. Graves and R. R. Graves, *The White Goddess: A Historical Grammar of Poetic Myth*, Creative Age Press, 1948.
1.52. H. M. Powell, 15. The structure of molecular compounds. Part IV. Clathrate compounds, *J. Chem. Soc.*, 1948, 61–73.
1.53. E. Weber and H.-P. Josel, A proposal for the classification and nomenclature of host-guest-type compounds, *J. Incl. Phenom.*, 1983, **1**, 79–85.
1.54. L. R. Nassimbeni, Physicochemical Aspects of Host−Guest Compounds, *Acc. Chem. Res.*, 2003, **36**, 631–637.
1.55. S. Boothroyd, A. Kerridge, A. Broo, D. Buttar and J. Anwar, Why Do Some Molecules Form Hydrates or Solvates?, *Cryst. Growth Des.*, 2018, **18**, 1903–1908.
1.56. A. K. Kwan, Hard boiled eggs - How to cook the perfect hard boiled eggs every time, https://tasteasianfood.com/hard-boiled-eggs/, (accessed 15 January 2022).
1.57. cyclonebill, *Vagtel-spejlæg*, 2009.
1.58. Stasroki, *Български: Омлет натюр*, 2011.

1.59. C. for D. C. and Prevention, *English: Chick and duckling*, 2006.
1.60. B. Ibragimov, A Simple Correlation between the Structures of Different Crystal Modifications of a Given Host–Guest Complex and their Crystallisation Temperatures, *J. Incl. Phenom.*, 1999, **34**, 345–353
1.61. B. T. Ibragimov, Z. G. Tiljakov, K. M. Beketov and S. A. Talipov, Polymorphism of Inclusion Complexes and Unsolvated Hosts. I. Trimorphism of the Host-Guest Complex of Gossypol with Dichloromethane. The Structure of the β-Phase, *J. Incl. Phenom.*, 1997, **27**, 99–104.
1.62. B. T. Ibragimov, Further development of the general rule on correlation between host–guest ratio and topology of polymorphic inclusion compounds and their crystallisation temperatures, *CrystEngComm, 2007, **9**, 111–118.*
1.63. M. Kitamura and T. Tanaka, Crystallisation behavior of polymorphous Ni-complex clathrate in the presence of 2-methylnaphthalene, *J. Cryst. Growth*, 1994, **142**, 165–170.
1.64. P. Natarajan, A. Bajpai, P. Venugopalan and J. N. Moorthy, Pseudopolymorphism of a Highly Adaptable Tetraarylpyrene Host that Exhibits Abundant Solid-State Guest Inclusion, *Cryst. Growth Des.*, 2012, **12**, 6134–6143.
1.65. A. Sayed, A. Jacobs and J. H. Taljaard, Solvent manipulation of N-methylacetamide inclusion compounds with a xanthenol host, *Z. Kristallogr. Cryst. Mater*., 2015, **230**, 167–175.
1.66. K. Tanaka and F. Toda, Solvent-Free Organic Synthesis, *Chem. Rev.*, 2000, **100**, 1025–1074.
1.67. P. S. Sidhu, G. D. Enright, K. A. Udachin and J. A. Ripmeester, Polymorphism and Structure in a Pentamorphic Guest−Host Material: The Tris(5-acetyl-3-thienyl) Methane (TATM) Inclusion Compound with 1,3-Dichloropropane, *Cryst. Growth Des.*, 2004, **4**, 1249–1257.
1.68. M. Lusi and L. J. Barbour, Solid–vapour reactions as a post-synthetic modification tool for molecular crystals: the enclathration of benzene and toluene by Werner complexes, *Chem. Commun.*, 2013, **49**, 2634–2636.
1.69. W. Ostwald, Studien über die Bildung und Umwandlung fester Körper: 1. Abhandlung: Übersättigung und Überkaltung, *Z. Phys. Chem.*, 1897, **22U**, 289–330.
1.70. Ch 10: Kinetic and Thermodynamic Control, http://www.chem.ucalgary.ca/courses/351/Carey5th/Ch10/ch10-3-3.html, (accessed 10 January 2022).
1.71. J. D. Badjic , S. J. Cantrill and J. F. Stoddart , *J. Am. Chem. Soc.*, 2004, **126** , 2288
1.72. A. S. M. Dyck , U. Kisiel and C. Bohne , *J. Phys. Chem. B*, 2003, **107** , 11652
1.73. P. Mukhopadhyay , P. Y. Zavalij and L. Isaacs , *J. Am. Chem. Soc.*, 2006, **128** , 14093
1.74. T. Oshikiri , Y. Takashima , H. Yamaguchi and A. Harada , *J. Am. Chem. Soc.*, 2005, **127** , 12186
1.75. J. C. Chapin , M. Kvasnica and B. W. Purse , *J. Am. Chem. Soc.*, 2012, **134** , 15000
1.76. Z. Urbanczyk-Lipkowska , K. Yoshizawa , S. Toyota and F. Toda , *CrystEngComm*, 2003, **5** , 114
1.77. H. Hosomi , S. Ohba , K. Tanaka and F. Toda , *J. Am. Chem. Soc.*, 2000, **122** , 1818
1.78. R. Boese , J. Benet-Buchholz , A. Stanger , K. Tanaka and F. Toda , *Chem. Commun.*, 1999, 319

1.79. O. Danylyuk, V. P. Fedin and V. Sashuk, Kinetic trapping of the Host–guest association intermediate and its transformation into a thermodynamic inclusion complex, *Chem. Commun.*, 2013, **49**, 1859–1861.
1.80. F. Sánchez-Férez and J. Pons, *Polymorphism and Supramolecular Isomerism: The Impasse of Coordination Polymers*, IntechOpen, 2021.
1.81. J. Bernstein, *Polymorphism in Molecular Crystals*, OUP Oxford, 2002.
1.82. L. R. Nassimbeni, Physicochemical Aspects of Host−Guest Compounds, *Acc. Chem. Res.*, 2003, **36**, 631–637.
1.83. L. R. Nassimbeni, Useful Techniques in Host-Guest Chemistry, *Supramol. Chem.*, 2000, **12**, 161–167.
1.84. A. M. Pivovar, K. T. Holman and M. D. Ward, Shape-Selective Separation of Molecular Isomers with Tunable Hydrogen-Bonded Host Frameworks, *Chem. Mater.*, 2001, **13**, 3018–3031.
1.85. M. du Plessis, V. I. Nikolayenko and L. J. Barbour, Record-Setting Selectivity for p-Xylene by an Intrinsically Porous Zero-Dimensional Metallocycle, *J. Am. Chem. Soc.*, 2020, **142**, 4529–4533.
1.86. A. I. Kitaigorodskii, The principle of close packing and the condition of thermodynamic stability of organic crystals, *Acta Crystallogr.*, 1965, **18**, 585–590.
1.87. N. B. Báthori and L. R. Nassimbeni, Selectivity of amides by host–guest inclusion, *CrystEngComm*, 2011, **13**, 3156–3161.
1.88. K. Beketov, E. Weber, J. Seidel, K. Köhnke, K. Makhkamov and B. Ibragimov, Temperature-controlled selectivity of isomeric guest inclusion: enclathration and release of xylenes by 1,1′-binaphthyl-2,2′-dicarboxylic acid, *Chem. Commun.*, 1999, 91–92.
1.89. C. Donzé, A. Chatjigakis and A. W. Coleman, Co-solvent modulation of the inclusion selectivity ofβ-cyclodextrin, *J. Incl. Phenom. Macrocycl. Chem.*, 1992, **13**, 155–161.
1.90. S. A. Bourne, K. C. Corin, L. R. Nassimbeni and F. Toda, Selective Enclathration of Picolines, *Cryst. Growth Des.*, 2005, **5**, 379–382.
1.91. J.-R. Wu and Y.-W. Yang, Geminiarene: Molecular Scale Dual Selectivity for Chlorobenzene and Chlorocyclohexane Fractionation, *J. Am. Chem. Soc.*, 2019, **141**, 12280–12287.
1.92. F. M. Amombo Noa, S. A. Bourne, H. Su and L. R. Nassimbeni, Guest Exchange in Halogenated Host–Guest Compounds: Structures and Kinetics, *Cryst. Growth Des.*, 2016, **16**, 1636–1642.
1.93. V. V. Gorbatchuk, A. K. Gatiatulin, M. A. Ziganshin, A. T. Gubaidullin and L. S. Yakimova, Unusually high efficiency of β-cyclodextrin clathrate preparation by water-free solid-phase guest exchange, *J. Phys. Chem. B*, 2013, **117**, 14544–14556.
1.94. A. Bacchi, S. Bourne, G. Cantoni, S. A. M. Cavallone, S. Mazza, G. Mehlana, P. Pelagatti and L. Righi, Reversible Guest Removal and Selective Guest Exchange with a Covalent Dinuclear Wheel-and-Axle Metallorganic Host Constituted by Half-Sandwich Ru(II) Wheels Connected by a Linear Diphosphine Axle, *Cryst. Growth Des.*, 2015, **15**, 1876–1888.
1.95. J. Maddox, Crystals from first principles, *Nature*, 1988, **335**, 201–201.
1.96. G. R. Desiraju, Crystal engineering: structure, property and beyond, *IUCrJ*, 2017, **4**, 710–711.

1.97. M. C. Etter, Hydrogen bonds as design elements in organic chemistry, *J. Phys. Chem.*, 1991, **95**, 4601–4610.
1.98. G. R. Desiraju, Crystal Engineering: From Molecule to Crystal, *J. Am. Chem. Soc.*, 2013, **135**, 9952–9967.
1.99. S. G. Fleischman, S. S. Kuduva, J. A. McMahon, B. Moulton, R. D. Bailey Walsh, N. Rodríguez-Hornedo and M. J. Zaworotko, Crystal Engineering of the Composition of Pharmaceutical Phases: Multiple-Component Crystalline Solids Involving Carbamazepine, *Cryst. Growth Des.*, 2003, **3**, 909–919.
1.100. B. Moulton and M. J. Zaworotko, From Molecules to Crystal Engineering: Supramolecular Isomerism and Polymorphism in Network Solids, *Chem. Rev.*, 2001, **101**, 1629–1658.
1.101. P. Metrangolo, F. Meyer, T. Pilati, G. Resnati and G. Terraneo, Halogen Bonding in Supramolecular Chemistry, *Angew. Chem., Int. Ed.*, 2008, **47**, 6114–6127.
1.102. D. Braga and F. Grepioni, Reactions Between or Within Molecular Crystals, *Angew. Chem., Int. Ed.*, 2004, **43**, 4002–4011.
1.103. C. B. Aakeröy, Crystal Engineering: Strategies and Architectures, *Acta Cryst. B*, 1997, **53**, 569–586.
1.104. C. B. Aakeröy and K. R. Seddon, The hydrogen bond and crystal engineering, *Chem. Soc. Rev.*, 1993, **22**, 397–407.
1.105. C. B. Aakeröy, N. R. Champness and C. Janiak, Recent advances in crystal engineering, *CrystEngComm*, 2009, **12**, 22–43.
1.106. T. Beyer, T. Lewis and S. L. Price, Which organic crystal structures are predictable by lattice energy minimisation?, *CrystEngComm*, 2001, **3**, 178–212.
1.107. A. Gavezzotti, Are Crystal Structures Predictable?, *Acc. Chem. Res.*, 1994, **27**, 309–314.
1.108. The Seventh CSP Blind Test - 2020 to 2022 - The Cambridge Crystallographic Data Centre (CCDC), https://www.ccdc.cam.ac.uk/Community/initiatives/cspblindtests/csp-blind-test-7/, (accessed 16 January 2022).
1.109. A. J. Cruz-Cabeza, Crystal structure prediction: are we there yet?, *Acta Cryst. B*, 2016, **72**, 437–438.
1.110. C. R. Groom and A. M. Reilly, Sixth blind test of organic crystal-structure prediction methods, *Acta Cryst. B*, 2014, **70**, 776–777.
1.111. E. Weber and M. Czugler, in *Molecular Inclusion and Molecular Recognition — Clathrates II*, ed. E. Weber, Springer, Berlin, Heidelberg, 1988, pp. 45–135.
1.112. E. Weber, S. Nitsche, A. Wierig and I. Csöregh, Inclusion Compounds of Diol Hosts Featuring Two 9-Hydroxy-9-fluorenyl or Analogous Groups Attached to Linear Spacer Units, *Eur. J. Org. Chem.*, 2002, **2002**, 856–872.
1.113. L. R. Nassimbeni, G. Ramon and E. Weber, Inclusion by a fluorenyl diol host with substituted pyridines, *J Therm. Anal. Calorim.*, 2007, **90**, 31–37.
1.114. The Nobel Prize in Chemistry 1913, https://www.nobelprize.org/prizes/chemistry/1913/summary/, (accessed 16 January 2022).
1.115. United States Patent, Union Oil Co., US3013091A, 1961.

CHAPTER 2: Methods

(a) 18 January 2016, taken as a new MSc student. (b) 12 December 2018, a naphthalene inclusion compound with **H3**, the co-solvent has evaporated and separated from the oily excess guest. (c) 12 March 2021, a 'two-vial' vapour sorption experiment, where one vial contains the powdered host, and the other the liquid guest. (d) 1 March 2021, NMR tubes. (e-g) 21 May 2017, sample holder to measure in-situ vapor absorption by host powders. (h, i) 6 May 2018, me with the polarized light microscope, and a section of the lab I in which I worked. (j) 10 July 2021, my lab coat hook. (k) 28 May 2021, starting material exposed to bromine vapour to prepare **H4**.

2.1 LITERATURE SEARCH

2.1.1 Cambridge Structural Database.

Each guest molecule is searched on the Cambridge Structural Database (CSD),[2.1] which stores published organic and inorganic crystal structures. All structures containing the guest molecule of interest are examined and used to inform the design of a new separation project. Noteworthy observations include the types of interactions between guests and other molecules and, therefore, which moieties a host should have to maximise the likelihood of forming an inclusion compound. Potential hosts are also searched and this provides useful information, such as which solvents can be used as a 'neutral' solvent, i.e., dissolves the host but does not yield a host-solvent compound.

2.2 SYNTHESIS OF INCLUSION COMPOUNDS

2.2.1 Recrystallisation.

Most inclusion compounds were prepared using the recrystallisation by slow evaporation technique. The preferred method was to dissolve a host in a liquid guest and allow the guest to evaporate slowly at ambient temperature ($\pm$25 °C) until crystals formed. This worked best if the guests were liquids with high vapour pressures, e.g., acetone is a liquid at room temperature and standard pressure (m.p. -95 °C) and boils at 56 °C.

However, in some cases, the host was sparingly soluble in the guest, and some guests were solids near room temperature or had high normal boiling points. For example, it was not possible to dissolve **H3** in 2-methylnapthalene (m.p. 33–35 °C, b.p. 240 °C). In such cases, a mutual solvent with high vapour pressure was first used to dissolve the host (e.g., methanol, chloroform), and to this solution the guest was added. As before, solutions were allowed to evaporate slowly and crystallise at room temperature.

In some experiments, the effect of crystallisation temperature on the structure of the resulting inclusion compounds was studied. In these cases, vials containing a solution of host and guest were sealed and allowed to crystallise at the specified temperatures.

2.2.2 Vapour Sorption and Guest Exchange.

In some experiments, powdered or single crystals of host or host-guest compounds were exposed to the vapour of volatile guest molecules using either a "two vial experiment" or a custom-built sample holder (Figure 2.1). In this way, it was possible to produce inclusion compounds from apohost, and sometimes transform one inclusion compound to another by exposure to the guest vapours.

Guest exchange experiments were performed using a "two-vial" method. Crystals of inclusion compounds or apohost were removed from mother liquor, patted dry, and (unless specified) crushed into a powder. This starting material was set in a short vial, while into a second vial was added the guest to be exchanged. Both vials were placed inside a sealed jar and left at room temperature.

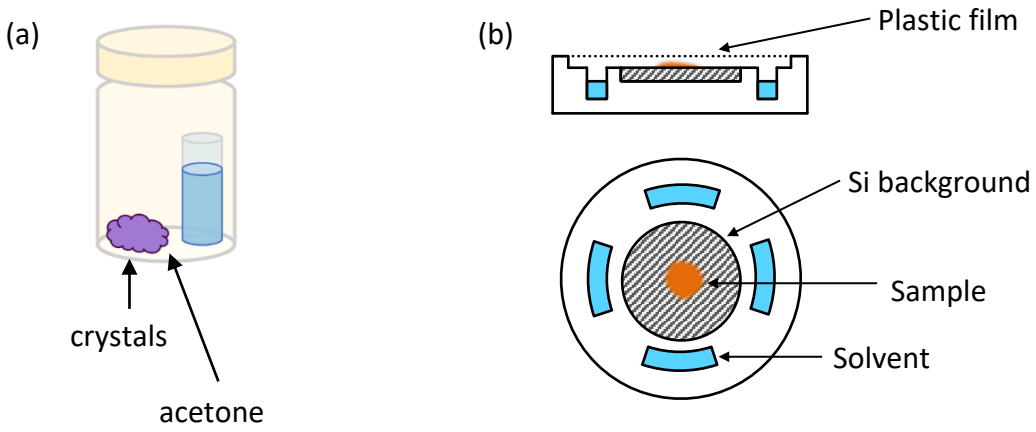

Figure 2.1. Methods of inclusion compound crystallisation by vapor absorption. a) "two vial" experimental set up, and (b) side on and top views of the powder X-ray sample holder.

2.3 THERMAL DECOMPOSITION

2.3.1 Thermogravimetric (TG) Analysis.

In thermogravimetric (TG) analysis, a sample's weight is measured as it is heated in an enclosed chamber while purged with a steady flow of inert N_2 gas. If a sample is an inclusion compound, then as the temperature increases the normal boiling point of the included guest, the guest will vaporise and be carried off the balance by the N_2 stream, causing the sample mass to decrease. Using this technique, it was possible to determine whether the materials under study contained any guest molecules, as no mass loss in the region of the guest's normal boiling point is indicative of an unsuccessful inclusion experiment. But if a mass loss was recorded, then the percentage mass loss value was used to confirm the ratio of host to guest molecules in the inclusion compound.

It is thought that if the energy required to remove guest A from the inclusion compound, H•A, is larger than the energy required to remove guest B from H•B, then H•A is the more stable inclusion compound and will be preferentially formed over H•B. The model-free method based on the Ozawa, Flynn and Wall method[2.2, 2.3] was used to determine the activation energy (E_a) of the guest desolvation reaction. This method requires that samples of the inclusion compound be heated at various rates (β). The temperature (T) that is reached by each sample, heated at different rates, is measured at regular intervals as the guest desolvation reaction progresses. Plotted are the heating rates vs temperature recorded for each chosen extent of reaction, more specifically, $\ln(\beta/\beta_0)$ is plotted against 1/T. These points join into straight lines, the slope of which can be multiplied by negative the universal gas constant (R) to give the activation energy (E_a) of guest desolvation:

$$\ln(\beta/\beta_0) = -\frac{E_a}{RT} + \ln A$$

Note, β_0 is the standard state (in this case 1 °C min^{-1}), used to remove units from the logarithmic calculation. The Kinetics Committee of the International Confederation for Thermal Analysis and Calorimetry[2.4] recommends that this process should be repeated for extents of reaction ranging from 5% to 95%. Suppose the resultant straight lines have different slopes and so give different activation energies. This indicates that the mechanism of desolvation has more than one step, and changes as the guest desolvation progresses.

TG samples were prepared by removing crystals from the mother liquor, blotting lightly on filter paper to remove excess solvent, and then lightly crushed to form a powder. The sample mass varied from between 4–10 mg. Sample material was evenly spread at the bottom of an open aluminium oxide pan to ensure consistent and reproducible results. A TA-Q500 thermogravimetric analyser was used with Universal Analysis 2000 software (v4.5A, TA Instrument-Waters LLC) and operating a dry nitrogen purge gas flow rate of 40 ml min^{-1}. To determine the activation energy of guest desolvation, the samples were heated at rates of 2, 4, 8, 16 and 32 °C min^{-1}, while 20 or 30 °C min^{-1} was used for most other TG experiments. Samples were heated from room temperature to ±40 °C after the temperature of desolvation, or just ±10 °C before the host melt.

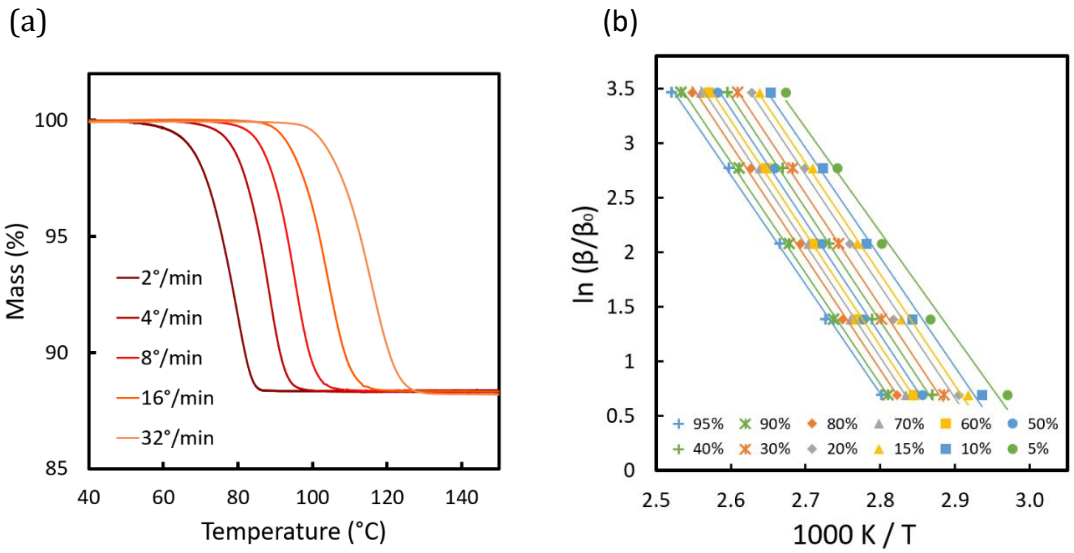

Figure 2.2. (a)TG traces collected at heating rates of 2, 4, 8, 16, and 32 °C/minute (b) Plots of ln (β/β_0) versus 1000 K / T at 5%, 10%, 15%, 20%, 30%, 40%, 50%, 60%, 70%, 80%, 90%, and 95% extent of the guest desorption reaction.

2.3.2 Differential Scanning Calorimetry.

In differential scanning calorimetry (DSC), the sample material is sealed in a lidded pan, and placed on a thermoelectric disk next to a second, empty reference pan. As the temperature is increased, heat is transferred to the sample and reference pan. However, the pan containing sample material can absorb and release additional heat energy, and when these events take place, a temperature difference between the sample and reference pans will result. Area thermocouples measure the temperature difference (ΔT), and the resultant heat flow (q) is determined by the thermal equivalent of Ohm's law: q = ΔT / R where R is the innate resistance of the thermoelectric disk. A heat flow vs temperature graph is plotted, showing

peaks and troughs caused by endothermic and exothermic events like melting, vaporisation, glass transitions, and recrystallisation. In particular, DSC can be used to determine enthalpy changes and onset and peak temperatures, associated with guest vaporisation. As with TG, guests that require higher temperatures to be vaporised from the crystal lattice are thought to form more stable host-guest compounds.

Crystals were removed from vials, blotted dry on filter paper, and gently crushed. Samples were weighed directly into an aluminium pan on an analytical balance, then sealed with a lid pierced with two small holes (so vapours can be vented). All samples had a mass of approximately 1–3 mg. The sample holder was continuously purged during the experiment with a dry nitrogen flow of 40 or 60 ml min^{-1}. All samples were heated at 20 or 30 °C min^{-1} from room temperature to a few degrees after the host melted. Experiments were performed using either a TA Instruments DSC-Q200 or Surface Solutions GmbH DSC XP-10 with data analysed using Universal Analysis 2000 software or a TA Instruments Discovery 25 instrument, with data analysed using the TRIOS Software programme from TA Instruments.

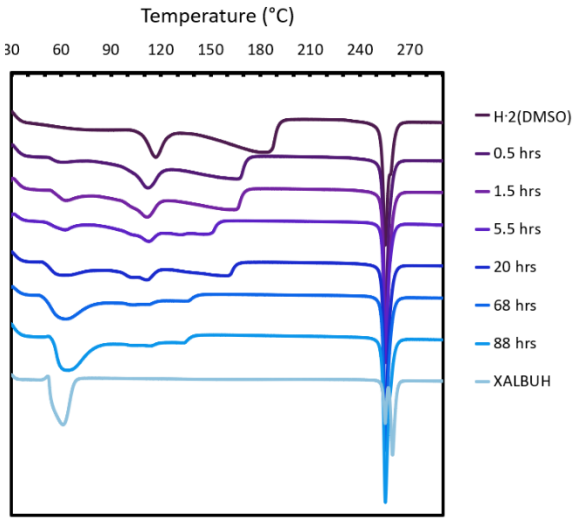

Figure 2.3. DSC traces collected at various amounts of time of **H4•2(DMSO)** exposure the vapor of acetone, showing the qualitative guest exchange process from DMSO to acetone, with a consistent melting point of the apohost.

2.4 SELECTIVITY

2.4.1 Competition Experiments.

In some cases, competition experiments were performed to determine the selectivity of a host towards a particular mixture of guests. The same experimental method was used when preparing inclusion compounds with only one guest: a known mass of host was dissolved into various binary mixtures of guests (Figure 2.4). In most cases, the solutions with mixed guests and co-solvent, were allowed to evaporate. The exception was in Chapter 5, when vials were sealed and crystallised at low temperatures. The resultant crystals were harvested, and analysed by either ^{1}H NMR spectroscopy or gas chromatography to determine the relative composition of guests.

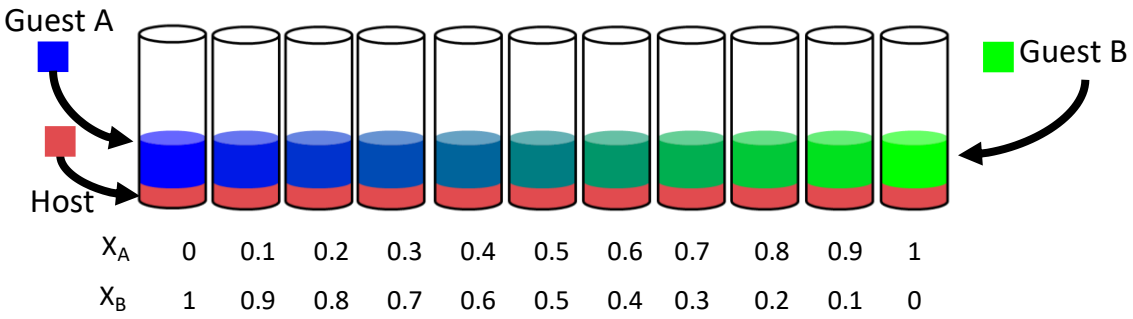

Figure 2.4. Example of setting up a competition experiment with varying amounts of guest A (blue) and guest B (green).

The resulting guest concentrations in the crystals are plotted as a function of the guest concentration in the starting solution. Three general types of selectivity curves generally arise. The host can show a mild selectivity preference for guest A (over guest B), a strong preference, or a concentration dependent preference, as seen in Figure 2.5, which is taken from Nassimbeni.[2.5]

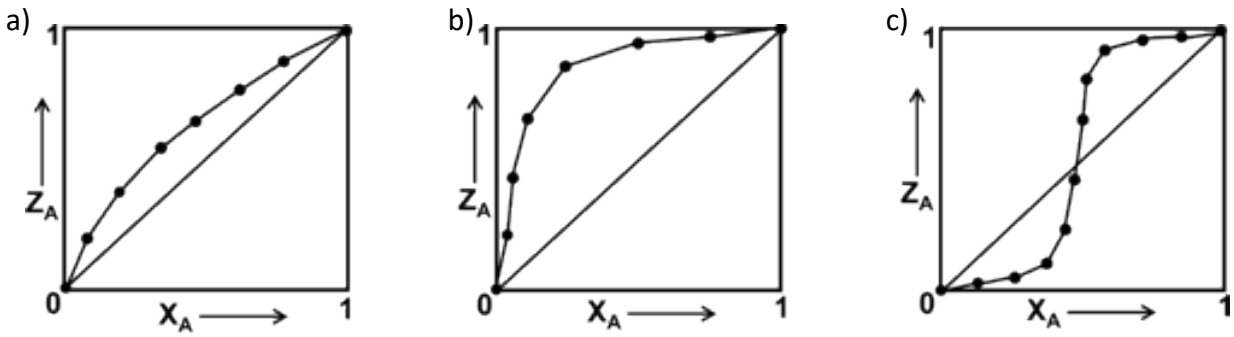

Figure 2.5. Three general types of selectivity curves generally arise. (a) mild selectivity for guest A (over guest B), (b) strong preference for guest A over B, (c) concentration dependent preference.

2.4.2 Proton Nuclear Magnetic Resonance (^{1}H NMR) spectroscopy.

Because the nuclei of hydrogen atoms are magnetically active (spin quantum number of ½), they behave like small magnets when molecules containing hydrogen atoms are placed in a strong magnetic field. A broad spectrum of radiofrequency waves is applied to the sample, causing the nuclei within the molecule to resonate at their own specific frequencies, each affected in different ways by the other hydrogen nuclei near them. All these resonant frequencies are measured, Fourier transformed to separate each wave component, and converted into an NMR spectrum. The spectrum displays peaks on a graph, where the peak area represents the number of hydrogen nuclei resonating at each specific frequency. The peaks can be attributed to each hydrogen atom in a molecule, owing to their size and shape.

^{1}H NMR spectroscopy was used to determine the stoichiometry of the host and guests in inclusion compounds, and particularly the ratio of different guests in crystals resulting from

competition experiments. Samples were dried on filter paper, and depending on the sample solubility, dissolved in 0.7 ml of deuterated chloroform ($CDCl_3$) or dimethyl sulfoxide (d_6-DMSO). The experiments were carried out using a Bruker Ultrashield 300 (300 MHz) or 400 plus (400 MHz) spectrometer. The data was analysed using the programme MestReNova.[2.6]

2.4.3 Gas chromatography.

Gas chromatography (GC) is used to separate compounds in a mixture by injecting a gaseous sample into the mobile phase, the carrier gas, which moves through a thin column, the stationary phase. Different compounds in the mixture will move at different paces, slowed down as they interact with the stationary phase. Columns can be fitted with different detectors. As the separated compounds exit the column, they are, e.g., combusted into ions by a hydrogen flame in a process known as flame ionisation detection (FID). In this detector, two electrodes create a potential difference, and the newly created cations are attracted to the anode. Upon reaching the anode, a current is induced, where the magnitude of the current is proportional to the concentration of eluted cation.

When it was not possible to determine the ratio of different guests in the crystals using ^{1}H NMR spectroscopy due to overlapping peaks, gas chromatography with a flame ionisation detector was used. This was done in both chapters 3 and 4. Crystals were removed from vials, blotted on filter paper, and left to dry to remove the surface solvent. Crystals were then added to a GC vial, heated, and then the vapour above the crystals is sampled by the GC needle.

The system used was an Agilent 6890 gas chromatograph/ 7697A Headspace sampler with a 50-m CB Wax 57 capillary column. The inlet temperature was kept constant at 250 °C and 220 °C, in chapters 3 and 4, respectively. Nitrogen was used as the carrier gas at a constant flow rate of 1.5 (chapter 4) or 2 ml/min (chapter 3).

In chapter 3, samples were subjected to an initial oven temperature of 50 °C for 2 min, which then increased to 180 °C at a rate of 8 °C/min, with no hold time. Samples were equilibrated for 15 min at 120 °C before being transferred to the detector (temperature kept constant at 250 °C), where the transfer line was set at 140 °C, and the loop temperature at 135 °C.

Similarly, in chapter 4, samples were subjected to an initial oven temperature of 70 °C for 2 min, which then increased by 8 °C each minute to 200 °C and held at 200 °C for 1 min. Samples were then equilibrated for 15 min at 110 °C, then transferred to the detector (temperature kept constant at 220 °C), where the transfer line was set at 120 °C, and the loop temperature at 115 °C. In both studies, the detector gas was hydrogen (30 ml/min), air (400 ml/min), and nitrogen (25 ml/min).

2.5 STRUCTURE

2.5.1 Ultraviolet-Visible Diffuse Absorbance Spectroscopy.

In chapter 6, solid-state Ultraviolet-visible (UV-VIS) absorption spectra were recorded using an Analytik Jena SPECORD 210 PLUS spectrophotometer utilising the integrating sphere attachment. All data were graphically analysed using the software package WinAspect PLUS 3.9.14.

2.5.2 Microscopy.

In chapter 6, photographs were taken with an Axiocam 105 colour camera attached to a Zeiss SteREO Discovery V8 microscope and processed using the ZEN 2 (blue edition) programme (Carl Zeiss Microscopy GmbH, 2011).

2.5.3 Single Crystal X-ray Diffraction.

Crystals are made of repeating arrangements of atoms in three dimensions, with covalently bonded atoms approximately 1–2 Å apart. When a crystal is placed in the path of a beam of electromagnetic waves having a similar wavelength (X-rays, ~1 Å) to the distance between the atoms, then most of the rays will be transmitted through the crystal, but some will be reflected. The waves can interfere with each other to cause a macroscopic pattern viewable using an appropriate detector.

Young first demonstrated the phenomenon of diffraction in 1801. He used the sun and needle holes pricked in paper, proving that for such patterns to form (as in Figure 2.5), light must act as a wave, and not as discrete particles as previously thought. This phenomenon can be easily observed using readily available pen lasers (Figure 2.5), which often come equipped with different tips containing diffraction gratings – sheets with slits that are roughly the same distance apart as the wavelength of visible light.

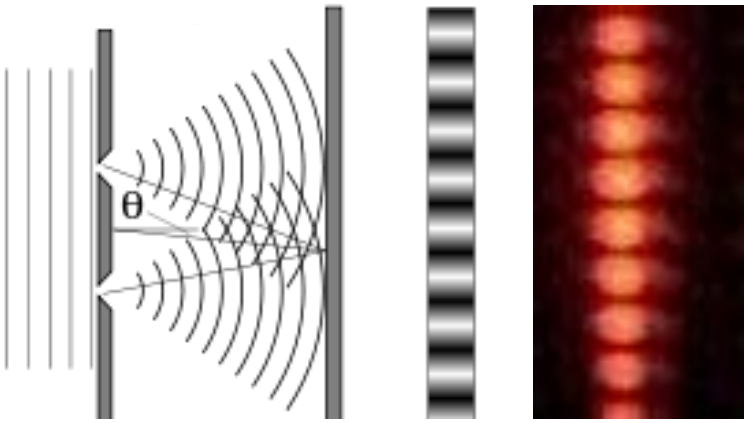

Figure 2.5. (a) Interference of waves passing through a double slit [2.7] (b) red laser light passed through a double-slit assembly (0.7 mm between slits).[2.8]

The duality of light was not known until Einstein discovered the photoelectric effect, showing that light can also behave as if it is composed of discrete particles, called photons.

When a crystal is placed in an X-ray beam, the intensity of the reflected rays is measured as a function of the incident ray angle (θ). Bragg's equation, nλ = 2d sinθ, (where n is an integer representing the reflection order and λ is the X-ray wavelength) is used to calculate the distance (d) between layers of atoms, from which crystal's unit cell parameters (see Figure 2.6) can be determined.

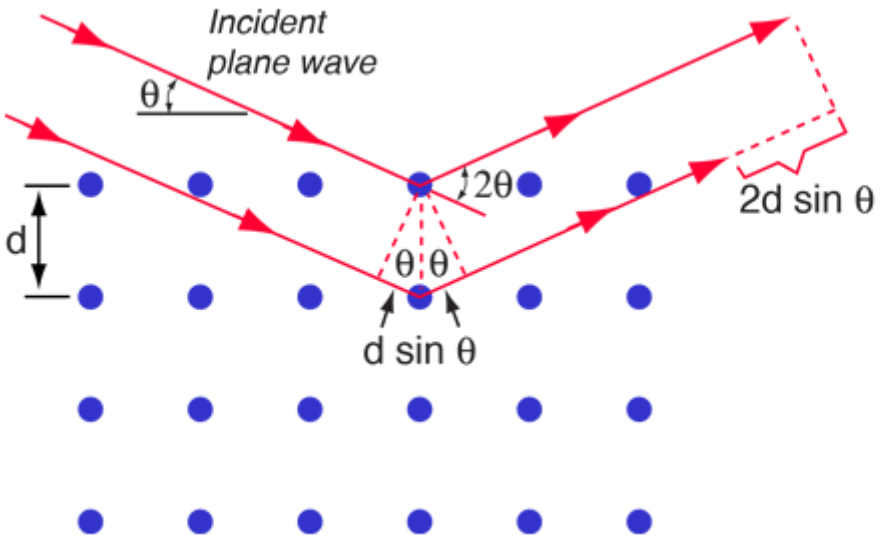

Figure 2.6 A representation of a single crystal[2.9] with layers separated by a distance d. When the path difference of reflected rays is equal to an integer multiple of the wavelength, then reflected X-rays constructively will constructively interfere, and appear as spots on the detector.

A single crystal was selected using a polarising microscope based on its size (between 0.1 to 0.35 mm in all dimensions) and quality (clear). The crystal was then coated in paratone oil and mounted onto a loop. The paratone oil helps to prevent decomposition and provides a rigid mount during low-temperature data collection.

Data for all crystals were collected on a Bruker KAPPA APEX[2.10] II DUO single crystal X-ray diffractometer with graphite monochromatic MoKα radiation (λ = 0.7107 Å). X-rays were generated by a Bruker K780 generator (50 kV, 30mA) at a temperature of -120 or -100 °C, achieved by a constant stream of nitrogen gas at a flow rate of 20 ml min^{-1}, produced by an Oxford cryostream 700.

The intensity data were collected using the phi scan and omega scan techniques, scaled and reduced with either DENZO-SMN[2.11, 2.12] or SAINT-Plus.[2.13] The correction of the collected intensities for absorption was done using the SADABS[2.14] programme. The space group was determined from the systematic reflection absences using the programme XPREP.[2.15] XPREP was also used to prepare the input data for the programmes SHELXS[2.16] and SHELXT[2.17] which implement direct methods to solve the structure, and SHELXL,[2.18] which uses the full-matrix least-squares method based on reflection $F^2$to refine the structure. These programmes were used in conjunction with the graphical interface, X-Seed.[2.19] Reflections at low angles and with observed intensities significantly lower than the calculated value were omitted due to potential truncation of these reflections by the beam-stop.

Hydrogen atoms were refined isotropically and assigned temperature factors that relate to the atom to which they are attached. Most hydrogen atoms were placed in idealised positions using a riding model. However, the O-H and N-H hydrogen atoms in host and guest compounds, were located in the final difference electron density map. Their bond lengths were fixed using the suggested formulae by Lusi and Barbour,[2.20] who studied the neutron data of D···A systems, where D and A are donor and acceptor atoms. They derived correlation formulae that yield sensible positions of the H atoms in such systems, based on the distances between the donor and acceptor atoms.

When all non-hydrogen atoms were refined satisfactorily with isotropic temperature factors, they were refined anisotropically. Some C−C and C−O bond lengths in disordered guest molecules were restrained. One structure was refined as a two-component twin using the HKLF 5 file and BASF instruction to specify the fractional volume contributions of the twin components.

Diagrams were generated using Mercury.[2.21, 2.22] To display and calculate the percentage volume of space occupied by guests within a crystal, all guest molecules were deleted, and Mercury's "contact surface" void space method was used with a default probe radius (1.2 Å), and approximate grid spacing of 0.7 Å. This clearly shows if guest molecules are located in channels, cavities or layers within the host framework.

Crystal Explorer was used to create Hirshfeld surface plots, which were used to investigate packing modes and the intermolecular interactions within a crystal structure.[2.23, 2.24]

PLATON[2.25] and WingGX[2.26] was used to calculate bond angles, torsion angles and bond lengths.

2.5.4 Powder X-ray Diffraction.

In powder X-ray diffraction (PXRD), a *powdered* sample is placed in the X-ray beam, and the intensity of the reflected rays is measured as a function of the angle of the incident rays. By measuring the intensity of the reflected rays at various incident θ angles, all possible diffraction directions of the lattice should theoretically be attained due to the random orientation of the powdered material. However, some samples still align in a preferred orientation, and this was mitigated by rotating the sample stage during each data collection.

Crystalline samples were lightly crushed into powders and mounted on a flat (zero-background) sample holder. PXRD data were recorded on a Bruker D2 phaser diffractometer using Cu Kα radiation (λ= 1.5418 Å) generated at 30 kV and 10 mA.

In situ PXRD experiments were carried out on a Bruker D8 powder X-ray diffractometer using Cu Kα radiation (λ= 1.5418 Å) generated at 30 kV and 40 mA. The sample holder is shown in Figure 2.1b. This allowed for changing powder patterns to be measured as compounds transformed upon exposure to guest vapours. In these kinetic experiments, powders were first sieved through a 106 μm filter to ensure all particles were the same size. Powder diffraction traces were recorded at 25 °C and repeated at intervals of 25 minutes.

For each compound, the single crystal X-ray data (unit cell parameters, space group symmetry, and atomic coordinates) were input into Mercury to produce idealised PXRD patterns using the same wavelength as that used experimentally in the single crystal structure determination. The experimentally obtained powder pattern, which results from many single crystals crushed together, is compared to the simulated PXRD pattern (simulated from one single crystal). If the patterns match, then it could be concluded that the single crystal chosen for structure collection is representative of all the crystals that formed. PXRD was also used to determine whether the desired compound had been obtained in subsequent crystallisation or vapour-sorption experiments.

2.6 REFERENCES

2.1 C. R. Groom, I. J. Bruno, M. P. Lightfoot and S. C. Ward, The Cambridge Structural Database, *Acta Cryst. B*, 2016, **72**, 171–179.

2.2 T. Ozawa, A New Method of Analyzing Thermogravimetric Data, *BCSJ*, 1965, **38**, 1881–1886.

2.3 J. H. Flynn and L. A. Wall, A quick, direct method for the determination of activation energy from thermogravimetric data, *J. Polym. Sci., Part B: Polym. Lett.*, 1966, **4**, 323–328.

2.4 S. Vyazovkin, A. K. Burnham, L. Favergeon, N. Koga, E. Moukhina, L. A. Pérez-Maqueda and N. Sbirrazzuoli, ICTAC Kinetics Committee recommendations for analysis of multi-step kinetics, *Thermochim. Acta*, 2020, **689**, 178597.

2.5 L. R. Nassimbeni, Physicochemical Aspects of Host−Guest Compounds, *Acc. Chem. Res.*, 2003, **36**, 631–637.

2.6 M. R. Willcott, MestRe Nova, *J. Am. Chem. Soc.*, 2009, **131**, 13180–13180.

2.7 E. svg: en:User:Lacatosias Epzcaw User:Stanneredderivative work:, *Diagram for the double-slit experiment*, 2011.

2.8 Jordgette, *English: Double-slit experiment: Difference between double-slit pattern and single-slit pattern, with interference.*, 2010.

2.9 Bragg's Law, http://hyperphysics.phy-astr.gsu.edu/hbase/quantum/bragg.html, (accessed 22 January 2022).

2.10 Bruker, APEX2, *Version* 1.0-27, Bruker, AXS Inc., 2005, Madison, Wisconsin, USA.

2.11 Z. Otwinowski, W. Minor, D. Borek and M. Cymborowski, DENZO and SCALEPACK, in *International Tables for Crystallography*, John Wiley & Sons, Ltd, 2012, pp. 282–295.

2.12 Z. Otwinowski and W. Minor, in *Methods in Enzymology*, Academic Press, 1997, vol. 276, pp. 307–326.

2.13 *SAINT-plus (including XPREP), Version 7.12*, Bruker AXS Inc., 2004, Madison, Wisconsin, USA.

2.14 G. M. Sheldrick, Program for Empirical Absorption Correction of Area Detector Data, *SADABS*, 1996.

2.15 Bruker, *XPREP, Version 6.14,* Bruker AXS inc., 2005, Madison, Wisconsin, USA.

2.16 G. M. Sheldrick, A short history of SHELX, *Acta Cryst. A*, 2008, **64**, 112–122.

2.17 G. M. Sheldrick, SHELXT – Integrated space-group and crystal-structure determination, *Acta Cryst. A*, 2015, **71**, 3–8.

2.18 G. M. Sheldrick, Crystal structure refinement with SHELXL, *Acta Cryst. C*, 2015, **71**, 3–8.

2.19 L. J. Barbour, X-Seed — A Software Tool for Supramolecular Crystallography, *Supramol Chem*., 2001, **1**, 189–191.
2.20 M. Lusi and L. J. Barbour, Determining Hydrogen Atom Positions for Hydrogen Bonded Interactions: A Distance-Dependent Neutron-Normalised Method, *Cryst. Growth Des.*, 2011, **11**, 5515–5521.
2.21 I. J. Bruno, J. C. Cole, P. R. Edgington, M. Kessler, C. F. Macrae, P. McCabe, J. Pearson and R. Taylor, New software for searching the Cambridge Structural Database and visualising crystal structures, *Acta Cryst. B*, 2002, **58**, 389–397.
2.22 C. F. Macrae, I. Sovago, S. J. Cottrell, P. T. A. Galek, P. McCabe, E. Pidcock, M. Platings, G. P. Shields, J. S. Stevens, M. Towler and P. A. Wood, Mercury 4.0: from visualisation to analysis, design and prediction, *J. Appl. Cryst.*, 2020, **53**, 226–235.
2.23 M. A. Spackman and J. J. McKinnon, Fingerprinting intermolecular interactions in molecular crystals, *CrystEngComm*, 2002, **4**, 378–392.
2.24 J. J. McKinnon, M. A. Spackman and A. S. Mitchell, Novel tools for visualising and exploring intermolecular interactions in molecular crystals, *Acta Cryst. B*, 2004, **60**, 627–668.
2.25 A. L. Spek, Single-crystal structure validation with the program PLATON, *J. Appl. Cryst.*, 2003, **36**, 7–13.
2.26 L. J. Farrugia, WinGX suite for small-molecule single-crystal crystallography, *J. Appl. Cryst.*, 1999, **32**, 837–838.

CHAPTER 3

Selective Enclathration of Methyl- and Dimethylpiperidines by Fluorenol Hosts

By Nicole M. Sykes, Hong Su, Edwin Weber, Susan A. Bourne, and Luigi R. Nassimbeni
In *Cryst. Growth Des.*, 2017, **17**, 819–826 (Published 15 December 2016)

2016 – year 1 – an MSc student

(a) 22 March, one of the first photographs I snapped with Prof. Nassimbeni's newly purchased microscope – the polarizer and analyser (Nicol prisms) are at 90° to each other, which produces the black background and shows the imperfections in the large crystal placed between them. (b) 26 April, I started feeling unwell, so we both donned surgical masks, a sight that used to be uncommon. (c) 5 April, an unfortunate beetle became an accidental crystal growth medium. (d) 14 June, crystal and image by Ruth Amoore, grown during her vac work in our lab. (e) 8 July, Ruth baked and decorated a cake to look like a host-guest lattice. (f) 28 August – 1 September my first poster presentation was at the European Crystallographic Meeting 30, held in Basel Switzerland. (g) My ID badge at the Messeplatz congress centre. (h) I thoroughly enjoyed my time in Switzerland – especially floating down the Rhine with my '*Wickelfisch*'- the official Basel dry-bag.

3.1 SYNOPSIS

This paper investigates the selectivity by two similar hosts, **H1** and **H2**, which consist of fluorenol groups separated by different spacers. Previous studies have shown that both **H1** and **H2** form complexes with the picoline isomers; and **H2** also forms complexes with lutidines. In all cases these host-guest complexes were stabilised by hydrogen bonds between host hydroxyl moieties and guest nitrogen atoms.

In this study, the three methylpiperidine (MP) isomers and two dimethylpiperidine (DMP) isomers were selected as guests to recrystallise with **H1** and **H2**. These guest molecules are structurally similar to the previously used picolines and lutidines, and have normal boiling points within 25 degrees of one another, which presents a separation challenge.

Eight new host-guest compounds were successfully grown, and their structures characterised by single X-ray diffraction and thermal analysis. Five of the compounds are of **H1** with each of the guests under study, and the remaining three are of **H2** with **2MP**, **2,6DMP**, and **3,5DMP** + H_2O. Attempts to crystallise **H2** with **3MP** and **4MP** resulted in gels, which generally form when two (or more) components interact and cross-link in such a way as to entrap a large volume of liquid [3.1 - 3.3] and does not flow – much like a properly set jelly. While interesting to ponder the subtle interactions at play that result in either crystals or gels, this was not further pursued.

Certain competition experiments were performed where **H1** or **H2** was mixed with an equal amount of two guests and the solution allowed to crystallise. The proportion of each guest in the resulting crystals was determined by GC-FID, however neither the GC nor the NMR could distinguish between **3MP** and **4MP,** and so these were excluded from the competition experiments.

Our results showed that at equimolar concentrations of each guest,

> **H1** is specific (100% selectivity) to **2MP** over **4MP**, which we note is in contrast with the literature result for 2- and 4-picoline, against which **H1** did not discriminate,
> **H1** prefers **2MP** over **3MP**, in the ratio 90 : 10,
> **H1** is specific to **3,5DMP** over **2,6DMP**,
> This was surprising to us as the compounds with **2MP** and **2,6DMP** have similar unit cells and packing, as do the compounds with **3MP** and **3,5DMP**. We expected then to observe the analogous selectivity result for **2,6DMP** vs. **3,5DMP** as for **2MP** vs. **3MP**, but this was not the case, and
> **H2** is specific to **2,6DMP** over **3,5DMP**. This was interesting, as it is directly opposite to the selectivity preference of **H1**.

In order to rationalise the competition results, lattice energies and the Hirshfeld surfaces of the guests of relevant inclusion compounds were calculated, but these unfortunately provided no further insights. Although, close study of the DSC curves in 2021 showed that the peak temperature of the guest endotherm (normalised by subtracting the guest boiling point)

corresponds to the selectivity preferences of **H1** and **H2**, where the larger $T_{peak} - T_{boil}$ value indicates the host preference:

For the **H1** structure with **2MP**, $T_{peak} - T_{boil} \approx +34°$ while with **4MP**, $T_{peak} - T_{boil} \approx +4°$ and +27° (**2MP** preferred by **H1**).

For the **H1** structure with **3MP**, $T_{peak} - T_{boil} \approx +27°$, while with **2MP** ≈ +34° (**2MP** preferred by **H1**).

For the **H2** structure with **3,5DMP** and H_2O, $T_{peak} - T_{boil} \approx -18°$, while with **2,6DMP**, $T_{peak} - T_{boil} \approx +24°$ (**2,6DMP** preferred by **H2**)

However, for the **H1** structure with **3,5DMP** and **2,6DMP** it is the **H1•2(2,6-DMP)** $T_{peak} - T_{boil}$ that is the larger, but only by 1 °C. Hence, this selectivity result, and the preference of **H1** for **3,5DMP** over **2,6DMP** could not be confirmed using this technique.

DSC results

Code	Compound	Normal boiling point (°C)	Guest release T_{peak} (°C)	Guest release $T_{peak} - T_{boil}$ (°C)
3.1	**H1•2(2MP)**	118.5	152.1	33.5
3.2	**H1•2(3MP)**	125.5	152.6	27.1
3.3	**H1•2(4MP)**	124	128.1 & 151.4	4.1 and 27.4
3.4	**H1•2(2,6DMP)**	127.5	143.0	15.5
3.5	**H1•2(3,5DMP)**	144	158.4	14.4
3.6	**H2•2(2MP)**	118.5	108.5 & 132	-10 & 13.5
3.7	**H2•2(2,6DMP)**	127.5	151.8	24.3
3.8	**H2•2(3,5DMP)•H_2O**	144	129.2	-17.8

3.2 INTRODUCTION

The separation of a given compound from a mixture is difficult when the various components have similar boiling points and molecular structures. In such circumstances the process of enclathration by a suitable host compound may be a practical option. Miyata[3.4] has reviewed the selectivity of cholic acid when exposed to mixtures of various aromatic guests and has studied the mechanism of this process. Barton[3.5] has recently discussed the separation of the three xylene isomers and ethylbenzene by employing the host TETROL and Ward[3.6] has employed guanidinium o-terphenyl-4-4'-disulfonate to separate the isomers of dimethylcyclohexane. Most of the separations by host-guest methods are carried out as batch experiments, but there are increasing contributions of continuous separation methods. Binev[3.7] has described a fluidised bed crystalliser for the crystallisation of ternary systems.

A particularly arduous aspect of this process is the case of the separation of enantiomers from a racemic modification, because they have identical physical properties such as melting points, boiling points, density, and refractive index. Their only difference is their ability to rotate plane polarized light in opposite directions.

The procedure of separation via host-guest chemistry or employing a resolving agent to separate enantiomers, is dependent on the phenomenon of molecular recognition and may be summarised as follows:
When a Host compound, H is exposed to a mixture of two guests G_1 and G_2

$$H_{(s,\alpha)} + n_1G_{1(\ell)} + n_2G_{2(\ell)} \rightarrow H \cdot m_1G_1 \cdot m_2G_{2\,(s,\beta)}$$

The solid host H, in its non-porous α-phase, the apohost, is dissolved in a known mixture of guests G_1 and G_2 and allowed to crystallise, yielding the inclusion compound. This, the β-phase, has the host: guests ratio 1: m_1m_2.
The values of $m_1$and m_2 can be established by various analytical techniques such as thermal gravimetry (TG), gas chromatography (GC) and NMR spectroscopy. It is noteworthy that m_1 and m_2 do not have to be integers or simple fractions as inclusion compounds are sometimes non-stoichiometric. However, it is important to establish accurate values of m_1 and m_2 in order to apply sensible site occupancy factors to the various molecular components of the crystal structure analysis.

Suppose the Host H has a greater affinity for G_1 than G_2. Then for a perfect separation the inclusion compound formed would simply be $H \cdot m_1G_1$ and $m_2$would be zero.

This seldom occurs in practice, and the extent of the selectivity can be calculated via the selectivity constant. [3.8]

$$K_{G_1:\,G_2} = {}^{Z_{G1}X_{G2}}/_{Z_{G2}X_{G1}} \quad \text{where} \quad X_{G1} + X_{G2} = 1$$

where X_{G1} and X_{G2} are the mole fractions of the guests G_1 and G_2 in the mother liquor and Z_{G1} and Z_{G2} are their mole fractions in the resulting crystallisation product. A selectivity constant ≥ 10 is regarded as a successful result for practical purposes.
The topic of selectivity in host-guest chemistry has been well documented[3.9 - 3.10] and goes back to Emil Fischer's lock-and-key hypothesis.[3.11]

In this work we employ two hosts with subtly differing structures in order to explore their selectivity towards selected isomers of methyl- and dimethylpiperidines. The structural formulae of the hosts together with those of the guests are shown in Scheme 3.1.

H1 and **H2** are both typical dumbbell shaped hosts which contain fluorenyl groups separated by a spacer. The hydroxyl moieties act as hydrogen bond donors to the piperidine guests. These bulky diol compounds have been proven to be a useful class of hosts in the synthesis of coordinatoclathrates.
H1 and **H2** form inclusion compounds with a variety of guests which include amines, aliphatic alcohols, ketones and aromatic hydrocarbons.[3.12] Several crystal structures of these compounds are listed in the Cambridge Structure Database, and their reference codes are given in the supplementary data.

Of particular interest is the result of the competition experiments between the guests ethanol and acetonitrile with **H1**, in which the selectivity profile was practically invariant over the

whole range of EtOH/ CH_3CN compositions, [3.13] and the details of the structural analyses of these mixed guest compounds is given.[3.14] An important result with **H2** was obtained by analysing its selectivity profile with the two guests, aniline and benzylamine, and noting how the results could be manipulated by changing the pH of the mother liquor.[3.15]

Scheme 3.1 Host and Guest Compounds

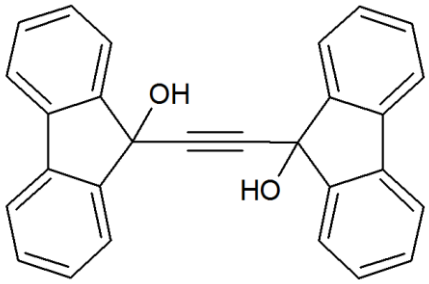

H1

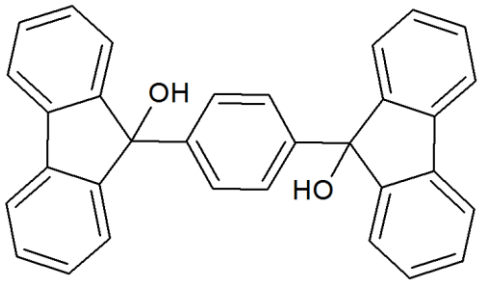

H2

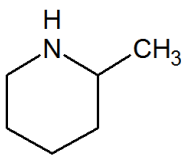

2MP

118-119 °C

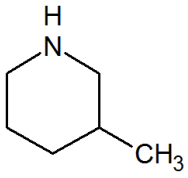

3MP

125-126 °C

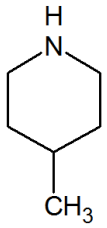

4MP

124 °C

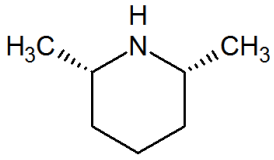

2,6DMP

127-128 °C

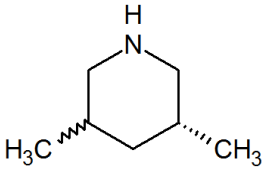

3,5DMP

144 °C

H1 = 9,9'-(ethyne-1,2-diyl)-bis(fluoren-9-ol)
H2 = 9,9'-(1,4-phenylene)-bis(fluoren-9-ol)
2MP = 2-methylpiperidine
3MP = 3-methylpiperidine
4MP = 4-methylpiperidine
2,6DMP = (*cis*)-2,6-dimethylpiperidine
3,5DMP = (*cis/trans*)-3,5-dimethylpiperidne

3.3 EXPERIMENTAL

3.3.1 Materials.

The host compounds, **H1** and **H2**, were synthesized by Weber[3.12] and were used without further purification. The piperidine guests were all purchased from Sigma Aldrich and used as received. Single crystals of the inclusion compounds were obtained by dissolving these two host compounds in a minimum volume of chloroform and adding an excess of the relevant guest or guest mixture. The resulting solutions were filtered and allowed to crystallise by slow evaporation.

3.3.2 X-ray Crystallography.

Single crystal X-ray diffraction data were collected on a Bruker DUO APEX[3.16] diffractometer for all structures using Mo Kα (λ = 0.71073 Å) at a temperature of 153 K. The intensity data were collected using the phi scan and omega scan techniques, scaled and reduced with DENZO-SMN[3.17, 3.18] or SAINT-Plus.[3.19] The correction of the collected intensities for absorption was done using the SADABS program. [3.20]

The structures were solved by direct methods using SHELXS-97[3.21] and refined using full-matrix least squares methods in SHELXL. The graphical interface used was the program X-SEED. [3.22] All non-hydrogen atoms were refined isotropically or anisotropically depending on the occurrence of disorder in the structures. All C-H hydrogen atoms were placed geometrically and with a riding model for their isotropic temperature factors. The O-H and N-H hydrogen atoms in the host and guest compounds, respectively, were located in the final difference electron density map. Their bond lengths were fixed using the suggested formulae by Lusi and Barbour[3.23] who studied the neutron data of the D-H···A systems, where D and A are donor and acceptor atoms. They derived correlation formulae which yield sensible positions of the H atoms in such systems, based on the distances between the donor and acceptor atoms. Diagrams were generated using POVRAY in X-SEED[3.22] and Mercury (3.5). [3.24]

3.3.3 Thermal Analysis.

Thermogravimetric analysis (TGA) was performed using a TA-Q500 Thermogravimetric Analyser and Differential Scanning Calorimetry (DSC) was performed using a TA Instruments DSC-Q200. Results were analysed using Universal Analysis 2000 software. The samples were crushed and blotted dry (4–10 mg for TGA and 1-3mg for DSC) and weighed directly into open aluminium oxide TGA crucibles or crimped, vented Tzero™ aluminium DSC pans. The experiments were performed over a temperature range of 20–350 °C at a heating rate of 20 °C min^{-1} under dry nitrogen with a flow rate of 40 ml min^{-1} in the TGA and 60 ml min^{-1} in the DSC.

3.3.4 Gas Chromatography Headspace.

The system used was an Agilent 6890 gas chromatograph/ 7697A Headspace sampler with a 50-m CB Wax 57 capillary column. Nitrogen was used as the carrier gas at a constant flow rate of 2 ml/min. The oven conditions included an initial temperature of 70 °C and an initial time of 2 min, 8 °C/min to 200 °C held for 1 min. The inlet temperature was kept constant at 250 °C, and the FID detector was set at 250 °C with flow rates of hydrogen at 30 ml/min, air at 400 ml/min and nitrogen at 25 ml/min. Samples were equilibrated for 15 min at 120 °C with a loop temperature of 135 °C and the transfer line set at 140 °C.

3.4 RESULTS AND DISCUSSION

3.4.1 Structures with H1.

Structure **3.1**, **H1•2(2MP)**, crystallises in the space group $P\bar{1}$ with Z = 1. The host is located on a centre of inversion at Wykoff position *f*. The host conformation can be defined in terms of

the O-C-C-O torsion angle (Figure 3.1a) and the crystal structure and refinement parameters for the five structures with **H1** are shown in Table 3.1.

The **2MP** guest, which lies in a general position, is disordered over two positions with site occupancies of 0.51/0.49. The structure is stabilized by (Guest)-N-H···O(Host) and (Host)-O-H ··· N(Guest) hydrogen bonds which may be described as $R_4^4(8)$ in Etter's graph set notation.[3.25] This is shown in Figure 3.1b. Hydrogen bonding data of all compounds are given in Table 3.2.

The packing is characterized by pairs of guests which are located in restricted channels running down [1 0 1] as shown in Figure 3.2. The metrics of the hydrogen bonding for this and all the remaining structures is given in Table 3.2.

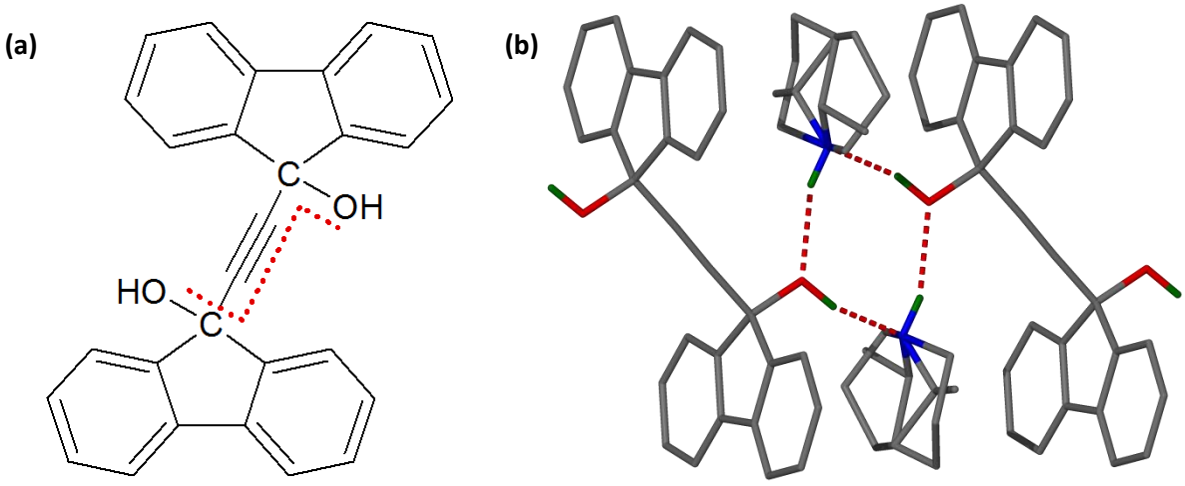

Figure 3.1. (a) O-C-C-O host torsion angle and (b) structure **3.1** showing two host **H1** molecules and two disordered **2MP** guests, linked by $R_4^4(8)$ H-bonding.

Structure **3.2**, **H1•2(3MP)**, crystallises in $P\bar{1}$ with Z = 2, with all host and guest atoms in general positions. The hydrogen bonding displays the same pattern as the previous structure with an $R_4^4(8)$ motif, as is the packing.

Structure **3.3** is similar to structure **3.2** in that there are two hosts and four guests in the unit cell, in the space group $P\bar{1}$. The two crystallographically independent **3MP** guests are *cis/trans* disordered and refined with site occupancies of 66/34 and 78/22% with *cis* being the major isomer in both cases. The hydrogen bonding follows the same pattern as the previous two structures and the packing, viewed close to the [1 -1 0] direction is shown in Figure 3.3.

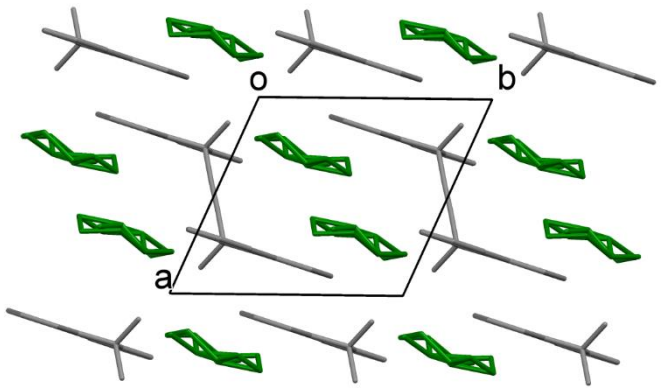

Figure 3.2. The packing of structure **3.1** showing guests in restricted channels viewed down the c axis.

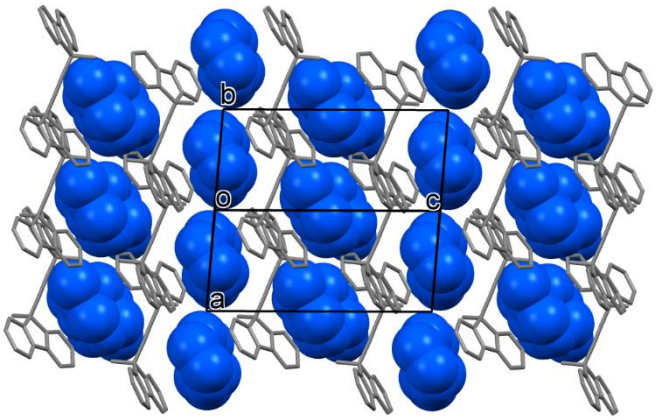

Figure 3.3 The packing of structure **3.3** viewed close to the [1 -1 0] direction showing guests in restricted channels.

Table 3.1. Crystallographic data parameters of the Host-Guest complexes of **H1** studied.

Compound	**3.1**	**3.2**	**3.3**	**3.4**	**3.5**
Code	**H1•2(2MP)**	**H1•2(3MP)**	**H1•2(4MP)**	**H1•2(2,6DMP)**	**H1•2(3,5DMP)**
Structural formula	C_{40} H_{44} N_2 O_2	C_{40} H_{44} N_2 O_2	C_{40} H_{44} N_2 O_2	C_{42} H_{48} N_2 O_2	C_{42} H_{48} N_2 O_2
Host: Guest ratio	1:2	1:2	1:2	1:2	1:2
Molecular mass (g·mol^{-1})	584.77	584.77	584.77	612.82	612.82
Data collection temp. (K)	153	153	153	153	153
Crystal system	Triclinic	Triclinic	Triclinic	Triclinic	Triclinic
Space group	$P\bar{1}$	$P\bar{1}$	$P\bar{1}$	$P\bar{1}$	$P\bar{1}$
a (Å)	8.2258(16)	10.025(2)	9.3643(19)	8.2556(17)	10.255(2)
b (Å)	9.3271(19)	12.285(3)	12.666(3)	9.4398(19)	12.742(3)
c (Å)	12.578(3)	14.447(3)	14.257(3)	12.922(3)	14.450(3)
α(°)	107.82(3)	82.73(3)	92.47(3)	108.57(3)	80.62(3)
β(°)	92.77(3)	88.42(3)	90.14(3)	95.34(3)	87.06(3)
γ(°)	111.70(3)	71.77(3)	100.34(3)	108.73(3)	70.86(3)
Volume(Å^3)	839.3(3)	1676.2(6)	1661.9(6)	882.4(3)	1760.0(6)
Z	1	2	2	1	2
Dc, calc density (g·cm^{-1})	1.157	1.159	1.169	1.153	1.156
θ range	1.73-27.90	1.42-27.92	1.43-27.94	1.70-28.45	1.43-27.64
Reflections collected	11091	19570	18922	4438	15307
No data I>2 sigma (I)	2761	4913	5652	3536	5319
Final R indices [I>2 sigma (I)]	0.0543	0.0536	0.0501	0.0448	0.0654
R indices (all data)	0.0819	0.0962	0.0753	0.0617	0.1015
Goodness-of-fit on F^2	1.042	1.027	1.034	1.025	1.042
Host torsion angle (°)	180	149.8	144.9	180	146.0
CCDC no.	1517588	1517590	1517591	1517587	1517589
CSD refcode	CANGAC	CANGIK	CANGOQ	CANFUV	CANGEG

Structure **3.4**, **H1•2(2,6DMP)**, crystallises in $P\bar{1}$ with Z = 1. The host is located at a centre of symmetry at Wykoff position *g*, and the structure is similar to structure **3.1**, with comparable unit cell parameters and packing.

Structure **3.5**, **H1•2(3,5DMP)**, is similar to structure **3.3** with Z = 2 in $P\bar{1}$ and a similar packing and hydrogen bonding pattern. The starting 3,5-dimethylpiperidine guest is a mixture of (71/29% *cis/trans*) as determined by ^{1}H NMR. The crystal structure shows the two crystallographically independent **3,5-DMP** guests to be *cis/trans* disordered. The refinement yielded 77/23 and 73/27%, with the major component being the *cis* isomer: similar to the starting mixture.

Table 3.2. Hydrogen bonding studied.

Compound	Donor (D)	Acceptor (A)	D···A/Å	D-H/Å	H···A/Å	D-H···A/°
3.1	O13	N1	2.714(2)	0.997(5)	1.745(8)	162(2)
	N1	O13[a]	2.930(2)	0.994(5)	1.995(9)	156(2)
3.2	O13	N1	2.676(3)	1.095(5)	1.588(7)	171(1)
	O13	N12	2.552(1)	1.095(5)	1.605(16)	141(2)
	O16	N6	2.735(3)	1.002(5)	1.737(7)	173(2)
	O16	N7	2.669(7)	1.002(5)	1.751(14)	150(2)
	N1	O13[b]	2.893(3)	0.997(5)	1.975(12)	152(2)
	N12	O13[b]	2.976(9)	1.001(5)	2.09(6)	147(9)
	N6	O16[c]	2.925(3)	0.996(5)	1.963(10)	162(2)
	N7	O16[c]	3.057(7)	0.999(5)	2.273(4)	135(4)
3.3	O13	N1'[d]	2.640(2)	1.000(5)	1.657(7)	166(2)
	O16	N1	2.659(2)	1.000(5)	1.697(8)	160(2)
	N1	O16[e]	3.039(2)	0.976(5)	2.092(8)	163(2)
	N1'	O13	3.016(2)	0.977(5)	2.076(7)	161(1)
3.4	O13	N1	2.718(2)	1.000(1)	1.765(7)	158(1)
	N1[f]	O13	3.005(2)	1.000(1)	2.030(5)	164(2)
3.5	N1	O16	2.993(2)	0.979(5)	2.056(11)	160(2)
	N1’	O13	2.908(2)	0.979(2)	2.000(12)	153(2)
	O16	N1[c]	2.655(2)	1.096(5)	1.584(9)	164(2)
	O13	N1’[b]	2.606(3)	1.096(5)	1.538(10)	163(2)
3.6	O13	N1	2.678(19)	0.986(5)	1.697(19)	173(2)
	O13	N2	2.766(12)	0.986(5)	1.786(13)	172(1)
	N1	O13[g]	3.091(8)	0.993(5)	2.163(8)	155(2)
	N2	O13[g]	3.121(5)	0.997(5)	2.163(8)	161(1)
3.7	O13	N1	2.773(2)	0.997(5)	1.780(6)	173(2)
	N1	O13[h]	3.234(2)	0.992(5)	2.278(7)	161(1)
3.8	O13	N6	2.691(2)	0.998(5)	1.698(6)	173(2)
	N6	O13[i]	3.032(2)	0.996(5)	2.105(12)	155(2)
	O1	O13	2.955(4)	1.011(5)	2.037(4)	150(1)

[a] -*x*, 2-*y*, 1-*z* [b] -*x*, 1-*y*, 1-*z* [c] 1-*x*, 1-*y*, -*z* [d] 1-*x*, -*y*, 1-*z* [e] -*x*, -*y*, -*z*

[f] -1-*x*, -*y*, -*z* [g] 1-*x*, 2-*y*, 2-*z* [h] -1-*x*, -1-*y*, -*z* [i] -*x*, *y*, -*z*- $\frac{1}{2}$

3.4.2 Structures with H2.

We obtained single crystals of **H2** with **2MP**, **2,6DMP**, and **3,5DMP**. We failed to obtain suitable crystals with **3MP** and **4MP** despite repeated attempts at crystallising the solutions of this host in the pure methylpiperidines by slow evaporation. The products obtained were invariably gels.
The crystal structure and refinement parameters for the inclusion compounds obtained with **H2** are given in Table 3.2; hydrogen bonding data are specified in Table 3.2. There is evidence of C-H $\cdots\pi$ interactions in structures **3.6**, **3.7**, **3.8**. We have used the distance criteria of C-H $\cdots\pi \leq 3.5$ [3.26] and have deposited the metrics of these interactions in the Supplementary Information.

Structure **3.6**, **H2•2(2MP)** crystallises in $P\bar{1}$ with Z = 1. The host is located at a centre of inversion at Wykoff position *c.* The structure is shown in Figure 3.4a. The **2MP** guest is disordered and shown in Figure 3.4b, with site occupancy factors of 59/41%.

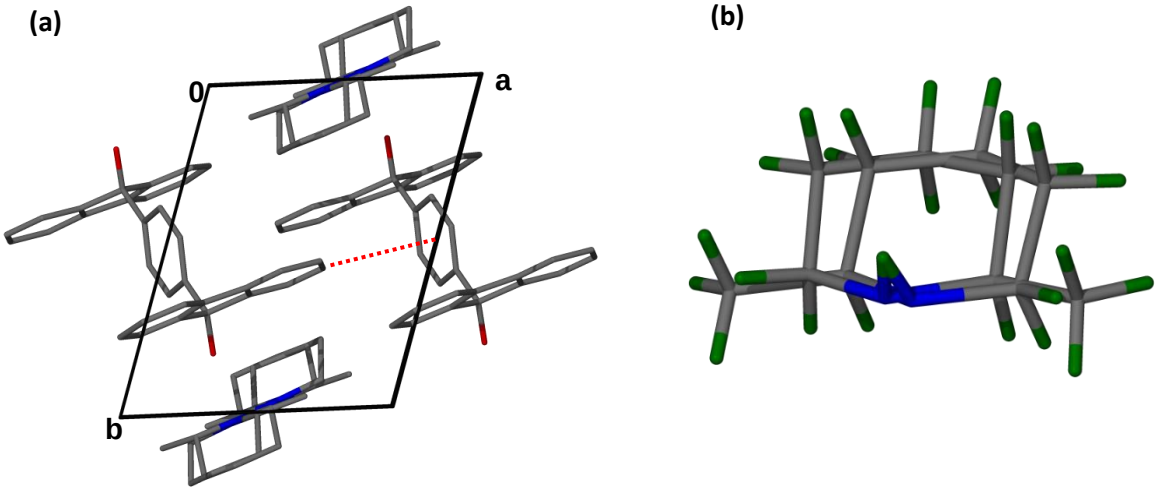

Figure 3.4. (a) The packing of structure **6** as viewed along [0 0 1] and (b) **2MP** guest disordered.

The hydrogen bonding pattern follows that displayed by the **H1•2(2MP)** structure and is again characterised by the $R_4^4(8)$ motif. The packing is characterised by planes of alternating **H2** and **2,6DMP** layers parallel to the *ac* plane.

Structure **3.7**, **H2•2(2,6DMP)**, also crystallises in $P\bar{1}$ with Z = 1 and the host on a centre of symmetry at Wykoff position *c*. The packing and hydrogen bonding are similar to that of structure **3.6** and it is noteworthy that the mode of disorder of **2MP** yields an overall molecular shape which is comparable to that of **2,6DMP**.

Structure **3.8**, **H2•2(3,5DMP)•H_2O**, crystallises in *C*2/*c* with Z = 4. The host is located at $\bar{1}$ at Wykoff position *a* and the **3,5DMP** guest is in a general position. The structure is a monohydrate, with the water oxygen located on the diad at Wykoff position *d*. The water hydrogens could not be located, but the interatomic distances of the water oxygen O1 to the hydroxyl oxygen O13 of the host is 2.96 Å, indicating a weak hydrogen bond. [3.27, 3.28] We

inserted the hydrogen atom with OH distance 1.01 Å. The ^{1}H NMR shows evidence of a small percentage of the *trans* **3,5DMP** stereoisomer (15%) in the dissolved crystals, but we could find no proof of the *trans* isomer in the refined crystal structure.
The packing is shown in Figure 3.5a, which displays a chain of host molecules interconnected by hydrogen bonding pairs of 3,5-dimethylpiperidine and the water molecules. The chain runs along [0 0 1] and the structure is characterised by restricted channels which accommodate the **3,5DMP** guests, and run along [0 1 0]. This is illustrated in Figure 3.5b.

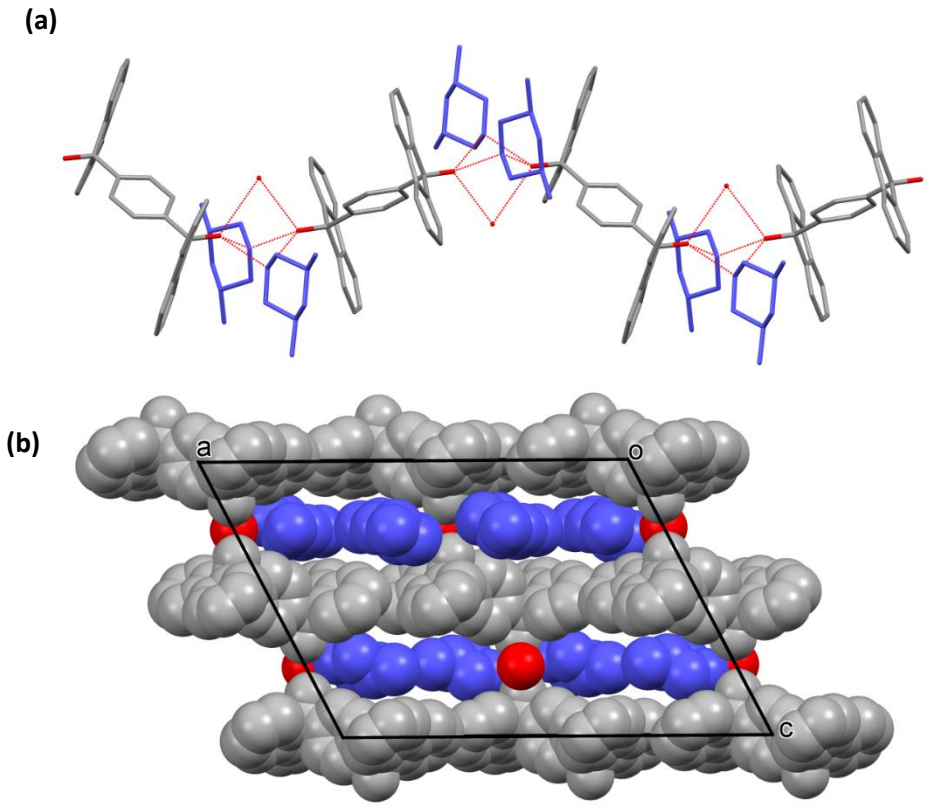

Figure 3.5. (a) Hydrogen bonding of structure **3.8** and (b) packing of structure **3.8** as viewed along [010] showing the guests located in restricted channels down this axis.

Table 3.3. Crystallographic data parameters of the Host-Guest complexes of **H2** studied.

Compound	**3.6**	**3.7**	**3.8**
Code	**H2•2(2MP)**	**H2•2(2,6DMP)**	**H2•2(3,5DMP)•H20**
Structural formula	$C_{44}\ H_{48}\ N_2\ O_2$	$C_{46}\ H_{52}\ N_2\ O_2$	$C_{46}\ H_{54}\ N_2\ O_3$
Host: Guest ratio	1:2	1:2	1:2:1
Molecular mass ($g{\cdot}mol^{-1}$)	636.84	664.90	682.91
Data collection temp. (K)	153	153	152
Crystal system	Triclinic	Triclinic	Monoclinic
Space group	$P\bar{1}$	$P\bar{1}$	$C2/c$
a (Å)	8.3533(17)	8.4600(17)	27.144(5)
b (Å)	10.505(2)	10.768(2)	8.3271(17)
c (Å)	11.159(2)	11.146(2)	19.643(4)
α(°)	95.51(3)	95.49(3)	90
β(°)	97.36(3)	97.73(3)	117.27(3)
γ(°)	106.39(3)	107.90(3)	90
Volume($Å^3$)	922.7(3)	947.3(3)	3946.4(14)
Z	1	1	4
Dc, calc density ($g{\cdot}cm^{-1}$)	1.146	1.166	1.149
θ range	1.86-28.04	1.86-27.85	1.69-27.89
Reflections collected	13906	22292	20467
No data I>2 sigma (I)	3564	3549	3636
Final R indices [I>2 sigma (I)]	0.0457	0.0470	0.0616
R indices (all data)	0.0572	0.0620	0.0781
Goodness-of-fit on F^2	1.040	1.052	1.051
Host torsion angle (°)	180	180	180
CCDC no.	1517593	1517592	1517594
CSD refcode	CANHAD	CANGUW	CANHEH

3.4.3 Competition Experiments.

In all the competition experiments, the molar ratio of host : total guest in the starting mother liquor was 1: 100, ensuring that the guests in the mixture were in excess. The guest ratio of the ensuing crystals was established by GC- HS.

H1 has been previously employed to discriminate between pyridine and the three isomers of picoline.[3.29] The competition experiment between 2-picoline and 4-picoline showed poor selectivity, but in the three-component experiment between pyridine, 2-picoline and 4-picoline, 2-picoline was favoured. We therefore investigated the selectivity between **2MP** and **4MP**, the results of which are displayed in Figure 3.6. These show that **2MP** is completely enclathrated when $X_{\mathbf{2MP}} \geq 0.3$.

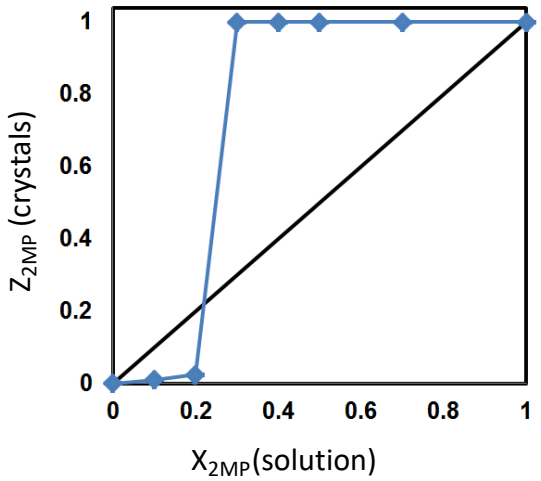

Figure 3.6. Results of the **2MP** vs. **4MP** competition experiments, showing a concentration dependent selectivity.

We also carried out simple selectivity experiments between **H1** and equimolar **2MP**/**3MP** yielding 90% **2MP** and **H2** and equimolar **2MP**/**3MP** yielding 57% **2MP**.

The structures containing the guests 2,6-dimethylpiperidine and 3,5-dimethylpiperidine were obtained with both **H1** and **H2**. Competition experiments were therefore performed by exposing each host to equimolar mixtures of **2,6DMP** and **3,5DMP**
The results were:

$$\mathbf{H1} + (\mathbf{2,6DMP} + \mathbf{3,5DMP})_{\text{equimolar}} \rightarrow \mathbf{H1 \cdot 2(3,5DMP)}$$
$$\mathbf{H2} + (\mathbf{2,6DMP} + \mathbf{3,5DMP})_{\text{equimolar}} \rightarrow \mathbf{H2 \cdot 2(2,6DMP)}$$

The results from the GC-HS analysis showed that the discrimination was complete (>99%) with only a small trace of the excluded guest showing on the GC trace.
The question that arises is: why does **H1** prefer **3,5DMP** while **H2** prefers **2,6DMP**?
We tackled this problem by analysing the final products of the competition experiments by a packing analysis of the structures with the program Crystal Explorer, [3.30 - 3.32] the calculation of lattice energies and the results of thermal analyses.

The Hirshfeld surface analysis of each of the four structures, **H1•2(2,6DMP)**, **H1•2(3,5DMP)**, **H2•2(2,6DMP)**, **H2•2(3,5DMP)•H_2O** and their corresponding fingerprint plots targeting the host molecule in each case, were computed. While we could interpret all the main features of the 2D fingerprint plots in terms of the various non-bonded interactions arising from the packing, the four plots were very similar. This was confirmed by the metrics giving the percentage interactions arising from H···H, H···C contacts and the hydrogen bonds. These values were close for the pairs of structures containing the same host, and the result was therefore inconclusive. We have deposited the fingerprint plots and the accompanying metrics in the supplementary information.

Lattice energy calculations using Gavezzotti's program[3.33, 3.34] AA-CLP were carried out. The values obtained for **H1•2(2,6DMP)** and **H1•2(3,5DMP)** were -325.8 kJmol^{-1} and - 324.3 kJmol^{-1}, respectively. These are within the margin of error of the calculation, and therefore cannot be used to discriminate between the two compounds. No calculations were carried out for the compounds with **H2** because the clathrate **H2•2(3,5DMP)• H_2O** is a monohydrate and this renders any comparison with the other compounds invalid.

3.4.4 Thermal analysis.

The results of the thermal analysis are shown in Figures 3.7 and 3.8 and summarised in Table 3.4.

The TG of the **H1•2(2MP)** compound displays a single step for the desorption reaction, with the DSC showing the corresponding endotherm. However, the DSC of the **H1•2(4MP)** crystals yielded two endotherms for the guest loss and the corresponding TG records a kink in its profile, indicating a more complex desorption reaction.

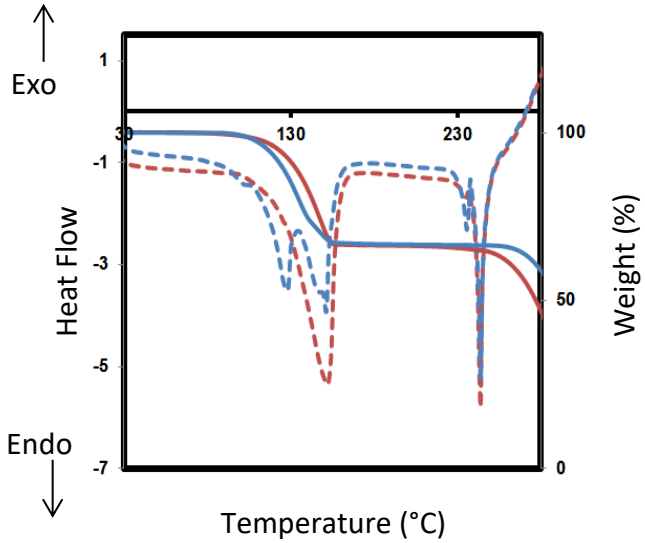

Figure 3.7. TGA (unbroken lines) and DSC (broken lines) traces for the **H1•2(2MP)** (red) and **H1•2(4MP)** (blue) compounds.

The TG traces for the **H1•2(2,6DMP)** and **H1•2(3,5DMP)** compounds both exhibit a single step reaction for the loss of the guests (red curve for **3,5DMP** and blue curve for **2,6DMP**). The accompanying table shows good agreement between observed and calculated percentage loss values.

The DSC curves (red broken line for **3,5DMP** and blue broken line for **2,6DMP**) are more instructive. Since the endotherms due to guest loss are rather broad, we could not evaluate onset temperatures T_{on} accurately and therefore report the peak temperatures T_{peak}. For **H1**, the endotherm corresponding to **3,5DMP** has T_{peak} = 158.4 °C, while that for **2,6DMP** has T_{peak} at 143.0 °C, 15.4 °C lower. The higher value of T_{peak} shows which guest is more strongly retained in the crystal structure.

In Figure 3.8b, however, the two guest loss endotherms occur the other way round. The higher T_{peak} for **2,6DMP** occurs at 151.8 °C while that for **3,5DMP** occurs at the lower temperature of 129.2 °C. This is in total agreement with the results of the competition experiment, a gratifying result.
Figures 3.8a and b both exhibit further smaller peaks before the melt endotherms of the respective hosts **H1** and **H2** with **2,6DMP**. These are attributed to possible polymorphic changes of the host after guest loss.

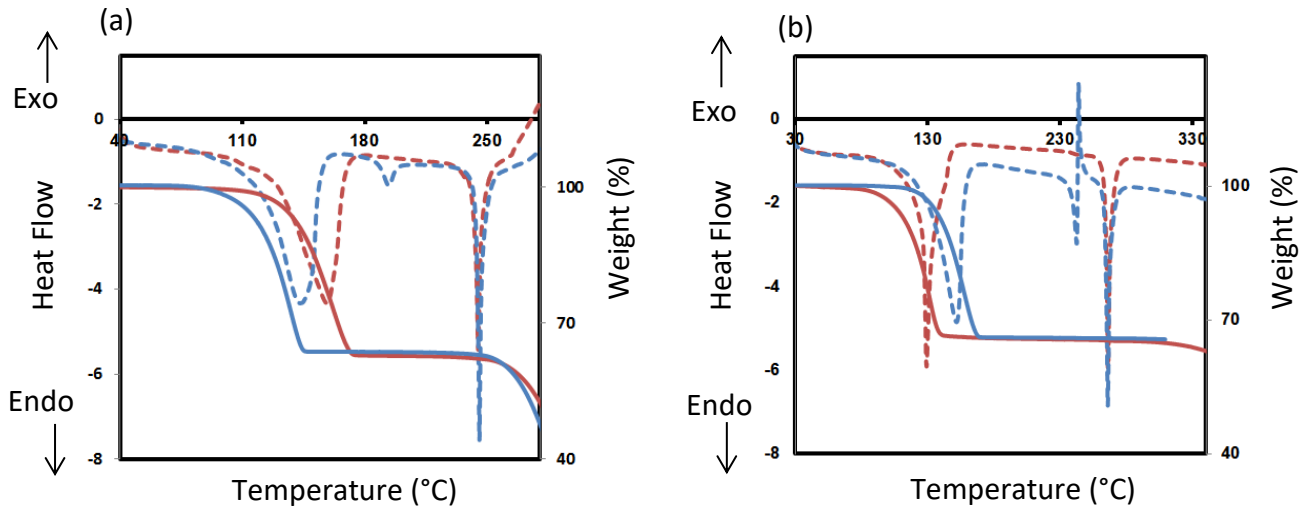

Figure 3.8. (a) TGA (unbroken lines) and DSC (broken lines) traces for the **H1•2(3,5DMP)** (red) and **H1•2(2,6DMP)** (blue) compounds and (b) TGA (unbroken lines) and DSC (broken lines) traces for the **H2•2(3,5DMP)•H_2O** (red) and **H2•2(2,6DMP)** (blue) compounds.

Table 3.4. Thermal analysis results.

Code	Compound	Mass loss (obsd) %	Mass loss (calc) %	Guest release T_{peak} /°C	Host melt T_{peak} /°C
3.1	**H1•2(2MP)**	33.5	33.9	152.1	243.9
3.3	**H1•2(4MP)**	33.0	33.9	128.1 & 151.4	244.1
3.4	**H1•2(2,6DMP)**	36.7	36.7	143.0	245.3
3.5	**H1•2(3,5DMP)**	37.0	36.7	158.4	244.6
3.7	**H2•2(2,6DMP)**	34.0	34.0	151.8	265.8
3.8	**H2•2(3,5DMP)·H_2O**	33.7	35.8	129.2	265.9

3.5 CONCLUSION

The inclusion compounds formed by **H1** and the various methylated piperidines display similar packings stabilized by O-H···N and N-H···O hydrogen bonds. The competition experiment of **H1** exposed to equimolar **2,6DMP** and **3,5DMP** results in the selection of **3,5DMP**. **H2**, however, yields the opposite result, preferring **2,6DMP**. This outcome could not be explained by packing analysis or lattice energy calculations, but is in agreement with the thermal analytical TG and DSC profiles. We surmise that the selectivity may be governed by kinetic effects of host-guest aggregation at the nucleation stage of host-guest aggregation.

3.6 REFERENCES

3.1 D. J. Adams, K. Morris, L. Chen, L. C. Serpell, J. Bacsa and G. M. Day, The delicate balance between gelation and crystallisation: structural and computational investigations, *Soft Matter.*, 2010, **6**, 4144–4156.

3.2 J. V. Alemán, A. V. Chadwick, J. He, M. Hess, K. Horie, R. G. Jones, P. Kratochvíl, I. Meisel, I. Mita, G. Moad, S. Penczek and R. F. T. Stepto, Definitions of terms relating to the structure and processing of sols, gels, networks, and inorganic-organic hybrid materials (IUPAC Recommendations 2007), *Pure Appl. Chem.*, 2007, **79**, 1801–1829.

3.3 S. Banerjee, R. K. Das and U. Maitra, Supramolecular gels 'in action', *J. Mater. Chem.*, 2009, **19**, 6649–6687.

3.4 N. Yoswathananont, M. Miyata, K. Nakano and K. Sada, Separation of Isomers and Enantiomers by Bile Acid Derivatives in *Separations and Reactions in Organic Supramolecular Chemistry*, John Wiley & Sons, Ltd, 2004, pp. 87–122.

3.5 B. Barton, E. C. Hosten and P. L. Pohl, Discrimination between o-xylene, m-xylene, p-xylene and ethylbenzene by host compound (R,R)-(–)-2,3-dimethoxy-1,1,4,4-tetraphenylbutane-1,4-diol, *Tetrahedron*, 2016, **72**, 8099–8105.

3.6 J. Kim, J. Yi, M. D. Ward and W.-S. Kim, Separation of dimethylcyclohexane stereoisomers by selective guest inclusion of host compound of guanidinium o-terphenyl-4,4'-disulfonate, *Sep. Purif. Technol.*, 2009, **66**, 57–64.

3.7 D. Binev, A. Seidel-Morgenstern and H. Lorenz, Continuous Separation of Isomers in Fluidized Bed Crystallizers, *Cryst. Growth Des.*, 2016, **16**, 1409–1419.

3.8 A. M. Pivovar, K. T. Holman and M. D. Ward, Shape-Selective Separation of Molecular Isomers with Tunable Hydrogen-Bonded Host Frameworks, *Chem. Mater.*, 2001, **13**, 3018–3031.

3.9 F. Toda and R. Bishop, *Separations and Reactions in Organic Supramolecular Chemistry*, John Wiley & Sons, 2004.

3.10 G. W. Gokel, *Crown Ethers and Cryptands*, Royal Society of Chemistry, 1991.

3.11 J.-P. Behr, *The Lock-and-Key Principle: The State of the Art--100 Years On*, Wiley, 1994.

3.12 E. Weber, S. Nitsche, A. Wierig and I. Csöregh, Inclusion Compounds of Diol Hosts Featuring Two 9-Hydroxy-9-fluorenyl or Analogous Groups Attached to Linear Spacer Units, *Eur. J. Org. Chem*., 2002, **2002**, 856–872.

3.13 T. le Roex, L. R. Nassimbeni and E. Weber, Clathrates with mixed guests, *Chem. Commun.*, 2007, 1124–1126.
3.14 T. le Roex, L. R. Nassimbeni and E. Weber, Selectivity and structure of mixed guest clathrates, *New J. Chem.*, 2008, **32**, 856–863.
3.15 S. A. Bourne, K. C. Corin, L. R. Nassimbeni and E. Weber, pH control of guest selectivity by inclusion, *CrystEngComm*, 2004, **6**, 54–55.
3.16 APEX 2, Version 1.0-27; Bruker AXS Inc.; Madison, WI, 2005.
3.17 Z. Otiwinowski and W. Minor In *Methods in Enzymology, Macromolecular Crystallography*; Carter, C.W., Jr., Sweet, R.M, Eds.; Academic Press: 1997; part A, Vol. 276, p 307.
3.18 Z. Otwinowski and W. Minor, Processing of X-ray diffraction data collected in oscillation mode in *Methods Enzymol.*, Elsevier, 1997, vol. 276, pp. 307–326.
3.19 SAINT-Plus, Version 7.12; Bruker AXS Inc.: Madison, Wisconsin, USA, 2004.
3.20 G. M. Sheldrick, Program for Empirical Absorption Correction of Area Detector Data, *SADABS*.
3.21 G. M. Sheldrick, SHELXS97, Program for the Solution of Crystal Structures, University of Göttingen, Germany 1997.
3.22 L. J. Barbour, X-Seed — A Software Tool for Supramolecular Crystallography, *Supramol. Chem.*, 2001, **1**, 189–191.
3.23 M. Lusi and L. J. Barbour, Determining Hydrogen Atom Positions for Hydrogen Bonded Interactions: A Distance-Dependent Neutron-Normalized Method, *Cryst. Growth Des.*, 2011, **11**, 5515–5521.
3.24 C. F. Macrae, I. J. Bruno, J. A. Chisholm, P. R. Edgington, P. McCabe, E. Pidcock, L. Rodriguez-Monge, R. Taylor, J. Van De Streek and P. A. Wood, Mercury CSD 2.0– new features for the visualization and investigation of crystal structures, *J. Appl. Crystallogr.*, 2008, **41**, 466–470.
3.25 M. C. Etter, J. C. MacDonald and J. Bernstein, Graph-set analysis of hydrogen-bond patterns in organic crystals, *Acta Cryst. B*, 1990, **46**, 256–262.
3.26 L. Loots and L. J. Barbour, Rudimentary Method for Classification of π···π Packing Motifs for Aromatic Molecules in *The Importance of Pi-Interactions in Crystal Engineering*, John Wiley & Sons, Ltd, pp. 109–124.
3.27 G. R. Desiraju and T. Steiner, *The Weak Hydrogen Bond: In Structural Chemistry and Biology*, Oxford University Press, 1999.
3.28 G. A. Jeffrey, *An Introduction to Hydrogen Bonding*, Oxford University Press, 1997.
3.29 L. Nassimbeni, G. Ramon and E. Weber, Inclusion by a fluorenyl diol host with substituted pyridines: Structures, selectivity and kinetics of desorption, *J. Therm. Anal. Calorim.*, 2007, **90**, 31–37.
3.30 M. A. Spackman and D. Jayatilaka, Hirshfeld surface analysis, *CrystEngComm*, 2009, **11**, 19–32.
3.31 S. K. Wolff, D. J. Grimwood, J. J. McKinnon, M. J. Turner, D. Jayatilaka and M. A. Spackman, CrystalExplorer (Version 3.1), *University of Western Australia*.
3.32 M. J. Turner, J. J. McKinnon, D. Jayatilaka and M. A. Spackman, Visualisation and characterisation of voids in crystalline materials, *CrystEngComm*, 2011, **13**, 1804–1813.
3.33 A. Gavezzotti, Calculation of Intermolecular Interaction Energies by Direct Numerical Integration over Electron Densities. I. Electrostatic and Polarization Energies in Molecular Crystals, *J. Phys. Chem. B*, 2002, **106**, 4145–4154.

3.34 A. Gavezzotti, Calculation of Intermolecular Interaction Energies by Direct Numerical Integration over Electron Densities. 2. An Improved Polarization Model and the Evaluation of Dispersion and Repulsion Energies, *J. Phys. Chem. B*, 2003, **107**, 2344–2353.

CHAPTER 4

Selectivity of aliphatic alcohols by host–guest chemistry

By Nicole M. Sykes, Hong Su, Edwin Weber, Susan A. Bourne, and Luigi R. Nassimbeni
In *Cryst. Growth Des.*, 2017, **17**, 819–826 (Published 19 June 2017)

2017 – year 2 – a PhD student

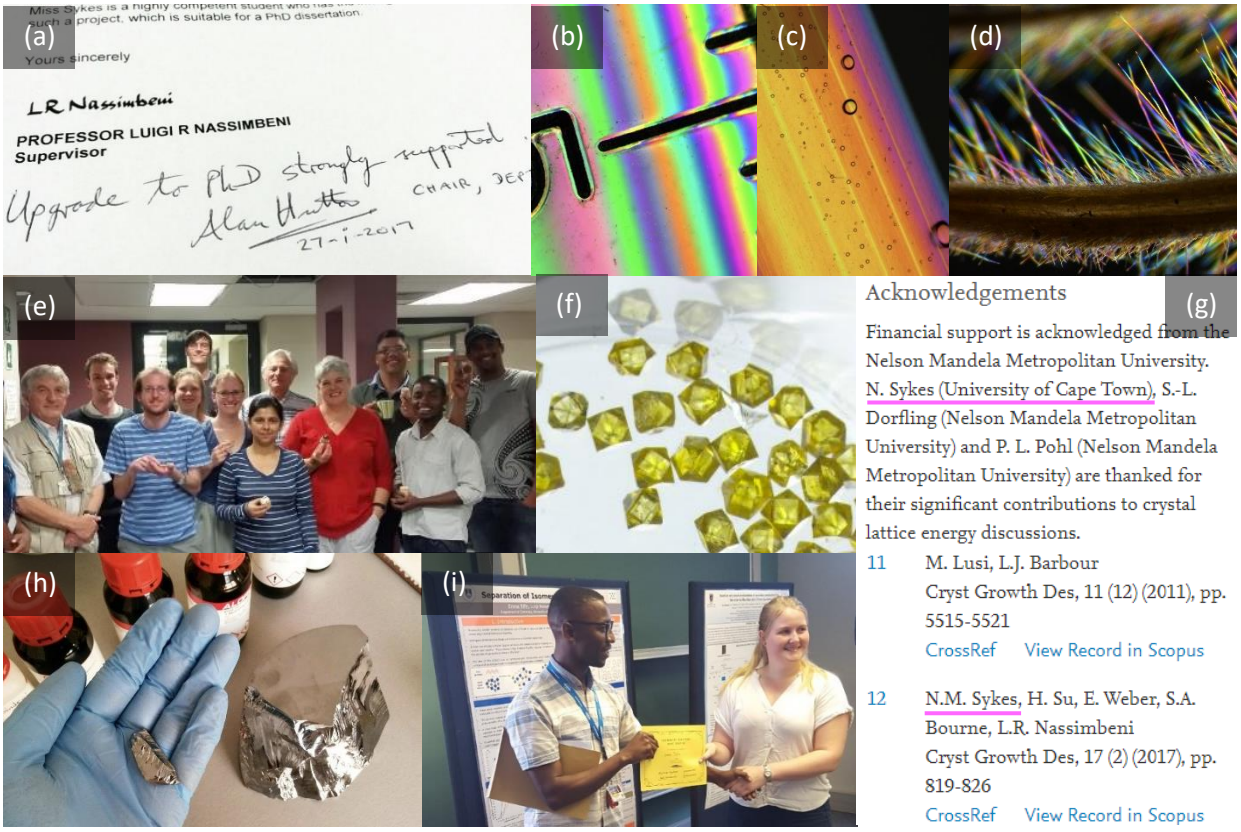

(a) 27 January, I was upgraded from the MSc to the PhD degree. (b) – (d) Rainbow colours under cross-polarized light: (b) 28 June, stress-induced birefringence of a plastic ruler. (c) 14 June, straw with water droplets. (d) 16 October, hairs on the stamen of a pincushion protea. (e) 28 November, cake in celebration of Dr Christelle Tekouo's first paper published at UCT. (f) 6 June, Prof. Nassimbeni's yellow diamonds, photo shared online by Chemical & Engineering News magazine. (g) 23 March, article by Benita Barton et al. (*Tetrahedron* **2017**, *73* (18), 2662–2673) marked my first paper citation (and thank you for my help). (h) 30 May, a chunk of monocrystalline silicon, gifted to Prof. Nassimbeni by Prof Buffler (Physics HOD), off which wafers were cut to be used as a low background surface in customised X-ray diffraction experiments. (i) 20 November, Emma Tiffin (my mentee) won best poster for her honours project.

4.1 SYNOPSIS

This paper investigates the selectivity by the same bulky diol host (**H1**) used in Chapter 3. In this work the guests chosen were similarly structured aliphatic alcohols with close boiling points. Unsuccessful enclathration attempts led to the crystallisation of two new polymorphs of the apohost (host without guest), which display different conformations, as characterised by the O-C-C-O torsion angle. The lattice energies of the polymorphs were calculated using Gavezzotti's AA-CLP programme, with the difference between them equal to 5.7 kJ mol^{-1}. The structure of the more stable polymorph contains hosts which display both the *cis* (O-C-C-O torsion angle ≈ 0°) and *trans* conformation (torsion angle = 180°). The polymorph with the higher lattice energy contains hosts that display the *cis* conformation only.

The relaxed potential energy of the gas-phase host molecule was scanned as a function of its O-C-C-O torsion angle. The results, computed using density functional theory (DFT), show a small maximum energy difference between all possible host conformations equal to ≈ 2 kJ mol^{-1}, which suggests that any conformers are accessible in the solid state.[4.1 - 4.3]

Reported also are four new inclusion compounds of **H1** with an alcohol guest, either 3-methylbutan-2-ol (**3MBUT**), 3-pentanol (**3PENT**), 2-pentanol (**2PENT**), or 1-butanol (**1BUT**). These four alcohols all boil within 2.5 °C of each other, which would make a mix of them challenging to separate by conventional methods. The apohost polymorphs and inclusion compounds were characterised by thermal analysis and X-ray diffraction.

It was noted that the three structures with pentanol isomers, which are secondary alcohols, are all comprised of a unit cell containing two guests and two hosts in the *trans* conformation, together forming a ring of hydrogen bonds described as $R_4^4(8)$ in Etter's graph set notation. While in the unit cell of **H1** with the smaller, but less bulky, **1BUT** (and also 1-propanol, denoted as IFAHOM in the CSD) there are instead four *gauche* hosts (torsion angle ≈ 100°) and four guests, which form a hydrogen bonded motif described as $R_8^8(16)$.

To determine the selectivity for these alcohols, the host was exposed to equimolar mixtures of two guests and allowed to crystallise. These competition experiments revealed that whenever **H1** was presented with an equal mix of **1BUT** and a pentanol, the pentanol was always preferred. It also was found that **H1** is selective towards **3PENT** over **3MBUT** in ratio 80:20, but only mildly selective towards **3PENT** over **2PENT** (63:37). In turn **H1** preferred **2PENT** over **3MBUT** in the ratio 71:29. The combined results yields the overall preference of the host for the four alcohols in the following order: **3PENT** > **2PENT** > **3MBUT**> **1BUT**.

To try account for these results, Hirshfeld surfaces of the inclusion compounds were computed, but revealed no great insight. It was, however, noted that the selectivity by the host could be linked to the DSC traces collected from the pure inclusion compounds. The peak temperature of the endotherm due to guest desorption (normalised by subtracting the guest boiling point) gives a measure of how strongly the guest is held within the host framework.[4.4] In the table below, the $T_{peak} - T_{boil}$ values correspond to the selectivity ranking assigned to that host-guest compound, where the less negative the $T_{peak} - T_{boil}$ value, the more preferred that alcohol guest is by the host.

DSC results in order of the host's preference for the four aliphatic alcohols

Compound	Guest	Guest normal boiling point (°C)	Guest release T_{peak} (°C)	Guest release $T_{peak} - T_{boil}$ (°C)	Selectivity ranking
3H1•6(3PENT)	3-pentanol	115	103	-11	1
H1•2(2PENT)	2-pentanol	119	92.3	-26.7	2
H1•2(3MBUT)	3-methyl-2-butanol	114	86.7	-27.3	3
H1•2(1BUT)	1-butanol	118	47 & 79	-40 & -71	4

4.2 INTRODUCTION

Selective enclathration, whereby a host compound preferentially combines with a given guest molecule in a mixture, depends on the phenomenon of molecular recognition. A quantitative measure of the efficiency of this process is the selectivity constant.

Consider a binary mixture of two liquid guests A and B of known composition. If a host H is dissolved in this mixture and the resulting solution is allowed to crystallise, the crystalline product can be harvested and analysed. If the mole fractions of the two guests in the mother liquor are X_A, X_B and those in the crystals are Z_A, Z_B then the selectivity constant,[4.5] :

$$K_{A:B} = {}^{Z_A}/_{Z_B} \times {}^{X_B}/_{X_A}$$

This is illustrated in Figure 4.1, where the starting mother liquor contains an equimolar mixture of the guests, and the crystals have a composition shown by point P. The selectivity constant is given by the ratio of the areas I/II. In Figure 4.1, the broken line represents the selectivity profile of the host in which A is preferred over B over the complete range of A/B compositions. Different kinds of selectivity curves may occur arising from the results of competition experiments. These have been described in detail[4.6] for binary mixtures and for three-component systems.[4.7]

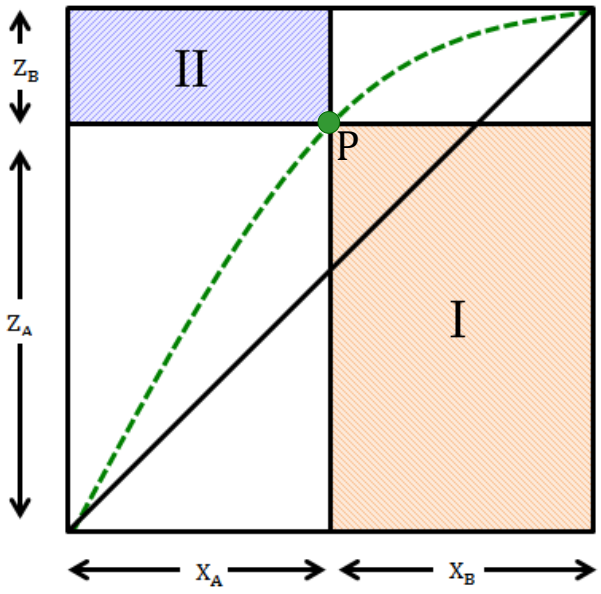

Figure 4.1. A competition experiment between an equimolar mixture of two guests A and B which yielded a greater percentage of A than of B in the inclusion compound.[4.8]

In this work, we have employed the host 9,9'-(ethyne-1,2-diyl)-bis(fluoren-9-ol) (**H1**) to study the separation of the four aliphatic alcohols 3-methylbutan-2-ol (**3MBUT**), 3-pentanol (**3PENT**), 1-butanol (**1BUT**) and 2-pentanol (**2PENT**).
The host **H1** and the guests are shown in Scheme 4.1. The four alcohols have boiling points from 114 °C to 119 °C, rendering separation by distillation impractical.

This host compound has been used previously in the study of its inclusion compounds with ethanol and acetonitrile, and its selectivity profile for mixtures of these guests has been determined.[4.9] The separation of the picoline isomers has been described[4.10] and the structures with caffeine and methanol have been characterised.[4.11] Recently, the selectivity of this host for methylated piperidines was studied by elucidating crystal structures and their packing, as well as analysing their decomposition profiles via Differential Scanning Calorimetry (DSC). [4.12]

Scheme 4.1. Host and Guest Compounds

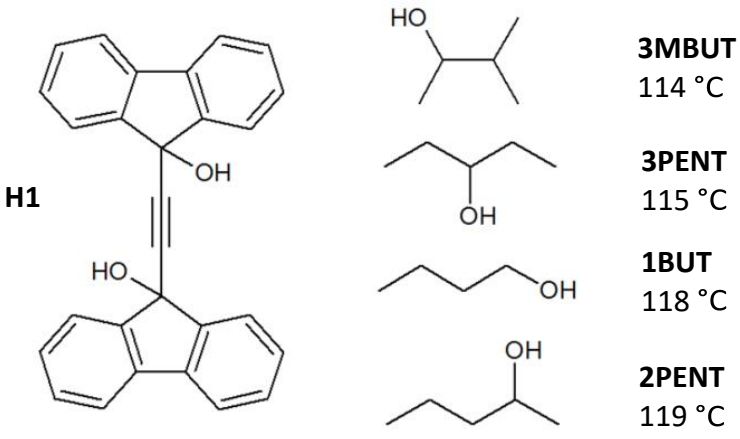

3MBUT
114 °C

3PENT
115 °C

1BUT
118 °C

2PENT
119 °C

4.3 EXPERIMENTAL

4.3.1 Materials.

The host compound, **H1** was synthesized by Weber[4.13] and used without further purification. The alcohol guests were all purchased from Sigma Aldrich and used as received. Single crystals of the inclusion compounds were obtained by dissolving **H1** in chloroform and adding an excess of the relevant guest or binary guest mixture. The resulting solutions were filtered and allowed to crystallise by slow evaporation at room temperature.

4.3.2 X-ray Crystallography.

Single crystal X-ray diffraction data were collected on a Bruker DUO APEX II[4.14] diffractometer for all structures using Mo Kα (λ = 0.71073 Å) at a temperature of 153 K. The intensity data were collected using the phi scan and omega scan techniques, scaled, and reduced with SAINT-Plus.[4.15] The correction of the collected intensities for absorption was done using the SADABS program.[4.16]

The structures were solved by direct methods using SHELX-97[4.17] and refined using full-matrix least squares methods in SHELXL.[4.17] The graphical interface used was the program X-SEED.[4.18] All C-H hydrogen atoms were placed geometrically and with a riding model for their isotropic temperature factors. The O-H hydrogen atoms were located in the final difference electron density map. Their bond lengths were fixed using the formulae suggested by Lusi and Barbour[4.19] who studied the neutron data of the O-H···O systems. Diagrams were generated using MERCURY (3.5).[4.20]

Powders were mounted on a flat zero-background sample holder. X-ray powder data were collected in a Bruker D2 PHASER Desktop X-ray diffractometer with copper radiation (Cu Kα, λ = 1.5406 Å) at 30 kV and 10 mA. Each sample was scanned between 4 and 50° 2θ with a step size of 0.02°.

4.3.3 Thermal Analysis.

Thermogravimetric analysis (TGA) was performed using a TA-Q500 Thermogravimetric Analyser. Results were analysed using Universal Analysis 2000 software. The samples were crushed and blotted dry (4–10 mg) and weighed directly into open aluminium oxide TGA crucibles. Differential scanning calorimetry (DSC) was performed using a Surface Solutions GmbH DSC XP-10. Crushed and dried samples (1–3 mg) were weighed directly into a vented aluminium pan on an analytical balance.
The experiments were performed over a temperature range of 20–300 °C at a heating rate of 20 °C min^{-1} under dry nitrogen with a flow rate of 40 ml/min.

4.3.4 Gas Chromatography Headspace.

The system used was an Agilent 6890 gas chromatograph/ 7697A Headspace sampler with a 50-m CB Wax 57 capillary column. Nitrogen was used as the carrier gas at a constant flow rate of 1.5 ml/min. The oven conditions included an initial temperature of 50 °C and an initial time of 2 min, 8 °C/min to 180 °C with no hold time. The inlet temperature was kept constant at 220 °C, and the FID detector was set at 220 °C with

flow rates of hydrogen at 30 ml/min, air at 400 ml/min and nitrogen at 25 ml/min. Samples were equilibrated for 15 min at 110 °C with a loop temperature of 115 °C and the transfer line set at 120 °C.

4.3.5 ^{1}H Nuclear Magnetic Resonance (NMR) Spectroscopy.

^{1}H NMR spectra were recorded on a Bruker 300MHz with DMSO as internal standard. Samples were blotted dry, crushed, and dissolved in deuterated d6-DMSO. The appropriate signals were integrated to determine the relative proportions of the guests.

4.4 RESULTS AND DISCUSSION

4.4.1 New Inclusion compounds.

Two polymorphs of the apohost were crystallised and their structures elucidated.

Apohost(α), was crystallised from a solution of the host dissolved in 3-methyl-1-butanol. The resulting structure crystallised in *C*2/*c* with Z = 8 and the conformation, as defined by the torsion angle O13-C13-C16-O16, (16.1°), may be regarded as *cis* (Figure 4.2a).
The packing is characterised by hydrogen bonded dimers

(Host)O-H···O(Host)
|
H

with d(O ··· O) = 2.89 Å (Figure 4.2b). The dimers are interlinked by (Host)O-H···π(Host)interactions with d(O-H…π) = 2.84 Å[4.21, 4.22] which give rise to Host molecular columns in the [001] direction (Figure 2c). The refinement parameters for all structures are given in Table 4.1 and the metrics of the hydrogen bonding for all structures are given in Table 4.2.

Apohost(β), was crystallised from a solution of the host dissolved in 1-butanol at 50 °C. The resulting structure crystallised in $P\bar{1}$ with Z = 3. One molecule, with torsion angle O-C-C-O at 0.7°, adopts a *cis*- conformation, while a second molecule is located on a centre of inversion at Wyckoff position *h*, and is necessarily *trans*-. It is noteworthy that this structure displays the host in both *cis*- and *trans*- conformations. Therefore, an energy calculation was performed on a single molecule in vacuo, varying the O-C-C-O torsion angle from 0° to 360°,[4.23 - 4.29] the details of which are given in the Supplementary Information.

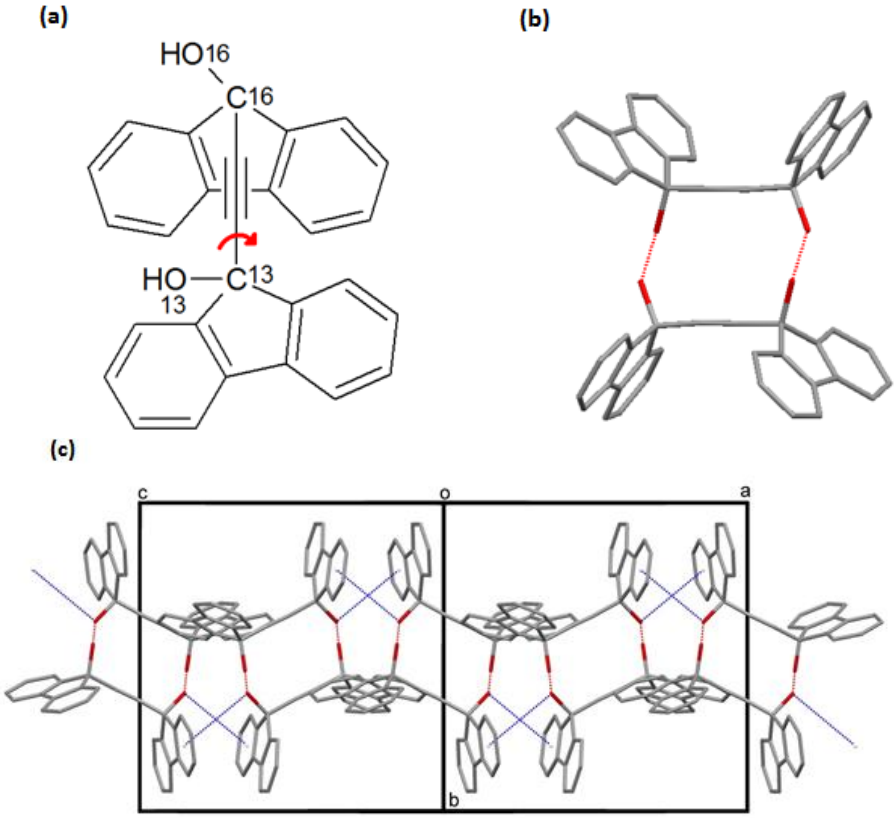

Figure 4.2. (a) O-C-C-O host torsion angle, (b) two host molecules connected by O-H···O hydrogen bonds and (c) **Apohost(α)**, showing host columns interlinked by O-H···O (red) and O-H··· π (blue) hydrogen bonds.

Table 4.1. Crystallographic data parameters of the Host-Guest complexes studied.

Compound	**Apohost (α)**	**Apohost (β)**	**H1•2(3MBUT)**	**3H1•6(3PENT)**	**H1•2(1BUT)**	**H1•2(2PENT)**
Structural formula	$C_{28}H_{18}O_2$	$C_{28}H_{18}O_2$	$C_{38}H_{42}O_4$	$C_{114}H_{125}O_{12}$	$C_{36}H_{38}O_2$	$C_{38}H_{42}O_4$
Host: Guest ratio	-	-	1:2	1:2	1:2	1:2
Molecular mass ($g{\cdot}mol^{-1}$)	386.45	386.45	562.75	1687.24	534.70	562.75
Data collection temp. (K)	153	153	123	153	153	153
Crystal system	Monoclinic	Triclinic	Triclinic	Triclinic	Triclinic	Triclinic
Space group	$C2/c$	$P\bar{1}$	$P\bar{1}$	$P\bar{1}$	$P\bar{1}$	$P\bar{1}$
a(Å)	18.455(4)	9.7243(19)	9.869(2)	9.6915(19)	8.8074(18)	8.5130(17)
b (Å)	14.363(3)	10.424(2)	13.153(3)	15.3801(31)	13.145(3)	9.5480(19)
c (Å)	15.938(3)	14.814(3)	14.18(3)	16.4385(33)	14.259(3)	12.017(2)
α(°)	90	94.05(3)	63.18(3)	91.21(3)	75.84(3)	101.52(3)
β(°)	113.45(3)	102.03(3)	86.31(3)	98.29(3)	75.56(3)	103.71(3)
γ(°)	90	93.31(3)	83.31(3)	91.87(3)	75.70(3)	114.49(3)
Volume($Å^3$)	3875.7(13)	1460.9(5)	1632.1(6)	2422.6(8)	1520.8(5)	813.1(3)
Z	8	3	2	1	2	1
Dc, calc density ($g{\cdot}cm^{-1}$)	1.325	1.318	1.145	1.156	1.168	1.149
θ range	1.86-27.98	1.41-28.43	1.61-28.30	1.25-27.94	1.52-27.96	1.85-27.94
Reflections collected	27944	39652	36160	73746	15786	11684
No data I>2 sigma (I)	4079	6144	6643	8408	5399	3211
Final R indices [I>2 sigma (I)]	0.0387	0.0418	0.0488	0.0466	0.0457	0.0455
R indices (all data)	0.0982	0.1000	0.1243	0.1104	0.1026	0.1139
Goodness-of-fit on F^2	1.040	1.025	1.030	1.026	1.022	1.032
Host torsion angle (°)	16.1	0.7 &180	157.6	151.7 & 180	101.4	180
CCDC no.	1540357	1540358	1540359	1540362	1540360	1540361
CSD refcode	PAZTUI	PAZTUI01	PAZVEU	PAZVUK	PAZVIY	PAZVOE

Table 4.2. Hydrogen bonding studied.

Compound	Donor (O)	Acceptor (O)	O···O (Å)	O-H (Å)	H···O (Å)	< O-H···O(°)
Apohost (α)	O16	O13[a]	2.886(15)	0.993(5)	1.905(6)	169(2)
Apohost (β)	O41	O16	2.927(2)	0.994(5)	1.996(9)	156(2)
	O13	O41[b]	2.876(1)	0.993(5)	1.886(6)	174(2)
H1•2(3MBUT)	O1	O13	2.752(3)	0.982(5)	1.787(5)	167(3)
	O1A	O13	2.612(9)	0.976(5)	1.787(5)	140(2)
	O13	O1[c]	2.678(3)	0.975(5)	1.748(5)	158(2)
	O13	O1A[c]	2.639(8)	0.975(5)	1.763(5)	148(2)
	O16[d]	O2	2.742(6)	0.977(5)	1.872(5)	147(3)
	O16[d]	O2A	2.685(9)	0.977(5)	1.890(5)	137(3)
	O16[d]	O2B	2.637(9)	0.977(5)	1.715(5)	156(3)
	O16	O2	2.749(7)	0.977(5)	1.787(5)	168(4)
	O16	O2A	2.641(10)	0.977(5)	1.667(5)	174(4)
	O16	O2B	2.715(11)	0.977(5)	1.820(5)	151(4)
	O2	O16	2.749(7)	0.979(5)	1.822(5)	157(4)
	O2A	O16	2.641(10)	0.981(5)	1.822(5)	139(4)
	O2B	O16	2.715(11)	0.978(5)	1.822(5)	150(4)
	O2	O16[d]	2.742(6)	0.976(5)	1.786(5)	166(5)
	O2A	O16[d]	2.685(9)	0.980(5)	1.786(5)	151(4)
	O2B	O16[d]	2.637(10)	0.982(5)	1.786(5)	143(3)
3H1•6(3PENT)	O36	O13	2.723(8)	0.965(5)	1.860(2)	147.25
	O36'	O13	2.777(8)	0.970(5)	1.860(2)	156.60
	O13	O36'	2.777(8)	0.968(5)	1.830(1)	165.34
	O13	O36	2.723(8)	0.968(5)	1.782(1)	163.23
	O13	O41[e]	2.739(2)	0.968(5)	1.779(8)	170.93
	O41[e]	O13	2.739(2)	0.968(5)	1.882(24)	146.13
	O41	O13'	2.709(2)	0.978(5)	1.768(15)	160.28
	O13'	O41	2.709(2)	0.979(5)	1.772(19)	158.92
	O41	O13[e]	2.739(2)	0.968(5)	1.882(24)	146.13
	O13[e]	O41	2.739(2)	0.968(5)	1.779(8)	170.93
	O36[e]	O13'	2.692(8)	0.969(5)	1.842(27)	144.72
	O36'[e]	O13'	2.745(8)	0.968(5)	1.842(27)	153.85
	O13'	O36[e]	2.692(8)	0.967(5)	1.742(13)	166.16
	O13'	O36'[e]	2.745(8)	0.967(5)	1.802(13)	164.00
	O16	O31	2.702(25)	0.980(5)	1.741(26)	165.98
	O16	O31'	2.673(7)	0.980(5)	1.700(10)	171.41
	O31[f]	O16	2.676(14)	0.964(5)	1.841(18)	143.10
	O31'[f]	O16	2.716(4)	0.969(5)	1.841(18)	148.72
	O16	O31[f]	2.676(14)	0.969(5)	1.815(31)	146.34
	O16	O31'[f]	2.716(4)	0.969(5)	1.9169	138.11

H1•2(1BUT)	O29’	O16	2.734(2)	0.965(5)	1.775(6)	172(2)
	O16	OA	2.681(20)	0.975(5)	1.714(21)	171(2)
	O16	OB	2.623(16)	0.975(5)	1.658(17)	170(2)
	O16	OC	2.689(11)	0.975(5)	1.722(23)	171(2)
	OA	O13[g]	2.737(5)	0.967(5)	1.782(6)	169(2)
	OB	O13[g]	2.724(5)	0.967(5)	1.782(6)	164(2)
	OC	O13[g]	2.739(5)	0.968(5)	1.782(6)	169(2)
	O13	O29’[c]	2.649(2)	0.977(5)	1.687(7)	167(2)
H1•2(2PENT)	O13	O16	2.670(1)	0.970(5)	1.726(1)	163(1)
	O16	O13[h]	2.781(2)	0.965(5)	1.891(1)	152(1)

Symmetry codes: (a) 1-x, 1-y, -z (b) x-1, y, z (c) 2-x, 1-y, 1-z (d) 1-x, 2-y, -z (e) -x, -y, -z (f) 1-x, 1-y, -1-z (g) 1+x, y, z (h) -x-1, -y, -z

The result is given in Figure 4.3, which shows that the energy profile is symmetrical, and the lowest energies occur at 75° and 285°, corresponding to ≈ gauche conformations. The energy difference between these and the *trans*- conformation is small, amounting to ≈ 2.2 kJ mol^{-1}: comparable to the thermal energy of an ideal gas at room temperature.
While this is not directly commensurate with values obtained from results in the solid state, it suggests that both conformations are likely to occur.

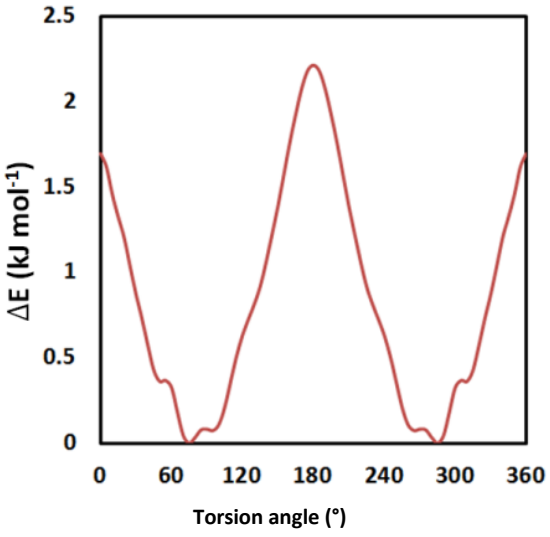

Figure 4.3. DFT calculations computed potential energy scans of the host molecule with varying torsion angles.

The packing of **Apohost(β)**, displays a double column of hydrogen-bonded *cis*- hosts, bridged by the *trans*- molecules, which run along [100]. The structure is also stabilised by (*cis*-Host)O-H ⋯π(*cis*-Host) interactions with d(O-H⋯π) = 2.64 Å.[4.21, 4.22] This is shown in Figure 4.4.

Comparison of the packing of the apohost polymorphs was carried out using Crystal Explorer,[4.30 - 4.32] and the fingerprint plots are shown in Figure 4.5.

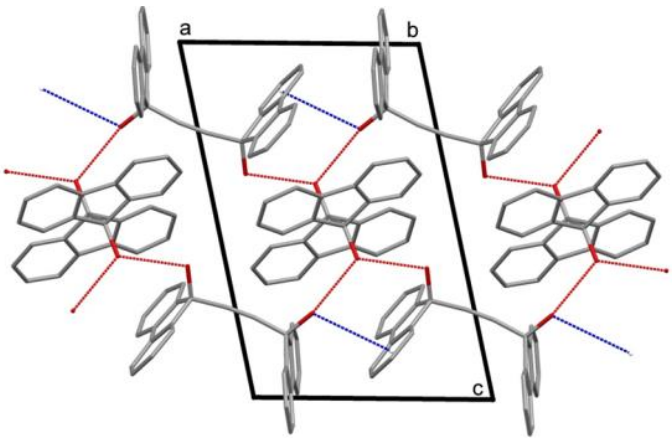

Figure 4.4. The packing of **Apohost(β)**, viewed down [010] showing columns of *cis*- host molecules interlinked by O-H···O (red) and O-H··· π (blue) hydrogen bonds; bridged by *trans*-host molecules.

For **Apohost(α)**, (Figure 4.5a) the peaks ① and ② represent the O-H···O hydrogen bonds and ③ represents the H···H contacts. For **Apohost(β)**, two fingerprint plots were calculated, targeting the *cis*- and *trans*- molecules respectively. Figure 4.5b (*cis*-conformer) is similar to that of the **Apohost(α)** structure, but the plot for the *trans*-conformer, Figure 4.5c, is different: although peaks ① and ② occur at di + de ≈ 1.90 Å as in the other structures, the H···H interaction peak ③ is clearly different, and the accompanying table recording the % of the main interactions shows that the (Host)OH···O hydrogen bond has a higher occurrence than in the other structures.

The full data with the percentage atom···atom interactions for all these structures have been deposited in the Supplementary Information.

The lattice energies of these two polymorphs have been calculated using Gavezzotti's programme[4.33, 4.34] AA-CLP. The result yielded -192.7 kJ mol^{-1} for polymorph (α) and -198.4 kJ·mol^{-1} for polymorph (β). The difference of 5.7 kJ mol^{-1} is small, but possibly significant.

For the remaining structures the host was practically insoluble in the liquid guests at 25 °C and we therefore employed $CHCl_3$ as a co-solvent.

H1·2(3MBUT), crystallises in $P\bar{1}$ with Z = 2, with all host and guest atoms in general positions. The guest molecules are disordered and were refined anisotropically.
The packing is shown in Figure 4.6 viewed along [100]. It is characterised by two hydrogen bonded rings centred on Wyckoff positions *a* and *h* and described as $R_4^4(8)$ in Etter's Graph Set Notation.[4.35] The 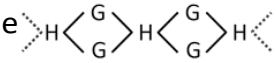 chains run in the [111] direction.

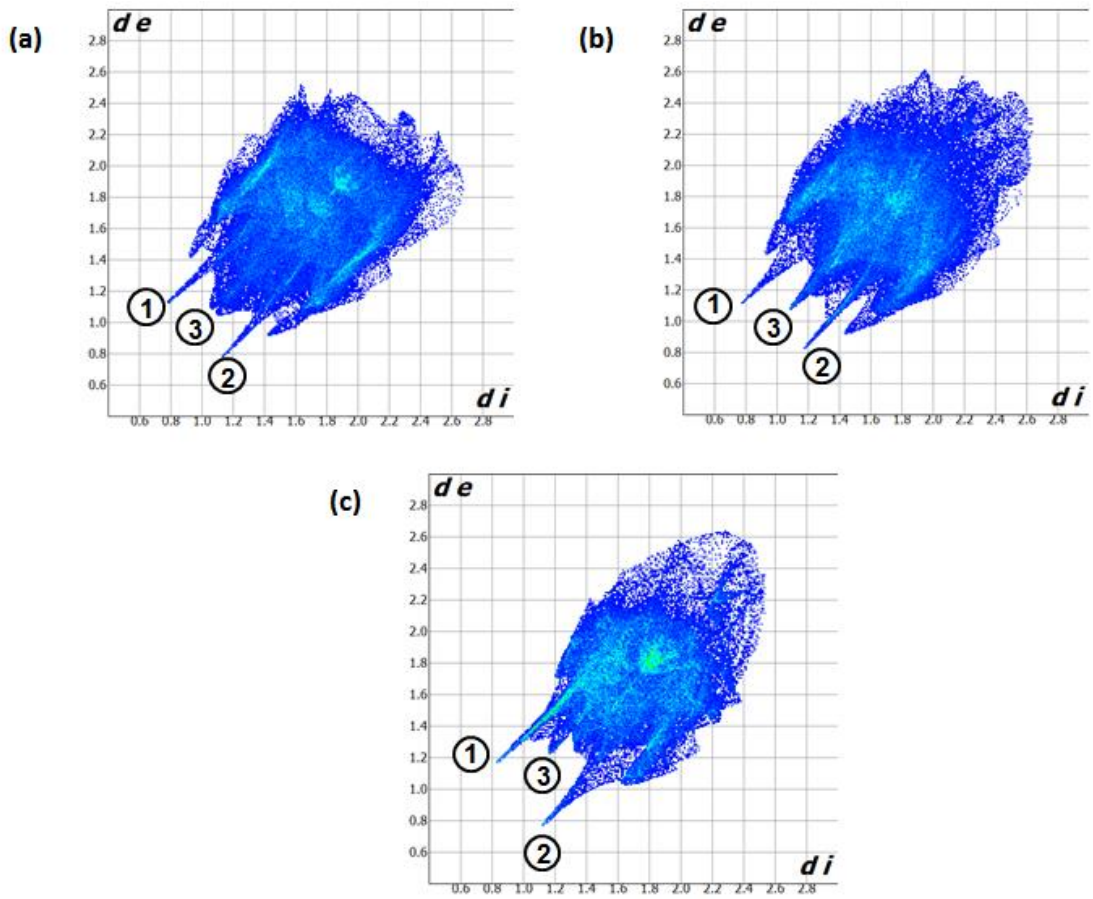

Figure 4.5. 2D fingerprint plots for (a) **Apohost(α)** (*cis*-) , and (b) **Apohost(β)** (*cis*-) and (c) **Apohost(β)** (*trans*-).

3H1•6(3PENT), also crystallises in $P\bar{1}$. In this case, however there are three host molecules in the unit cell, one of which lies on a centre of inversion at Wyckoff position *a*, and six guest molecules. The packing is similar to that of structure **Apohost(α)**, with the hydrogen bonded Host···Guest···Host chains also running along [111]. The 3-pentanol guests are again disordered over two positions.

The **H1•5(1BUT)** compound, crystallises in $P\bar{1}$, Z = 2, with all the molecules in general positions and one of the guests is disordered. The packing, however, is different from those of **H1•2(3MBUT)** and **3H1•6(3PENT)**, in that four guests and four hosts form a host-guest ring, $R_8^8(16)$, and the rings are bridged by a pair of host molecules. The resulting chains are shown in Figure 7 and run along [100].
The packing is similar to that of the **H1•2(1-propanol)** (IFAHOM) structure which was previously published by Edwin Weber.

H1•2(2PENT), crystallises in $P\bar{1}$, Z = 1, with one host on a centre of symmetry at Wyckoff position *a*. The guest is disordered over two positions and the packing is similar to that of structures **H1•2(3MBUT)** and **3H1•6(3PENT)**, with the host-guest chains running along [100].

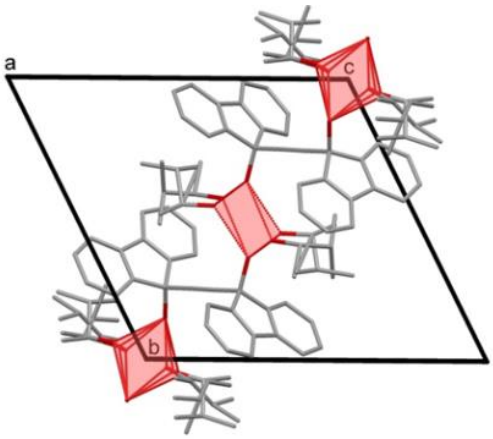

Figure 4.6. H1•2(3MBUT) viewed down [100] with $R_4^4(8)$ hydrogen bond motif shaded in red.

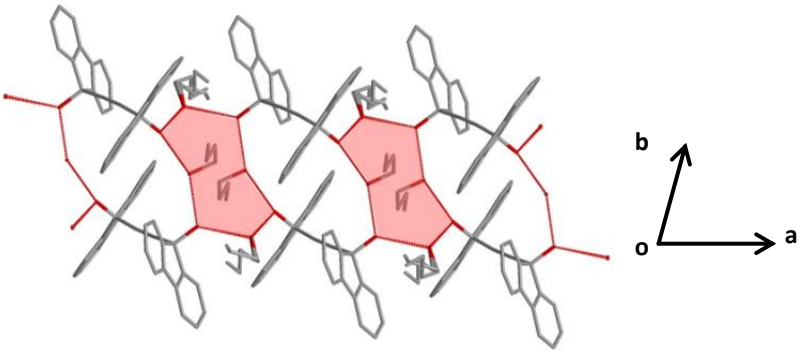

Figure 4.7. H1•2(1BUT) with $R_8^8(16)$ hydrogen bond motif shaded in red.

4.4.2 Selectivity.

A series of competition experiments was carried out at 300 K where equimolar binary mixtures of the four alcohols under investigation were exposed to the host molecule.

The solutions were allowed to crystallise, and the ensuing crystals were analysed by gas chromatography- headspace (GC) or ^{1}H NMR spectroscopy. The results of the competition experiments are given in Table 4.3; we estimate the experimental errors to be ± 2% for GC and ± 5% for NMR.
The preference of this host for the four alcohols is therefore: **3PENT > 2PENT > 3MBUT > 1BUT**.

Table 4.3. Competition experiment results.

Starting mother liquor (50/50)	Method	End crystals mol %
3PENT / 3MBUT	GC	**80/20**
2PENT / 3MBUT	NMR | GC	**74/26 | 68/32**
2PENT / 1BUT	GC	**98/2**
3MBUT / 1BUT	GC	**85/15**
3PENT / 2PENT	NMR | GC	**63/37 | 63/37**
3PENT / 1BUT	GC	**98/2**

We subjected the four inclusion compounds to thermal analysis, with results shown in Table 4.4.
The corresponding DSC and TGA profiles are shown in Figures 4.8a and 4.8b. The DSC curves display an initial endotherm due to the guest loss followed by an endotherm associated with the melting of the residual host.

Table 4.4. Thermal analysis results.

Compound	TG exp (%)	TG calc (%)	DSC T_{peak} (°C)	DSC T_{melt} (°C)
3H•6(3PENT)	31.1	31.3	103.3	252.1
H•2(2PENT)	31.0	31.3	92.3	251.8
H•2(3MBUT)	31.1	31.3	86.7	251.9
H•2(1BUT)	26.6	27.7	47.3 & 78.5	244.6 & 251.5

The guest-loss endotherms are broad and the peak temperatures T_{peak} are reported instead of the onset values T_{on}. The T_{peak} values are a measure of the thermal stability of the inclusion compound, and it is gratifying that they follow the same sequence that was observed from the competition experiments.

The melting endotherm for **H1•2(1BUT)** shows two peaks which are probably due to a polymorphic change.

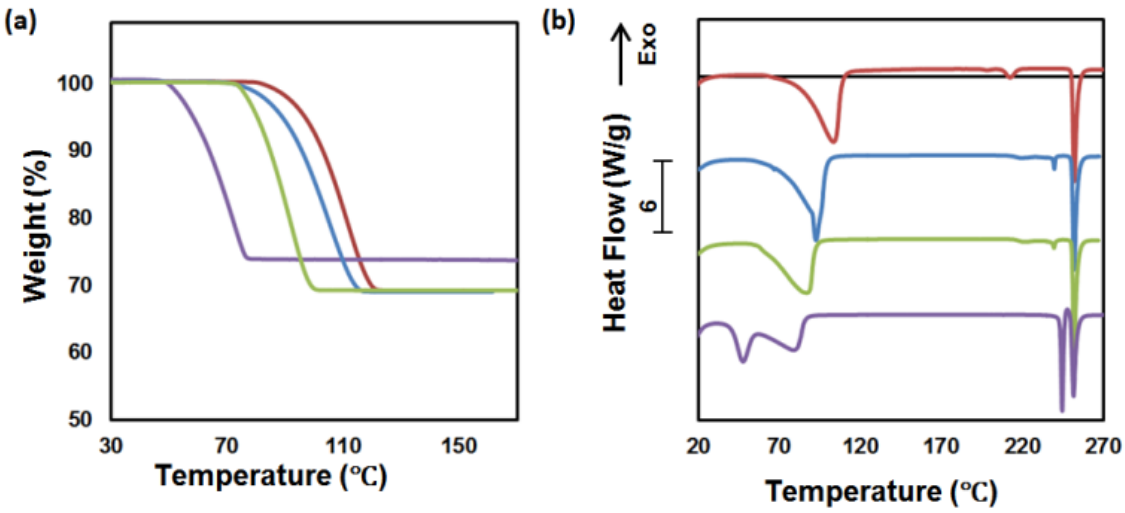

Figure 4.8. (a) TGA traces and (b) DSC traces for compounds **3H1·6(3PENT)** (red), **H1•2(2PENT)** (blue), **H1•2(3MBUT)** (green), and **H1•2(1BUT)** (purple).

The competition experiments and the TG/ DSC results both yield the sequence of preferential selectivity by the host for the guest alcohols. Intuitively one may surmise that the packing is more efficient for the guest of first preference and that the corresponding structure has the lowest (most negative) lattice energy. The packing may be analysed qualitatively using the Crystal Explorer programme[4.30 - 4.32]. However, lattice energy calculations were not carried out because the guest molecules showed considerable disorder, rendering atom to atom potential calculations invalid.

The fingerprint plot derived from the Hirshfeld surface for the **H1•2(2PENT)** structure is shown in Figure 4.9a. This is similar to those calculated for **3H•6(3PENT)** and **H1•2(3MBUT)**. The plot for the **H1•2(1BUT)** (Figure 4.9b) structure is similar in that

both display two spikes due to the two O-H···O hydrogen bonds, but the peak labelled ① occurs at the sum of the external + internal contacts at 2.2 Å for **H·2(2PENT)** and 2.4 Å for **H1•2(1BUT)**. In addition, the % of H···H contacts are 63.8% and 55.8% for **H1•2(2PENT)** and **H1•2(1BUT)** respectively, indicating a looser packing for **H1•2(1BUT)**.

(a) **(b)**

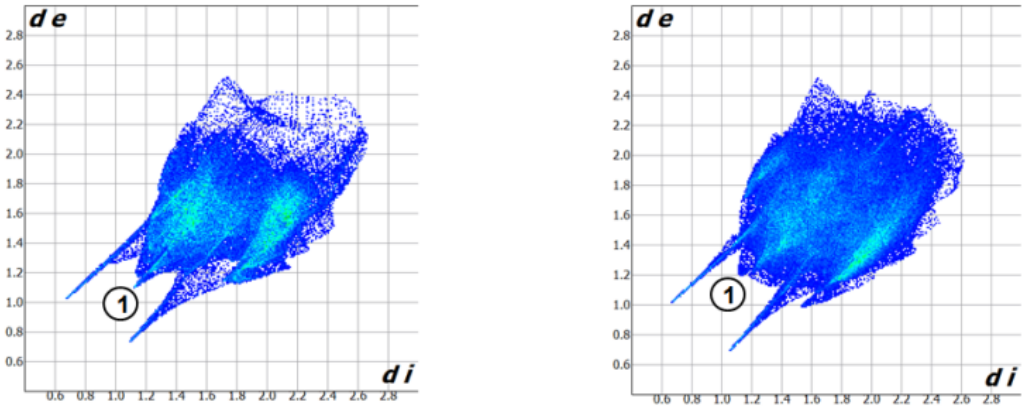

Figure 4.9. 2D fingerprint plots for (a) **H1•2(2PENT)** and (b) **H1•2(1BUT)**.

4.5 CONCLUSION

The host compound **H1**, 9,9'-(ethyne-1,2-diyl)-bis(fluoren-9-ol), yields two polymorphs of the apohost which exhibit both *cis*- and *cis*-/*trans*- conformations having similar lattice energies. Competition experiments conducted between pairs of alcohols with close boiling points showed that the selectivity preference was **3PENT** > **2PENT** > **3MBUT** > **1BUT**. The hydrogen bonding exhibited by the structures which contain the secondary alcohols is different from that with 1-butanol as guest.

4.6 REFERENCES

4.1. B. A. Nogueira, C. Castiglioni and R. Fausto, Color polymorphism in organic crystals, *Commun Chem*, 2020, **3**, 1–12.

4.2. A. J. Cruz-Cabeza and J. Bernstein, Conformational Polymorphism, *Chem. Rev.*, 2014, **114**, 2170–2191.

4.3. A. Nangia, Conformational Polymorphism in Organic Crystals, *Acc. Chem. Res.*, 2008, **41**, 595–604.

4.4. L. R. Nassimbeni, Physicochemical Aspects of Host–Guest Compounds, *Acc. Chem. Res.*, 2003, **36**, 631–637.

4.5. A. M. Pivovar, K. T. Holman and M. D. Ward, Shape-Selective Separation of Molecular Isomers with Tunable Hydrogen-Bonded Host Frameworks, *Chem. Mater.*, 2001, **13**, 3018–3031.

4.6. N. B. Báthori and L.R. Nassimbeni, *Supramolecular Chemistry: From Molecules to Nanomaterials*, ed. P. Gale, J. Steed, Wiley, Chichester, 2012, vol. 6, p.p. 3009-3016.

4.7. A. Jacobs, L. R. Nassimbeni, K. L. Nohako, H. Su and J. H. Taljaard, Inclusion with Mixed Guests: Structure and Selectivity, *Cryst. Growth Des.*, 2008, **8**, 1301–1305.

4.8. Adapted from D. W. Breck, Zeolite Molecular Sieves, 1974, Wiley, New York.
4.9. T. le Roex, L. R. Nassimbeni and E. Weber, Clathrates with mixed guests, *Chem. Commun.*, 2007, 1124–1126.
4.10. L. Nassimbeni, G. Ramon and E. Weber, Inclusion by a fluorenyl diol host with substituted pyridines: Structures, selectivity and kinetics of desorption, *J. Therm. Anal. Calorim.*, 2007, **90**, 31–37.
4.11. A. Jacobs, L. R. Nassimbeni, K. L. Nohako, G. Ramon and B. K. Sebogisi, Inclusion of Caffeine by a Diol Host, *J. Chem. Crystallogr.*, 2011, **41**, 610–616.
4.12. N. M. Sykes, H. Su, E. Weber, S. A. Bourne and L. R. Nassimbeni, Selective Enclathration of Methyl- and Dimethylpiperidines by Fluorenol Hosts, *Cryst. Growth Des.*, 2017, **17**, 819–826.
4.13. E. Weber, S. Nitsche, A. Wierig and I. Csöregh, Inclusion Compounds of Diol Hosts Featuring Two 9-Hydroxy-9-fluorenyl or Analogous Groups Attached to Linear Spacer Units, *Eur. J. Org. Chem.*, 2002, **2002**, 856–872.
4.14. APEX 2, Version 1.0-27; Bruker AXS Inc.; Madison, WI, 2005.
4.15. SAINT-Plus, Version 7.12; Bruker AXS Inc.: Madison, Wisconsin, USA, 2004.
4.16. G. M. Sheldrick. *SADABS: Program for Area Detector Adsorption Correction*; University of Göttingen: Germany, 1997; pp. 33-38.
4.17. G. M. Sheldrick *SHELX-97: Program for Crystal Structure Solution and Refinement*; University of Göttingen: Germany, 1997; p 1456.
4.18. L. J. Barbour, X-Seed — A Software Tool for Supramolecular Crystallography, *Supramol. Chem.*, 2001, **1**, 189–191.
4.19. M. Lusi and L. J. Barbour, Determining Hydrogen Atom Positions for Hydrogen Bonded Interactions: A Distance-Dependent Neutron-Normalized Method, *Cryst. Growth Des.*, 2011, **11**, 5515–5521.
4.20. C. F. Macrae, I. J. Bruno, J. A. Chisholm, P. R. Edgington, P. McCabe, E. Pidcock, L. Rodriguez-Monge, R. Taylor, J. Van De Streek and P. A. Wood, Mercury CSD 2.0– new features for the visualization and investigation of crystal structures, *J. Appl. Crystallogr.*, 2008, **41**, 466–470.
4.21. G. Gilli and P. Gilli, *The Nature of the Hydrogen Bond: Outline of a Comprehensive Hydrogen Bond Theory*, Oxford University Press, Oxford, 2009.
4.22. G. R. Desiraju and T. Steiner, *The Weak Hydrogen Bond: In Structural Chemistry and Biology*, Oxford University Press, 1999.
4.23. A. D. Becke, Density-functional thermochemistry. III. The role of exact exchange, *J. Chem. Phys.*, 1993, **98**, 5648–5652.
4.24. C. Lee, W. Yang and R. G. Parr, Development of the Colle-Salvetti correlation-energy formula into a functional of the electron density, *Phys. Rev. B*, 1988, **37**, 785–789.
4.25. P. J. Stephens, F. J. Devlin, C. F. Chabalowski and M. J. Frisch, Ab Initio Calculation of Vibrational Absorption and Circular Dichroism Spectra Using Density Functional Force Fields, *J. Phys. Chem.*, 1994, **98**, 11623–11627.
4.26. F. Weigend and R. Ahlrichs, Balanced basis sets of split valence, triple zeta valence and quadruple zeta valence quality for H to Rn: Design and assessment of accuracy, *Phys. Chem. Chem. Phys.*, 2005, **7**, 3297–3305.
4.27. S. Grimme, J. Antony, S. Ehrlich and H. Krieg, A consistent and accurate ab initio parametrization of density functional dispersion correction (DFT-D) for the 94 elements H-Pu, *J. Chem. Phys.*, 2010, **132**, 154104.

4.28. S. Grimme, S. Ehrlich and L. Goerigk, Effect of the damping function in dispersion corrected density functional theory, *J. Comput. Chem.*, 2011, **32**, 1456–1465.
4.29. Gaussian 09, Revision A.02, M. J. Frisch, G. W. Trucks, H. B. Schlegel, G. E. Scuseria, M. A. Robb, J. R. Cheeseman, G. Scalmani, V. Barone, G. A. Petersson, H. Nakatsuji, X. Li, M. Caricato, A. Marenich, J. Bloino, B. G. Janesko, R. Gomperts, B. Mennucci, H. P. Hratchian, J. V. Ortiz, A. F. Izmaylov, J. L. Sonnenberg, D. Williams-Young, F. Ding, F. Lipparini, F. Egidi, J. Goings, B. Peng, A. Petrone, T. Henderson, D. Ranasinghe, V. G. Zakrzewski, J. Gao, N. Rega, G. Zheng, W. Liang, M. Hada, M. Ehara, K. Toyota, R. Fukuda, J. Hasegawa, M. Ishida, T. Nakajima, Y. Honda, O. Kitao, H. Nakai, T. Vreven, K. Throssell, J. A. Montgomery, Jr., J. E. Peralta, F. Ogliaro, M. Bearpark, J. J. Heyd, E. Brothers, K. N. Kudin, V. N. Staroverov, T. Keith, R. Kobayashi, J. Normand, K. Raghavachari, A. Rendell, J. C. Burant, S. S. Iyengar, J. Tomasi, M. Cossi, J. M. Millam, M. Klene, C. Adamo, R. Cammi, J. W. Ochterski, R. L. Martin, K. Morokuma, O. Farkas, J. B. Foresman, and D. J. Fox, Gaussian, Inc., Wallingford CT, 2016.
4.30. M. A. Spackman and D. Jayatilaka, Hirshfeld surface analysis, *CrystEngComm*, 2009, **11**, 19–32.
4.31. S. K. Wolff, D. J. Grimwood, J. J. McKinnon, M. J. Turner, D. Jayatilaka, M. A. Spackman. Crystal Explorer (Version 3.1), University of Western Australia, 2010.
4.32. M. J. Turner, J. J. McKinnon, D. Jayatilaka and M. A. Spackman, Visualisation and characterisation of voids in crystalline materials, *CrystEngComm*, 2011, **13**, 1804–1813.
4.33. A. Gavezzotti, Calculation of Intermolecular Interaction Energies by Direct Numerical Integration over Electron Densities. I. Electrostatic and Polarization Energies in Molecular Crystals, *J. Phys. Chem. B*, 2002, **106**, 4145–4154.
4.34. A. Gavezzotti, Calculation of Intermolecular Interaction Energies by Direct Numerical Integration over Electron Densities. 2. An Improved Polarization Model and the Evaluation of Dispersion and Repulsion Energies, *J. Phys. Chem. B*, 2003, **107**, 2344–2353.
4.35. M. C. Etter, J. C. MacDonald and J. Bernstein, Graph-set analysis of hydrogen-bond patterns in organic crystals, *Acta Cryst. B*, 1990, **46**, 256–262.

CHAPTER 5
Crystallisation temperature control of stoichiometry and selectivity in host–guest compounds

By Nicole M. Sykes, Hong Su, Edwin Weber, Susan A. Bourne, and Luigi R. Nassimbeni
In *CrystEngComm*, 2017, **19**, 5892–5896. Published 18 September 2017

2018 – year 3 – Summering in Switzerland

(a) 2 July, at the Swiss Light Source electron synchrotron , where I helped collect over 30 structures during an 8-hour shift. (b) 29 August, poster presentation after three months as a Next Generation Scientist (NGS) intern at Novartis. (c) and (f) 30 June with Ana, Cintia, Alet and Ireen (South Africa) we drove to Riquewihr, a small Alsace town, serendipitously on the day of this Venetian parade. (d) with fellow NGS interns Ana (Brazil) and Cintia (Argentina) off to float down the Rhine on our Wickelfisch (e) 18 August, with Marian (the Philippines) and Mary (Ghana) on the bridge between Rheinfelden (Germany) and Rheinfelden (Switzerland). (g) 29 August, all the interns together on our last day. (h) 13 July, with UCT Prof Neil Ravenscroft one Friday afternoon in Zurich. (i) 11 July, posing with my UCT fellow, Dickson (Zambia), at the University of Basel pharmacy museum.

5.1 SYNOPSIS

This chapter presents the continued study on the same diol host (**H1**) used in chapters 3 and 4, and the compounds formed with alcohols as guests. Here studied is the effect of the crystallisation temperature on the separation by **H1** of 2-propanol (**2-PROP**) and tertiary butanol (**t-BUT**), which have practically the same normal boiling points (82.2 °C vs 82.6 °C).

Six new inclusion compounds were successfully synthesized, and their structures elucidated via single crystal X-ray crystallography. The inclusion compounds, with one exception (where the structure additionally contains one molecule of solvent) can be categorised into one of three phases, corresponding to their guest/host ratio and the conformation displayed by the host molecules.

Crystallising the host from **2-PROP** at different temperatures yielded two similar inclusion compounds. Both structures were labelled as "phase 1", having a guest/ host ratio of 1⅓ and a unit cell containing two *trans* and two *cis* host molecules.

H1 crystallised from **t-BUT** yielded host-guest compounds with two distinct phases. At a higher temperature of crystallisation, the resultant inclusion compound has a "phase II" structure, with a guest/host ratio equal to 2 and with host molecules displaying the *trans* conformation only. However, when a solution of **H1** and tertiary butanol was left to evaporate at room temperature, the resultant inclusion compound's structure is of "phase III". The structure also contains only *trans* hosts, but with the guest/host ratio increased to 4. This agrees with the many reports that the guest/host ratio of inclusion compounds increases as the temperature of crystallisation is decreased.

Inspired by the work of Huskić et al, a custom PXRD sample holder was built in house by which the kinetics of inclusion by vapour sorption was monitored for the reaction of **H1** with **t-BUT** at room temperature. The resulting material was of phase III, and so matches the compound obtained when **H1** is exposed to liquid **t-BUT** at the same temperature.

The most interesting results were recorded when the host was crystallised from equimolar mixtures of **2-PROP** and **t-BUT** at various temperatures. At a high temperature of crystallisation, the ensuing material was determined to have a "phase I" structure, and contained equal amounts of **2-PROP** and **t-BUT**. However, when the crystallisation temperature was lowered, the ensuing crystals were determined to have a "phase II" structure with improved selectivity – containing mostly **t-BUT** (90%). Lowering the temperature of crystallisation even further did not improve the host's preference for tertiary butanol, but did yield crystalline material with a "phase III" structure and a guest/host ratio = 4.

5.2 INTRODUCTION

One of the important uses of host-guest chemistry is to synthesise host compounds which are selective to a particular guest molecule in a mixture of guests. This is most important when the guest molecules have similar structures and comparable boiling points, rendering standard distillation methods ineffective for the purposes of separation, and providing strong motivation for host design.

The process of host-guest selectivity is based on the phenomenon of molecular recognition, a topic that has attracted considerable attention, and has been reviewed by several authors, particularly in respect to crystal engineering and supramolecular chemistry. [5.1 - 5.3]

The specificity of non-covalent interactions is what gives rise to selectivity of a host for a particular guest and the quantitative difference between two such guests may be subtle, as may occur between isomers. In this work we investigate the changes in selectivity as a function of the temperature of crystallisation from the host-guest mother liquor. The variation of temperature of crystallisation on the guest: host ratio in inclusion compounds is known[5.4 - 5.7], but its effect on selectivity has not received extensive attention.

We present the preparation, structure, and selectivity of inclusion compounds by the host 9,9'-(ethyne-1,2-diyl)bis(fluoren-9-ol), **H1**, with two guests of similar boiling points: 2-propanol (**2-PROP**, b.p. 82.6 °C) and tertiary butanol (**t-BUT**, b.p. 82.2 °C) shown in Scheme 5.1.

This host has been employed in the synthesis of several inclusion compounds and has proved useful in the separation of picoline isomers[5.8], methylated piperidines[5.9] and various alcohols.[5.10] As this host has shown its utility for separation of close isomers, we chose to use it in this study on the dependence on crystallisation temperature of the separation of **2-PROP** and **t-BUT**. In addition to the phases obtainable by crystallisation we studied the kinetics of transformation on uptake of a guest vapour by the apohost, using a specially developed sample holder to carry out *in situ* experiments.

The structures of two polymorphs of the apohost have been previously elucidated[5.10]; these displayed two distinct conformations as defined by the O-C-C-O torsion angle, which may be ≈ 0° (cis-) or ≈ 180° (trans-).

Scheme 5.1. Host and Guest Compounds

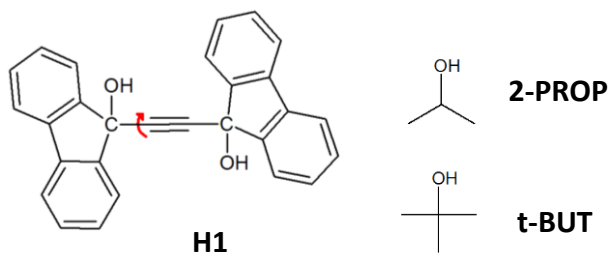

H1

5.3 EXPERIMENTAL

5.3.1 Materials.

The host compound 9,9'-(ethyne-1,2-diyl)bis(fluoren-9-ol), **H1** was synthesized by Weber[5.11] and used without further purification. The alcohol guests were purchased from Sigma Aldrich and used as received. Single crystals of the inclusion compounds were obtained by dissolving **H1** in chloroform and adding an excess of the guest or binary guest mixture. The resulting solutions were filtered and allowed to crystallise at various temperatures. Heating mantles were used to achieve the temperatures of +30 °C and +50 °C and vials were left open to slowly evaporate. This is acceptable given that the vapour pressures of the two guests are so similar; at 20 °C the vapour pressure of 2-propanol is 4.24 kPa and that of tertiary butanol is 3.98 kPa. At the lower temperatures vials were capped and sealed with parafilm; +5 °C and -20 °C were realised by using a standard fridge and freezer. The low temperatures of -41 °C and -61 °C were achieved by allowing solutions to crystallise in a slurry of acetonitrile/ dry ice and chloroform/dry ice respectively.

5.3.2 X-ray Crystallography.

Single crystal X-ray diffraction data were collected on a Bruker DUO APEX II[5.12] diffractometer for all structures using Mo Kα (λ = 0.71073 Å) at a temperature of 153 K. The intensity data were collected using the phi scan and omega scan techniques, scaled and reduced with SAINT-Plus.[5.13] The correction of the collected intensities for absorption was done using the SADABS program.[5.14]

The structures were solved by direct methods using SHELX-97[5.15] and refined using full-matrix least squares methods in SHELXL.[5.15] The graphical interface used was the program X-SEED.[5.16] All C-H hydrogen atoms were placed geometrically and with a riding model for their isotropic temperature factors. The O-H hydrogen atoms were located in the final difference electron density map. Their bond lengths were fixed using the formulae suggested by Lusi and Barbour[5.17] who studied the neutron data of the O-H···O systems. Diagrams were generated using MERCURY (3.9).[5.18]

Powders were mounted on a flat zero-background sample holder. X-ray powder data were collected in a Bruker D8 Advance X-ray diffractometer with copper radiation (Cu Kα, λ = 1.5406 Å) at 30 kV and 40 mA. Each sample was scanned between 4 and 32° 2θ with a step size of 0.02°.

5.3.3 ^{1}H Nuclear Magnetic Resonance (NMR) Spectroscopy.

^{1}H NMR spectra were recorded on a Bruker 300MHz with DMSO as internal standard. Samples were blotted dry, crushed, and dissolved in deuterated d6-DMSO. The appropriate CH_3 signals were integrated to determine the relative proportions of the guests.

5.4 RESULTS AND DISCUSSION

The structures of the inclusion compounds with the pure guests **2-PROP** and **t-BUT**, as well as those obtained from their equimolar mixtures, were characterised by single crystal and powder X-ray diffraction and the relative guest quantities obtained from the competition experiments were determined by ^{1}H Nuclear Magnetic Resonance (NMR) spectroscopy. The crystallisation experiments were carried out at the following temperatures: -61 °C, -41 °C, -20 °C, +5 °C, +30 °C, and +50 °C and are summarised in Table 5.1. Host-Guest structures give rise to different phases, labelled **I**, **II** and **III**. Structures which have the same phase possess the same G/H ratio and display similar Powder X-ray Diffraction (PXRD) patterns.

Table 5.1. Summary of results

	2-PROP			**t-BUT**			**Equimolar Competition**			
Temp (°C)	Structure no.	Phase	G/H	Structure no.	Phase	G/H	Structure no.	Phase	G/H	2-PROP/ t-BUT
+50	**5.1**	I	$1\frac{1}{3}$	**5.2**	II	2	**5.3**	I	$1\frac{1}{3}$	50/50
+30	**5.1**	I	$1\frac{1}{3}$	**5.4**	III	4	-	I & II	Various	50/50 - 10/90
+5		-		**5.4**	III	4	**5.2**	II	2	10/90
-20	a) **5.5** b)**5.6**	a)atypical b) I	a) 2 b)$1\frac{1}{3}$		-		**5.2**	II	2	10/90
-41		-			-		-	II & III	Various	10/90
-61		-			-		**5.4**	III	4	10/90

Structure **5.1**, phase **I**, was obtained by crystallising the host **H1** in **2-PROP** at 50 °C. The resulting compound crystallises in $P\bar{1}$ with six **H1** and eight **2-PROP** molecules per unit cell. The G/H ratio is $1\frac{1}{3}$, and the asymmetric unit contains one *trans*- and two *cis*-host molecules. This and the hydrogen bonding pattern are shown in Figure 5.1.

Structure **5.2**, phase **II**, obtained at 50 °C from **H1** and **t-BUT**, crystallises in $P\bar{1}$ with one host and two **t-BUT** molecules. The host is located on a centre of inversion at Wyckoff position *h* and is therefore *trans*.

The packing is dominated by a series of (Host)O-H···O-H(Guest) rings linked by host molecules, described as $R_4^4(8)$ in Etter's Graph Set Notation.[5.19] This is shown in Figure 5.2.

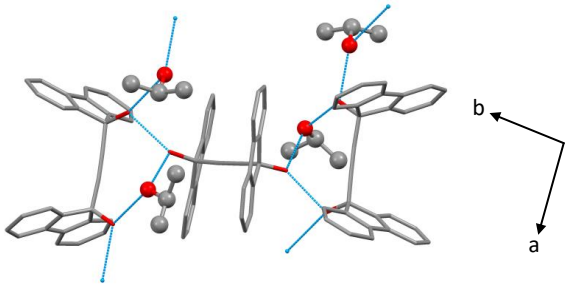

Figure 5.1. Structure **5.1**, phase **I**, asymmetric unit with hydrogen bonded chains along [1 0 0] shown in blue.

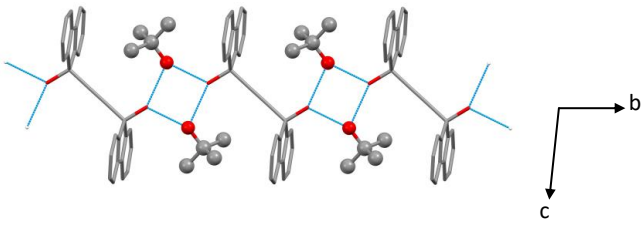

Figure 5.2. Structure **5.2**, phase **II**, with hydrogen bonded Host and Guest molecules forming a ring which propagates along [0 1 0] (blue).

At 30 °C, the result of the host crystallisation with **2-PROP** yielded the same result as structure **5.1**. This was ascertained by PXRD.

Structure **5.4**, phase **III**, was grown at 30 °C from the host in **t-BUT**. It crystallises in $P\bar{1}$ with Z = 1 and **H1** located on $\bar{1}$ at Wyckoff position *a*. The G/H ratio is 4 and the packing displays a $R_6^6(12)$ motif shown in Figure 5.3, and this is propagated with chains by the host molecules in a similar manner to structure **2.**

It is interesting to compare the packings of structures **5.2** and **5.4**. Although they have differing G/H ratios of 2 and 4 respectively, the superposition shows the host molecules display similar configurations and close positions of two pairs of the **t-BUT** guests. This is shown in Figure 5.4.

At -20 °C the experiments with **2-PROP** yielded two distinct structures, **5.5** and **5.6**.

Structure **5.5** crystallises in $P\bar{1}$ with the asymmetric unit comprising two **H1** molecules in *cis*-configuration, three **2-PROP** and one chloroform molecules. The packing displays hydrogen- bonded chains linking **2-PROP** and **H1** molecules.

Structure **5.6**, obtained from crystallisation from pure **2-PROP** at the same temperature also crystallises in $P\bar{1}$, and contains both *cis*- and *trans*- molecules, the structure being of phase **I**, but with slight differences in the hydrogen-bonded pattern.

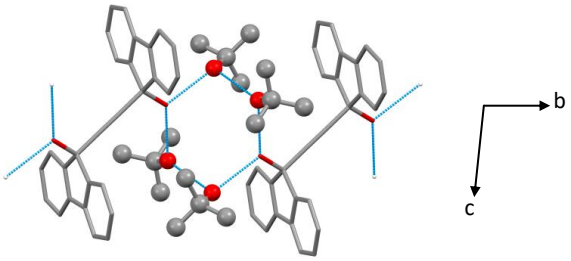

Figure 5.3. Structure **5.3**, phase **III**, with hydrogen bonded rings, forming a chain of Host and Guests along [0 1 0] (blue).

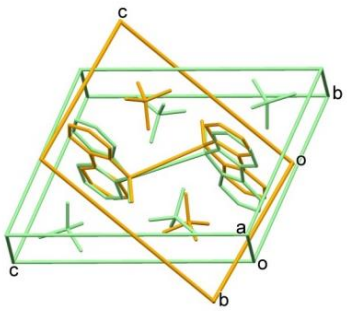

Figure 5.4. Overlay of structure **5.2** (orange) and structure **5.4** (green).

The selectivity experiments carried out at -61 °C, -41 °C, -20 °C and +5 °C all resulted in selectivities of **2-PROP**/**t-BUT** of 10/90 as measured by NMR spectroscopy. The PXRD spectra at -61 °C showed only phase **III** (Figure S8.12 Supplementary Data) and at -41°C revealed a mixture of phase **II** and phase **III**, while those at -20 °C and +5 °C show only phase **II**.

Structure **5.3**, phase **I**, which was crystallised at 50 °C from an equimolar mixture of **2-PROP** and **t-BUT**, is similar to structure **5.1** although one of its cell lengths is halved. The asymmetric unit contains one (*cis*-) host and half a (*trans*-) host molecule. There is one **2-PROP** and **t-BUT** guest molecule, and the G/H ratio is $1\frac{1}{3}$ and the packing is similar. NMR spectroscopy confirmed the ratio of **2-PROP**/**t-BUT** in the bulk crystals to be 50/50. The selectivity thus jumps from 10/90 mole fraction at low temperatures to 50/50 at +50 °C.

The results of the competition experiments carried out at +30 °C were variable; ten experiments were carried out with new vials into which were added fixed masses of host compound, chloroform, and the equimolar mixture of **2-PROP** and **t-BUT**.

The harvested crystals were analysed by NMR spectroscopy and the selectivity results varied from **2-PROP**/**t-BUT** of 10/90 to 50/50.

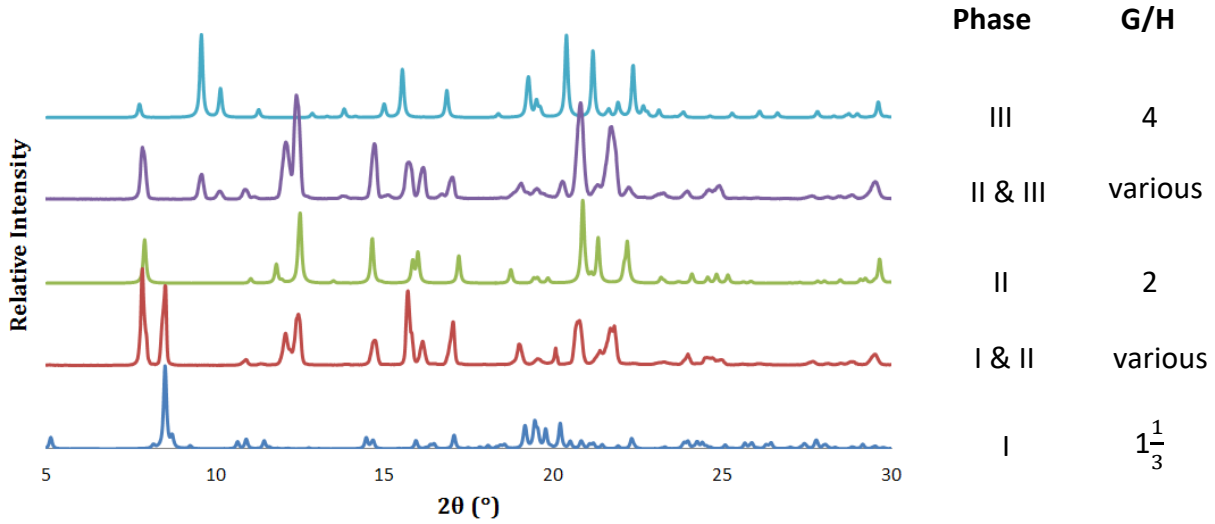

Figure 5.5. Powder X-ray diffraction data of the various phases observed.

Although due care was taken to be consistent in the preparation of these host / solvent / guest mixtures, we cannot account for the variation in selectivity. The details of the NMR and PXRD data are recorded in the Supplementary Information.

We studied the packing of the structures using the programme Crystal Explorer[5.20] and by calculating the lattice energy using Gavezzotti's programme AA-CLP.[5.21, 5.22] Details of these are given in the Supplementary Data; both analyses showed similar interactions and similar lattice energies for each structure. Thus, these analyses did not provide insight into the selectivity observed.

In situ competition experiments were also carried out with the guests in vapour form. These were executed by constructing a sample holder for a Bruker D8 powder X-ray diffractometer similar to that described by Friščić[5.23], in which the powdered sample of the host is placed on a polished Si crystal surface (zero background), shown in Figure 5.6. The powder diffraction traces were recorded at 25 °C and repeated at intervals of 12 min.

In the first experiment, we exposed the apohost to pure **t-BUT** vapour, and the result, shown in Figure 5.7a displays the traces of the apohost as time-resolved peaks, whose colours vary from black (background) through red to yellow (most intense). The red product PXRD trace shown in Figure 7a corresponds to the phase **III**, structure **5.4** compound which has a G/H ratio of 4.

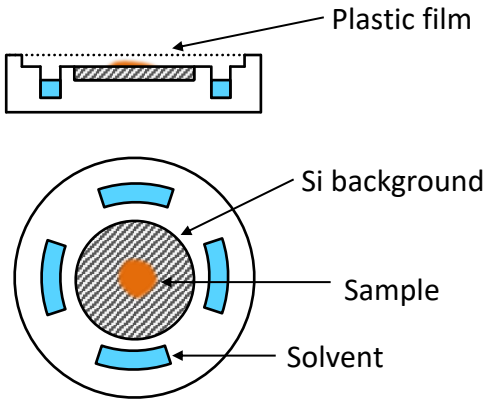

Figure 5.6. Side on and top views of the sample holder[5.23]

The related Figure 5.7b displays time resolved changes in the intensities of the reflection at $2\theta \approx 12.2°$ (apohost) and the (001) reflection of structure **5.4**. Using the intensity data of the apohost peak versus time we obtained the raw kinetic data for the enclathration reaction.

The data were normalised to yield the extent of the reaction versus time curve. This was fitted to the decreasing volume equation:

$$1 - (1-\alpha)^{1/3} = k\,t$$

where α represents the extent of reaction and k is the rate constant for the decay of the apohost phase.[5.24] The rate law held over an α range from 0 to 0.98 with r = 0.990. The kinetic trace yielded a rate constant of 3.7×10^{-3} min^{-1} which corresponds to a half-life of 55.4 min.

In the second and third experiments we demonstrated other changes in phase with **t-BUT** and with the guest mixture which correspond to results obtained from the liquid (Supplementary Information).

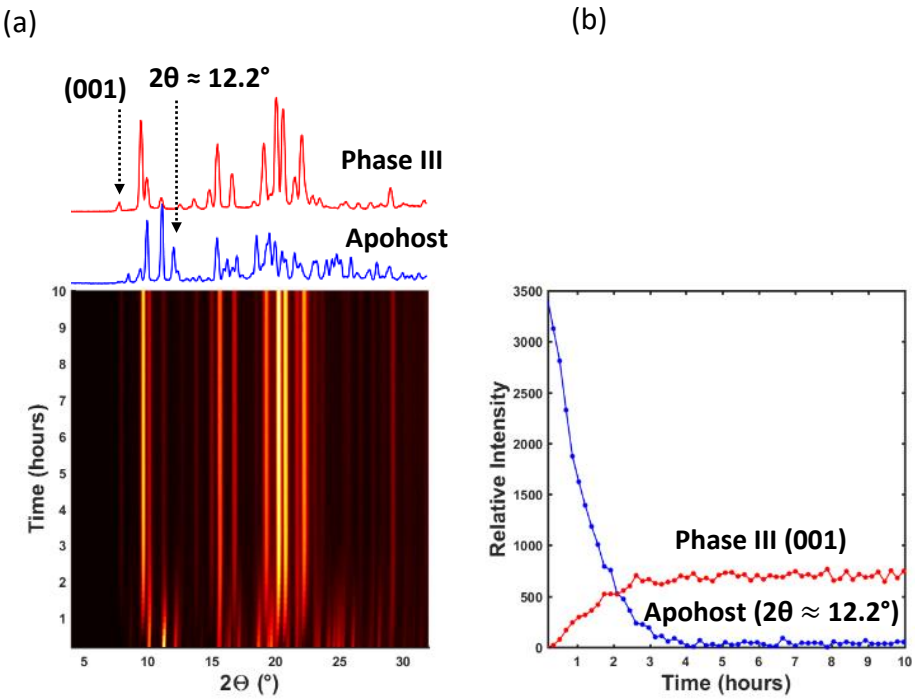

Figure 5.7. (a)Time - resolved *in situ* powder X-ray diffractogram for apohost exposed to **t-BUT** vapour for 10 hours and (b) Time -resolved changes in intensity of X-ray reflection 2θ ≈ 12.2° of the apohost and the (001) reflection of the product which is phase **III**.

5.5 CONCLUSION

In summary, at the low temperature of -61 °C there is a good selectivity with **2-PROP**/**t-BUT** of 10/90 and the concomitant phase **III**. At -41 °C the selectivity remains at 10/90 but both phases **II** and **III** are evident. When the temperature is further raised to -20 °C and +5 °C the selectivity holds at 10/90, but only phase **II** is evident. The high crystallisation temperature of +50 °C displays no selectivity (50/50) and a structure of phase **I.** The variable results obtained at 30 °C fit in between the outcomes at +50 °C and +5 °C and justify the structural results of the mixture of **I** and **II** phases.

5.6 REFERENCES

5.1. G. R. Desiraju, J. J. Vittal and A. Ramanan, *Crystal Engineering: A Textbook*, World Scientific, 2011.

5.2. F. Cramer, *The Lock and Key principle*, ed J-P. Behr, Wiley, Chichester, 1994, Chapter 1.

5.3. E. V. Anslyn and D. A. Dougherty, *Modern Physical Organic Chemistry*, University Science Books, California, 2006, Chapter 3.

5.4. B. Ibragimov, A Simple Correlation between the Structures of Different Crystal Modifications of a Given Host–Guest Complex and their Crystallization Temperatures, *J. Incl. Phenom.*, 1999, **34**, 345–353.

5.5. K. Beketov, E. Weber, J. Seidel, K. Köhnke, K. Makhkamov and B. Ibragimov, Temperature-controlled selectivity of isomeric guest inclusion: enclathration and release of xylenes by 1,1'-binaphthyl-2,2'-dicarboxylic acid, *Chem. Commun.*, 1999, 91–92.

5.6. L. R. Nassimbeni and H. Su, Controlled host:guest ratio in an inclusion compound, *J. Phys. Org. Chem.*, 2000, **13**, 368–371.

5.7. L. R. Nassimbeni and H. Su, Inclusion compounds of a diol host with xylidines: controlled stoichiometries, *Acta Cryst. B*, 2002, **58**, 251–259.

5.8. L. Nassimbeni, G. Ramon and E. Weber, Inclusion by a fluorenyl diol host with substituted pyridines: Structures, selectivity and kinetics of desorption, *J. Therm. Anal. Calorim.*, 2007, **90**, 31–37.

5.9. N. M. Sykes, H. Su, E. Weber, S. A. Bourne and L. R. Nassimbeni, Selective Enclathration of Methyl- and Dimethylpiperidines by Fluorenol Hosts, *Cryst. Growth Des.*, 2017, **17**, 819–826.

5.10. N. M. Sykes, H. Su, E. Weber, S. A. Bourne and L. R. Nassimbeni, Selectivity of aliphatic alcohols by host–guest chemistry, *CrystEngComm*, 2017, **19**, 3682–3688.

5.11. E. Weber, S. Nitsche, A. Wierig and I. Csöregh, Inclusion Compounds of Diol Hosts Featuring Two 9-Hydroxy-9-fluorenyl or Analogous Groups Attached to Linear Spacer Units, *Eur. J. Org. Chem.*, 2002, **2002**, 856–872.

5.12. APEX 2, Version 1.0-27; Bruker AXS Inc.; Madison, WI, 2005.

5.13. SAINT-Plus, Version 7.12; Bruker AXS Inc.: Madison, Wisconsin, USA, 2004.

5.14. G. M. Sheldrick. SADABS: Program for Area Detector Adsorption Correction; University of Göttingen: Germany, 1997; pp. 33-38.

5.15. G. M. Sheldrick SHELX-97: Program for Crystal Structure Solution and Refinement; University of Göttingen: Germany, 1997; p 1456. 1

5.16. L. J. Barbour, X-Seed — A Software Tool for Supramolecular Crystallography, *Supramol. Chem.*, 2001, **1**, 189–191.

5.17. M. Lusi and L. J. Barbour, Determining Hydrogen Atom Positions for Hydrogen Bonded Interactions: A Distance-Dependent Neutron-Normalized Method, *Cryst. Growth Des.*, 2011, **11**, 5515–5521.

5.18. C. F. Macrae, I. J. Bruno, J. A. Chisholm, P. R. Edgington, P. McCabe, E. Pidcock, L. Rodriguez-Monge, R. Taylor, J. Van De Streek and P. A. Wood, Mercury CSD 2.0– new features for the visualization and investigation of crystal structures, *J. Appl. Crystallogr.*, 2008, **41**, 466–470.

5.19. M. C. Etter, J. C. MacDonald and J. Bernstein, Graph-set analysis of hydrogen-bond patterns in organic crystals, *Acta Cryst. B*, 1990, **46**, 256–262.

5.20. M. J. Turner, J. J. McKinnon, S. K. Wolff, D. J. Grimwood, P. R. Spackman, D. Jayatilaka and M. A. Spackman, CrystalExplorer17 (2017). University of Western Australia.
5.21. A. Gavezzotti, Calculation of Intermolecular Interaction Energies by Direct Numerical Integration over Electron Densities. I. Electrostatic and Polarization Energies in Molecular Crystals, *J. Phys. Chem. B*, 2002, **106**, 4145–4154.
5.22. A. Gavezzotti, Calculation of Intermolecular Interaction Energies by Direct Numerical Integration over Electron Densities. 2. An Improved Polarization Model and the Evaluation of Dispersion and Repulsion Energies, *J. Phys. Chem. B*, 2003, **107**, 2344–2353.
5.23. I. Huskić, J.-C. Christopherson, K. Užarević and T. Friščić, In situ monitoring of vapour-induced assembly of pharmaceutical cocrystals using a benchtop powder X-ray diffractometer, *Chem. Commun.*, 2016, **52**, 5120–5123.
5.24. M. E. Brown, in *Introduction to Thermal Analysis: Techniques and applications*, ed. M. E. Brown, Springer Netherlands, Dordrecht, 1988, pp. 1–4.

CHAPTER 6

Enclathration by Werner Hosts: Selectivity and Polymorphism

By Nicole M. Sykes, Hong Su, Susan A. Bourne, and Luigi R. Nassimbeni
In *Cryst. Growth Des.*, 2020, **20**, 1, 274–280 (Published 26 November 2019)

2019 – year 4 – Celebrations

(a) – (c) 11 April, picnic at Kirstenbosch gardens in celebration of Prof. Susan Bourne being chosen as one of twelve IUPAC Distinguished Women in Chemistry award recipients. We presented Susan with framed messages of congratulations and appreciation of her inspiring example. (d) and (g) 17–18 October, celebrating Prof. Luigi Nassimbeni's 80th birthday with a 'crystal' cake made by Alex and Giselle Vicatos. (e) 30 May, with Vice-Chancellor Prof. Mamokgethi Phakeng to receive a research scholarship award. (f) 27 November, celebrating this chapter's publication acceptance. (h) – (i) 12 December, congratulating Emma Tiffin on her MSc graduation.

6.1 SYNOPSIS

This was an invited paper to remember the legacy of Joel Bernstein, a scientist at the forefront of polymorphism research. I heard him talk at the 31st European Crystallographic Meeting (2016) in Basel, Switzerland, and greatly enjoyed his lecture on consulting as an expert witness in patent lawsuits regarding polymorphic forms of active pharmaceutical ingredients.

This chapter investigates the inclusion compounds formed by a Werner type host, $Ni(NCS)_2(4\text{-phenylpyridine})_4$ (**H3**) and 1- and 2-methylnaphthalene (**1-MN** and **2-MN**) guests. The guests' close boiling points, which range from 240–243 °C, make these isomers impractical to separate via distillation.

Four new inclusion compounds with the individual guests were successfully grown and their structures elucidated. Two of these (**6.1** and **6.2**) are a polymorphic pair with **1-MN** as guest, and a guest/host ratio = 4. Initially the first polymorph (**6.1**) crystallises and is coloured blue. After sufficient evaporation the oily **1-MN** guest liquid separates from the methanol co-solvent to form a bubble about crystals of **6.1**. The crystals subsequently transition to the second polymorph (**6.2**) and are coloured purple. Solid-state UV spectra of **6.1** and **6.2** quantified their different colours, and this disparity was attributed to the slight variation in the Ni—N(4-PhPy) bond length between the two compounds.

Another two inclusion compounds were grown (**6.3** and **6.4**) containing **2-MN** as guest. These both had a lower guest/host ratio = 3 (compared to 4 for **1-MN** compounds). However, **6.3** and **6.4** have different molecular formulas and so are not polymorphs. This comes about because structure **6.4** contains a different host – *in situ* a dimer was formed from two **H3** molecules connected via the Ni ion by two bridging NCS ligands - the formula of this 'host' is $Ni_2(NCS)_4(4\text{-phenylpyridine})_6$. The compound (**6.4**) was produced by recrystallising **H3** from a low concentration of **2-MN**. This formation of a host dimer is not unique; there are many examples in the literature of metal ions with pyridine ligands being bridged by NCS ligands to form dimers, [6.1 - 6.3] and even 1D chain [6.4 - 6.9] or 2D sheet [6.10 - 6.13] polymeric structures.

To test the preference of the host to the two guests it was exposed to an equimolar mix of **1-MN** and **2-MN**. The resulting crystals were blue, and unusual in that the structure (**6.5**) was found to contain two methylnaphthalene guests and one methanol solvent molecule for each **H3** molecule - clearly methanol has not acted as a neutral solvent. The NMR result revealed that these crystals comprised a guest mixture of 87% **1-MN** (13% **2-MN**), and **1-MN** was the only guest located in the electron difference density map of the structure. After allowing crystals of **6.5** to remain in the mother liquor for some time the crystals turned from blue to purple. The resulting structure (**6.6**) has a guest/host ratio = 3 and is very similar to structure **6.3** which is the inclusion compound with **2-MN**. However, the NMR result indicates that these crystals of structure **6.6** now contained approximately equal quantities of both **1-MN**

The d orbitals of transition metal ions are split into different energy levels by its ligands. These d electrons absorb photons of light, causing them to "jump" to the higher energy level. When the electrons fall back to their ground state, they release energy with a specific intensity and wavelength, perceived by our eyes as the colour of the material.

and **2-MN**. Here then is an example of a labile host-guest system where the selectivity preference of the host decreases over time and concomitant evaporation of co-solvent.

6.2 INTRODUCTION

Host coordination compounds of general formula MX_2L_4 (Werner clathrates) form inclusion compounds with a wide variety of guests, G, usually an organic aromatic compound. In a Werner clathrate M is a divalent cation (typically Fe, Co, Ni, Cu, Zn), X is an anionic ligand (NCS^-, NCO^-, NO_3^-, halide) and L is a neutral ligand, usually a substituted pyridine. These host compounds are able to absorb various organic guests reversibly and were first used to separate mixtures by Schaeffer et al.[6.14] The physical chemistry of Werner clathrates has been reviewed and their structures, separation capabilities, and thermal properties have been described.[6.15 - 6.17] Early important contributions in this field are attributed to Noman Smith[6.18] who discussed selectivity trends from competitions experiments. Lipkowski[6.19] analysed the thermokinetics of the enclathration reactions of xylenes by the apohost α-$Ni(NCS)_2$(4-methylpyridine)$_4$ and discussed the various concomitant structural and thermodynamic processes.

We have carried out a brief survey of the structures of Werner clathrates which contain $M(NCS)_2L_4$ with M = transition metal, L = 4-methylpyridine, 4-vinylpyridine, 4-phenylpyridine, and other similar bases and their various aromatic guests (CSD 2019 v. 2), which are relevant to this study. There are 200 such structures which have been deposited as Table S6.1 in the Supplementary Information. The guests comprise a variety of aromatic molecules, the most common being derivatives of benzene, various alcohols, and common chlorinated solvents. Table S6.1 contains the CSD REFCODE's, the ligand L and the enclathrated guest. The host $Ni(NCS)_2$(4-methylpyridine)$_4$ remains the most representative (65 structures) with $Ni(NCS)_2$(4-vinylpyridine)$_4$ second (28 structures).

The related coordination compounds based on dibenzoylmethanates have been shown to form a wide variety of inclusion compounds and display polymorphism.[6.20] More recently Lusi and Barbour[6.21] demonstrated that the host $Ni(NCS)_2$(4-phenylpyridine)$_4$ could be employed to separate the isomers of xylene in their vapor phase, and the compound containing isoquinolines as the neutral ligands was crystallised with xylenes, and their kinetics of thermal decomposition were studied.[6.22] A Werner host with mixed ligands, $Ni(NCS)_2$(isoquinoline)$_2$(4-phenylpyridine)$_2$ was employed to study the selectivity of xylene isomers and the host-guest secondary interactions were analyzed.[6.23]

In this work we present the results of the separation of the isomers 1-methylnaphthalene and 2-methylnaphthalene by the host $Ni(NCS)_2$(4-phenylpyridine)$_4$ (**H3**) their structures with the single guests and their selectivity obtained from the guest-competition experiments. We further report on the unusual occurrence of polymorphism in Werner inclusion compounds, with concomitant colour changes of the crystalline products.

The boiling points of the methylnaphthalenes, 240–243 °C and 241–243 °C are too close to allow their separation by fractional distillation, hence the choice of host-guest chemistry to

pursue selective enclathration. The structural formulas of the host and guest molecules are shown in Scheme 6.1.

Scheme 6.1. Host and Guest compounds

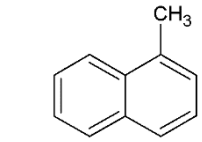

1-methylnaphthalene
1-MN
b.p. = 240–243 °C

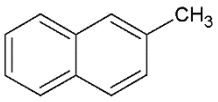

2-methylnaphthalene
2-MN
b.p. = 241–243 °C

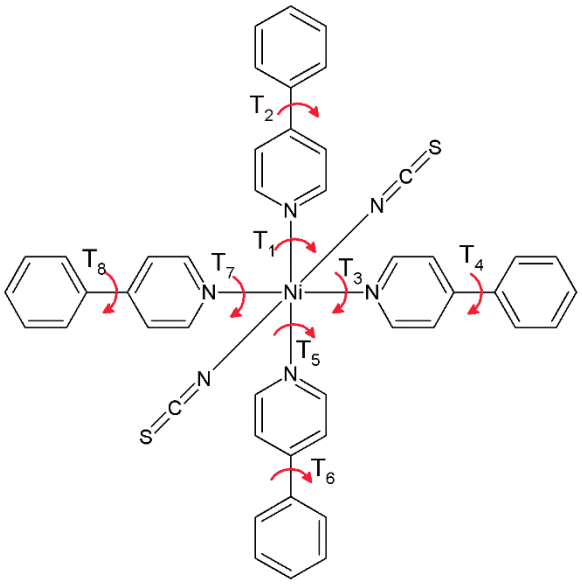

Host **H3** = $Ni(NCS)_2(4\text{-}PhPy)_4$
4-PhPy = 4-phenylpyridine

6.3 EXPERIMENTAL

6.3.1 Materials.

The host compound, **H3**, was synthesized according to a previously published method,[6.24] recrystallised once with methanol and deemed sufficiently pure via thermal gravimetric analysis. Methanol and methylnaphthalene guests were purchased from Sigma Aldrich and used without further purification.

6.3.2 X-ray Crystallography.

Single crystal X-ray diffraction data were collected on a Bruker DUO APEXII diffractometer for all structures using Mo Kα (λ = 0.71073 Å) at a temperature of 173 K. The intensity data were collected using the φ scan and ω scan techniques, scaled, and reduced with SAINT-Plus.[6.25] The correction of the collected intensities for absorption was done using the SADABS program[6.26] XPREP[6.27] was used to process and prepare input files for SHELXT 2014/5[6.28] and SHELXL 2015[6.29] which were used to solve and refine the structures using the X-seed graphical interface.[6.30] All non-hydrogen atoms were refined isotropically or anisotropically depending on the occurrence of disorder in the structures. Some C-C bond lengths in disordered guest molecules were restrained. All C–H hydrogen atoms were placed geometrically and refined with a riding model for their isotropic temperature factors, while the O-H hydrogen atom in MeOH was found in the difference electron density map. Diagrams were generated using

Mercury (3.10).[6.31] The default settings (probe radius of 1.2 Å) was chosen to display void spaces.

6.3.3 Thermal Analysis.

Samples were prepared by removing crystals from mother liquor, blotting dry on filter paper, lightly crushing and weighing directly into open aluminium oxide crucibles in the case of thermogravimetric analysis (TGA) or crimped, vented aluminium pans for differential scanning calorimetry (DSC). 4−10 mg was used for TGA and 1−3 mg for DSC. Experiments were performed over a temperature range of 20−400 °C at a heating rate of 30 min^{-1} under dry nitrogen with a flow rate of 40 cm^3 min^{-1} in the TGA and 60 cm^3 min^{-1} in the DSC. Thermogravimetric analysis was performed using a TA-Q500 thermogravimetric analyser, and differential scanning calorimetry was performed using a Q200 (TA Instruments). TG results were analysed using TA Instruments Universal Analysis 2000 software.

6.3.4 ^{1}H NMR Analysis.

^{1}H NMR spectra were recorded on a Bruker 300MHz with $CDCl_3$ as internal standard. Crystals were blotted dry, crushed, and dissolved in deuterated $CDCl_3$. The host compound is unstable in chloroform, and the resulting solution, enriched in methylnaphthalenes, was filtered into the NMR tube. The CH_3 singlets were integrated in MestReNova (v.6.0.2) to determine the relative proportions of the **1-MN** and **2-MN** guests.

6.3.5 UV-VIS Diffuse Absorbance Spectroscopy.

Solid-state UV-visible absorption spectra were recorded using an Analytik Jena SPECORD 210 PLUS spectrophotometer utilizing the integrating sphere attachment. All data were graphically analysed using the software package WinAspect PLUS 3.9.14.

6.3.6 Microscopy.

Photographs were taken with an Axiocam 105 colour camera attached to a Zeiss SteREO Discovery V8 microscope and processed using the ZEN 2 (blue edition) program (Carl Zeiss Microscopy GmbH, 2011).

6.3.7 Preparation.

Single crystals of inclusion compounds were obtained by dissolving host and guest in methanol (MeOH), filtering solutions into 10 cm^3 vials which were then capped with pierced lids and allowed to evaporate slowly at room temperature.

Structure **6.1**: 10 mg of host **H3** and 60 mg 1-methylnaphthalene (**1-MN**) guest were dissolved in 2 g MeOH and yielded large pale blue needles after two days.

Structure **6.2**: After crystallisation of structure **6.1**, we allowed the mother liquor to evaporate further. After ~14 days **1-MN** oil separates from the remaining MeOH and forms a bubble around crystals which subsequently transform into small pale violet plates over the course of ~ 16 hours.

Structure **6.3**: 10 mg of host **H3** and 120 mg **2-MN** were dissolved in 2 g MeOH which yielded pale violet plates within 4 days.

Structure **6.4**: 10 mg of host **H3** and 15 mg **2-MN** were dissolved in 2 g MeOH, yielding small pale blue crystals after 8 days.

6.3.8 Competition Experiments.

A bulk competition experiment was performed by dissolving 250 mg **H3** and 2.5 g of a 50:50 mixture of the methylnaphthalenes in 50 g MeOH and filtering into a 200 cm^3 beaker, placed in a desiccator with a lid opening of 2.5 cm in diameter.

Structure **6.5**: after 2 days large pale blue block like crystals were removed, the structure refined and allocated as **6.5**.

Structure **6.6**: After 3 weeks crystals began turning from pale blue to pale violet, and a pale violet crystal was chosen at random, and the structure refined as form **6.6**.

6.4 RESULTS AND DISCUSSION

Table 6.1 summarizes the structural and refinement parameters for the six host-guest structures, labelled **6.1** to **6.6**, as well as the calculated and experimental TG mass loss percentages. The refinement parameters of the apohost are included for comparison.

Crystals of structure **6.1** crystallised as pale blue needles from the mother liquor after 2 days. Structure **6.1**, **H3•4(1-MN)** crystallises in $P2_1/c$ with Z = 2. The Ni ion is located at a centre of inversion at Wykoff position *d* (Figure. 6.1). The **1-MN** guests are each disordered over two positions, and the packing is characterized by the host molecules lying in layers in the bc plane, with the guests slotted in the remaining spaces as shown in Figure 6.2.

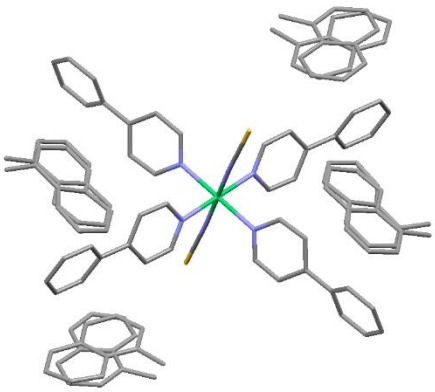

Figure 6.1. the asymmetric unit of structure **6.1** which has been grown to show 1 full host and 4 guest molecules, hydrogen atoms removed for clarity.

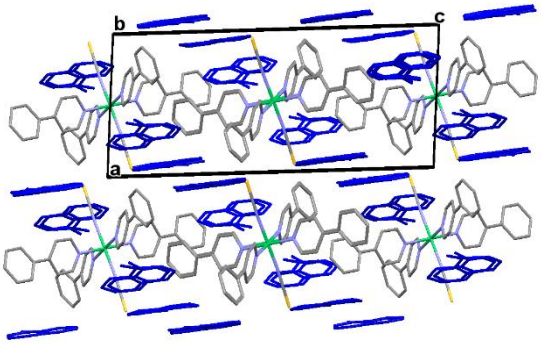

Figure 6.2. packing of structure **6.1** viewed down [010], with H atoms removed, and **1-MN** guest molecules coloured blue for clarity.

After a further 14 days of slow evaporation of the mother liquor, the crystals of **6.1** transformed to pale violet plates of a new polymorph, structure **6.2**. This crystallises in $P\bar{1}$ with Z = 2. This new polymorph retains the host : guest ratio of 1:4, but the host and three of the 1-methylnaphthalenes (disordered) are in general positions. The remaining **1-MN** molecule lies on centres of inversion at Wykoff positions *b* and *c* and their disorders were modelled with site occupancy factors of 0.5. The asymmetric unit is shown in Figure 6.3. The packing is characterized by channels which run in the $[0\bar{1}1]$ direction, shown in Figure 6.4, and contain the **1-MN** guest molecules.

Figure 6.5 is a transmission photograph of the crystals of structure **6.1** (pale blue) which transform into the pale violet polymorph, structure **6.2**, after approximately 16 hours.

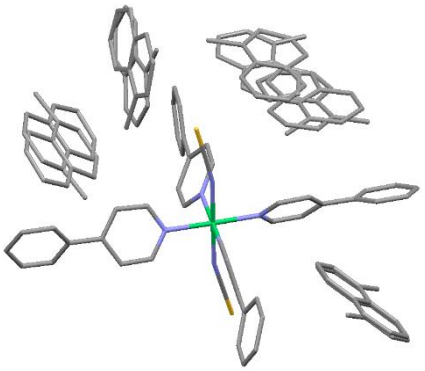

Figure 6.3. asymmetric unit of structure **6.2** with hydrogen atoms hidden, and the two guests lying on inversion centres were grown to show their disorder.

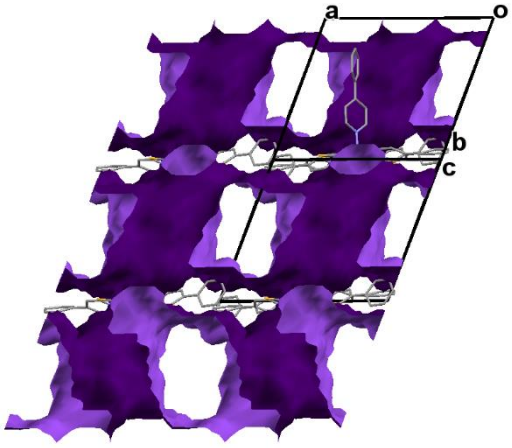

Figure 6.4. structure **6.2** viewed down $[0\bar{1}1]$. The **1-MN** guest molecules were removed.

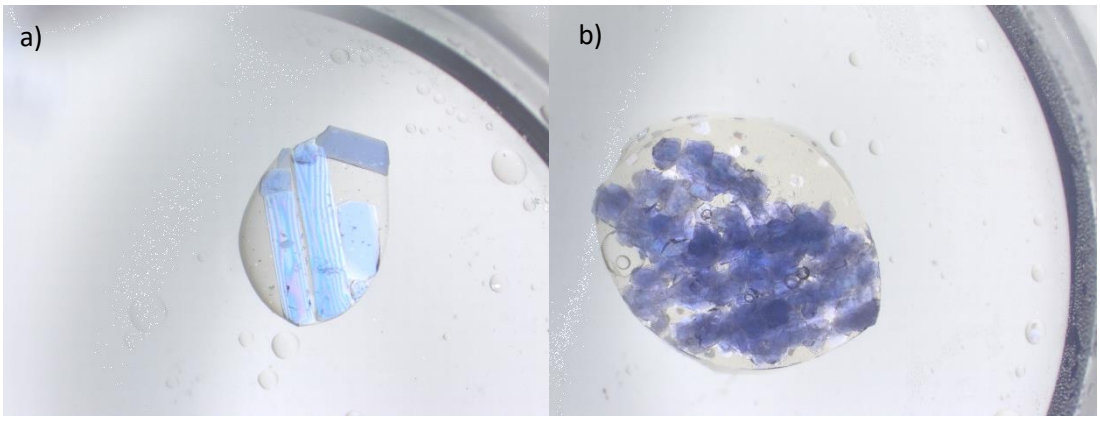

Figure 6.5. 1-MN crystals transforming from pale blue, structure **6.1** (a) to the pale violet polymorph, structure **6.2** (b); photos taken ~16 hours apart.

Table 6.1: Crystallographic and thermal data of compounds **6.1** to **6.6**, and the apohost of **H3**

CCDC refcode	VOVKUP	OVKUP01	VOVLEA	VOVLIE	VOVLOK	VOVLUQ	FOPREH[6.33]
CCDC deposition code	1949658	1949659	1949660	1949661	1949662	1949663	-
compound code	**6.1**	**6.2**	**6.3**	**6.4**	**6.5**	**6.6**	apohost
host	monomer	monomer	monomer	dimer	monomer	monomer	monomer
guest	**1-MN**	**1-MN**	**2-MN**	**2-MN**			-
guest/host	4	4	3	3	2	3	-
compound formula	$C_{90}H_{76}N_6S_2Ni_1$	$C_{90}H_{76}N_6S_2Ni_1$	$C_{79}H_{66}N_6S_2Ni_1$	$C_{103}H_{84}N_{10}S_4Ni_2$	$C_{69}H_{60}N_6O_1S_2Ni_1$	$C_{79}H_{66}N_6S_2Ni_1$	$C_{46}H_{36}N_6S_2Ni_1$
structural moieties (H•nG)	$C_{46}H_{36}N_6S_2Ni_1 \cdot 4(C_{11}H_{10})$	$C_{46}H_{36}N_6S_2Ni_1 \cdot 4(C_{11}H_{10})$	$C_{46}H_{36}N_6S_2Ni_1 \cdot 3(C_{11}H_{10})$	$C_{70}H_{54}N_{10}S_4Ni_2 \cdot 3(C_{11}H_{10})$	$C_{46}H_{36}N_6S_2Ni_1 \cdot 2(C_{11}H_{10}) \cdot HOCH3$	$C_{46}H_{36}N_6S_2Ni_1 \cdot 3(C_{11}H_{10})$	$C_{46}H_{36}N_6S_2Ni_1$
formula weight ($g \cdot mol^{-1}$)	1364.45	1364.45	1222.25	1707.51	1111.09	1222.25	759.36
data collection temp (K)	173	173	173	173	173	173	293
crystal system	monoclinic	triclinic	monoclinic	triclinic	monoclinic	monoclinic	orthorhombic
space group	*P2₁/c*	*P*$\bar{1}$	*C2/c*	*P*$\bar{1}$	*C*2/*c*	*C2/c*	*Pbca*
a (Å)	10.005(1)	14.745(2)	10.227(4)	9.989(5)	28.461(2)	10.291(2)	12.846
b (Å)	15.857(2)	15.099(2)	23.732(8)	12.7512(7)	9.4866(7)	24.070(5)	16.160
c (Å)	22.944(2)	18.590(2)	26.002(9)	17.8175(9)	24.296(2)	26.056(5)	39.377
α (°)	90	78.569(2)	90	94.084(11)	90	90	90
β (°)	93.922(2)	87.219(2)	99.488(7)	90.261(10)	117.330(1)	100.27(3)	90
γ (°)	90	64.594(2)	90	111.727(9)	90	90	90
volume ($Å^3$)	3631.37	3661.18	6224.31	2101.70	5827.66	6350.91	8174.32
Z	2	2	4	1	4	4	8
calc. density ($g \cdot cm^{-3}$)	1.25	1.24	1.30	1.35	1.27	1.28	1.29
θ range (°)	4.389-45.63	4.893-45.25	4.387-46.03	4.962-51.89	4.66-59.40	5.910-56.55	2-50
reflections collected	70068	151801	60510	9758	77172	75085	7948
no data I > 2σ(I)	5607	12573	6180	6269	5663	6158	1788
final R indices [I > 2σ(I)]	0.0856	0.0683	0.0895	0.0768	0.0632	0.0834	0.0691
R indices (all data)	0.1285	0.0995	0.1292	0.1321	0.0805	0.1015	0.0900
goodness of fit on F^2	1.045	1.031	1.053	1.020	1.057	1.039	-
calculated TG mass loss (%)	87.0	87.9	85.4	79.7	84.1	85.4	78.0
experimental TG mass loss (%)	87.2	87.2	85.7	79.5	85.0	86.6	77.2

Structure **6.3** comprises the host **H3** with **2-MN**, with stoichiometry 1:3, and crystallises in the space group *C*2/*c*, forming pale violet crystals with Z = 4. The host thus lies on the diad at Wykoff position *e* and the **2-MN** guests are disordered, one of them located about a centre of inversion at Wykoff position *b*. The packing has the **2-MN** guests located in channels running along [100] as shown in Figure 6.6.

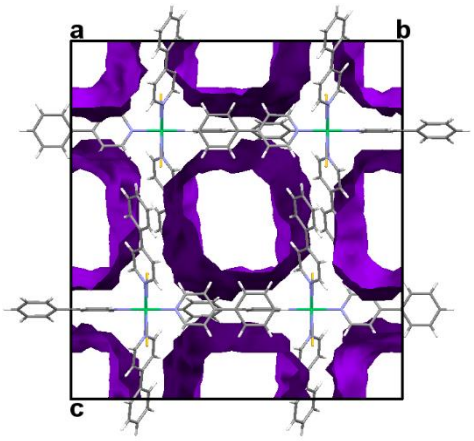

Figure 6.6. packing of structure III viewed down [100], with guest molecules removed. Void spaces have been displayed, showcasing that **2-MN** molecules reside in channels.

Crystals of structure **6.4** are grown via a low concentration of **2-MN**. These were shown to be pale blue host dimers of H: G stoichiometry 1:3; therefore, a different compound was formed. **6.4** crystallises in $P\bar{1}$ with Z = 1, the unit cell comprises one dimer (Figure 6.7) formed about the centre of inversion, Wykoff position *h*, and three **2-MN** guests one of which is disordered over a centre of symmetry at Wykoff position *d*. The packing (Figure 6.8) displays channels along [100] which contain the guests.

a)

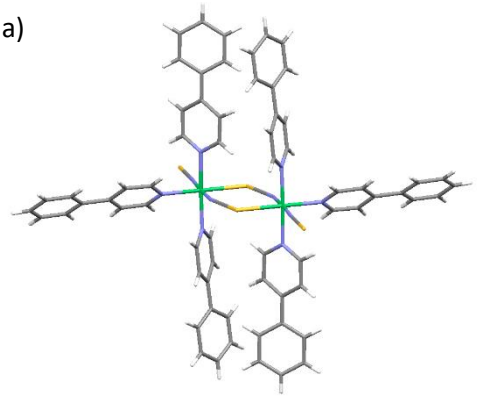

Figure 6.7. host dimer in structure **6.4**.

b)

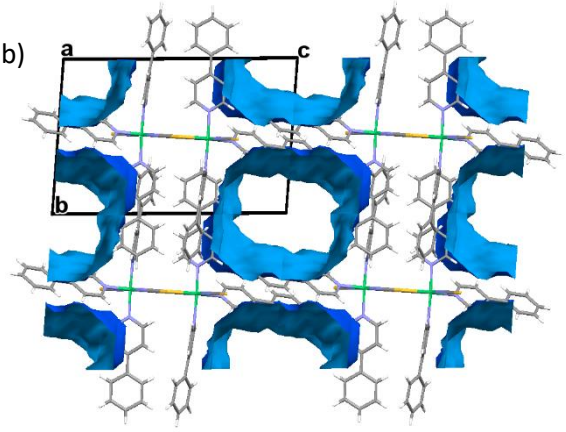

Figure 6.8. packing of structure **6.4** viewed down [100]. Guest molecules have been removed and void space displayed; the **2-MN** guests reside in channels.

Competition experiments yielded crystalline products from mother liquors which initially contained equimolar **1-MN**/**2-MN**, with the initial solution containing host to total equimolar guest of 1: 50. The resulting pale blue crystals were harvested after 4 days and subjected to ^{1}H NMR and single crystal analysis, yielding structure **6.5**. The formula is **H3•2(1-MN)•1(MeOH)** (Figure S6.36 in the Supplementary Information). The space group is *C*2/*c* with Z = 4, and the Ni cation is located on a centre of inversion at Wykoff position *b*. The MeOH molecule was disordered about the diad at Wykoff position *e*. The NMR analysis showed **1-MN** as 87% and **2-MN** as 13%. The former was the only guest located in the difference electron density map and is disordered over two positions. We have noted in previous studies that when the minor guest component less than 15% it is difficult to observe in the final difference electron density map of the structure.

The blue crystals of **6.5** changed colour with time, and after a total of 20 days the crystals had all turned pale violet, and were again harvested. The ^{1}H NMR result was **1-MN**/**2-MN** = 54%/ 46% (Figure S6.25) and the PXRD spectrum (Figure S6.12) indicated that the bulk was a mixture of **6.2** and **6.3**. A single crystal (pale violet) was chosen at random and the structure collected, **6.6**. This structure, **6.6**, has a unit cell which is very close to that of **6.3**, and the torsion angles of the host (Table S6.8, Figure S6.35) and PXRD patterns of the structures (Figure S6.34) are also very similar. It crystallises in *C*2/*c* with the host on a diad at Wykoff position *e*. We assigned one disordered **2-MN** molecule on a centre of inversion at Wykoff position *a*, with site occupancy factors 0.5. We also assigned one full **1-MN** molecule in the ASU, disordered over two positions. The final model required the fixing of U_{iso} for the two C(methyl) atoms of **1-MN**. This corresponds to a ratio of 67% **1-MN** : 33% **2-MN** in this structure. However, it must be noted that the assignment was difficult due to the severe disorder of the guest molecules.
This host-guest system is labile, and while the NMR results are a measure of the bulk host-guest product, the corresponding structure of the chosen single crystal is not representative of the bulk. Its structure displays severe disorder of the **1-MN** and **2-MN** guests and its unit cell parameters are similar to those of **6.3**.

The propensity of Werner host compounds to form inclusion compounds with aromatic guests has been associated with the torsional flexibility of the substituted pyridines ligated to the metal ion. This has been demonstrated by Lipkowski who studied the clathrates formed by the host $Ni(NCS)_2(4\text{-methylpyridne})_4$ with a variety of guests.[6.17]

The crystals of **6.1**, $Ni(NCS)_2(4\text{-PhPy})_4 \cdot 4$(**1-MN**) (pale blue) has the host molecule located on a centre of inversion. In contrast, its violet isomer structure **6.2** crystalizes in $P\bar{1}$ with Z = 2 and the host molecule therefore lies in a general position, with no symmetry restriction. This impinges on the torsion angles governing the pyridine and phenyl moieties which twist to accommodate the 1-methylnaphthalene guests. There are four independent torsion angles in the host of structure **6.1** (pale blue), but eight independent torsion angles on the host of structure **6.2**. The latter has double the degrees of torsional freedom, and it is surmised that this forms the more stable structure, hence the conversion of the from **6.1** (blue) to **6.2** (violet). The colour change from pale blue to pale violet is associated with *d-d* electronic transitions in the nickel ion, and the octahedral geometry of the six ligands surrounding the Ni. The solid-state UV-VIS spectra of the crystals of **6.1** (pale blue) and **6.2** (pale violet) are

shown in Figure 6.9. There is a small shift of the peak maximum for **6.1** (pale blue) 594.6 nm to 585.2 nm for **6.2** (pale violet).

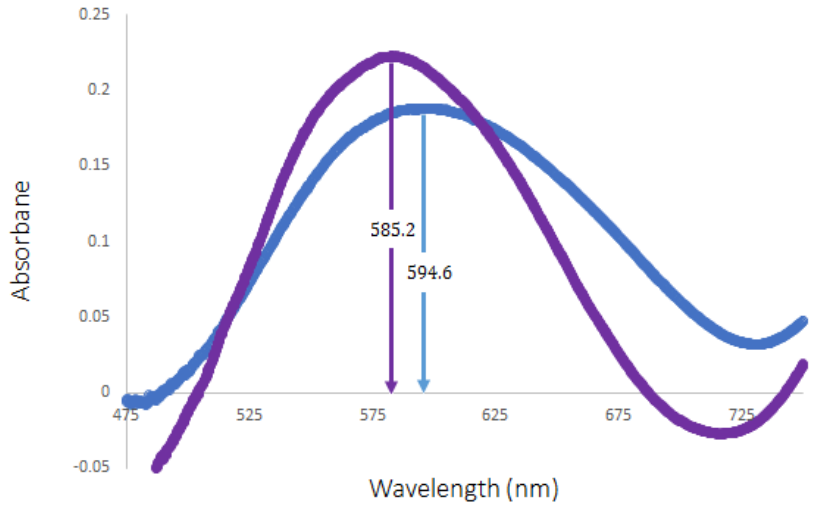

Figure 6.9. absorption UV visible spectra of structure **6.1** (blue) and **6.2** (purple).

We have measured the bond lengths about the octahedral Ni(II) ion for structure **6.1** and **6.2**. The results, reported in the Supplementary Information Table S6.3, have been averaged and summarized as follows:
For **6.1**, Ni-N(NCS) = 2.050(3) Å and Ni-N(4-PhPy) = 2.158(4) Å
For **6.2**, Ni-N(NCS) = 2.053(3) Å and Ni-N(4-PhPy) = 2.132(4) Å
The latter bond lengths are subtly different, and the corresponding shifts in the peaks of the absorbance spectra are correspondingly small.
The twelve N-Ni-N bond angles about the Ni^{2+} ion for structures **6.1** and **6.2** are also recorded (Supplementary Information Table S6.4) and show that there is only one significant deviation from 90° which occurs in structure **6.1**; the angles between the equatorial (4-PhPy)N-Ni-N(4-PhPy) vary as 85.4(1)° and 94.6(1)°.
We studied the overall deviation from ideality in the host molecules of **6.1** and **6.2** by measuring the angle subtended by Ni(II) from the C atom in the para-position of opposite phenyl rings. This is necessarily 180° for **6.1** but varies to as much as 176.2° in **6.2** and 158.5° in the apohost; this is a result of secondary interactions from the molecular packing.

We have also recorded the torsion angles that govern the conformation of the 4-phenylpyridines in **6.1** and **6.2**, deposited in the Supplementary Information, Table S6.5. For structure **6.2** we labelled the torsion angles as N(x)-Ni-N(y1)-C(y2) with x = 1 and y = 1(T1), y= 2(T3), and x = 2, y = 3(T5), y = 4(T7) and their corresponding intraligand torsion angles as C(z3)-C(z4)-C(z11)-C(z12) with z = 1(T2), z= 2(T4), z= 3 (T6), z = 4(T8).[6.32] The host molecules of **6.1** and **6.2** were compared using Mercury's 'Automatic Molecule Overlay' feature, and the corresponding atoms of structure **6.1** were labelled to match **6.2** where possible, taking the symmetry of the molecule into account.

The host molecules have different conformations, and we can summarize the torsion angles for each ligand in pairs as follows:
6.1: -+, +-, +-, -+
6.2: +-, ++, +-, +-
We analysed these differences in torsion angles governing the confirmation of the host molecules in structures **6.1** and **6.2** by measuring close contacts between the atoms in the host phenyl rings and guest and host atoms. This is recorded in the Supplementary Information Table S6.6 and S6.7.

The overlaid host structures in Figure S6.28 show structure **6.1** in blue (centrosymmetric with centre of inversion on Ni ion) and structure **6.2** in purple with no symmetry constraints. One observes that in structure **6.1** the phenyl ring conformation governed by T2 is significantly different from the equivalent ring in structure **6.2**. In structure **6.1** we have noted four close contacts between the host phenyl ring governed by T2 and guest atoms, whereas in structure **6.2** we note only one close contact to the corresponding host phenyl ring. The same obtains for the phenyl rings of structures **6.1** and **6.2** which are governed by T4 where the phenyl ring of structure **6.1** has one close contact, and in structure **6.2** there are none. The centrosymmetric structure **6.1** is clearly more constrained than structure **6.2**, by close contacts with either guests or an adjacent host.

6.5 CONCLUSION

The Werner host **H3** = $Ni(NCS)_2(4\text{-}PhPy)_4$ forms inclusion compounds with two isomers of methylnaphthalene. The structure with 1-methylnaphthalene has a host to guest ratio of 1:4. This crystalline compound (pale blue) changes to pale violet over 14 days and the structures of the two polymorphs have been elucidated. The solid-state absorbance spectra have been recorded and the geometry about the Ni^{2+} ion analysed. Competition experiments of this host with equimolar mixtures of 1-methylnaphthalene (**1-MN**) and 2-methylnaphthalene (**2-MN**) show that the ratio of **1-MN** : **2-MN** changes with time, rendering a labile system.

We shall all miss Joel Bernstein, his wide knowledge of crystallography, his expertise of polymorphism, and his genial personality.

The authors would like to thank the National Research Foundation (Pretoria) for research grants. We also thank Leonard Barbour and Lisa van Wyk at the University of Stellenbosch for the solid-state UV-VIS measurement.

6.6 REFERENCES

6.1. J. Lipkowski and G. D. Andreetti, Synthesis and structure of dimeric bis(isothiocyanato)tris (4-methylpyridine)nickel (II), *Transit. Met. Chem*, 1978, **3**, 117–121.
6.2. J. V. Handy, G. Ayala and R. D. Pike, Structural comparison of copper(II) thiocyanate pyridine complexes, *Inorg. Chim. Acta*, 2017, **456**, 64–75.

6.3. S. Wöhlert, T. Fic, Z. Tomkowicz, S. G. Ebbinghaus, M. Rams, W. Haase and C. Näther, Structural and Magnetic Studies of a New Co(II) Thiocyanato Coordination Polymer Showing Slow Magnetic Relaxations and a Metamagnetic Transition, *Inorg. Chem.*, 2013, **52**, 12947–12957.

6.4. T. Neumann, I. Jess and C. Näther, catena-Poly[[bis(pyridine-κN)nickel(II)]-di-μ-thiocyanato-κ2N:S;κ2S:N], *Acta Cryst. E*, 2014, **70**, m196–m196.

6.5. G. Chen, Z.-P. Bai and S.-J. Qu, catena-Poly[[dipyridylcopper(II)]-di-μ-thiocyanato], *Acta Cryst. E*, 2005, **61**, m2718–m2719.

6.6. J. Werner, T. Neumann and C. Näther, Synthesis, Structures, and Properties of Transition Metal Thiocyanato Coordination Compounds with 4-(4-Chlorobenzyl)pyridine as Ligand, *Z. Anorg. Allg. Chem.*, 2014, **640**, 2839–2846.

6.7. R. E. Marsh, P1 or P1¯? Or something else?, *Acta Cryst. B*, 1999, **55**, 931–936.

6.8. M. Taniguchi, Y. Sugita and A. Ouchi, The Crystal and Molecular Structures of Bis(2-methylpyridine)-, and Bis(3-methylpyridine)bis(thiocyanato)cadmium(II) in Polymeric Forms, $[Cd(SCN)_2(CH3C5H4N)_2]n$, *BCSJ*, 1987, **60**, 1321–1326.

6.9. M. Rams, Z. Tomkowicz, M. Böhme, W. Plass, S. Suckert, J. Werner, I. Jess and C. Näther, Influence of metal coordination and co-ligands on the magnetic properties of 1D $Co(NCS)_2$ coordination polymers, *Phys. Chem. Chem. Phys.*, 2017, **19**, 3232–3243.

6.10. A. Jochim, I. Jess and C. Näther, Structural diversity in Cd(NCS)2-3-cyanopyridine coordination compounds: synthesis, crystal structures and thermal properties, *Z. Naturforsch. B*, 2020, **75**, 163–172.

6.11. S. Wöhlert, J. Boeckmann, M. Wriedt and C. Näther, Coexistence of Metamagnetism and Slow Relaxation of the Magnetization in a Cobalt Thiocyanate 2D Coordination Network, *Angew. Chem. Int. Ed.*, 2011, **50**, 6920–6923.

6.12. M. G. Barandika, M. L. Hernández-Pino, M. K. Urtiaga, R. Cortés, L. Lezama, M. I. Arriortua and T. Rojo, Solvent control in the synthesis of [Mn(NCS)2(bpe)2(H2O)2] and [Mn(NCS)2(bpe)1.5(CH3OH)]n (bpe = 1,2-bis(4-pyridyl)ethene): structural analysis and magnetic properties, *J. Chem. Soc., Dalton Trans.*, 2000, 1469–1473.

6.13. T. Neumann, C. dos S. Cunha, H. Terraschke, L. S. Germann, R. E. Dinnebier, I. Jess, and C. Näther, Synthesis, Structures, and Physical Properties of Thiocyanate Coordination Compounds with 3-Hydroxymethylpyridine, *Z Anorg. Allg. Chem.*, 2017, **643**, 1497–1507.

6.14. W. D. Schaeffer, W. S. Dorsey, D. A. Skinner and C. G. Christian, Separation of Xylenes, Cymenes, Methylnaphthalenes and Other Isomers by Clathration with Inorganic Complexes, *J. Am. Chem. Soc.*, 1957, **79**, 5870–5876.

6.15. J. Lipkowski, Inclusion compounds formed by Werner MX_2A_4 coordination complexes In *Inclusion Compounds: Structural aspects of inclusion compounds formed by inorganic and organometallic host lattices.* J. L. Atwood, J. E. D. Davies and D. D. MacNicol, *Inclusion compounds*, Academic Press : Oxford University Press, London; Oxford, 1984.

6.16. J. Hanotier, P. de Radzitzky, Inclusion compounds of diisothiocyanatotetrakis(*α*-arylalkylamine)nickel(II) complexes In *Inclusion Compounds: Structural aspects of inclusion compounds formed by inorganic and organometallic host lattices.* Atwood, J.L., Davies, J.E.D., MacNicol, D.D. Eds.; Academic Press: London, 1984.

6.17. J. Lipkowski, Werner Clathrates In *Comprehensive Supramolecular Chemistry*. J. L. Atwood, J. E. Davies, D. D. MacNicol, F. Vögtle, Vol 6. *Solid State Supramolecular Chemistry: Crystal Engineering*, Elsevier Science: Oxford, 1996.
6.18. H. L. Wiener, L. Ilardi, P. Liberati, L. Dengler, S. A. Jeffas, S. Saba and N. O. Smith, Competition among aromatic guests for the host tetrakis(4-methylpyridine)nickel(II) isothiocyanate and a basis for the observed selectivity, *J. Incl. Phenom.*, 1986, **4**, 415–427.
6.19. P. Starzewski, W. Zielenkiewicz and J. Lipkowski, A thermokinetic study of the clathration of isomeric xylenes by the Ni(NCS)2 (4-methylpyridine)4 host, *J. Incl. Phenom.*, 1984, **1**, 223–232.
6.20. D. V. Soldatov and J. A. Ripmeester, Novel 4-vinylpyridine-extended metal-dibenzoylmethanate host frameworks: structure, polymorphism, and inclusion properties, *Chemistry*, 2001, **7**, 2979–2994.
6.21. M. Lusi and L. J. Barbour, Solid–Vapor Sorption of Xylenes: Prioritized Selectivity as a Means of Separating All Three Isomers Using a Single Substrate, *Angew. Chem. Int. Ed.*, 2012, **51**, 3928–3931.
6.22. M. M. Wicht, N. B. Báthori and L. R. Nassimbeni, Isoquinoline-based Werner clathrates with xylene isomers: aromatic interactions vs. molecular flexibility, *Dalton Trans.*, 2015, **44**, 6863–6870.
6.23. M. M. Wicht, N. B. Báthori and L. R. Nassimbeni, Enhanced selectivity towards xylene isomers of a mixed ligand Ni(II) thiocyanato complex, *Polyhedron*, 2016, **119**, 127–133.
6.24. D. R. Bond in Structures of Werner Clathrates, MSc thesis, University of Cape Town, 1982.
6.25. Bruker SAINT-Plus. Bruker AXS Inc., Madison, Wisconsin, USA, 2012.
6.26. G. M. SHELDRICK, Program for Empirical Absorption Correction of Area Detector Data, *SADABS*.
6.27. XPREP, Data Preparation and Reciprocal Space Group Exploration, Version 2008/2, © Bruker AXS Inc., Madison, Wisconsin, USA, 2008.
6.28. G. M. Sheldrick, SHELXT – Integrated space-group and crystal-structure determination, *Acta Cryst. A*, 2015, **71**, 3–8.
6.29. G. M. Sheldrick, Crystal structure refinement with SHELXL, *Acta Cryst. C*, 2015, **71**, 3–8.
6.30. L. J. Barbour, X-Seed - A software tool for supramolecular crystallography, *J. Supramol. Chem*. **2001**, 1, 189-191.
6.31. C. F. Macrae, P. R. Edgington, P. McCabe, E. Pidcock, G. P. Shields, R. Taylor, M. Towler and J. van de Streek, Mercury: visualization and analysis of crystal structures, *J Appl. Cryst.*, 2006, **39**, 453–457.
6.32. L. R. Nassimbeni, M. L. Niven and M. W. Taylor, Studies in Werner Clathrates. Part 7. Structures of bis(isothiocyanato)tetrakis(4-phenylpyridine)nickel(II) and its Clathrates with ortho-xylene, meta-xylene and para-xylene + dimethylsulphoxide, *Inorg. Chim. Acta*, 1987, **132**, 67–73.

CHAPTER 7

Enclathration By A Halogenated Host: Structures, Polymorphism, Kinetics And Guest Exchange

By Nicole M. Sykes, Hong Su, Susan A. Bourne, and Luigi R. Nassimbeni
In *Cryst. Growth Des.*, 2021, **21**, 6465–6472. (Published 6 October 2021)

2020 & 2021 – years 5 & 6 – PhD in a pandemic

(a) 15 December 2020, Dr Roxanne Mohunlal's virtual graduation. (b) 14 September 2021, we re-took our 2016 photo (see Chapter 3). (c) 28 September 2020, a poster I made of the Greek myths behind the elements they are named for. (d) 22 September 2021, Prof Nassimbeni and I. (e) 27 September 2021, all four co-authors of our 2021 article together - Prof Susan Bourne, Dr Hong Su, myself, and Prof. Luigi Nassimbeni. (f) 27 September 2021, CSCR group photo.(g) 27 September 2021, Alexios Vicatos, Dr Adrien Ndamyberra, and I all had publications accepted within a few weeks of each other.

7.1 SYNOPSIS

In 1954 the first crystallographic study of halogen bonding[7.1] yielded a structure with bromine and 1,4-dioxane, held together by a strong Br ··· O interaction of length = 2.71 Å – much shorter than sum of the Bondi[7.2] van der Waals radii (3.35 Å). This study aimed to create inclusion compounds containing strong Br ··· O interactions between the racemic brominated host tetrakis(*p*-bromophenyl)ethylene (**H4**) and achiral guests similar to 1,4-dioxane in that all contain an oxygen atom.

Five new inclusion compounds were synthesized, however none of the crystal structures contain close Br ··· O contacts and are instead held together by host-to-host Br ··· Br contacts and van der Waals forces. Interestingly, the structures of these compounds were shown to be either chiral or racemic – racemic structures had equal amounts of left- and right-handed **H4**, whereas single crystals of chiral structures contained only the one enantiomer.

Two of the newly prepared inclusion compounds in this publication are a polymorphic pair with 1,4-dioxane (**H•DIOX 1** and **H•DIOX 2**) as guest. **H•DIOX 1** crystallises in a chiral space group, while **H•DIOX 2** is racemic. Their activation energies of decomposition were calculated by non-isothermal TG. This indicated that the second polymorph, **H•DIOX 2**, is the more stable, as measured by the slightly higher activation energy of 90 $\pm$1 kJ·mol^{-1} compared to 83 $\pm$ 2 kJ·mol^{-1}for **H•DIOX 1**. The increased stability of **H•DIOX 2** was further supported by the peak temperature of the endotherm associated with dioxane desorption as measured by DSC, recorded as 118 °C for **H•DIOX 2**, and the lower peak temperature of 106 °C for **H•DIOX 1**. Structural investigations of the polymorphic compounds by Hirshfeld Surface analysis showed that the **H•DIOX 2** structure contains Br ··· Br interactions that are shorter, and so stronger, than those observed in **H•DIOX 1**.

Guest exchange studies showed that **H•DIOX 1** could be produced by exposing the similarly structured **H•PENT** to dioxane vapor. In contrast **H•DIOX 2** could be formed by instead starting with **H•CYNO** and exchanging the cyclohexanone by exposing the compound to dioxane vapor. It was also possible to exchange the cyclohexanone in **H•CYNO** for 3-pentanone to produce the **H•PENT** compound. The latter reaction was monitored by *in-situ* powder X-ray diffraction where distinct peaks at certain two theta values either increased or decreased as the exchange progressed. Processing of this kinetic data revealed that the reaction obeys a deceleratory model, the decreasing area mechanism R2, with the rate law $kt = 1 - \sqrt{(1 - \alpha)}$ with k = 0.0069 min^{-1} at 25 °C, where t = time, and α is the extent of reaction.

7.2 INTRODUCTION

The formation of inclusion compounds by halogenated phenylethylenes was first declared by Tanaka, Fujimoto and Toda.[7.3] They showed that tetra(*p*-halophenyl)ethylene derivatives form stable inclusion complexes with various halogenated alkanes and alkenes. These host compounds were found to yield inclusion compounds which were chiral with guest compounds which were achiral, and this was attributed to halogen-halogen interactions occurring between host molecules.[7.4, 7.5] This phenomenon was further demonstrated by a

solid-vapour reaction which occurred between the *p*-bromophenyl derivative of the host and gaseous *p*-xylene.[7.6] The kinetics of enclathration and desolvation of the inclusion compounds of the *p*-bromophenyl host and its p-iodophenyl analogue with halogenated methanes have been analysed and their structures elucidated.[7.7] The bromophenyl inclusion compound with 1,2-dischloroethane (DCE) was subjected to the vapours of methyl iodide (MeI) and the reaction was monitored by NMR spectroscopy. A single crystal was removed which contained 48.6% MeI and its structure elucidated, displaying a stoichiometry of 6H•3DCE•2MeI[7.8] revealing the mechanism of the guest exchange reaction.

In this work we present the structures of the inclusion compounds formed by the host **H4**, tetrakis(*p*-bromophenyl)ethylene with dimethyl sulfoxide (DMSO), 1,4-dioxane (DIOX), cyclohexanone (CYNO), and 3-pentanone (PENT), analyse their kinetics of thermal decomposition, monitor their guest exchange reactions and comment on the relevant halogen-halogen interactions. The structural formulae of the host and guests are shown in Scheme 7.1.

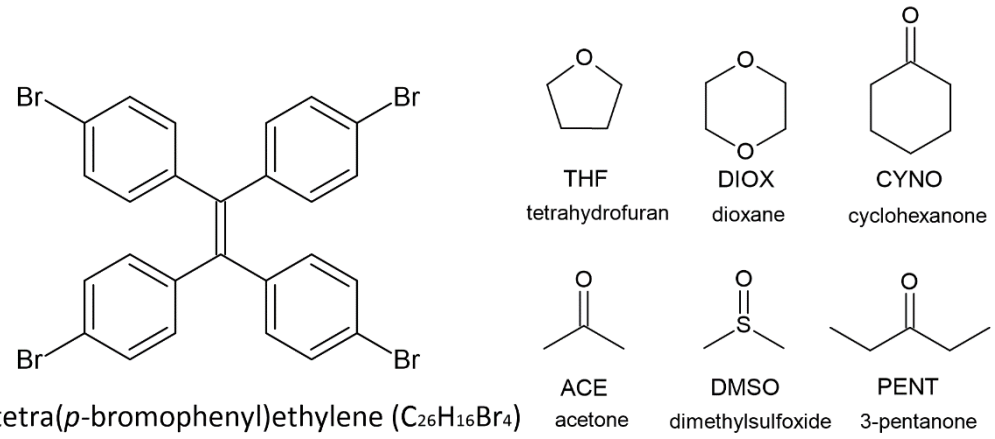

Scheme 7.1: Host compound (left) and guests under study (right).

7.3 EXPERIMENTAL

7.3.1 Materials.

The host compound, **H4**, was synthesized according to a known method,[7.7] where tetraphenylethylene was exposed to bromine vapour overnight, (stirred occasionally to prevent a crust forming), then dissolved in hot chloroform and precipitated out with ethanol. Guest solvents were bought from Sigma-Aldrich and used without further purification.

7.3.2 Preparation.

Single crystals of the inclusion compounds were obtained by dissolving the host in an excess of the relevant guest and then leaving the solution to crystallize by slow evaporation. The first polymorph of the host with dioxane was made in this way, while the second polymorph was found by allowing crystals to age for two weeks in the dioxane solvent at room temperature. Dioxane solutions with the same concentrations of host produce either form when seeded with the desired polymorph. The two polymorphs of the apohost (host without guest) were synthesized according to known methods with slight modifications; apohost 1 (CSD **MALGOV**)

was recrystallized from *m*-xylene,[7.5] and apohost 2 (CSD **MALGOV01**) was formed by recrystallizing the apohost from a mix of chloroform and acetonitrile.[7.7]

7.3.3 X-ray Crystallography.

Single crystal X-ray diffraction (SXRD) data were collected on a Bruker DUO APEX II diffractometer for all structures using Mo Kα (λ = 0.71073 Å) at a temperature of -100 or -173 °C. The intensity data were collected using the φ scan and ω scan techniques, scaled, and reduced with SAINT-Plus.[7.9] The correction of the collected intensities for absorption was carried out using the SADABS program.[7.10] XPREP[7.11] was used to process and prepare input files for SHELXT 2014/5[7.12] and SHELXL 2018[7.13] which were used to solve and refine the structures using the X-seed graphical interface.[7.14] All non-hydrogen atoms were refined isotropically or anisotropically depending on the occurrence of disorder in the structures. Some C−C and C−O bond lengths in disordered guest molecules were restrained. All C−H hydrogen atoms were placed geometrically and refined with a riding model for their isotropic temperature factors. **H•PENT** was refined as a two-component twin using the HKLF 5 file and BASF instruction to specify the fractional volume contributions of the twin components.[7.12]
Diagrams were generated using Mercury (2020 3.0).[7.15] To display and calculate the percentage volume of voids we used the Mercury default probe radius (1.2 Å), approx. grid spacing (0.7 Å), and "contact surface" method.

Powder X-ray diffraction (PXRD) was recorded on a Bruker D2 phaser diffractometer using Cu Kα radiation (λ = 1.5418 Å) generated at 30 kV and 10 mA. Simulated powder patterns of crystal structures were calculated using Mercury and compared with the experimental patterns to confirm bulk phase purity.
An *in situ* PXRD experiment was also carried on a Bruker D8 powder X-ray diffractometer using Cu Kα radiation (λ = 1.5418 Å) generated at 30 kV and 40 mA. The CYNO compound was sieved through a 106-μm filter and exposed to 3-pentanone vapour using a modified sample holder as previously described.[7.16] Powder diffraction traces were at recorded at 25 °C and repeated at intervals of 25 minutes.

7.3.4 Thermal Analysis.

Samples were prepared by removing crystals from mother liquor, blotting on filter paper, and leaving to dry. Crystals were gently crushed, sieved and exposed to solvent vapour (if specified), and weighed directly into open aluminium oxide crucibles in the case of thermogravimetric analysis (TGA) or crimped, vented aluminium pans for differential scanning calorimetry (DSC). 4−10 mg was used for TGA and 1−3 mg for DSC. Unless specified, experiments were performed over a temperature range of 30−290 °C at a heating rate of 20 °C/min under dry nitrogen with a flow rate of 40 cm^3min^{-1} in the TGA and 60 cm^3min^{-1} in the DSC. Thermogravimetric analysis was performed using a TA-Q500 thermogravimetric analyser, and differential scanning calorimetry was performed using a Q200 (TA Instruments). TG results were analysed using TA Instruments Universal Analysis 2000 software.

7.3.5 Guest Exchange.

Guest exchange experiments were performed using a "two-vial" method. Crystals of inclusion compounds or apohost were removed from mother liquor, patted dry, and (unless specified) crushed into a powder. This starting material was set in a short vial, while into a second vial was added the guest to be exchanged. Both vials were then placed inside a sealed jar and left

at room temperature. Guest exchange was considered successful when the resulting PXRD pattern of the starting material changed to that of the new host-guest compound. When patterns were similar, ^{1}H NMR was used to confirm presence of the exchanged guest.

7.4 RESULTS AND DISCUSSION

7.4.1 Structures with H4.

The crystallographic data and structure parameters are presented in Table 1a. To these we have added in Table 7.1b the relevant data of the structures with tetrahydrofuran (THF) and acetone (ACE), and the two polymorphs of the apohost obtained from the Cambridge Structural Database which are pertinent to the discussion.[7.3, 7.4]

Structure **7.1**, **H•DIOX 1**, crystallizes in the space group $P2_12_12_1$ with Z = 4 with one host and one guest in the asymmetric unit. The guests are located within isolated cages of size 113 Å^3 each. The packing diagrams for all structures are displayed in Figure 7.1. Toda *et al*[7.4] recorded the synthesis of this compound (by both recrystallisation and vapour sorption, but did not elucidate its structure).
Structure **7.1** and Structure **7.2**, **H•DIOX 2**, are polymorphs with very close unit cell volumes. Structure **7.2** crystallizes in *C*2/*c* with Z = 4. The asymmetric unit consists of one-half host molecule which lies on a 2-fold axis at Wykoff position *e* (0, y, ¼), and one-half guest molecule, which is disordered over two positions (63%/ 37%) and lies about a centre of symmetry at Wykoff position *c* (¾, ¼, ½). The nature of the dioxane disorder causes the guest molecules to reside in slightly enlarged isolated cages (120 Å^3), in comparison to those of dioxane polymorph 1 (113 Å^3).

Structure **7.3**, **H•CYNO** crystallizes in *C*2/*c*, and has a similar unit cell and packing to that of Structure **7.2**, **H•DIOX 2**. The asymmetric unit consists of one half-host which lies on a two-fold axis at Wykoff position *e* (0, y, ¼) and one-half guest, which is located about a centre of inversion at Wykoff position *d*. (¼, ¼, ½). The guests are located within isolated cages of size 132 Å^3 each.

Structure **7.4**, **H•PENT**, crystallizes in the space group $P2_1$. The asymmetric unit consists of two host molecules and two guest molecules. The two guests together occupy an elongated cage, totalling 149 Å^3. One guest takes on the most stable zig-zag conformation (*trans-trans*), while the second guest displays the *trans-gauche* conformer, the next most stable of the four conformers of 3-pentanone.[7.17]

Structure **7.5**, **H•2(DMSO)** crystallizes in the space group $P2_12_12_1$. The asymmetric unit consists of one host molecule and two DMSO guest molecules. One of the DMSO molecules is disordered, and was refined over three positions totalling occupancies of 32%, 47%, and 21% respectively. We note that the structure and packing are similar to that of the host-guest compounds formed with ACE and THF.[7.4] When the DMSO guests are removed and void spaces displayed, channels along [100] are evident (Figure S7.1).

While the packing of host molecules can produce either chiral or racemic structures, the shape of the tetrakis(*p*-bromophenyl)ethylene molecules remains consistent. In each case the host displays a propeller conformation with torsion angles amongst the compounds ranging from +41° to +62° (Table S7.1).

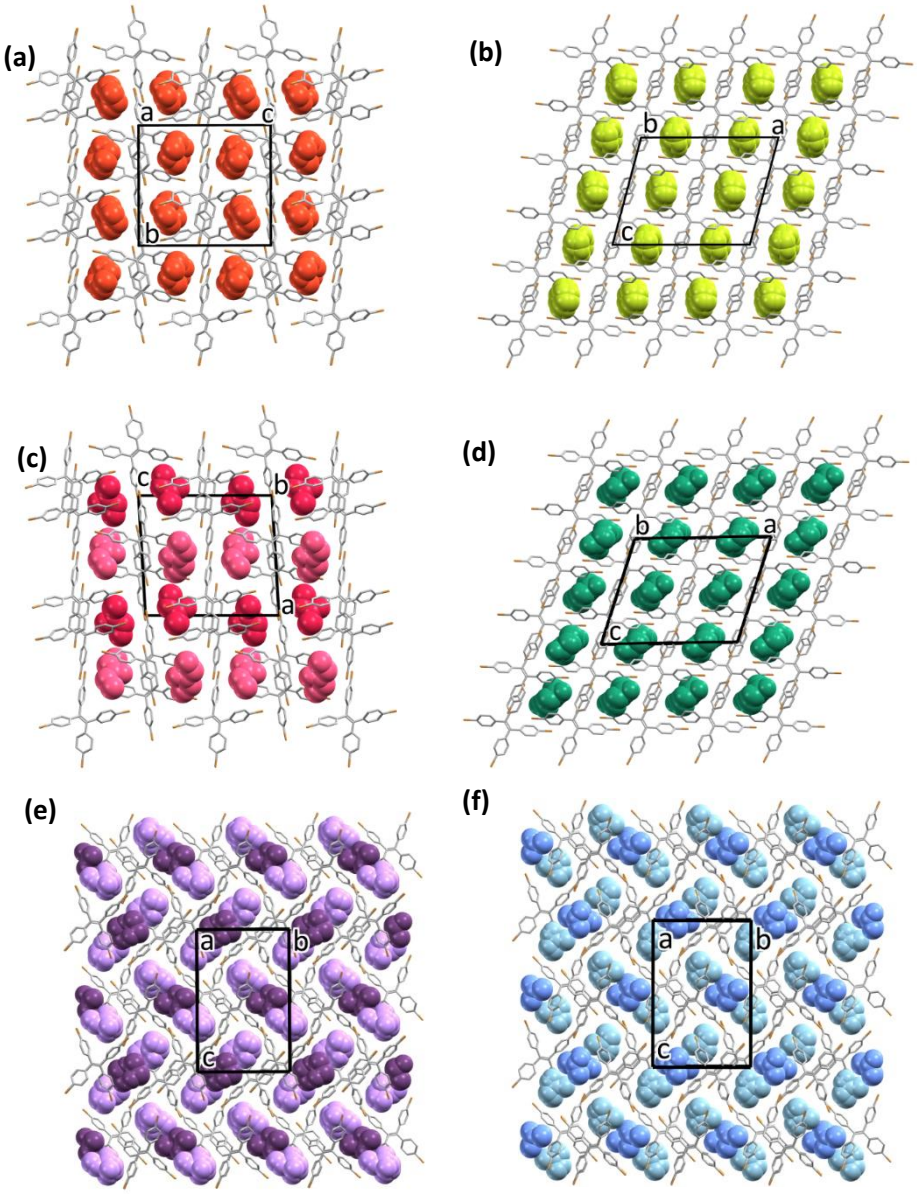

Figure 7.1. Packing diagrams of tetra(*p*-bromophenyl)ethylene inclusion compounds with guests drawn in the space fill style: a) **H•DIOX 1**, b) **H•DIOX 2,** c) **H•PENT**, d) **H•CYNO**, e) **H•2(DMSO)**, f) **H•2(ACE)** (CIF refcode XALBUH).

Table 7.1a. Crystallographic data parameters of new host-guest compounds

Compound	**H•DIOX 1**	**H•DIOX 2**	**H•CYNO**	**H•PENT**	**H•2(DMSO)**
chirality	chiral	racemic	racemic	chiral	chiral
Guest	dioxane	dioxane	cyclohexanone	3-pentanone	DMSO
Structural formula of ASU	C_{26} H_{16} Br_4, C_4 H_8 O_2	½ (C_{26} $H_{16}Br_4$, C_4 H_8 O_2)	½ (C_{26} H_{16} Br_4, C_6 H_{10} O_1)	2(C_{26} H_{16} Br_4, C_5 H_{10} O_1)	C_{26} H_{16} Br_4, 2(C_2 H_{61} S_1)
Guest/ Host ratio	1	1	1	1	2
Molecular mass ($g \cdot mol^{-1}$)	736.10	736.10	746.17	734.16	804.30
Data collection temp (K)	173(2)	173(2)	173(2)	100(2)	173(2)
Crystal system	Orthorhombic	Monoclinic	Monoclinic	Monoclinic	Orthorhombic
Space group	$P2_12_12_1$	$C2/c$	$C2/c$	$P2_1$	$P2_12_12_1$
a (Å)	9.535(2)	20.338(1)	20.206(1)	16.645(3)	9.550(2)
b (Å)	16.387(3)	8.721(1)	9.2124(6)	9.355(2)	14.598(3)
c (Å)	17.956(4)	16.410(1)	16.455(1)	18.532(4)	22.552(5)
α (°)	90	90	90	90	90
β (°)	90	105.076(1)	108.710(1)	93.34(3)	90
γ (°)	90	90	90	90	90
Volume ($Å^3$)	2805	2810	2901	2880	3143
Z	4	4	4	4	4
Calc. density ($g \cdot cm^{-1}$)	1.743	1.740	1.708	1.693	1.699
θ range (°)	2.27-25.02	2.56-27.74	2.45-28.26	2.20-27.89	2.28-27.64
Reflections collected	57777	26219	27428	37052	95335
Unique reflections ($I > 2\sigma(I)$)	6068	2961	3124	7109	6294
Final R indices ($I > 2\sigma(I)$)	0.0304	0.0291	0.0243	0.0239	0.0412
R indices (all data)	0.0406	0.0392	0.0314	0.0262	0.0750
Goodness-of-fit on F^2	1.033	1.050	1.037	1.047	1.013
CCDC deposition number	2101407	2101408	2101406	2101410	2101409
CSD refcode	DANQAO	DANQAO01	DANPUH	DANQOC	DANQIW

Table 1b. Crystallographic data parameters of previous compounds with this host

Compound (CSD refcode)	**MALGOV**[7.5]	**MALGOV01**[7..7]	**XALBUH**[7.4]	**XALCAO**[7.4]
Chirality	racemic	racemic	chiral	chiral
Guest	-	-	acetone	THF
Structural formula	C_{26} H_{16} Br_4	C_{26} H_{16} Br_4	C_{26} H_{16} Br_4, 2(C_3 H_6 O_1)	C_{26} H_{16} Br_4, 2(C_4 H_8 O_1)
Guest/ Host ratio	-	-	2	2
Molecular mass (g·mol^{-1})	648.03	648.03	764.19	792.24
Crystal system	Orthorhombic	Monoclinic	Orthorhombic	Orthorhombic
Space group	*Pccn*	$P2_1/n$	$P2_12_12_1$	$P2_12_12_1$
A (Å)	16.173(2)	20.520(1)	9.203(1)	9.3337(2)
b (Å)	16.512(1)	9.787(1)	14.969(2)	15.1835(3)
c (Å)	18.024(2)	24.004(1)	22.418(3)	21.9443(5)
α(°)	90	90	90	90
β(°)	90	91.60(1)	90	90
γ(°)	90	90	90	90
Volume (Å^3)	4813	4818	3088	3109
Z	8	8	4	4
Dc, calc density (g·cm^{-1})	1.789	1.787	1.644	1.692

7.4.2 Kinetics of desolvation of the two polymorphs of dioxane.

Crystals of each polymorph were sieved through a 106 µm filter, then exposed to dioxane vapour at room temperature for at least one hour to replace any volatile guest lost during sieving. The polymorph phase was confirmed by PXRD. The TG traces were collected at heating rates (β) of 2, 4, 8, 16, and 32 °C/minute (Figure 7.2). For both **H•DIOX 1** and **H•DIOX 2** the average mass loss (%) came to 11.7%; the calculated mass loss for a H•DIOX compound is 12.0%. In order to determine the activation energy of decomposition we made use of the method developed by Flynn, Wall, and Ozawa [7.18, 7.19] and plotted ln (β/ β_0) versus 1000 K/T using temperature points from when the extent of reaction (α) was 5%, 10%, 15%, 20%, and 30% complete (Figure 7.3). For **H•DIOX 1** the activation energy of desolvation was calculated to be 84 $\pm$2 kJ·mol^{-1}, whereas for **H•DIOX 2** the activation energy was slightly higher, at 90 $\pm$2 kJ·mol^{-1}. This trend agrees with the DSC results (Figure S7.4), which show an endothermic peak due to dioxane desorption at 106 °C for **H•DIOX 1** and at a higher temperature of 118 °C for **H•DIOX 2**.

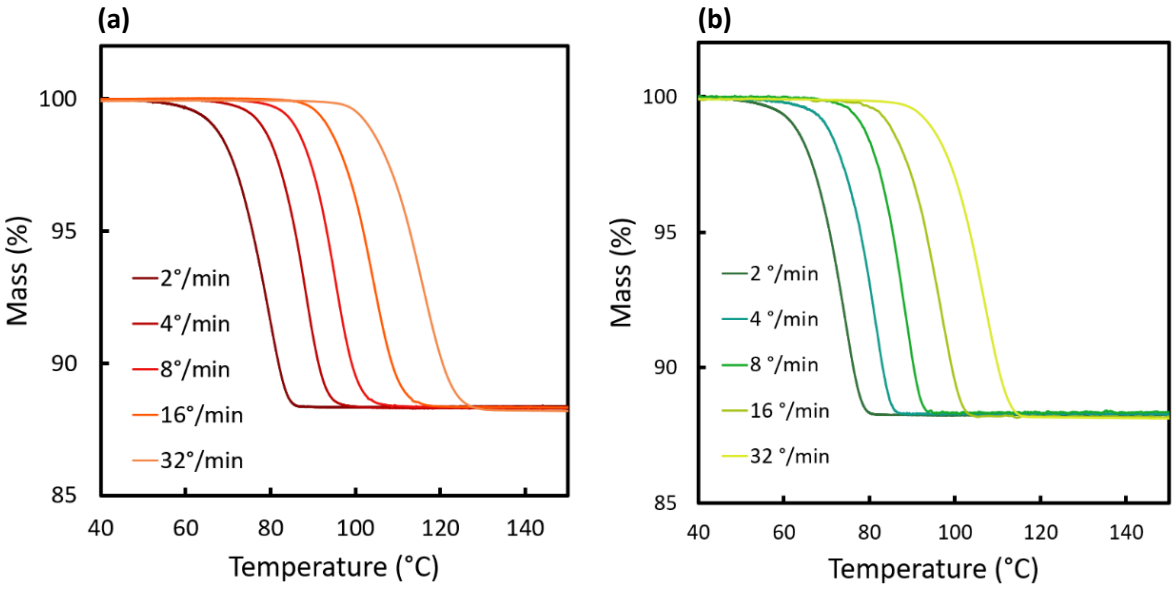

Figure 7.2. TG traces collected at heating rates of 2, 4, 8, 16, and 32 °C/minute of a) **H•DIOX 1** and b) **H•DIOX 2**.

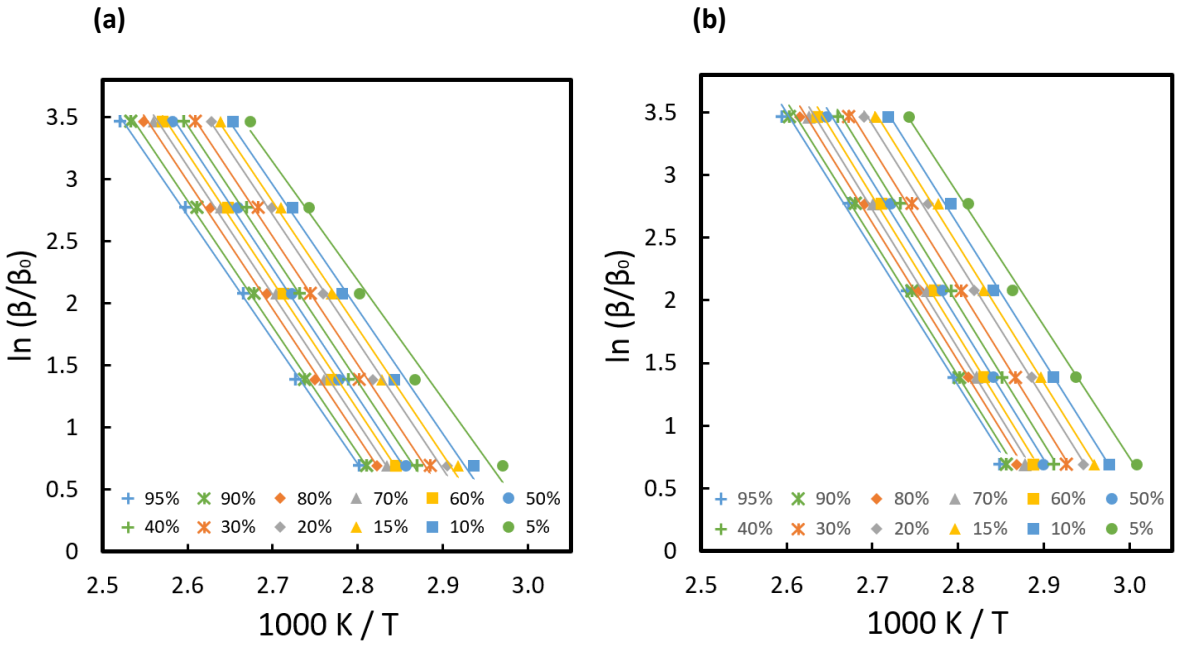

Figure 7.3. Plots of ln (β/β_0) versus 1000 K / T at 5%, 10%, 15%, 20%, 30%, 40%, 50%, 60%, 70%, 80%, 90%, and 95% extent of the guest desorption reaction for a) **H•DIOX 1** and b) **H•DIOX 2**.

7.4.3 Structural differences in the two dioxane polymorphs.

Whilst the thermal data suggests that **H•DIOX 2** is more stable than **H•DIOX 1**, it is not obvious structurally why that should be the case.

We compared the packing of the dioxane polymorphs by using the programme, Crystal Explorer.[7.20] In each analysis the dioxane molecules were selected as the target, and the resulting fingerprint plots (Figure 7.4) visualize the contacts from each dioxane guest molecule to the surrounding host. We note that the **H•DIOX 2** has a spike due to a (dioxane)H···Br(host) interaction of length 3.06 Å, which is not seen in **H•DIOX 1**.

In the **H•DIOX 1** structure there are four Br···Br interactions (Table S7.2). The **H•DIOX 2** structure contains only two Br···Br interactions, however at 3.48 Å they are shorter than those present in **H•DIOX 1**, and correspond to an approximately 6% reduction in the sum of the Bondi[7.21] van der Waals radii (3.70 Å).

We also more closely inspected the void spaces produced by deleting the dioxane guest molecules. We found that the originally cage-type voids displayed in **H•DIOX 2** are in fact joined, forming restricted channels down [010] (Figure S7.5b), while those in **H•DIOX 1** remain as isolated cages (Figure S7.5a). This was done by adjusting Mercury's default settings to a probe radius = 1 Å and an approx. grid spacing = 0.1 Å. This may be attributed to the disorder of the dioxane molecule which requires more space in the packing of the structures.

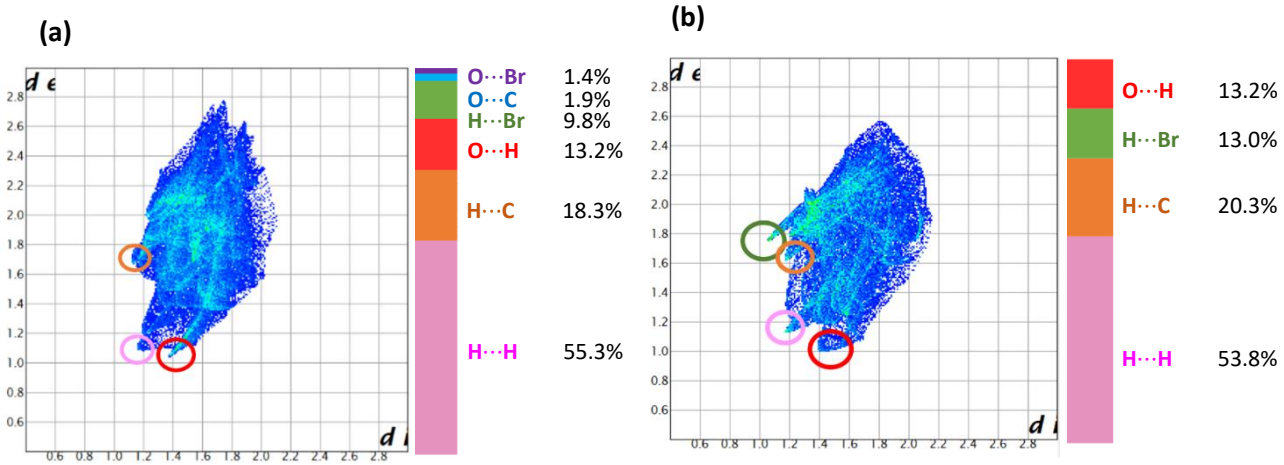

Figure 7.4. Hirshfeld fingerprint plots with dioxane selected as target in (a) **H•DIOX 1** and (b) **H•DIOX 2** (surface created about both disordered guests). Circled are spikes due to short O···H (red), H···H (pink), H···C (orange), and H···Br (green) interactions. The adjoining bar graphs display the percentage breakdown of the types of non-bonded interactions.

7.4.4 Guest exchanges.

When **H•CYNO** is exposed to dioxane vapour, the result is the **H•DIOX 2** polymorph which is not surprising because **H•CYNO** and **H•DIOX 2** are isomorphous. (Figure S7.11 – S7.13). The **H•PENT** compound exchanges PENT for DIOX to form the similar **H·DIOX 1** compound (Figure S7.11, S7.14, S7.15). Interestingly, we found that both single crystals and powders of **H·DIOX 1** would slowly transform to **H•DIOX 2** over time, if left in mother liquor or exposed to dioxane vapour, respectively. This again suggests that **H•DIOX 2** is the more stable polymorph.

Both polymorphs of the apohost also form **H•DIOX 1** upon exposure to dioxane vapour. Apohost 1 does not form **H•CYNO** when exposed to the vapour of CYNO according to Toda et al.,[7.5] however, **H•CYNO** is formed when apohost 2 is exposed to CYNO vapour for 4 days (Figure S7.18). Similarly, Toda et al.[7.4] previously found that the host-guest complex with acetone (**XALBUH)** is not formed by exposure of the apohost 1 to acetone vapour. Again, we found that the inclusion compound **XALBUH** (H•2(ACE)) is formed when apohost 2 is exposed to acetone vapour for 3 days (Figure S7.20).

We exposed DMSO crystals to gaseous acetone at 40 °C using a simple "two-vial" set-up (Figure 7.5a). The DSC profile of the **H•2(DMSO)** compound shows two broad endotherms for the DMSO desorption peaking at 115 and 180 °C while the third endotherm (256–258 °C) is associated with the melt of the apohost. As the reaction proceeds the guest profiles change and after 88 hours at 40 °C the exchanged compound yields a DSC trace almost identical to that collected from the pure acetone compound **H•2(ACE)** (Figure 7.5b). We emphasise that this method does not yield values of rate constants or define the mechanism laws of the reaction.[7.22]

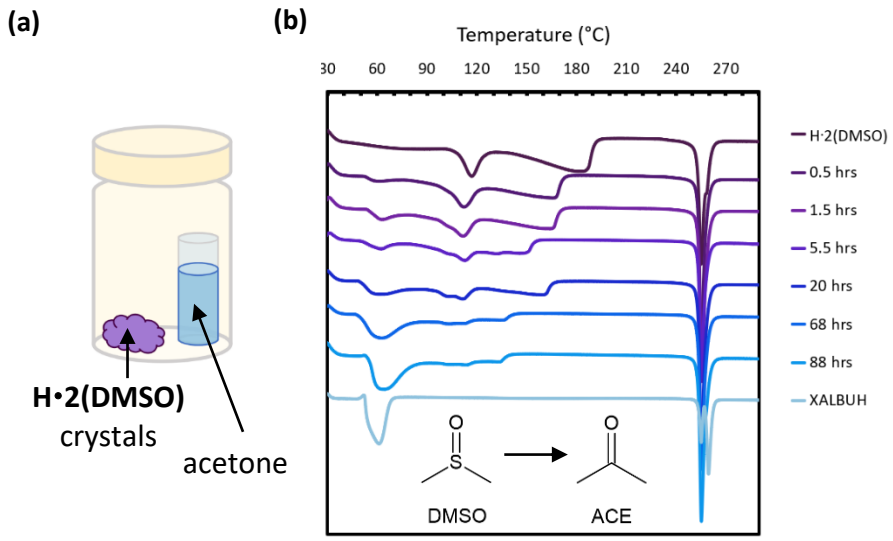

Figure 7.5. guest exchange experiment carried out at 40 °C from **H•2(DMSO)** (purple) to the isomorphous acetone structure, **H•2(ACE)** (blue). a) scheme of the "two vial" experimental set up, and b) DSC traces at specified times over 88 hours.

We monitored the kinetics for the exchange reaction:
H•CYNO$_{(s)}$ + PENT$_{(g)}$ → H • (xCYNO•(1-x)PENT)$_{(s)}$ → **H•PENT**$_{(s)}$
by employing a custom *in situ* sample holder as previously described. [7.16, 7.23]

The X-ray powder diffraction spectra of **H•CYNO** and **H•PENT** display distinct peaks
The **H•CYNO** compound has a peak at 2θ = 12.12° due to the (20-2) reflection that decreases with time, while **H•PENT** has a peak at 2θ = 7.35° due to the (101) reflection that increases correspondingly.

Powder diffraction traces were recorded at room temperature and repeated at intervals of 25 min. The result, shown in Figure 7.6a, displays the traces as time-resolved peaks, whose colours vary from dark grey (background) through red to yellow (most intense). Overlaid are the calculated PXRD traces of the **H•CYNO** (green) and **H•PENT** (pink) compounds.

The related Figure 7.6b displays time resolved changes in the area measured due to the (101) reflection of **H•CYNO**, and the (20-2) reflection of **H•PENT**. This raw kinetic data for the guest exchange reaction were normalised to yield the α vs time curve (Figure 7.6c) which followed the contracting surface area law R2: $1 - \sqrt{(1-\alpha)}$ = kt (Sharp-Hancock formalism), where α represents the extent of reaction and k is the rate constant for the exchange reaction (Figure 6d).[7.24] The rate law held over an α range from 0 to 1.0 with r = 0.996 for the **H•CYNO** reflection, and α range from 0 to 0.86 with r = 0.996 for the **H•PENT** reflection. The kinetic traces yielded an average rate constant of 0.0069 min^{-1} at 25 °C which corresponds to a half-life of approximately 42 minutes.

7.5 DISCUSSION AND CONCLUSION

The host compound tetrakis(*p*-bromophenyl)ethylene forms inclusion compounds with a series of guests yielding structures which are either chiral ($P2_1$ or $P2_12_12_1$) or racemic ($C2/c$). The compounds with 1,4-dioxane form two distinct polymorphs, **H•DIOX 1** ($P2_12_12_1$) and **H•DIOX 2** ($C2/c$), and their kinetics of thermal decomposition at various heating rates has shown that the activation energy of the **H•DIOX 2** polymorph has an activation energy of 90 kJ·mol^{-1}, somewhat higher than that of **H•DIOX 1** at 84 kJ·mol^{-1}. This suggests that the dioxane guest is more tightly held by the secondary interactions of the surrounding host molecules and is supported by the DSC traces of **H•DIOX 1** and **H•DIOX 2** (Figure S7.3). Structurally this is backed up by the nonbonded interactions between host and dioxane atoms which are less than the sum of the van der Waals radii.

The kinetics of guest exchange were carried out by two different methods.
For the exchange of DMSO by acetone in the reaction **H•2(DMSO)**$_{(s)}$ + ACE$_{(g)}$ → **H•2(ACE)**$_{(s)}$, the kinetics was followed by DSC and showed DMSO peaks decreasing, while those due to ACE vapour increasing. After 88 minutes the final profile is practically identical to that of the pure **H•2(ACE)** compound. The DSC method is only a qualitative method of following the exchange reaction, but is visually convincing.
The second reaction, **H•CYNO**$_{(s)}$ + PENT$_{(g)}$ → **H•PENT**$_{(s)}$ was followed by the changing X-ray powder spectra. The intensities of the disappearing peaks of the **H•CYNO** structure, and the

growing peaks of the **H•PENT** structure were measured as a function of time. This allowed the extent of reaction to be monitored and modelled. The reaction profile fitted the contracting area law R2: kt = $1 - \sqrt{(1-\alpha)}$.

Both the DSC and X-ray powder diffraction methods are strongly dependent on two factors, namely temperature, which governs the vapour pressure of the incoming guest, and the particle size of the starting inclusion compounds. A narrow size fraction of particles size ensures that diffusion barriers of the incoming gas ensure are kept constant. Therefore, sieving of the powder samples for these kinetic experiments is recommended.

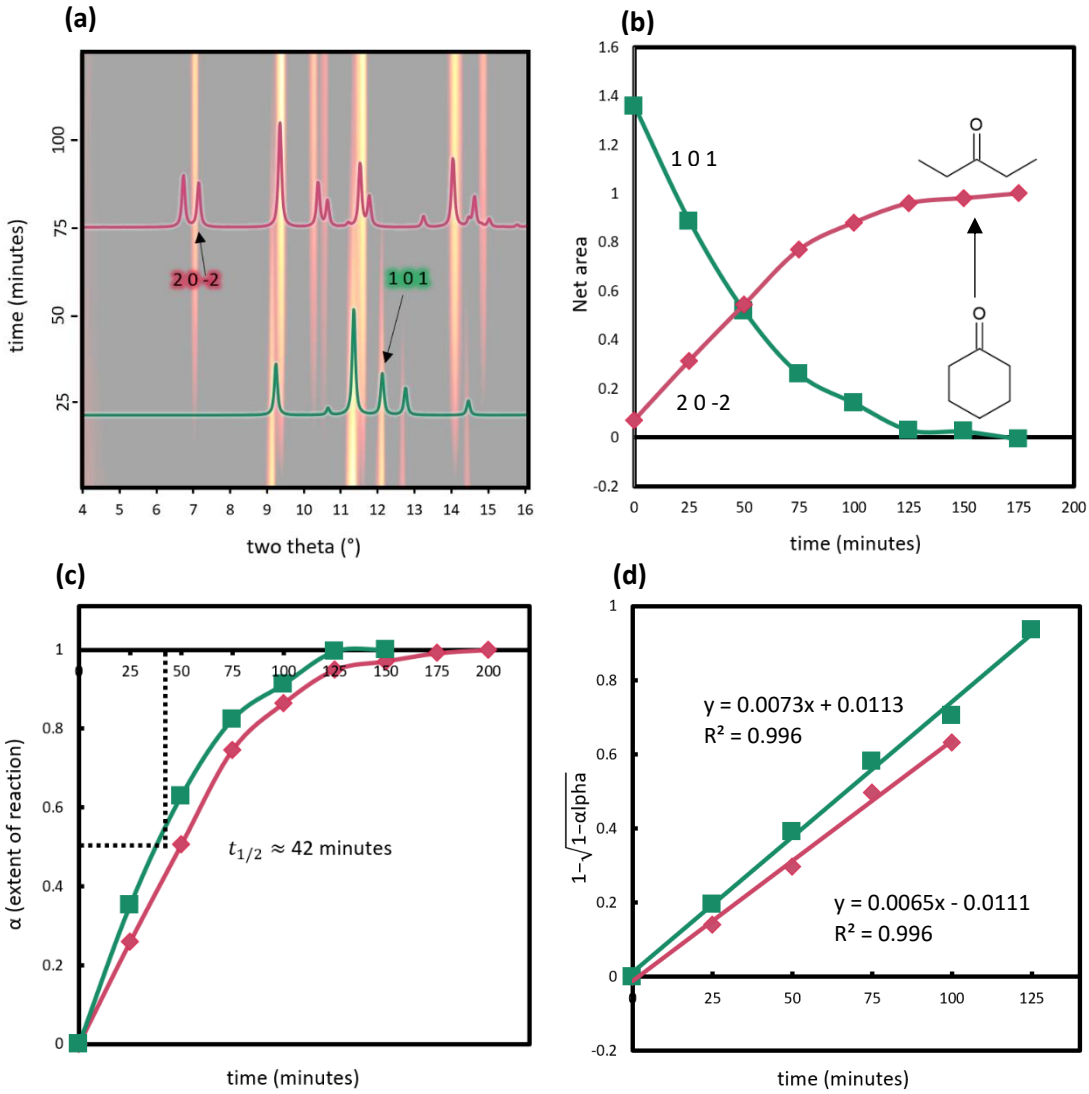

Figure 7.6. Guest exchange of powdered CYNO (green) with 3-pentanone resulting in PENT (pink). (a)Time-resolved in situ powder X-ray diffractogram for **H•CYNO** exposed to 3-pentanone vapour for 3 hours (b) time -resolved changes in relative net area of X-ray reflection (1 0 1) of **H•CYNO** and the (2 0 -2) reflection of the product **H•PENT** (c) alpha vs time curve with the reaction half-life marked at 42 minutes (d) plot of $1 - \sqrt{(1-\alpha)}$ vs. time indicating that the exchange reaction follows the contracting surface area law.

7.6 REFERENCES

7.1. O. Hassel, J. Hvoslef, E. H. Vihovde and N. A. Sörensen, The Structure of Bromine 1,4-Dioxanate., *Acta Chem. Scand.*, 1954, **8**, 873–873.

7.2. A. Bondi, van der Waals Volumes and Radii, *J. Phys. Chem.*, 1964, **68**, 441–451.

7.3. K. Tanaka, D. Fujimoto and F. Toda, Inclusion complex formation of tetra(p-halophenyl)ethylenes with halogenated guest compounds through halogen–halogen interaction, *Tetrahedron Lett.*, 2000, **41**, 6095–6099.

7.4. K. Tanaka, D. Fujimoto, A. Altreuther, T. Oeser, H. Irngartinger and F. Toda, Chiral inclusion crystallization of achiral tetrakis(p-halophenyl)ethylenes with achiral guest compounds, *J. Chem. Soc., Perkin Trans. 2*, 2000, 2115–2120.

7.5. K. Tanaka, D. Fujimoto, T. Oeser, H. Irngartinger and F. Toda, Chiral inclusion crystallization of tetra(p-bromophenyl)ethylene by exposure to the vapor of achiral guest molecules: a novel racemic-to-chiral transformation through gas–solid reaction, *Chem. Commun.*, 2000, 413–414.

7.6. L. R. Nassimbeni, M. L. Niven and M. W. Taylor, Studies in Werner Clathrates. Part 7. Structures of bis(isothiocyanato)tetrakis(4-phenylpyridine)nickel(II) and its Clathrates with ortho-xylene, meta-xylene and para-xylene + dimethylsulphoxide, *Inorg. Chim. Acta*, 1987, **132**, 67–73.

7.7. F. M. Amombo Noa, S. A. Bourne and L. R. Nassimbeni, Halogen Bonding in Host–Guest Compounds: Structures and Kinetics of Enclathration and Desolvation, *Cryst. Growth Des.*, 2015, **15**, 3271–3279.

7.8. F. M. Amombo Noa, S. A. Bourne, H. Su and L. R. Nassimbeni, Guest Exchange in Halogenated Host–Guest Compounds: Structures and Kinetics, *Cryst. Growth Des.*, 2016, **16**, 1636–1642.

7.9. Bruker (2012). SAINT-Plus. Bruker AXS Inc., Madison, Wisconsin, USA, 2012.

7.10. G. M. Sheldrick, Program for Empirical Absorption Correction of Area Detector Data, *SADABS*.

7.11. XPREP, Data Preparation and Reciprocal Space Group Exploration, Version 2008/2, © Bruker AXS Inc., Madison, Wisconsin, USA, 2008.

7.12. G. M. Sheldrick, SHELXT – Integrated space-group and crystal-structure determination, *Acta Cryst. A*, 2015, **71**, 3–8.

7.13. G. M. Sheldrick, Crystal structure refinement with SHELXL, *Acta Cryst. C*, 2015, **71**, 3–8.

7.14. L. J. Barbour, X-Seed — A Software Tool for Supramolecular Crystallography, *Journal of Supramolecular Chemistry*, 2001, **1**, 189–191.

7.15. C. F. Macrae, I. Sovago, S. J. Cottrell, P. T. A. Galek, P. McCabe, E. Pidcock, M. Platings, G. P. Shields, J. S. Stevens, M. Towler and P. A. Wood, Mercury 4.0: from visualization to analysis, design and prediction, *J. Appl. Cryst.*, 2020, **53**, 226–235.

7.16. N. M. Sykes, H. Su, E. Weber, S. A. Bourne and L. R. Nassimbeni, Crystallisation temperature control of stoichiometry and selectivity in host–guest compounds, *CrystEngComm*, 2017, **19**, 5892–5896.

7.17. N. Kuze, E. Kojima, H. Fujiwara, H. Takeuchi, T. Egawa and S. Konaka, Gas-phase structure and conformation of diethyl ketone studied by molecular orbital constrained electron diffraction, *Comput. Theor. Chem.*, 1996, **375**, 231–241.

7.18. J. H. Flynn and L. A. Wall, A quick, direct method for the determination of activation energy from thermogravimetric data, *J. Polym. Sci. B: Polym. Phys.*, 1966, **4**, 323–328.

7.19. T. Ozawa, A New Method of Analyzing Thermogravimetric Data, *BCSJ*, 1965, **38**, 1881–1886.
7.20. P. R. Spackman, M. J. Turner, J. J. McKinnon, S. K. Wolff, D. J. Grimwood, D. Jayatilaka and M. A. Spackman, CrystalExplorer: a program for Hirshfeld surface analysis, visualization and quantitative analysis of molecular crystals, *J. Appl. Cryst.*, 2021, **54**, 1006–1011.
7.21. A. Bondi, van der Waals Volumes and Radii, *J. Phys. Chem.*, 1964, **68**, 441–451.
7.22. M. A. A. Ibrahim and N. A. M. Moussa, Unconventional Type III Halogen···Halogen Interactions: A Quantum Mechanical Elucidation of σ-Hole···σ-Hole and Di-σ-Hole Interactions, *ACS Omega*, 2020, **5**, 21824–21835.
7.23. I. Huskić, J.-C. Christopherson, K. Užarević and T. Friščić, In situ monitoring of vapour-induced assembly of pharmaceutical cocrystals using a benchtop powder X-ray diffractometer, *Chem. Commun.*, 2016, **52**, 5120–5123.
7.24. M. E. Brown, Ed., in *Introduction to Thermal Analysis: Techniques and Applications*, Springer Netherlands, Dordrecht, 2001, pp. 19–54.

CHAPTER 8: Summary, Conclusion, Future Work

(a) 2017: Pieter de Kock, Prof. Mino Caira, Karin Badenhorst, and Prof Luigi Nassimbeni. (b) 17 September 2021: CSCR group (+friends) at our joint paper celebration. (c) 2016: Ruth 'Ubered' a guide-dog-in-training to visit the lab. (d) 2021: important discussions with Prof Susan Bourne, Prof Luigi Nassimbeni, and Tristan Theunissen. (e) – (h) 27 March 2019: snaps from a day in the lab. (i) 2021: with Ces. (j) 2017: with Emma, Alexios, Savannah, and Terence. (k) 2021: joint paper celebration with Alexios. (l), (m) enjoying *pastéis de nata* with Roxanne outside PD Hahn (Chemistry building). (n) playtime with Ces' kitten, Frankie. (o) Meeting baby Tintin, with Nabanita, and her husband Sauvik.

8.1 SUMMARY AND CONCLUSION

This thesis deals with host-guest chemistry and its application to separating organic mixtures. This is particularly relevant in cases where the individual compounds have similar physical properties, such as molecular shape, polarities, and boiling points, as can occur with isomers.

This thesis gave rise to five publications in the international literature, focusing on various aspects of molecular recognition of compounds crystallised from carefully selected hosts and mixtures of organic guests. Four host compounds were used to prepare 29 new inclusion compounds. Two of these hosts were similar bulky diols and were synthesised by Weber (**H1** and **H2**). The other two, a Ni-based Werner-type host (**H3**) and a brominated host (**H4**), were synthesised by known methods.

Various analytical techniques were used to analyse the resulting compounds, including single crystal structure elucidation and refinement, nuclear magnetic resonance spectroscopy, gas chromatography, thermal analysis, and the measurement of the kinetics of decomposition and enclathration. A combination of these techniques yielded insight into the intermolecular interactions within the prepared crystals, and the selectivity displayed by the studied host compounds.

In chapter 3, eight inclusion compounds were prepared with hosts **H1** and **H2** and guests methyl- and dimethylpiperidines (DMP). The selectivity observed by the hosts could be rationalised by the thermal stability results of inclusion compounds containing single guests, where both hosts showed a greater preference for guests which formed more thermally stable inclusion compounds. This was true in all cases, except for the competition experiment of **H1** recrystallised from an equimolar mixture of **2,6-** and **3,5-DMP**. The resulting crystals contained only **3,5-DMP**. However, the measured thermal stabilities of the **H1·3,5-DMP** and **H1·2,6-DMP** compounds were very similar.

Chapter 4 presents the preparation of two polymorphs of **H1** alone, and four inclusion compounds comprising single guests of three pentanol isomers, and 1-butanol. One of the apohost polymorphs was recrystallised from 3-methyl-1-butanol at room temperature, and the other polymorph from 1-butanol at 50 °C. It was found that **H1** displays a preference for the pentanol isomers over 1-butanol in the order: **3PENT** > **2PENT** > **3MBUT**> **1BUT**. It was again noted that the selectivity by the host could be linked to the thermal stability of the pure inclusion compounds.

In chapter 5, six inclusion compounds containing **H1** were prepared with various combinations of the guests, 2-propanol and tertiary butanol. The results of equimolar competition studies showed that **H1** includes both guests equally at high recrystallisation temperatures, displaying no selectivity. However, the selectivity displayed by **H1** increases towards tertiary butanol as the temperature of crystallisation is decreased. In addition, it was observed that the guest/host ratio of the inclusion compounds increases as the crystallisation temperature decreases, in agreement with observations made by Ibragimov.

In chapter 6, six inclusion compounds were prepared with the host **H3** and guests 1- and 2-methylnaphthalene (MN). A similar investigation has been conducted by Toda et al., but with

the Werner host's ligand being 4-methylpyridine (vs 4-*phenyl*pyridine in **H3**). A polymorphic pair of inclusion compounds with **1-MN** are reported. The less symmetrical (and therefore, higher entropy, and more thermodynamically stable) polymorph recrystallises second, after the concentration of **1-MN** has been sufficiently increased by the evaporation of co-solvent. Two inclusion compounds (not polymorphs) were prepared with **2-MN**, and their formation is also dependent on the guest concentration. When recrystallised from an equimolar guest mixture, the preference by **H3** for **1-MN**/ **2-MN** was 87/13. However, the crystallised compound has a different structure, with one co-solvent molecule present for every host molecule. With the evaporation of co-solvent, and the ensuing increase in guest concentration, a mechanical mixture of inclusion compounds are recrystallised, as indicated by PXRD, and NMR analysis of the bulk confirmed that both guests were present in equal amounts.

In chapter 7, the structures of five inclusion compounds were prepared with **H4** and guests containing an oxygen atom. The structures of these compounds were found to contain host to host bromine interactions, but none had significant contacts from host bromine atoms to guest oxygen atoms. Two compounds are polymorphic and are formed by recrystallisation of **H4** from liquid 1,4-dioxane. The one polymorph crystallises in a centrosymmetric space group, and the other crystallises as a mechanical mixture of non-centrosymmetric crystals. These different polymorphs could easily be prepared by exposing other inclusion compounds to 1,4-dioxane vapour, where the polymorph formed was the one which maintained the chirality of the starting inclusion compound. Other inclusion compounds were exposed to gaseous guests, and the kinetics of guest exchange from the **CYNO** to the **PENT** compound was measured by calculating the area of representative PXRD peaks during the guest-exchange reaction.

8.2 WHAT OF THE FUTURE?

While many structurally similar isomers share similar properties, they can also sometimes be remarkably different. For example, there are ten distinct isomers of dimethylnaphthalene, with melting points ranging from -18 to +112 °C. How does this guest melting point disparity affect the behaviour of inclusion compounds? It would be interesting to measure the temperatures that such binary mixtures (with various compositions) freeze. Such a phase diagram could then be compared with the host selectivity preference measured at different crystallisation temperatures and from different ratios of guests.

In addition, it is still not possible to accurately predict the crystal structure of multi-component compounds, and current algorithms do not factor in experimental conditions. Needed are the development of new methods that consider such factors, like the type and amount of co-solvent used, and the crystallisation method and temperature. For this to be possible further studies are needed correlating the structures of polymorphic multi-component systems with the crystallisation conditions from which they form.

1810	H. Davy prepares a chlorine hydrate [A1]
1823	M. Faraday confirms Davy's observation and determines the composition of the chlorine hydrate [A2]
1840	A. Damour observes the reversible dehydration of zeolite crystals [A3]
1841	C. Shafhäutl prepares the graphite intercalates [A4]
1849	F. Wohler prepares a β-quinol· H_2S molecular complex [A5]
1891	A. Villiers prepares the first cyclodextrin inclusion compounds [A6]
1893	S. U. Pickering publishes a study of alkylamine hydrates [A7]
1894	E. Fischer introduces the "lock and key" principle [A8]
1895	Discovery of X-rays by Röntgen
1897	Preparation of Hofmann's benzene inclusion compound: $Ni(CN)_2{\cdot}NH_3{\cdot}C_6H_6$ [A9]
1903	Preparation of Hofmann's compound with aniline and phenol [A10]
1906	Preparation of inclusion compounds of triphenylmethane [A11]
1909	Preparation of tri-o-thymotide (TOT) benzene inclusion compound [A12]
1914	Synthesis of Dianin's compound: 4-(4-hydroxyphenyl)-2,2,4-trimethylchroman [A13]
1914	Nobel prize for Physics M.T.F. von Laue for his discovery of the diffraction of x-rays by crystals
1915	Nobel prize for Physics: W.H. Bragg and W.L. Bragg for their services in the analysis of crystal structures by means of X-rays
1916	H. Wieland and H. Sorge prepare the first choleic acid inclusion compounds [A14]
1930	Gas hydrates block natural gas pipelines in USA and USSR at temperatures higher than for normal ice formation – this results in a renewed interest in gas hydrates [A15]
1932	The term "molecular sieve' is coined to describe the behaviour of some microporous charcoals and zeolites [A16]
1935	E. Terres and W. Vollmer publish the preparation of phenol molecular complexes [A17]
1936	O. Kratky and G. Giacomello elucidate the crystal structure of choleic acid [A18]
1940	M.F. Bengen patents the preparation of urea inclusion compounds [A19]

1947	F.F. Mikus, R.M. Hixon and R.E. Rundle publish the preparation of amylose inclusion compounds [A20]
1948	D. E. Palin and H.M. Powell publish the crystal structures of the β-quinol· H_2S inclusion compound[A21]. Powell announces the term, "clathrate" [A22]
1951	D.J Cram and H. Steinberg publish the synthesis of [2,2]paracyclophane [A23]
1951	M. von Stackelberg and H.R. Müller [A24]; W.F. Claussen[A25]; L. Pauling and R.E. Marsh [A26]**Error! Reference source not found.** all propose crystal structures for the two types of gas hydrates and recognise them as clathrates
1957	W.D. Schaeffer et al. publish an article entitles: "Separation of xylenes, cymenes, methylnaphthalenes and other isomers by clathration of inorganic complexes", using Werner clathrates [A27]
1964	Publication of "Non Stoichiometric Compounds" by L. Mandelcorn [A28]
1967	C.J. Pedersen publishes the preparation of crown ethers [A29]
1969	J.L. Atwood "accidentally" prepares first liquid clathrates [A30]
1969	J.-M. Lehn and co-workers publish the preparation of cryptands [A31]
1972	R.J. Argauer and G.R. Landolt describe zeolite ZSM5 [A32]
1974	D.J. Cram and J.M. Cram introduce the terms "host", "guest" and "host-guest complexation" [A33]
1976	D.D. MacNicol synthesises first hexa-hosts [A34]
1978	J.-M. Lehn introduces the concept and term "supramolecular chemistry" [A35]
1979	G.D. Andreetti, R. Ungaro and A. Pochini report the crystal structure of p-tert-butyl-calix[4]arene with toluene included in the cavity [A36]
1980	J. Lipkowski describes the physical chemistry of Werner clathrates [A37]
1980	Institute of physical Chemistry of the Polish Academy of Science hosts the First International Symposium on "Clathrate Compounds and Molecular inclusion phenomena" in Jachranka, near Warsaw.
1983	First issue of J. of Inclusion Phenomena is published, editors J.L. Atwood and J.E.D. Davies [A38]
1983	E. Weber and H.-P. Josel propose nomenclature and classification of host-guest type compounds [A39]
1984	First volume of Inclusion Compounds is published by Academic Press, London [A40]

1985	Nobel prize for Chemistry: J. Karle and H.A. Hauptman for developing direct phasing methods to determine X-ray crystal structures
1987	J.F. Stoddart and co-workers publish the synthesis of the first catenanes and rotaxanes [A41]
1987	Nobel prize for Chemistry: D.J. CramA42, J.-M. LehnA43, C.J. Pederson [A44] for their respective work in the field of supramolecular chemistry
1992	First issue of Supramolecular Chemistry is published, editors J.L. Atwood and G.W. Gokel [A45]
1993	Herbstein gives classification scheme for binary adducts [A46]
1994	First issue of Supramolecular Science is published, editor-in-chief W. Knoll [A47]
1996	Publication of Comprehensive Supramolecular Chemistry, Vol. 1-11, Executive editors: J.L. Atwood, J.E.D. Davies, D.D. MacNicol and F Vögtle, Pergamon Press [A48]
1998	First issue of Crystal Engineering is published, editors R.D. Rogers and M. Zaworotko [A49]
1999	First issue of CrystEngComm is published, editor-in-chief Dario Braga [A50]
2000	J.W. Steed and J.L. Atwood publish Supramolecular Chemistry text [A51]
2001	First issue of Crystal Growth and Design is published, editor-in-chief R.D. Rogers [A52]
2004	Publication of 'Encyclopaedia of Supramolecular Chemistry, vols 1-2, Editors J.L. Atwood and J.W. Steed **Error! Reference source not found.**
2009	Nobel prize for Chemistry: V. Ramakrishnan, T.A. Steitz, and A.E. Yonath for studied of the structure and function of the ribosome
2011	Nobel prize for Chemistry: D. Shechtman for the discovery of quasicrystals
2012	Publication of 'Supramolecular Chemistry: from molecules to nanomaterials', vols 1-8, editors-in-chief P.A. Gale and J.W. Steed [A54]
2016	Nobel prize for Chemistry: J.-P. Sauvage, F. Stoddard, and B. Feringa for the design and synthesis of molecular machines
2017	Publication of "Comprehensive Supramolecular Chemistry II", vols 1-9, editors J.L. Atwood, G.W. Gokel, and L. BarbourA55

References

A1 H. Davy, I. The Bakerian Lecture. On some of the combinations of oxymuriatic gas and oxygene, and on the chemical relations of these principles, to inflammable bodies, *Philosophical Transactions of the Royal Society of London*, 1811, **101**, 1–35.

A2 M. Faraday, On hydrate of chlorine. *Q.Jl Sci.Lit.Arts.* 1823, **15**, 71–74.

A3 A. Damour, Über das Bleigummi und thonerdhaltiges phosphorsaures Bleioxyd von Huelgoat. *Ann. Mines*., 1840, **17**, 191.

A4 C. Schafhaeutl, Ueber die Verbindungen des Kohlenstoffes mit Silicium, Eisen und anderen Metallen, welche die verschiedenen Gattungen von Roheisen, Stahl und Schmiedeeisen bilden. *J Prakt Chem*. 1840, **20**, 465–485.

A5 F. Wöhler, Ueber einige verbindungen aus der chinonreihe. *Justus Liebigs Ann. Chem*. 1849, **69**, 294–300.

A6 A. Villiers, Sur la fermentation de la fécule par l'action du ferment butyrique. *Hebd. Seances Acad. Sci*., 1891, **112**, 536–538.

A7 S. U. Pickering, X.—The hydrate theory of solutions. Some compounds of the alkyl-amines and ammonia with water, *J. Chem. Soc., Trans.*, 1893, **63**, 141–195.

A8 E. Fischer, Einfluss der configuration auf die wirkung der Enzyme. *Ber. Deutsch. Chem. Ges*. 1894, **27**, 2985-2993.

A9 K. A. Hofmann and F. Küspert, Verbindungen von kohlenwasserstoffen mit metallsalzen. *Z. Anorg. Allg. Chem*. 1897, **15**, 204–207.

A10 K. A. Hofmann and F. Höchtlen, Abnorme verbindungen des nickels. *Chem. Ber.* 1903, **36**, 1149–1151.

A11 H. Hartley and N. G. Thomas, CV.—The solubility of triphenylmethane in organic liquids with which it forms crystalline compounds, *J. Chem. Soc., Trans.*, 1906, **89**, 1013–1033.

A12 R. Spallino and G. Provenzal, Sulla preparazione dell'acido ortotimotico e di alcuni suoi derivati, *Gazz. Chim. Ital*., 1909, **39**, 325–336.

A13 A. P. Dianin, On the condensation of phenols with unsaturated ketones. Condensation of phenols with mesitylene oxide. *J. Soc. Phys. Chem. Russe*., 1914, **46**, 1310–1319.

A14 H. Wieland and H. Sorge, Untersuchungen über die gallensäuren. II. Mitteilung. Zur kenntnis der choleinsäure*. Z. Physiot Chem*. Hoppe-Seyler's. 1916, **97**, 1–27.

A15 E. G. Hammerschmidt, Formation of Gas Hydrates in Natural Gas Transmission Lines, *Ind. Eng. Chem.*, 1934, **26**, 851–855.

A16 J. W. McBain, *The Sorption of Gases and Vapours by Solids*, G. Routledge, 1932.

A17 E. Terres and W. Z. Vollmer, Die Löslichkeit von Mineralöl- und Teerbestandteilen in flüssigem Schwefelwasserstoff, *Petroleum Z*. 1935, **31**, 1–19.

A18 O. Kratky and G. Giacomello, Der kristallbau der paraffin carboncholeinsäuren, *Monatsh. Chem*., 1936, **69**, 427–436.

A19 M. F. Bengen. German Patent Application 02123438. March 18, 1940.

A20 F. F. Mikus, R. M. Hixon and R. E. Rundle, The Complexes of Fatty Acids with Amylose, *J. Am. Chem. Soc.*, 1946, **68**, 1115–1123.

A21 D. E. Palin and H. M. Powell, 50. The structure of molecular compounds. Part III. Crystal structure of addition complexes of quinol with certain volatile compounds, *J. Chem. Soc.*, 1947, 208–221.

A22 H. M. Powell, 15. The structure of molecular compounds. Part IV. Clathrate compounds, *J. Chem. Soc.*, 1948, 61–73.
A23 D. J. Cram and H. Steinberg, Macro Rings. I. Preparation and Spectra of the Paracyclophanes, *J. Am. Chem. Soc.*, 1951, **73**, 5691–5704.
A24 M. Von Stackelberg and H. R. Müller, On the structure of gas hydrates. J. *Chem. Phys*., 1951, **19**, 1319–1320.
A25 W. F. Claussen, Suggested Structures of Water in Inert Gas Hydrates, *J. Chem. Phys.*, 1951, **19**, 259–260.
A26 L. Pauling and R. E. Marsh, The Structure of Chlorine Hydrate, *Proc. Natl. Acad. Sci. U S A*, 1952, **38**, 112–118.
A27 W. D. Schaeffer, W. S. Dorsey, D. A. Skinner and C. G. Christian, Separation of Xylenes, Cymenes, Methylnaphthalenes and Other Isomers by Clathration with Inorganic Complexes, *J. Am. Chem. Soc.*, 1957, **79**, 5870–5876.
A28 L. Mandelcorn, *Non-stoichiometric compounds.*, Academic Press, New York, 1964.
A29 C. J. Pedersen, Cyclic polyethers and their complexes with metal salts, *J. Am. Chem. Soc.*, 1967, **89**, 2495–2496.
A30 J. L. Atwood, P. A. Milton and S. K. Seale, Thermal behavior of anionic organoaluminum thiocyanates, *Journal of Organometallic Chemistry*, 1971, **28**, C29–C30.
A31 B. Dietrich, J. M. Lehn and J. P. Sauvage, Diaza-polyoxa-macrocycles et macrobicycles, *Tetrahedron Lett.*, 1969, **10**, 2885–2888.
A32 R. J. Argauer and G. R. Landolt, Crystalline zeolite zsm-5 and method of preparing the same. United States, US3702886A, 1972.
A33 D. J. Cram and J. M. Cram, Host-Guest Chemistry, *Science*, 1974, **183**, 803–809.
A34 D. D. MacNicol and D. R. Wilson, New strategy for the design of inclusion compounds: discovery of the 'hexa-hosts', *J. Chem. Soc., Chem. Commun.*, 1976, 494–495.
A35 J. M. Lehn, Cryptates: inclusion complexes of macropolycyclic receptor molecules, *Pure and Applied Chemistry*, 1978, **50**, 871–892.
A36 G. D. Andreetti, R. Ungaro and A. Pochini, Crystal and molecular structure of cyclo{quater[(5-t-butyl-2-hydroxy-1,3-phenylene)methylene]} toluene (1 : 1) clathrate, *J. Chem. Soc., Chem. Commun.*, 1979, 1005–1007.
A37 J. Lipkowski, Structure and Physico-chemical Behaviour of Clathrates Formed by the $Ni(NCS)_2(4\text{-Methylpyridine})_4$ Complex. Accademia Polacca delle Scienze, Biblioteca e centro di studi a Roma Conferenze, 1980, **81**, 1–27.
A38 J. E. D. Davies, W. Kemula, H. M. Powell and N. O. Smith, Inclusion compounds — Past, present, and future, *J. Incl. Phenom.*, 1983, **1**, 3–44.
A39 E. Weber and H.-P. Josel, A proposal for the classification and nomenclature of host-guest-type compounds, *J. Incl. Phenom.*, 1983, **1**, 79–85.
A40 J. L. Atwood, D. D. MacNicol and J. E. D. Davies, *Inclusion Compounds: Physical Properties and Applications. - 1984*, Academic Press.
A41 B. L. Allwood, N. Spencer, H. Shahriari-Zavareh, J. F. Stoddart and D. J. Williams, Complexation of Paraquat by a bisparaphenylene-34-crown-10 derivative, *J. Chem. Soc., Chem. Commun.*, 1987, 1064–1066.
A42 D. J. Cram, The design of molecular hosts, guests, and their complexes, *J. Incl. Phenom.*, 1988, **6**, 397–413.

A43 J.-M. Lehn, Supramolecular Chemistry—Scope and Perspectives Molecules, Supermolecules, and Molecular Devices (Nobel Lecture), *Angew. Chem., Int. Ed. Engl.*, 1988, **27**, 89–112.

A44 C. J. Pedersen, The Discovery of Crown Ethers (Nobel Lecture), *Angew. Chem., Int. Ed. Engl.*, 1988, **27**, 1021–1027.

A45 J. L. Atwood, G. W. Gokel and Y. Murakami, Comments from the Editors, *Supramol. Chem.*, 1992, **1**, 1.

A46 F. H. Herbstein, Structural principles in the classification of crystalline binary adducts (molecular compounds and complexes). *Acta Chim. Hung*., 1993, **130**, 377–386.

A47 W. Knoll, Editorial. Supramolecular Science. 1994, **1**, 3.

A48 J. L. Atwood and J.-M. Lehn, *Comprehensive supramolecular chemistry*, Pergamon, New York, 1996.

A49 A. Anthony, G. R. Desiraju, R. K. R. Jetti, S. S. Kuduva, N. N. L. Madhavi, A. Nangia, R. Thaimattam and V. R. Thalladi, Crystal Engineering: Some Further Strategies, *Cryst. Eng.*, 1998, **1**, 1–18.

A50 L. R. MacGillivray, J. L. Reid and J. A. Ripmeester, Solvent provides a trap for the guest-induced formation of 1D host frameworks based upon supramolecular, deep-cavity resorcin[4]arenes, *CrystEngComm*, 1999, **1**, 1–4.

A51 J. W. Steed and J. L. Atwood, *Supramolecular Chemistry*, Wiley, 2000.

A52 R. D. Rogers, Editorial, *Cryst. Growth Des.*, 2001, **1**, 1–2.

A53 J. L. Atwood and J. W. S. Durham, *Encyclopedia of Supramolecular Chemistry*, CRC Press, Boca Raton, 2004.

A54 *Supramolecular Chemistry, 8 Volume Set: From Molecules to Nanomaterials*, Wiley, 2012. Editors P. A. Gayle and J. W. Steed.

A55 G. W. Gokel and L. Barbour, *Comprehensive Supramolecular Chemistry II*, Elsevier, 2017.

3.7.1 Table S3.1. Compounds of interest with H1 as listed in the Cambridge Structural Database in 2017.

Guest	REFCODE	Reference
2-picoline	CISPEA	Nassimbeni, L. R.; Ramon, G.; Weber, E. Inclusion by a Fluorenyl Diol Host with Substituted Pyridines. *J Therm Anal Calorim* **2007**, *90* (1), 31–37.
3-picoline	CISPIE	
4-picoline	CISPOK	
pyridine	CISPUQ	
ethanol	DEZBUG	
Ethanol and acetonitrile	DEZCAN	
Ethanol and acetonitrile	DIFDEC	
Ethanol and acetonitrile	DIFDIG	
Acetonitrile and water	DEZBOA01	Roex, T. le; Nassimbeni, L. R.; Weber, E. Selectivity and Structure of Mixed Guestclathrates. *New J. Chem.* **2008**, *32* (5), 856–863.
ethanol	DEZBUG01	
Acetonitrile and water	DEZCAN01	
Ethanol and acetonitrile	DIFDEC01	
Ethanol and acetonitrile	DIFDIG01	
ethanol	GIZPOV	

3.7.2 Table S3.2. Compounds of interest with H2 on the Cambridge Structural Database in 2017.

Guest	REFCODE	Reference
Aniline	EVUGEH	Bourne, S. A.; Corin, K. C.; Nassimbeni, L. R.; Weber, E. PH Control of Guest Selectivity by Inclusion. *CrystEngComm* **2004**, *6* (12), 54–55.
Benzylamine	EVUGIL	
2,4-lutidine	OBELEM	Caira, M. R.; Nassimbeni, L. R.; Vujovic, D.; Weber, E.; Wierig, A. Separation of Lutidine Isomers by Inclusion. *Structural Chemistry* **1999**, *10* (3), 205–211.
3,5-lutidine	OBELIQ	
2,6-lutidine	OBELOW	
2-picoline	OTOBOP	
3-picoline	OTOBUV	
4-picoline	OTOCAC	
pyridine	OTOCOQ	

3.7.3 Figure S3.1. Hirshfeld surface analysis of inclusion compounds with the hosts selected as target.

a) H1•2(2MP) Minor component

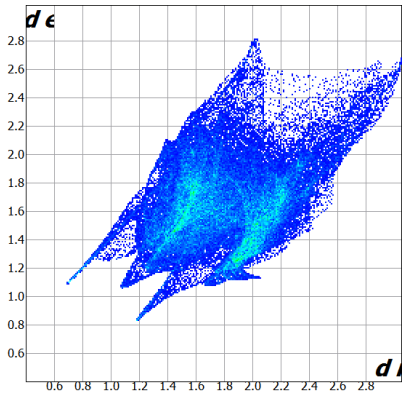

In (%)	Out (%) C	H	N	O
C	0	26.9	0	0
H	1.3	66.0	1.5	0.2
O	0	4.1	0	0

b) H1•2(2MP) Major component

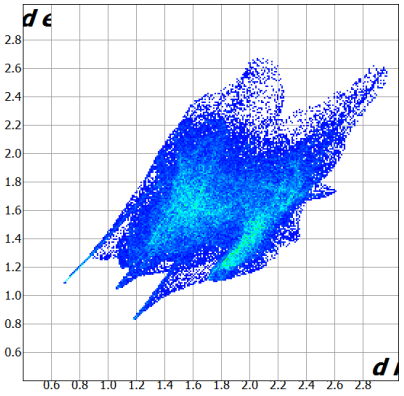

In (%)	Out (%) C	H	N	O
C	0	26.7	0	0
H	1.0	66.1	1.6	0.3
O	0	4.3	0	0

c) H1•2(3MP) Major component

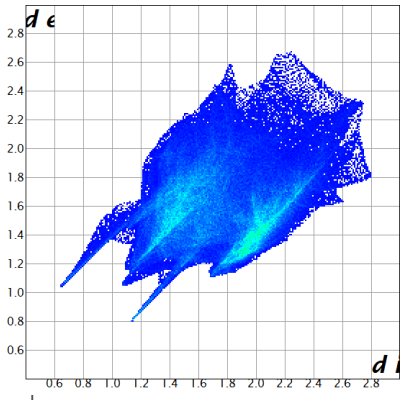

In (%)	Out (%) C	H	N	O
C	0	27.1	0	0
H	2.1	62.4	2.1	1.4
O	0	4.8	0	0

d) H1•2(3MP) Minor component

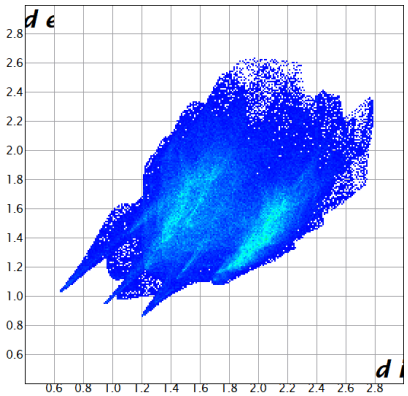

In (%)	Out (%) C	H	N	O
C	0	27.3	0	0
H	1.9	62.3	1.9	1.7
O	0	5.0	0	0

g) H1•2(3,5DMP)
(cis portion of guest only)

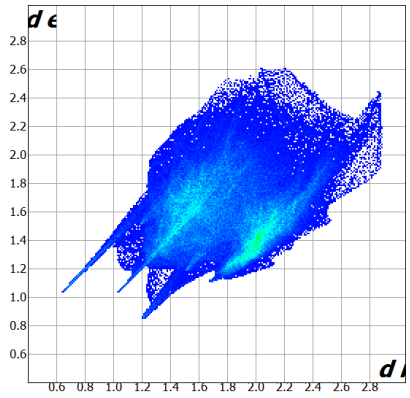

In (%)		Out (%) C	H	N	O
	C	0	26.9	0	0
	H	1.5	62.5	2.0	1.9
	O	0	5.2	0	0

h) H2•2(2,6DMP)

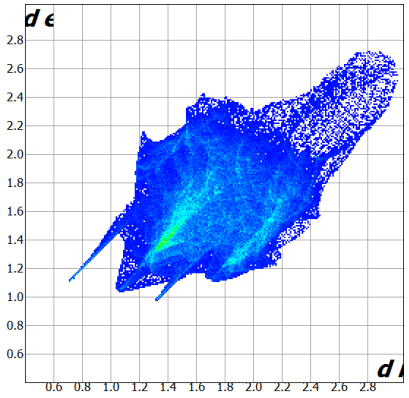

In (%)		Out (%) C	H	N
	C	0.8	21.9	0
	H	7.6	65.6	1.5
	O	0	2.6	0

i) H2•2(3,5DMP)•H_2O

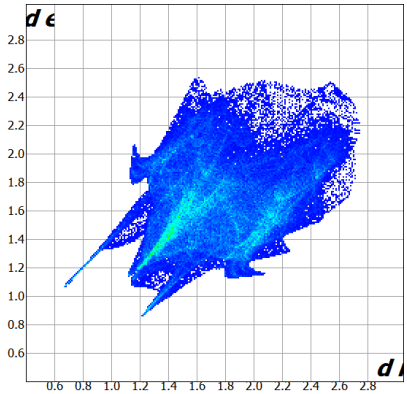

In (%)		Out (%) C	H	N	O
	C	0	22.0	0	0
	H	8.5	64.6	1.8	0.5
	O	0	2.6	0	0

3.7.4 $\pi - \pi$ interactions in H2.

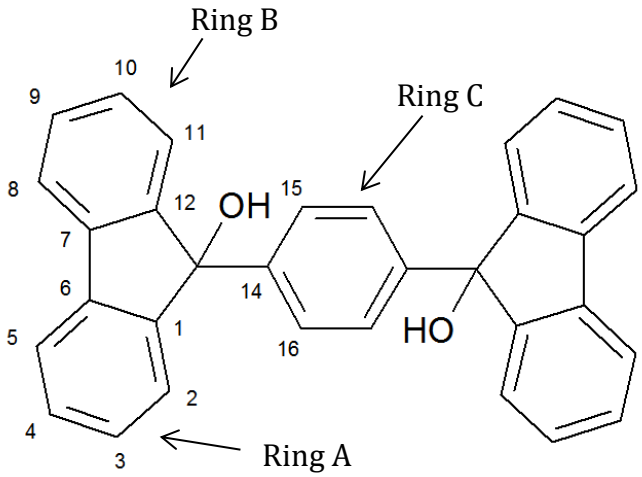

Ring A: C1, C2, C3, C4, C5, C6
Ring B: C7, C8, C9, C10, C11, C12
Ring C: C14, C15, C16

Table S3.3. Edge to face π interactions in compounds **3.6** – **3.8**

Compound	C-H ⋯ π	C ⋯ π (Å)	H ⋯ π (Å)	C-H ⋯ π (°)
H2•2(2MP)	π(**A**) C3[a]-H3[a]⋯ π(**C**)	3.822	2.881	171
H2•2(2,6DMP)	π(**B**) C10[b]-H10[b]⋯ π(**C**)	3.888	2.951	169
H2•2(3,5DMP)·H₂O	π(**B**) C10[c]-H10[c]⋯ π(**C**)	3.732	2.800	167

[a]1-*x*, 1-*y*, 2-*z*
[b]-*x*-1, -*y*, 1-*z*
[c]*x*, 1+*y*, *z*

3.7.5 Figure S3.3 TG and DSC traces of inclusion compounds.

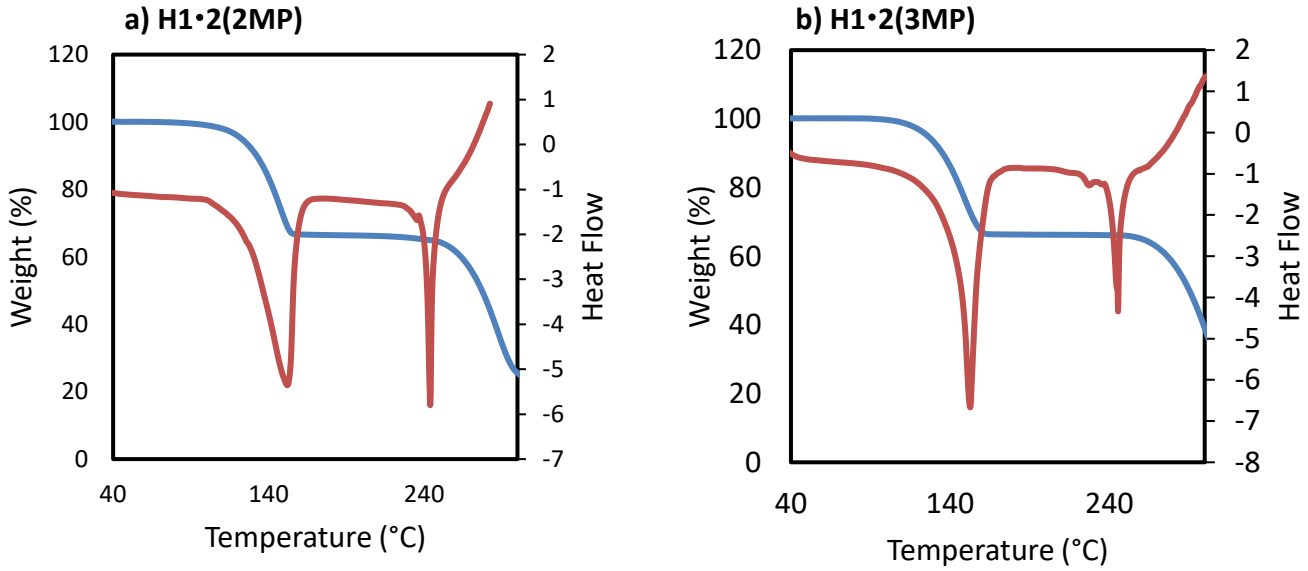

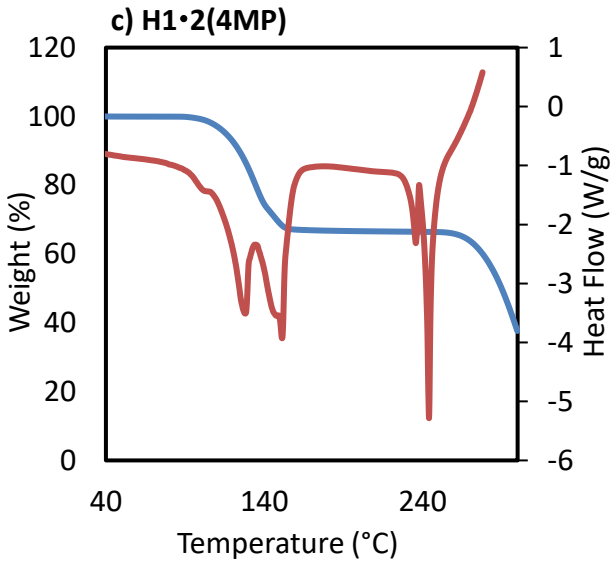
c) H1•2(4MP)
Weight (%)
Heat Flow (W/g)
Temperature (°C)

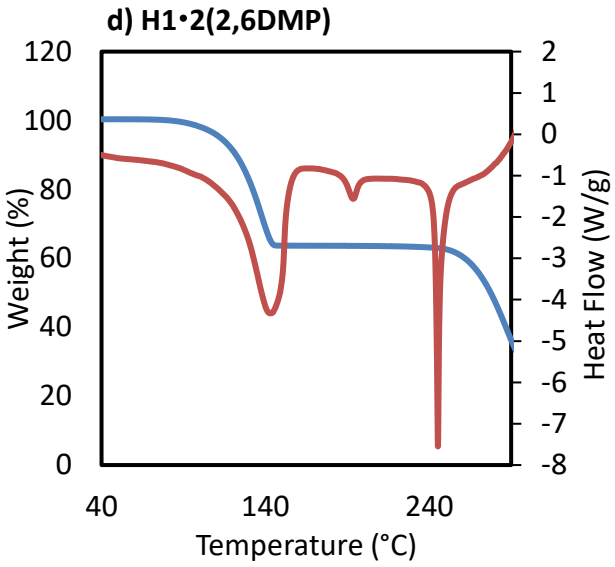
d) H1•2(2,6DMP)
Weight (%)
Heat Flow (W/g)
Temperature (°C)

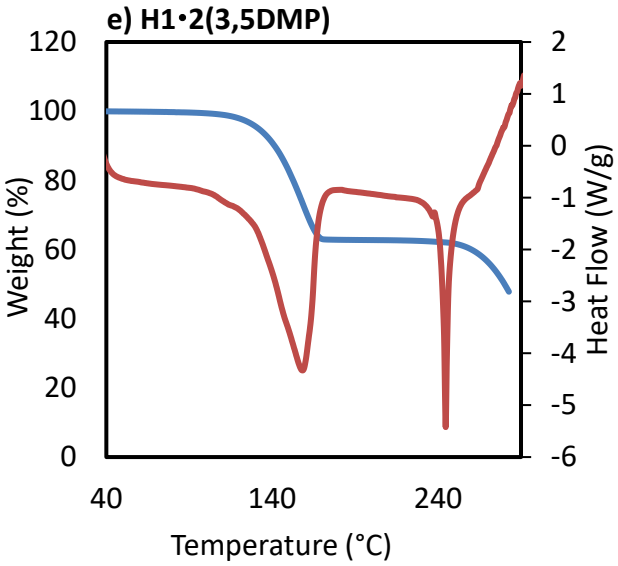
e) H1•2(3,5DMP)
Weight (%)
Heat Flow (W/g)
Temperature (°C)

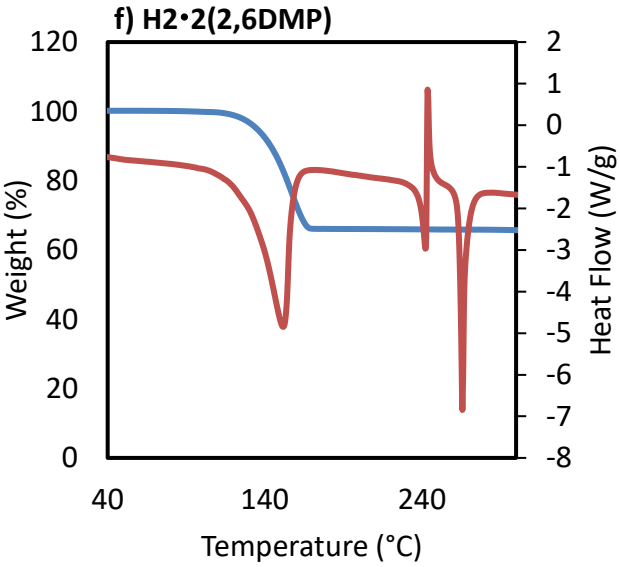
f) H2•2(2,6DMP)
Weight (%)
Heat Flow (W/g)
Temperature (°C)

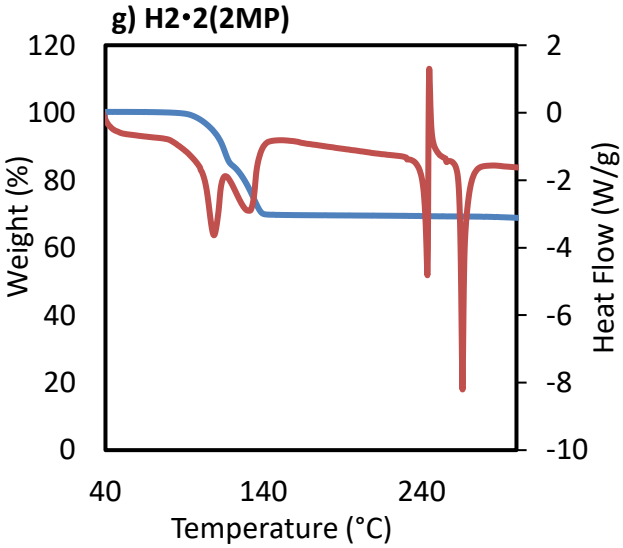
g) H2•2(2MP)
Weight (%)
Heat Flow (W/g)
Temperature (°C)

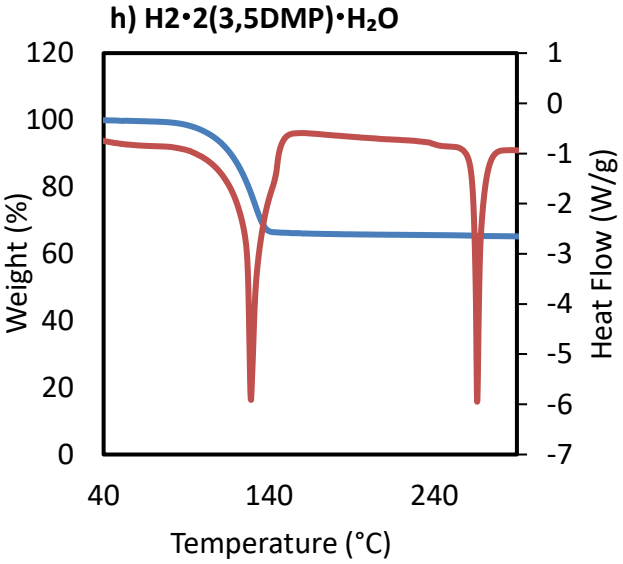
h) H2•2(3,5DMP)•H₂O
Weight (%)
Heat Flow (W/g)
Temperature (°C)

4.7.1 Table S4.1. CSD analysis of the host (H1), 9,9'-(ethyne-1,2-diyl)-bis(fluoren-9-ol).

Guest	Host torsion angle (°)	REFCODE	Reference
2,6-dimethylpiperidine	180	CANFUV	N. M. Sykes, H. Su, E .Weber, S. A. Bourne and L. R. Nassimbeni, Cryst. Growth Des., 2017, **17**, 819-826.
2-methylpiperidine	180	CANGAC	
3,5-methylpiperidine	146	CANGEG	
3-methylpiperidine	150	CANGIK	
4-methylpiperidine	145	CANGOQ	
2-picoline	180	CISPEA	L. R. Nassimbeni, G. Ramon and E. Weber, *J. Therm. Anal. Cal*., 2007, **90**, 31-37.
3-picoline	180	CISPIE	
4-picoline	180	CISPOK	
Pyridine	180	CISPUQ	
Acetonitrile and water	18, 13	DEZBOA	T. le Roux, L. R. Nassimbeni and E. Weber, *Chem. Commun*., 2007, 1124-1126.
Ethanol	5, 180	DEZBUG	
Ethanol and acetonitrile	4, 180	DEZCAN	
Ethanol and acetonitrile	4, 180	DIFDEC	
Ethanol and acetonitrile	4, 180	DIFDIG	
Acetonitrile and water	-	DEZBOA01	T. le Roux, L. R. Nassimbeni and E. Weber, *New J. Chem.*, 2008**, 32***,* 856-863.
Acetonitrile	1	ROBGAR	
Ethanol	5, 180	DEZBUG01	
Acetonitrile and water	18, 13	DEZCAN01	
Ethanol and Acetonitrile	4, 180	DIFDEC01	
Ethanol and Acetonitrile	4, 180	DIFDIG01	
Ethanol	0	GIZPOV	
1-propanol	96	IFAHOM	E. Weber, S. Nitsche, A. Wierig, I. Csoregh; *Eur.J.Org.Chem,* 2002, 856
Cyclohexanol	180	IFAHAS	
Tetrahydrofuran	94, 180	IFAJAA	
9H-fluoren-9-one	14, 14	QIZLES	J. Gabriel Garcia, F. R. Fronczek; Private Communication (2014)
9H-fluoren-9-one	12, 14	QIZLES01	Varshni Singh, F. R. Fronczek, S. F. Watkins; Private Communication (2012)
Caffeine	180	UPIWAS	A. Jacobs, L. Nassimbeni, K. L. Nohako, G. Ramon, B. K. Sebogisi; *J.Chem.Cryst*, 2011, **41**, 610
Caffeine and Methanol	43, 43, 15	UPIWEW	
Methanol	4, 5, 5	UPIWIA	

4.7.2 ORTEP and Packing Figures.

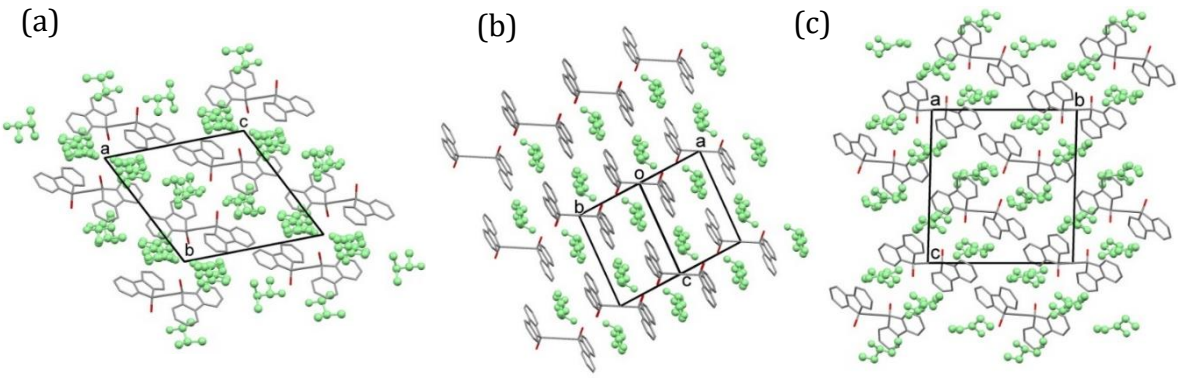

Figure S4.1. The packing of (a) **H•2(3MBUT**) viewed down [100] (b) **H•2(2PENT)** and (c) **3H•6(3PENT)** viewed down [100], with guest atoms shown in green.

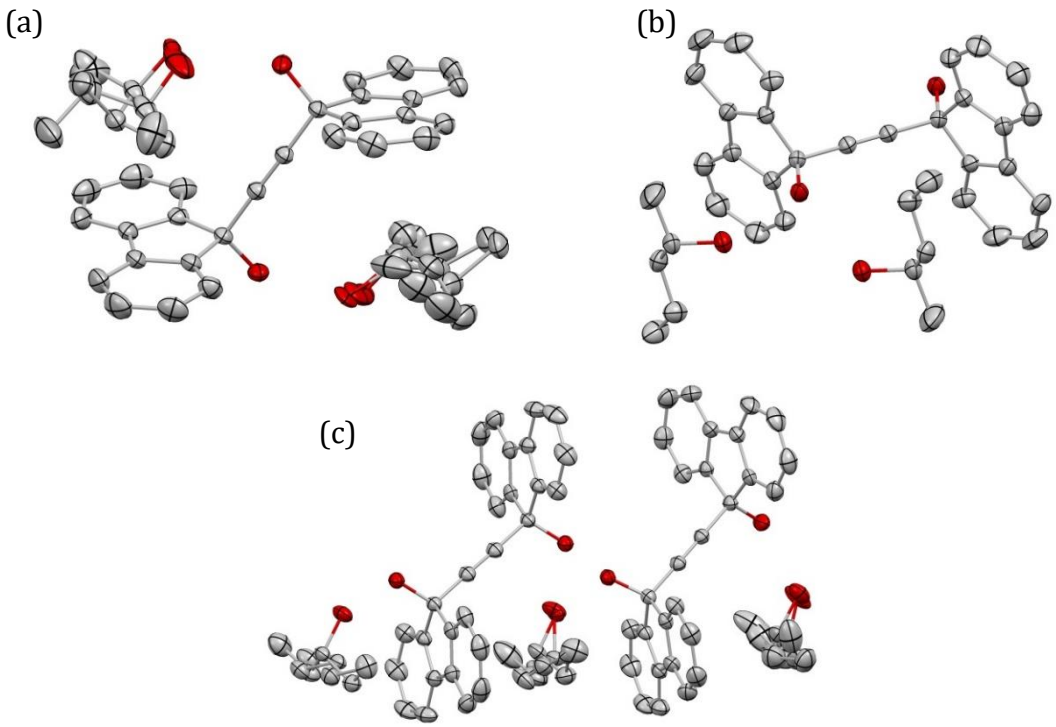

Figure S4.2. ORTEP diagrams of (a) **H•2(3MBUT)** (b) **H•2(2PENT)** and (c) **3H•6(3PENT)**

4.7.3 DSC and PXRD traces of Apohost(α) and Apohost(β).

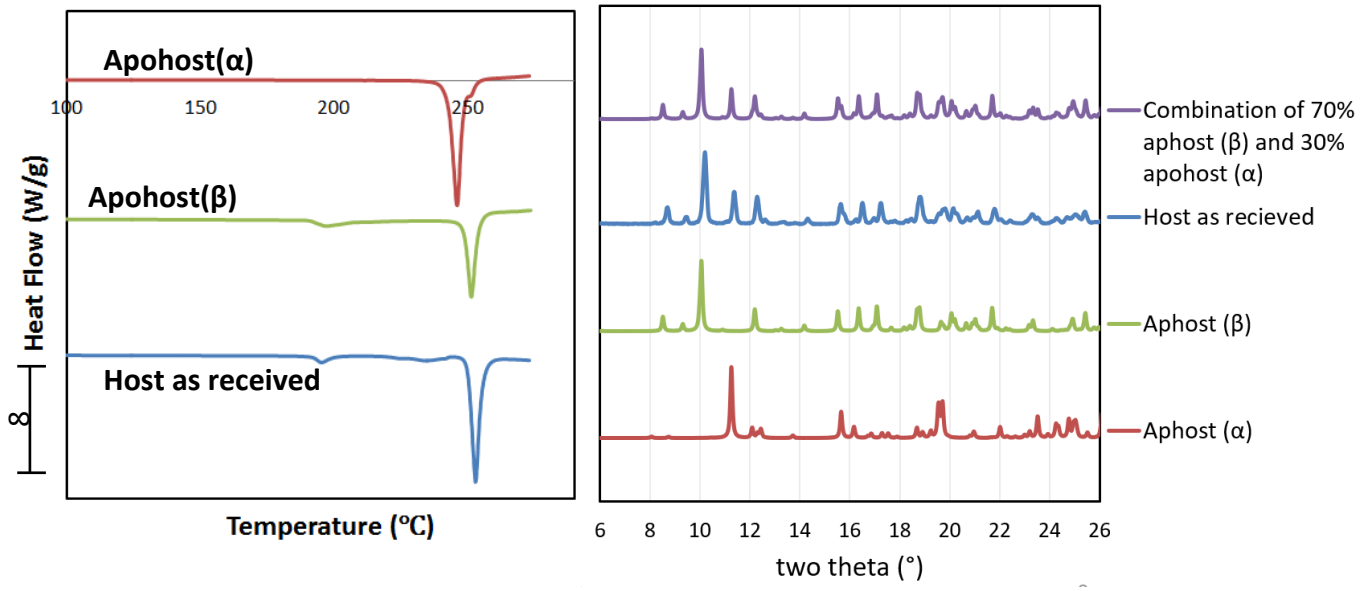

Figure S4.3. DSC (left) and PXRD (right) traces of **Apohost(α)**, **Apohost(β)**, and the Host (**H1**) as received.

4.7.4 DFT calculation.

Relaxed potential energy scans were computed using density functional theory (DFT), employing the B3LYP hybrid exchange-correlation functional[C1 - C3] and the def2-SVP basis set.[C4] Dispersion effects were taken into account by adding the D3 correction of Grimme, with Becke-Johnson (BJ) dampening[C5, C6]. This level of theory is denoted B3LYP-D3/def2-SVP. The Gaussian 09 package was used[C7].

References

C1 A. D. Becke, Density-functional thermochemistry. III. The role of exact exchange, *J. Chem. Phys.*, 1993, **98**, 5648–5652.

C2 C. Lee, W. Yang and R. G. Parr, Development of the Colle-Salvetti correlation-energy formula into a functional of the electron density, *Phys. Rev. B*, 1988, **37**, 785–789.

C3 P. J. Stephens, F. J. Devlin, C. F. Chabalowski and M. J. Frisch, Ab Initio Calculation of Vibrational Absorption and Circular Dichroism Spectra Using Density Functional Force Fields, *J. Phys. Chem.*, 1994, **98**, 11623–11627.

C4 F. Weigend and R. Ahlrichs, Balanced basis sets of split valence, triple zeta valence and quadruple zeta valence quality for H to Rn: Design and assessment of accuracy, *Phys. Chem. Chem. Phys.*, 2005, **7**, 3297–3305.

C5 S. Grimme, J. Antony, S. Ehrlich and H. Krieg, A consistent and accurate ab initio parametrization of density functional dispersion correction (DFT-D) for the 94 elements H-Pu, *J. Chem. Phys.*, 2010, **132**, 154104.

C6 S. Grimme, S. Ehrlich and L. Goerigk, Effect of the damping function in dispersion corrected density functional theory, *J. Comput. Chem.*, 2011, **32**, 1456–1465.

C7 Gaussian 09, Revision A.02, M. J. Frisch, G. W. Trucks, H. B. Schlegel, G. E. Scuseria, M. A. Robb, J. R. Cheeseman, G. Scalmani, V. Barone, G. A. Petersson, H. Nakatsuji, X. Li, M. Caricato, A. Marenich, J. Bloino, B. G. Janesko, R. Gomperts, B. Mennucci, H. P. Hratchian, J. V. Ortiz, A. F. Izmaylov, J. L. Sonnenberg, D. Williams-Young, F. Ding, F. Lipparini, F. Egidi, J. Goings, B. Peng, A. Petrone, T. Henderson, D. Ranasinghe, V. G. Zakrzewski, J. Gao, N. Rega, G. Zheng, W. Liang, M. Hada, M. Ehara, K. Toyota, R. Fukuda, J. Hasegawa, M. Ishida, T. Nakajima, Y. Honda, O. Kitao, H. Nakai, T. Vreven, K. Throssell, J. A. Montgomery, Jr., J. E. Peralta, F. Ogliaro, M. Bearpark, J. J. Heyd, E. Brothers, K. N. Kudin, V. N. Staroverov, T. Keith, R. Kobayashi, J. Normand, K. Raghavachari, A. Rendell, J. C. Burant, S. S. Iyengar, J. Tomasi, M. Cossi, J. M. Millam, M. Klene, C. Adamo, R. Cammi, J. W. Ochterski, R. L. Martin, K. Morokuma, O. Farkas, J. B. Foresman, and D. J. Fox, Gaussian, Inc., Wallingford CT, 2016.

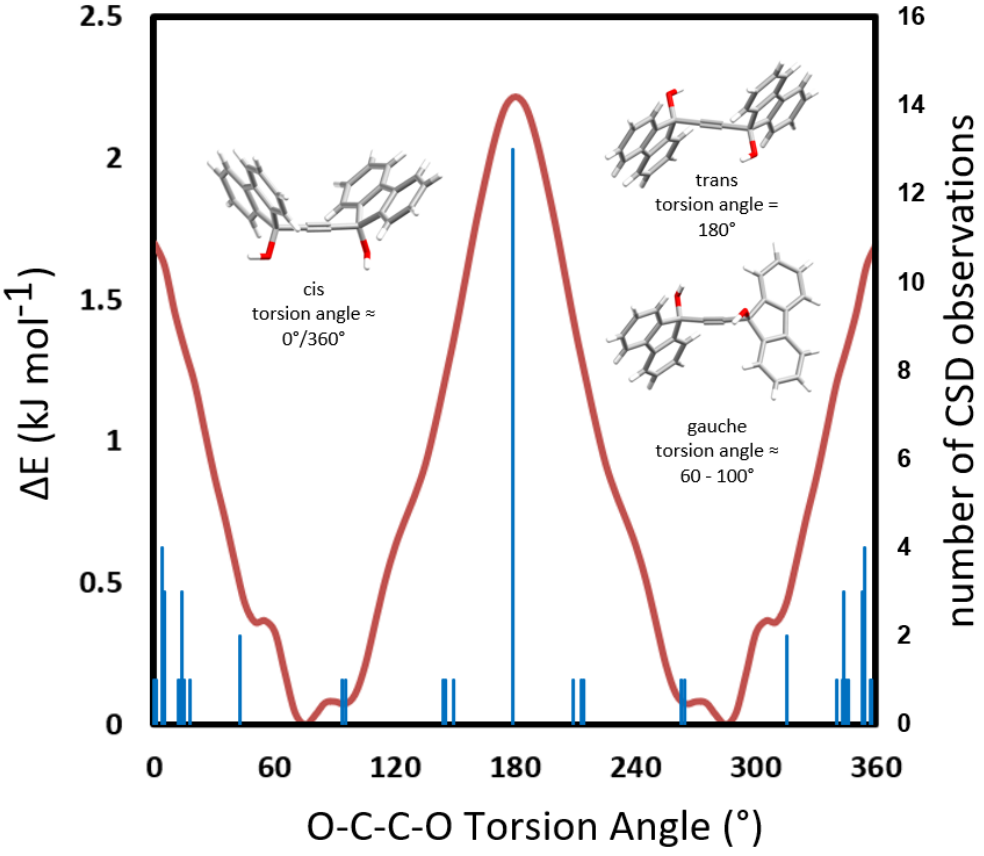

Figure S4.4. The red trace is the gas-phase relative conformational energy plotted as a function of the host's O-C-C-O torsion angle. Overlaid in blue is the number of occurrences on the Cambridge Structural database of the host's conformations.

4.7.5 Hirshfeld Analysis (host selected as target).

a) Apohost(α)

	Out %		
In %	**C**	**H**	**O**
C	6.8	20.5	0
H	16.3	46.9	4.2
O	0	5.3	0

b) Apohost(β) *trans*

	Out %		
In %	**C**	**H**	**O**
C	9.2	18.1	0.1
H	8.5	48.9	10.2
O	0.4	4.6	0

c) Apohost(β) *cis*

	Out %		
In %	**C**	**H**	**O**
C	5.2	21.9	0.2
H	20.2	46.3	1.5
O	0	4.8	0

d) H•2(3MBUT)

	Out %		
In %	**C**	**H**	**O**
C	0	27.2	0.1
H	2.5	62.1	4.0
O	0	4.2	0

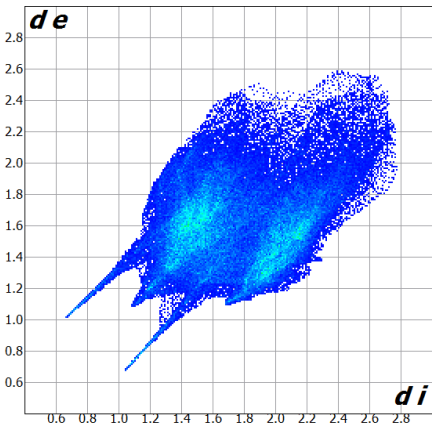

e) 3H•6(3PENT) *trans*

	Out %		
In %	**C**	**H**	**O**
C	0	26.4	0
H	3.7	60.3	3.8
O	0	5.3	0

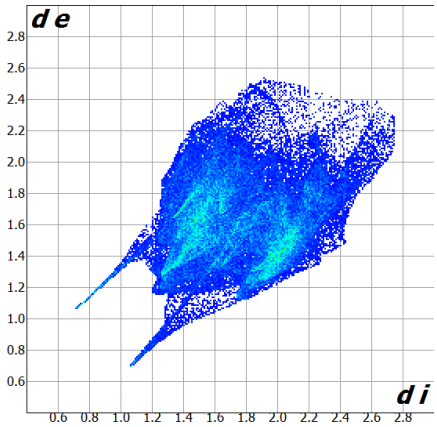

f) 3H•6(3PENT)

	Out %		
In %	**C**	**H**	**O**
C	0	27.4	0
H	2.9	60.7	3.9
O	0	5.1	0

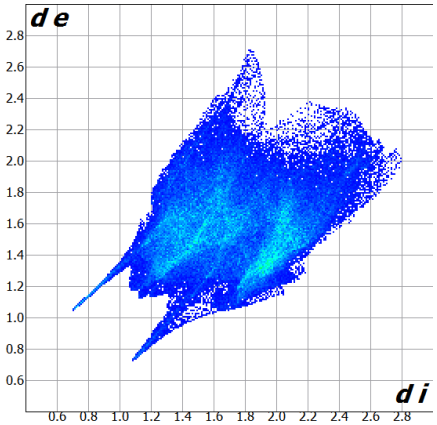

h) H•2(2PENT)

	Out %		
In %	**C**	**H**	**O**
C	0	26.8	0
H	2.0	62.8	3.9
O	0	4.5	0

i) H•2(1BUT)

	Out %		
In %	**C**	**H**	**O**
C	0.8	27.0	0
H	7.4	55.8	4.4
O	0	4.7	0

4.7.6 Competition experiment results.

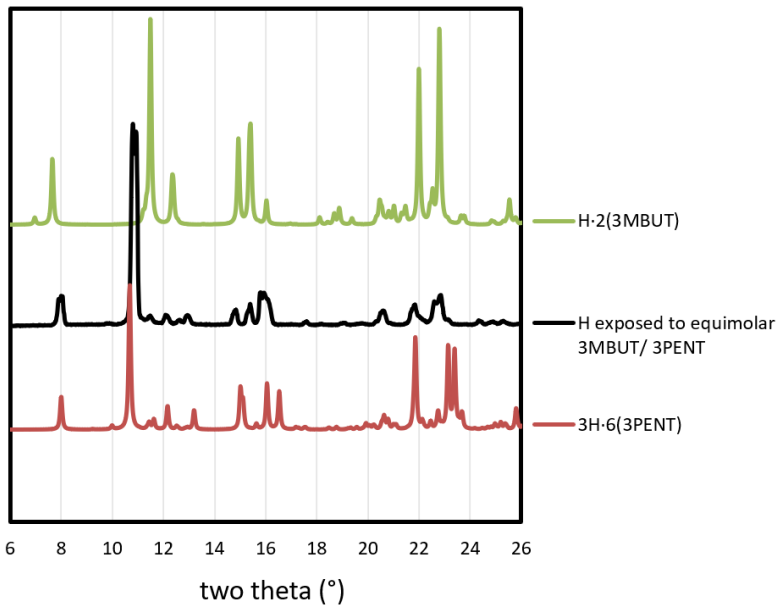

Figure S4.6. Calculated PXRD traces of **3H•6(3PENT)** (red) and **H•2(3MBUT)** (green) compared to the experimental trace (black) of the material collected from the recrystallisation of **H** from a 50/50 mixture of 3-methyl-2-butanol and 3-pentanol. The GC result indicated that 3-pentanol accounted for 80% of the guest contained within the crystals.

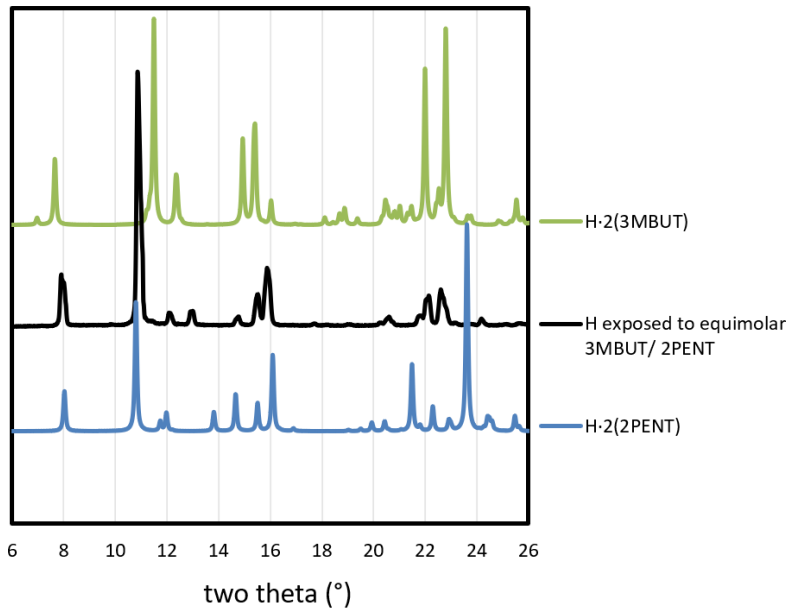

Figure S4.7. Calculated PXRD traces of **H•2(2PENT)** (blue) and **H•2(3MBUT)** (green) compared to the experimental trace (black) of the material collected from the recrystallisation of **H** from a 50/50 mixture of 3-methyl-2-butanol and 2-pentanol. The GC and NMR results indicated that 2-pentanol accounted for ~71% of the guest contained within the crystals.

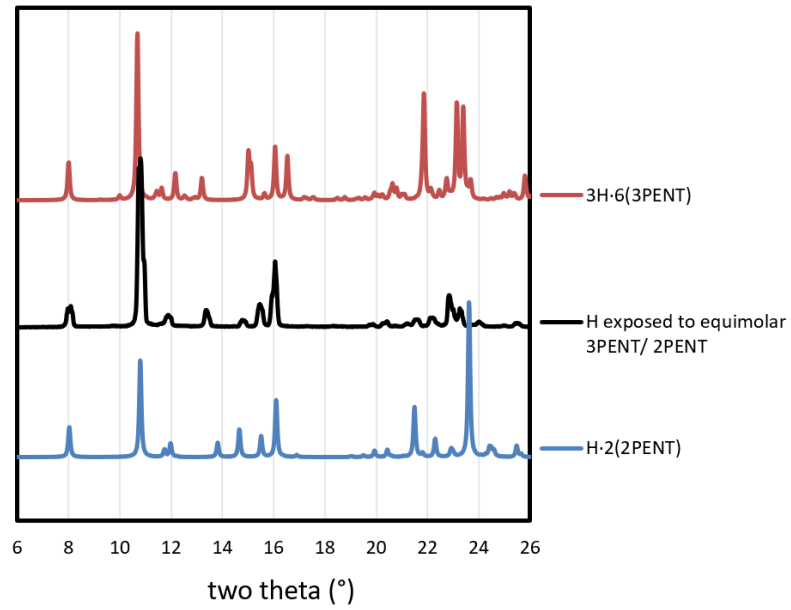

Figure S4.7. Calculated PXRD traces of **3H•6(3PENT)** (red) and **H•2(2PENT)** (blue) compared to the experimental trace (black) of the material collected from the recrystallisation of **H** from a 50/50 mixture of 3-pentanol and 2-pentanol. The GC and NMR results indicated that 3-pentanol accounted for 63% of the guest contained within the crystals.

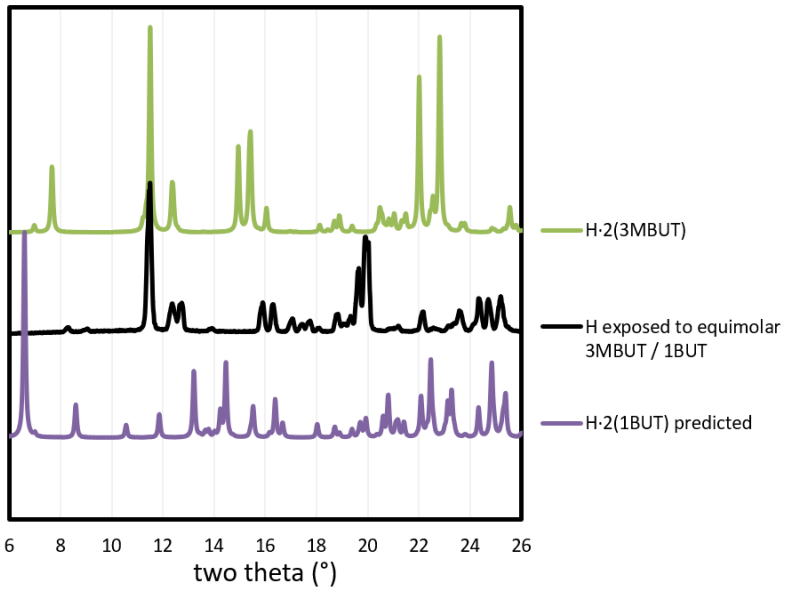

Figure S4.8. Calculated PXRD traces of **H•2(3MBUT)** (green) and **H•2(1BUT)** (purple) compared to the experimental trace (black) of the material collected from the recrystallisation of **H** from a 50/50 mixture of 3-methyl-butanol-2-ol and 1-butanol. The GC result indicated 3-methyl-butanol-2-ol accounted for 85% of the guest contained within the crystals.

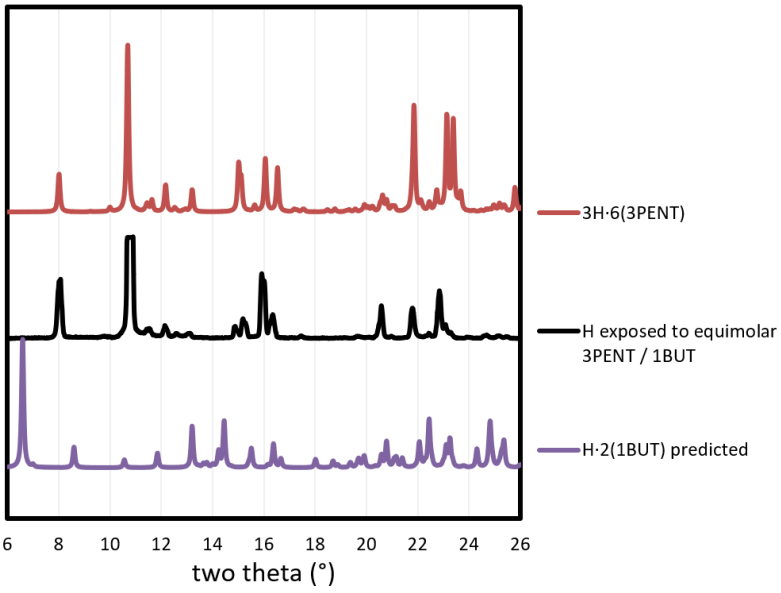

Figure S4.9. Calculated PXRD traces of **3H•6(3PENT)** (red) and **H•2(1BUT)** (purple) compared to the experimental trace (black) of the material collected from the recrystallisation of **H** from a 50/50 mixture of 3-pentanol and 1-butanol. The GC result indicated 3-pentanol accounted for 98% of the guest contained within the crystals.

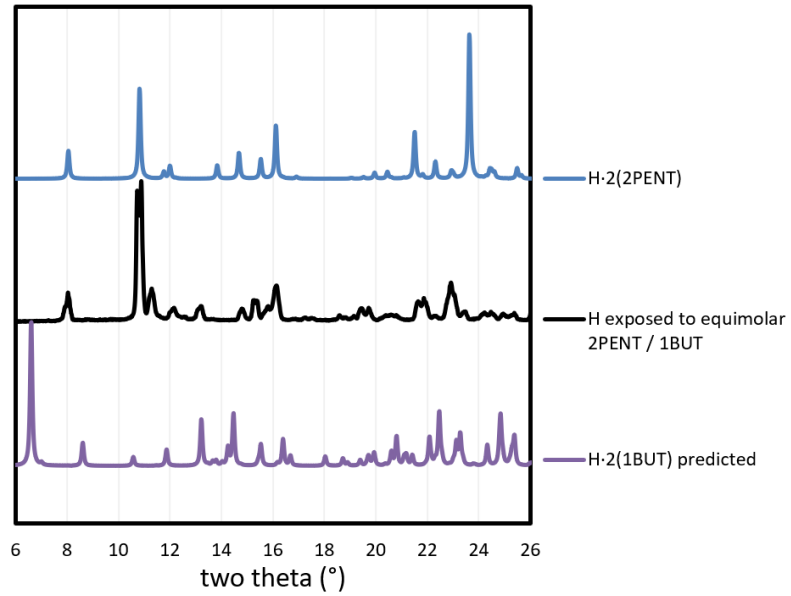

Figure S4.10. Calculated PXRD traces of **H•(2PENT)** (blue) and **H•2(1BUT)** (purple) compared to the experimental trace (black) of the material collected from the recrystallisation of **H** from a 50/50 mixture of 2-pentanol and 1-butanol. The GC result indicated 2-pentanol accounted for 98% of the guest contained within the crystals.

5.7.1 Table S5.1. Crystallographic data parameters of the Host-Guest complexes studied.

Compound	**5.1**	**5.2**	**5.3**	**5.4**	**5.5**	**5.6**
Structural formula	$C_{96}H_{86}O_{10}$	$C_{36}H_{38}O_4$	$C_{98}H_{90}O_{10}$	$C_{44}H_{58}O_6$	$C_{66}H_{61}Cl_3O_7$	$C_{96}H_{86}O_{10}$
Host: Guest ratio	$1:1\frac{1}{3}$	1:2	$1:1\frac{1}{3}$	1:4	1:2	$1:1\frac{1}{3}$
Molecular mass (g·mol^{-1})	1399.74	534.66	1427.79	682.90	1072.50	1399.74
Data collection temp. (K)	153	153	153	153	153	153
Crystal system	Triclinic	Triclinic	Triclinic	Triclinic	Triclinic	Triclinic
Space group	$P\bar{1}$	$P\bar{1}$	$P\bar{1}$	$P\bar{1}$	$P\bar{1}$	$P\bar{1}$
a(Å)	10.314(2)	8.5974(17)	10.328(2)	9.4041(19)	9.6930(19)	10.150(2)
b (Å)	18.768(4)	9.1212(18)	11.176(2)	9.4706(19)	14.066(3)	10.397(2)
c (Å)	20.269(4)	11.602(2)	18.112(4)	12.423(3)	21.052(4)	18.780(4)
α(°)	83.06(3)	92.96(3)	75.76(3)	111.38(3)	83.94(3)	104.29(3)
β(°)	81.59(3)	102.02(3)	79.16(3)	96.88(3)	82.70(3)	94.58(3)
γ(°)	82.49(3)	117.04(3)	88.31(3)	95.54(3)	89.93(3)	96.70(3)
Volume(Å^3)	3827.2(13)	781.3(3)	1989.9(7)	1011.0(4)	2831.0(10)	1895.2(7)
Z	2	1	1	1	2	1
Dc, calc density (g·cm^{-1})	1.215	1.136	1.191	1.122	1.258	1.226
θ range	1.42-27.90	1.82-27.95	1.18-27.75	1.79-28.00	1.52-27.96	2.03-27.97
Reflections collected	55397	12457	26269	13319	68486	34826
No data I>2 sigma (I)	11137	3214	6986	3458	11569	7144
Final R indices [I>2 sigma (I)]	0.0576	0.0490	0.0476	0.0574	0.0449	0.0451
R indices (all data)	0.1313	0.1324	0.1181	0.1363	0.1118	0.1089
Goodness-of-fit on F^2	1.029	1.060	1.042	1.030	1.038	1.057
Host torsion angle (°)	0.8, 7.7, 175.2	180	2.4, 180	180	1.3, 8.7	180, 0.2
CCDC no.	1558129	1558130	1558131	1558132	1558133	1558134
CSD refcode	DEBQUZ	DEBRAG	DEBREK	DEBRIO	DEBROU	DEBQUZ01

5.7.2 Table S5.2. Hydrogen bonding.

Compound	Donor (O)	Acceptor (O)	O···O (Å)	O-H (Å)	O···A (Å)	<O-H···O (°)
5.1	O16	O41	2.743(2)	0.967(5)	1.785(7)	171(2)
	O41	O95	2.707(2)	0.979(5)	1.729(6)	177(3)
	O95	O13	2.761(2)	0.969(5)	1.829(10)	161(2)
	O13	O92	2.753(2)	0.966(5)	1.787(5)	179(3)
	O92	O16[a]	2.931(2)	0.946(5)	2.080(15)	149(2)
	O89	O69	2.891(2)	0.955(5)	2.033(18)	148(3)
	O69	O44	2.726(2)	0.968(5)	1.770(7)	169(2)
	O44	O86	2.646(2)	0.989(5)	1.663(7)	172(3)
	O86	O72	2.744(2)	0.969(5)	1.812(11)	160(3)
	O72	O89[b]	2.768(2)	0.970(5)	1.802(7)	173(3)
5.2	O16	O13	2.770(2)	0.965(5)	1.825(8)	165(2)
	O13	O16[c]	2.668(2)	0.971(5)	1.745(9)	158(2)
5.3	O16	O41	2.739(2)	0.964(5)	1.781(6)	171(2)
	O41	O44	2.689(2)	0.978(5)	1.713(6)	176(2)
	O44	O13	2.766(2)	0.967(5)	1.817(7)	166(2)
	O13	O48	2.753(2)	0.964(5)	1.792(6)	175(2)
	O48	O16[a]	2.885(2)	0.948(5)	2.03(15)	148(2)
5.4	O13	O20	2.680(2)	0.977(5)	1.706(6)	175(2)
	O20	O16	2.706(2)	0.977(5)	1.736(6)	171(2)
	O16	O13[d]	2.781(2)	0.967(5)	1.816(6)	176(2)
5.5	O13	O62	2.674(2)	0.976(5)	1.698(5)	178(2)
	O62	O41	2.834(1)	0.945(5)	1.895(6)	172(2)
	O41	O16	2.723(2)	0.963(5)	1.761(5)	177(2)
	O16	O65	2.753(2)	0.964(5)	1.799(7)	169(2)
	O65	O44	2.853(2)	0.946(5)	1.913(6)	172(2)
	O44	O59	2.674(2)	0.973(5)	1.701(5)	176(2)
	O59	O13[e]	2.719(2)	0.964(5)	1.759(6)	174(2)
5.6	O16	O47	2.704(2)	0.964(5)	1.748(5)	171(2)
	O47	O41	2.753(2)	0.968(5)	1.790(6)	174(2)
	O41	O43	2.672(2)	0.975(5)	1.723(8)	163(2)
	O43	O13	2.814(2)	0.954(5)	1.869(9)	171(4)

Symmetry codes: (a) 1-x, 1-y, -z (a) x-1, y, z (b) x+1, y, z (c) 1-x, -y, 1-z (d) -x, 1-y, -z (e) x, y-1, z

5.7.3 Structure diagrams.

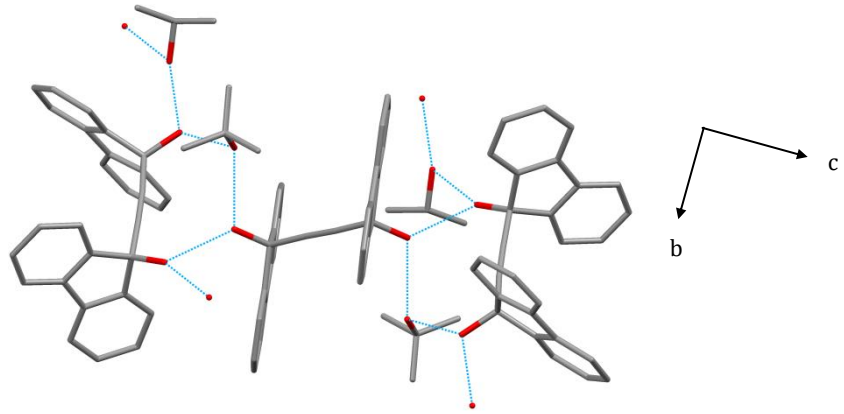

Figure S5.1: Structure **5.3**, grown at 50 °C from an equimolar guest mixture of **2-PROP** and **t-BUT** with hydrogen bonding shown in blue. Both **2-PROP** and **t-BUT** are included.

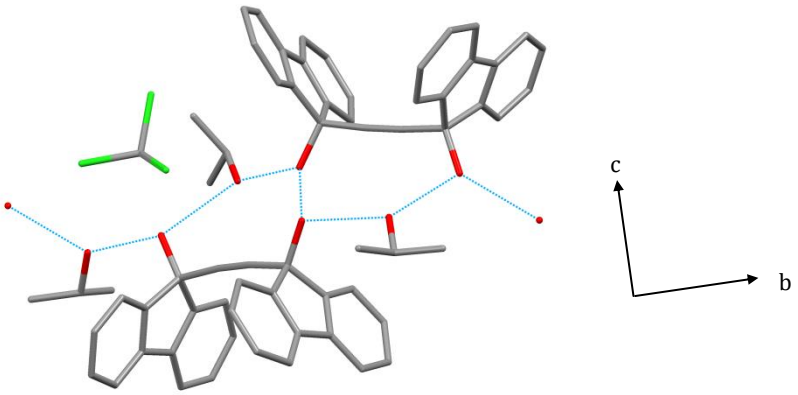

Figure S5.2: Structure **5.5**, grown from **2-PROP** and $CHCl_3$ at -20 °C with hydrogen bonding shown in blue.

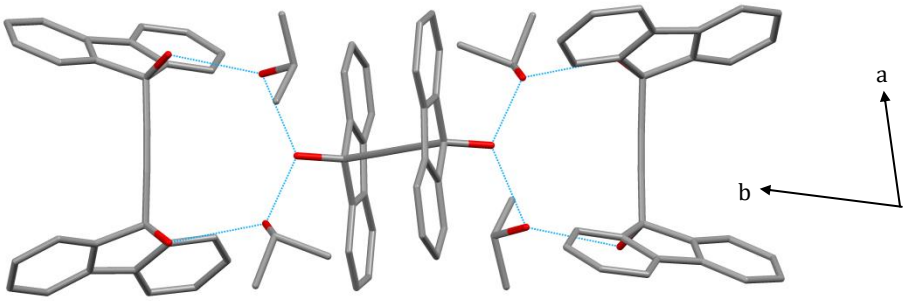

Figure S5.3: Structure **5.6**, grown from **2-PROP** only at -20 °C, with hydrogen bonding shown in blue.

5.7.4 Lattice Energy.

We also computed the lattice energies of the various compounds by employing Gavezzotti's programme AA-CLP.[D1, D2] There are several problems with the calculated lattice energies firstly because the structures are not isomeric and secondly because some of the guest molecules suffer from disorder, and Professor Gavezzotti states that such results are strictly invalid.

However, we normalised the stoichiometries to that of structure **5.2**. What is relevant is that structure **5.2** (phase **II**) yielded -357.0 kJ·mol^{-1} while structure **5**.**3** (phase **I**) gave -341.6 kJ·mol^{-1}, a difference of 15.4 kJ·mol^{-1}, which is not significant.

References

D1 A. Gavezzotti, Calculation of Intermolecular Interaction Energies by Direct Numerical Integration over Electron Densities. I. Electrostatic and Polarization Energies in Molecular Crystals, *J. Phys. Chem. B*, 2002, **106**, 4145–4154.

D2 A. Gavezzotti, Calculation of Intermolecular Interaction Energies by Direct Numerical Integration over Electron Densities. 2. An Improved Polarization Model and the Evaluation of Dispersion and Repulsion Energies, *J. Phys. Chem. B*, 2003, **107**, 2344–2353.

Table S5.3. Lattice Energies

Structure	Molar mass (g/mol)	Calculated Lattice Energy (kJ/mol)	Normalised Lattice Energy relative to structure 2 (kJ/mol)	Normalised $E_{structure\ i} - E_{structure\ 2}$ i = 1-6 (kJ/mol)
5.1	1399.74	-906.5	-346.3	+10.7
5.2	534.70	-357.0	-357.0	0
5.3	1427.79	-912.1	-341.6	+15.4
5.4	682.94	-520.5	-407.5	-50.5
5.5	1072.57	-680.4	-339.2	+17.8
5.6	1399.74	-877.8	-335.3	+21.7

5.7.5 Representative Inclusion Experiments.

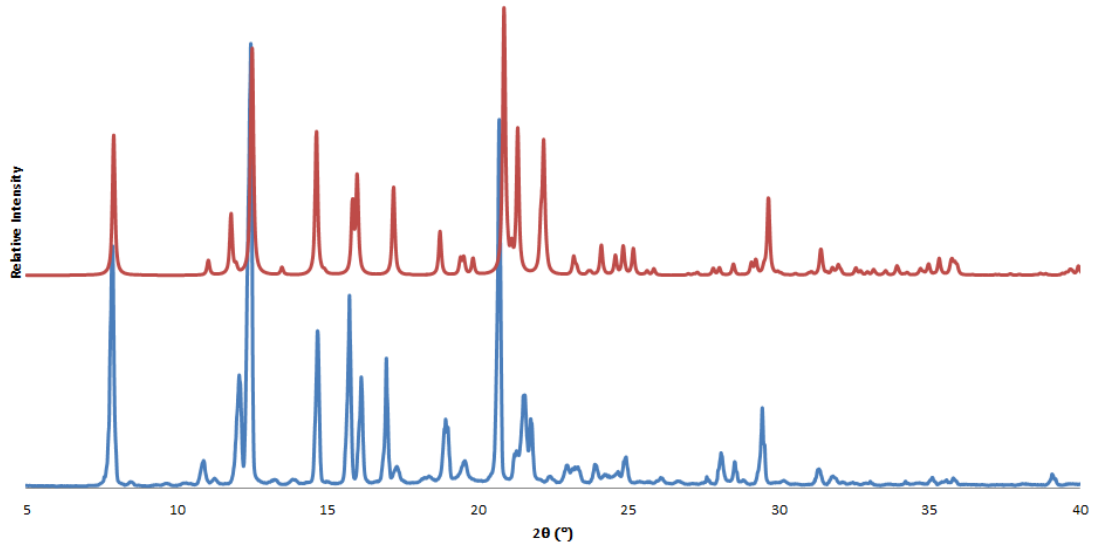

Figure S5.4. PXRD pattern of structure **5.2** (blue) grown from the single guest at 50 °C and predicted PXRD of **5.2** (red)

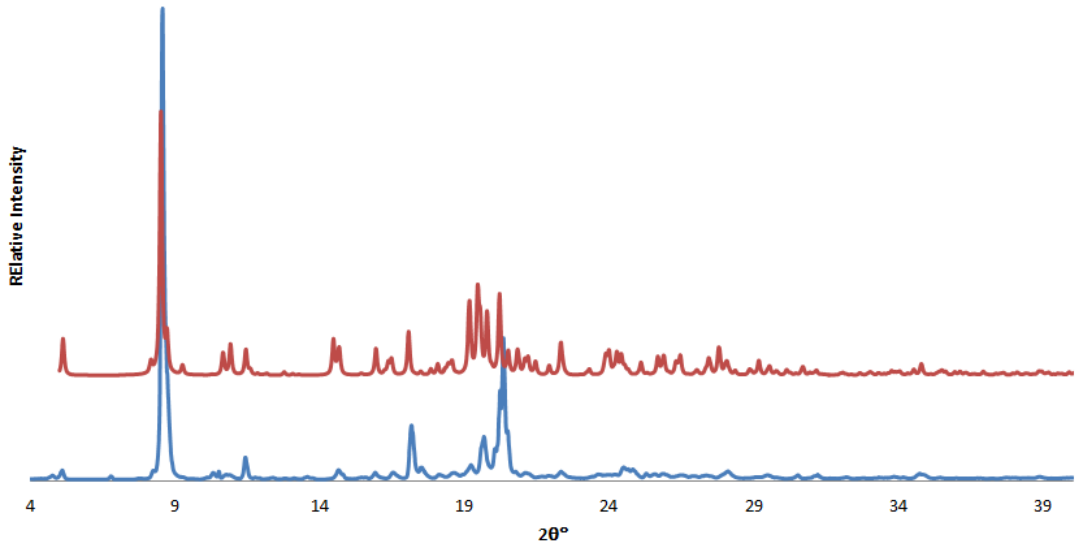

Figure S5.5. PXRD pattern of structure **5.1** (blue) grown from the single 2-propanol guest at 30 °C and simulated PXRD pattern of **5.1** (red)

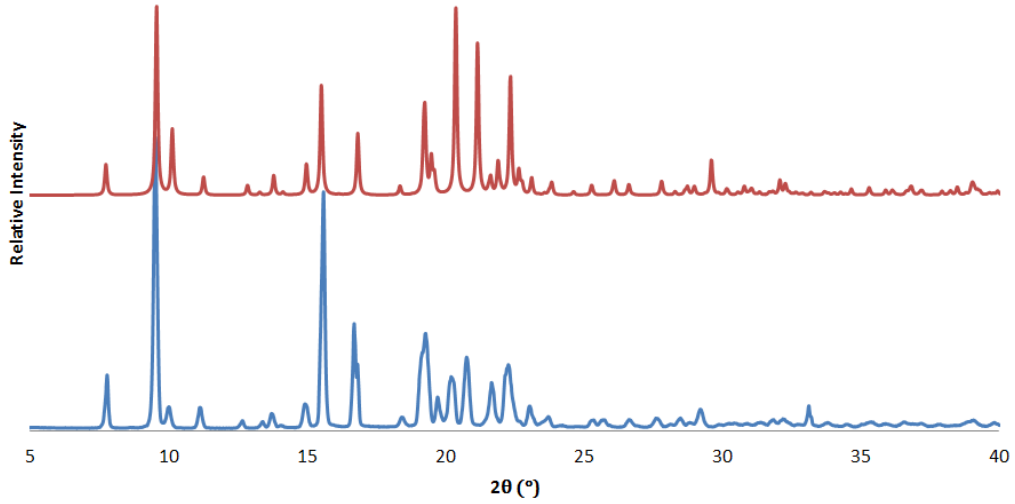

Figure S5.6. PXRD pattern of structure **5.4** (blue), grown from the single tertiary butanol guest at 30 °C and predicted PXRD pattern of **5.4** (red)

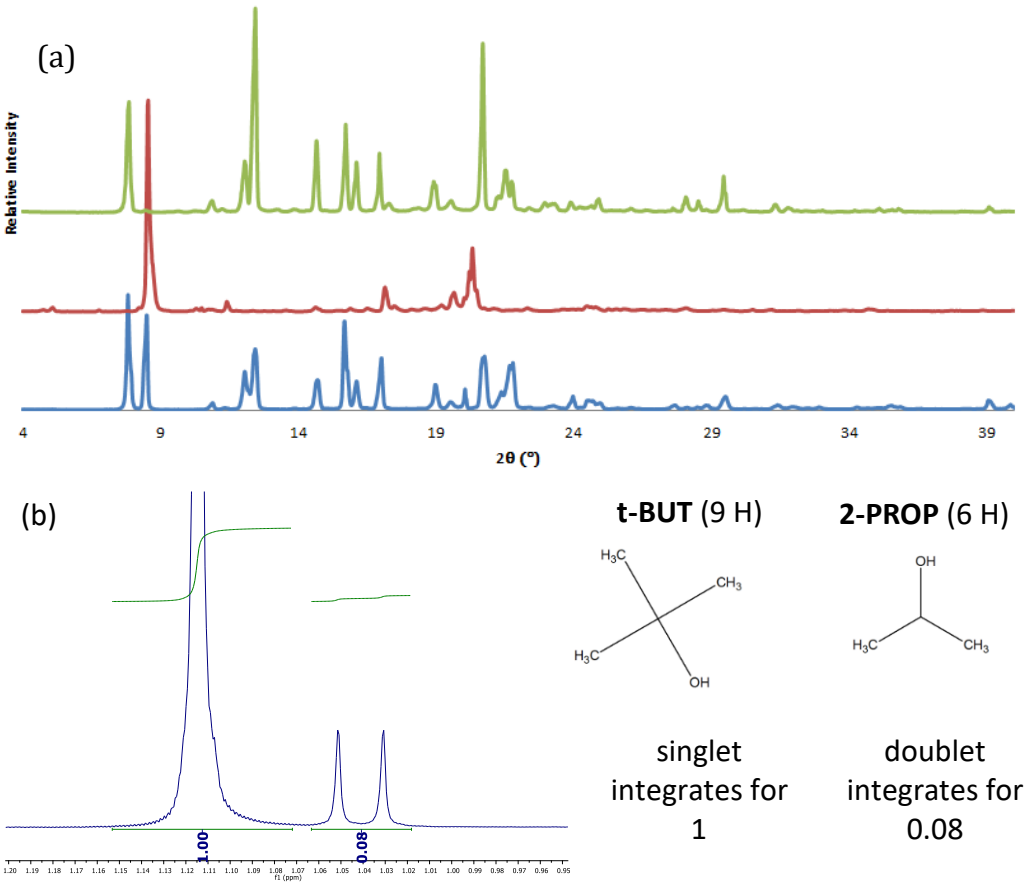

Figure S5.7. (a) PXRD pattern of the result of the equimolar competition carried out at 30 °C (blue), predicted PXRD pattern of **5.3** (red) and PXRD pattern of **5.2** at 50 °C (green) and (b) CH_3 region of ^1H NMR spectrum showing **t-BUT** integrating for 1 and **2-PROP** integrating for 0.08 indicating 10.7% 2-propanol in the mixture.

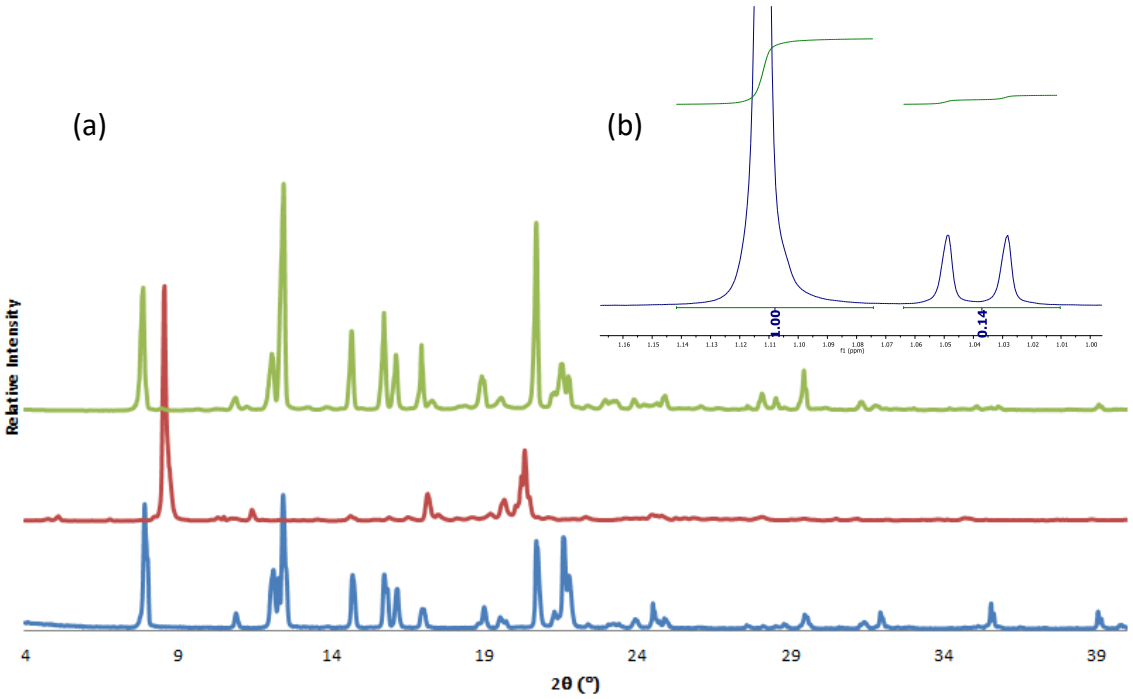

Figure S5.8. (a) PXRD pattern of the result of the equimolar competition carried out at 30 °C (blue), predicted PXRD pattern of **3** (red) and PXRD pattern of **2** at 50 °C (green) and (b) CH_3 region of ^1H NMR spectrum showing **t-BUT** integrating for 1 and **2-PROP** integrating for 0.14 indicating 17.4% 2-propanol in the mixture.

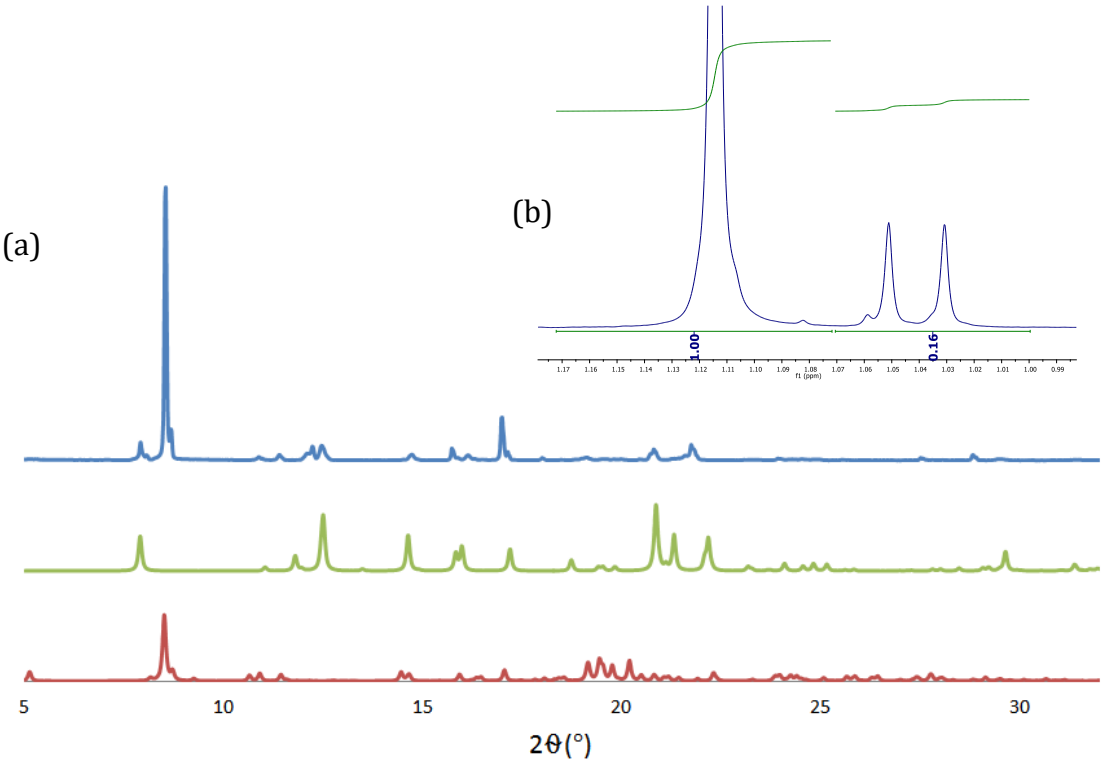

Figure S5.9. (a) PXRD pattern of the result of the equimolar competition carried out at 30 °C (blue), predicted PXRD pattern of **3** (red) and PXRD pattern of **2** at 50 °C (green) and (b) CH_3 region of ^1H NMR spectrum showing **t-BUT** integrating for 1 and **2-PROP** integrating for 0.016 indicating 19.4% 2-propanol in the mixture.

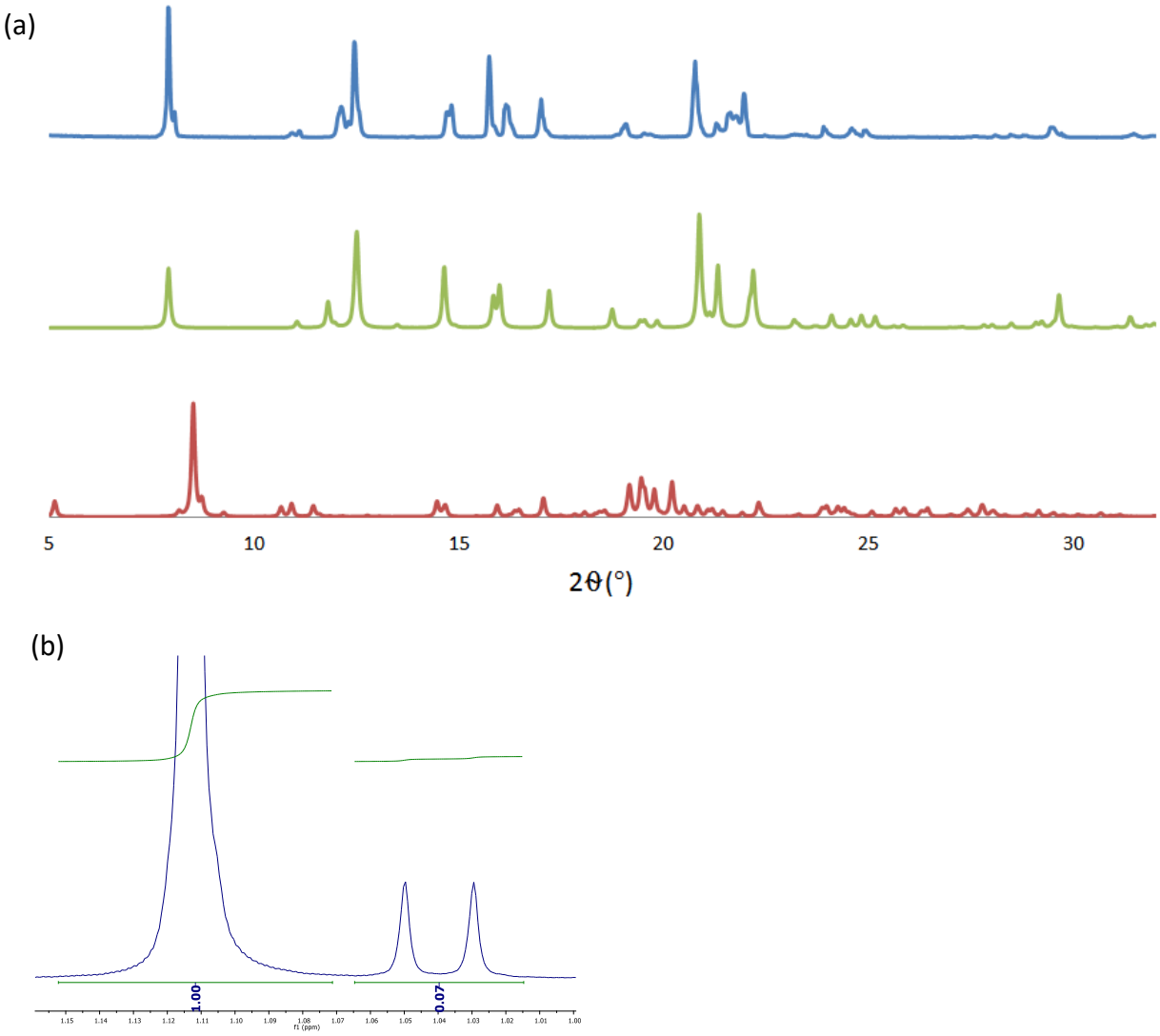

Figure S5.10. (a) PXRD pattern of the result of the equimolar competition carried out at 30 °C (blue), predicted PXRD pattern of **3** (red) and PXRD pattern of **2** at 50 °C (green) and (b) CH_3 region of ^1H NMR spectrum showing **t-BUT** integrating for 1 and **2-PROP** integrating for 0.07 indicating 9.5% 2-propanol in the mixture.

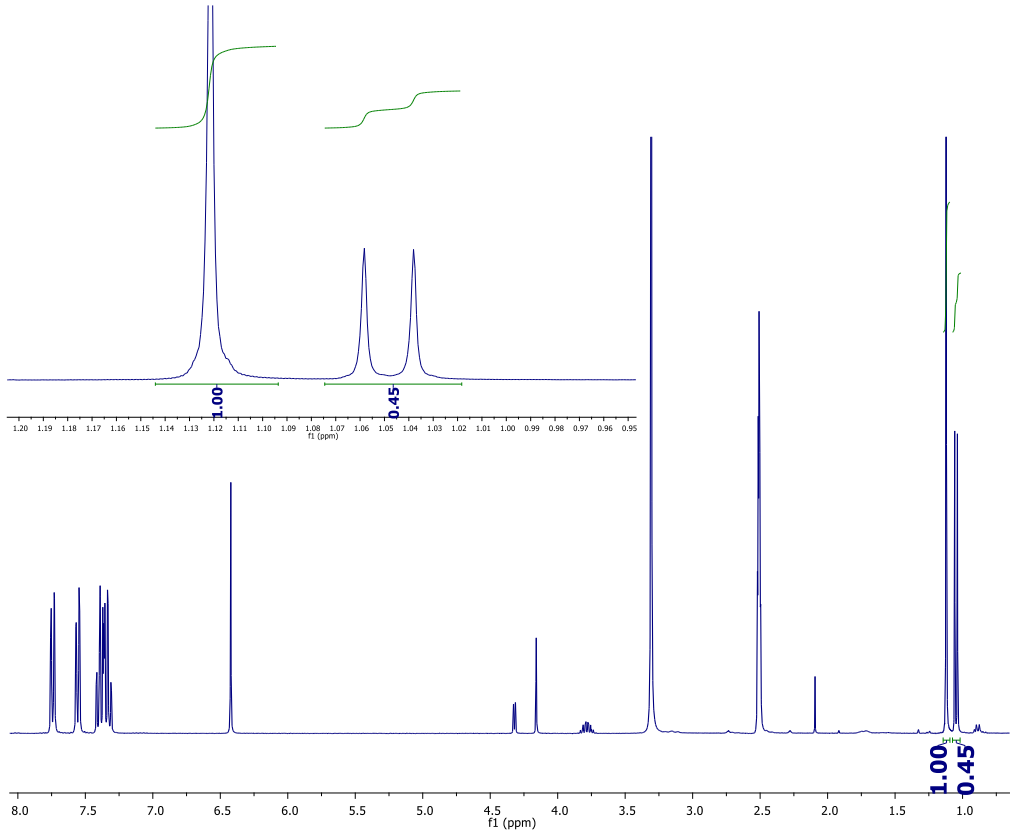

Figure S5.11. ^{1}H NMR spectrum of the crystals grown at 30 °C from an equimolar mixture of **2-PROP** and **t-BUT** showing **t-BUT** integrating for 1 and **2-PROP** integrating for 0.45 indicating 40.3% **2-PROP** in the mixture.

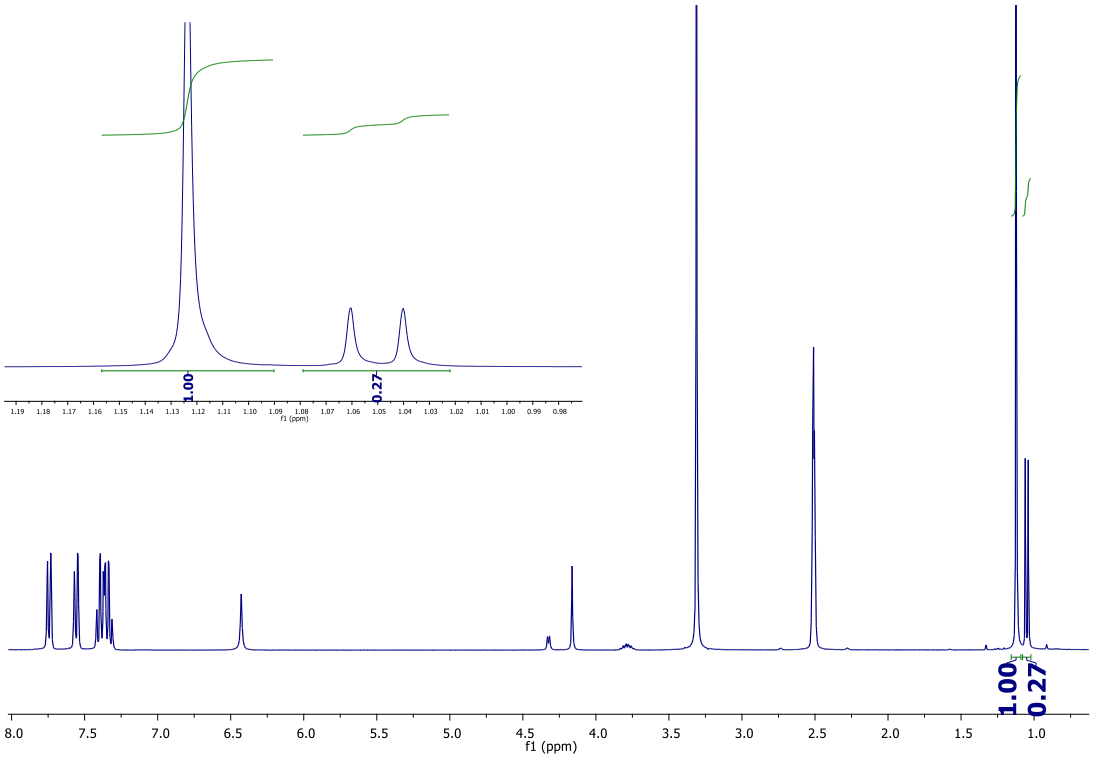

Figure S5.12. ^{1}H NMR spectrum of the crystals grown at 30 °C from an equimolar mixture of **2-PROP** and **t-BUT** showing **t-BUT** integrating for 1 and **2-PROP** integrating for 0.27 indicating 28.8% **2-PROP** in the mixture.

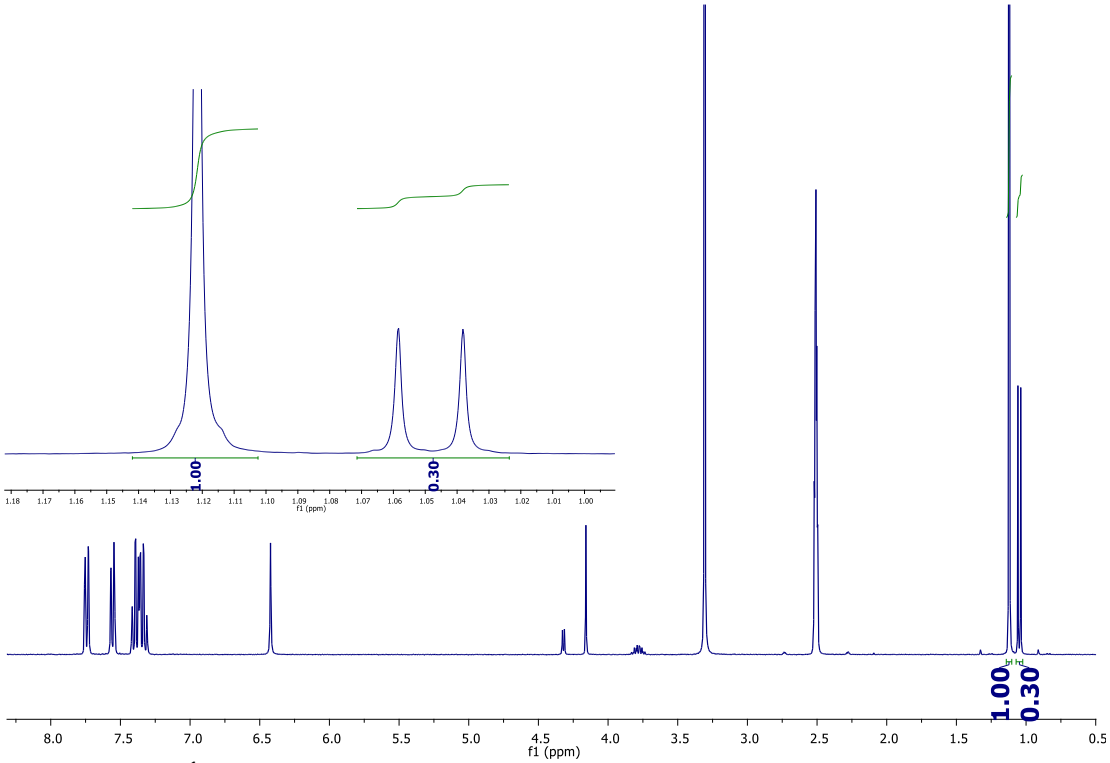

Figure S5.13. ^{1}H NMR spectrum of the crystals grown at 30 °C from an equimolar mixture of **2-PROP** and **t-BUT** showing **t-BUT** integrating for 1 and **2-PROP** integrating for 0.30 indicating 31% **2-PROP** in the mixture.

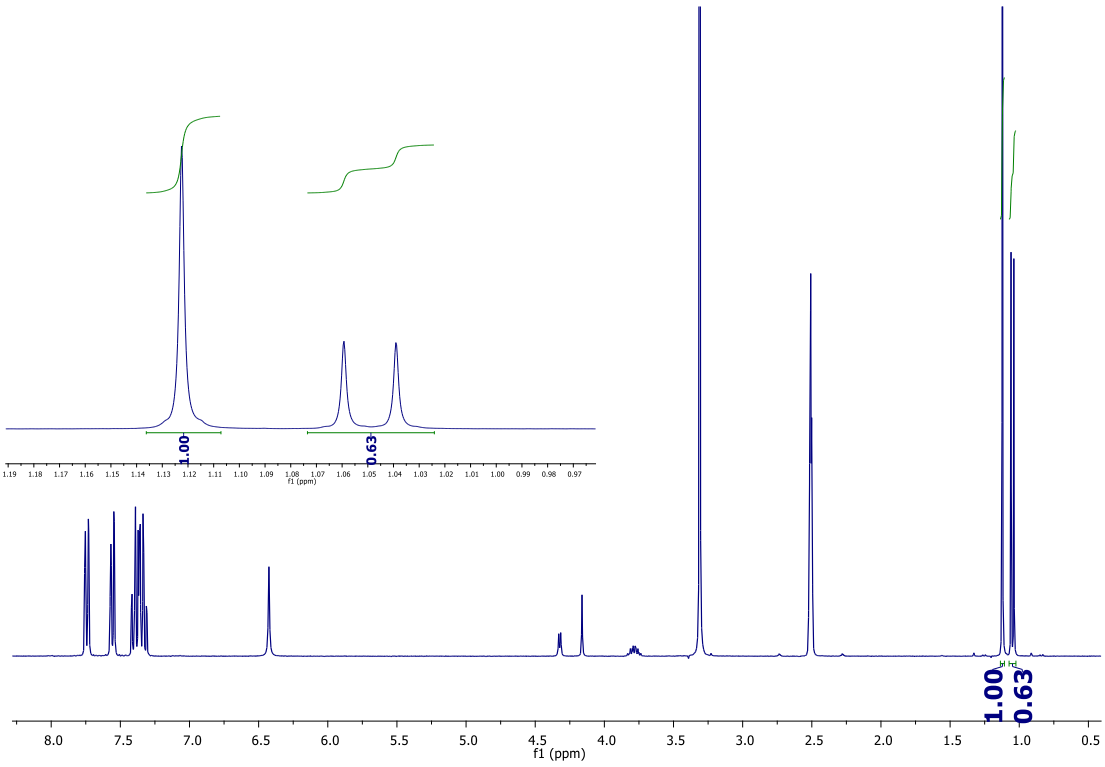

Figure S5.14. ^{1}H NMR spectrum of the crystals grown at 30 °C from an equimolar mixture of **2-PROP** and **t-BUT** showing **t-BUT** integrating for 1 and **2-PROP** integrating for 0.63 indicating 48.6% **2-PROP** in the mixture.

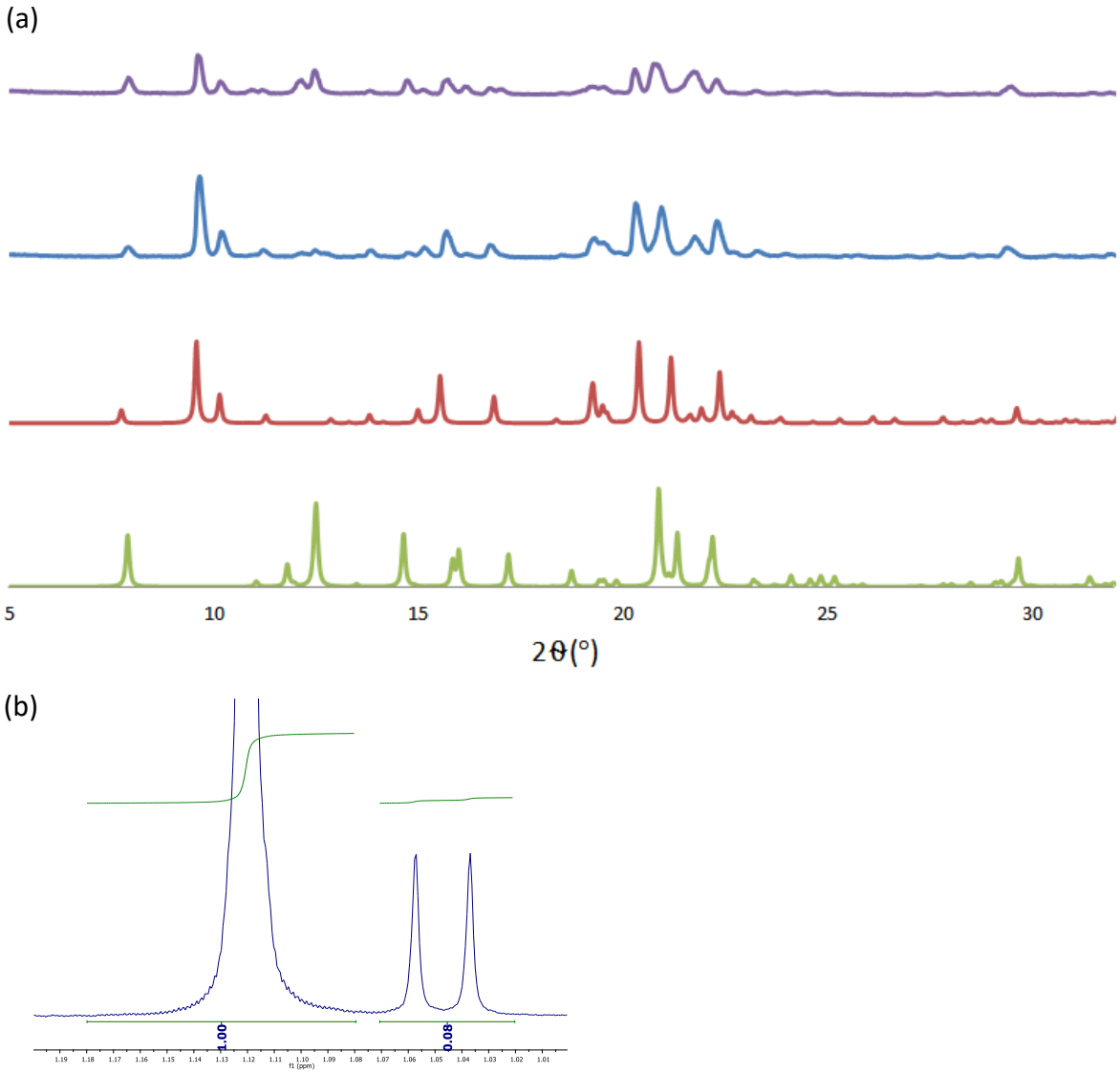

Figure S5.15. (a) PXRD pattern of the result of the equimolar competition carried out at -61 °C. The blue trace is the resulting powder diffractogram and the purple trace is the diffractogram collected immediately afterwards. This is compared to the predicted PXRD pattern of **5.2** (green) and predicted PXRD pattern of **5.3** (red) and (b) CH_3 region of ^1H NMR spectrum showing **t-BUT** integrating for 1 and **2-PROP** integrating for 0.08 indicating 10.7% **2-PROP** in the mixture.

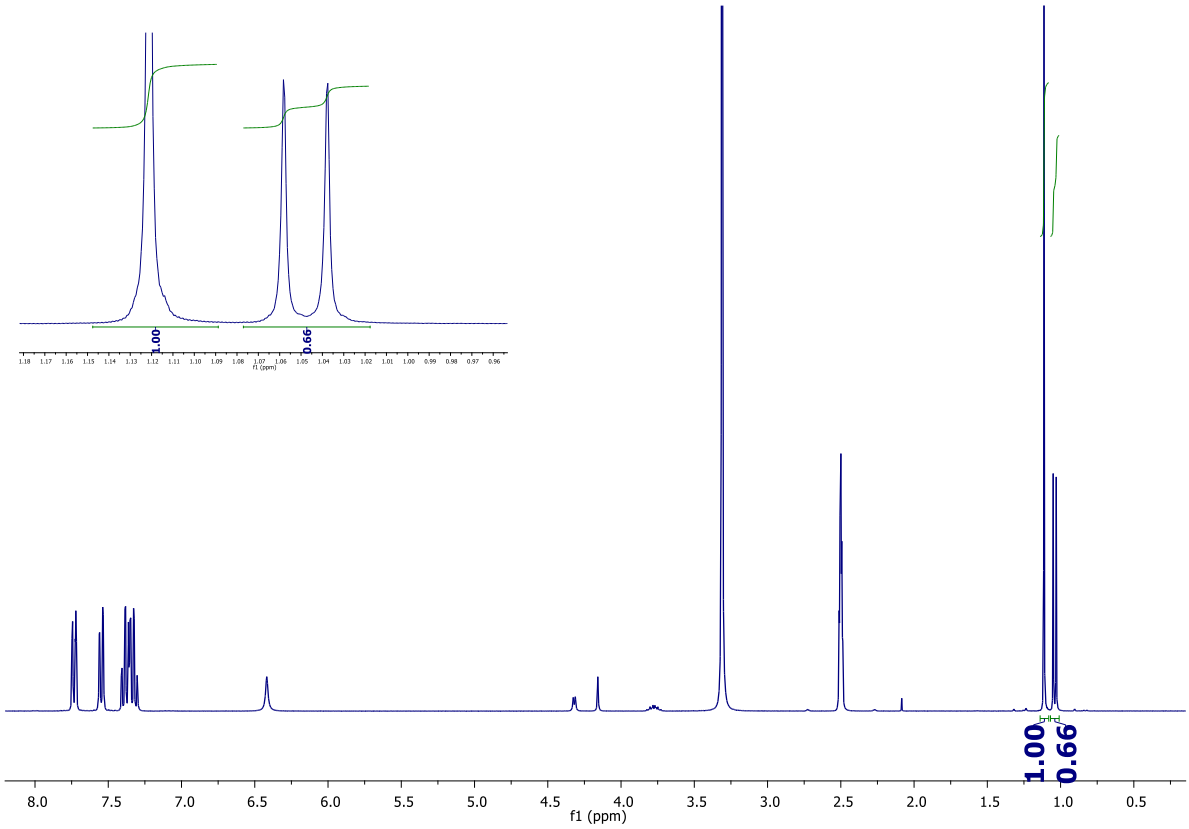

Figure S5.16. ^{1}H NMR spectrum of the crystals grown at 50 °C from an equimolar mixture of **2-PROP** and **t-BUT** showing **t-BUT** integrating for 1 and **2-PROP** integrating for 0.66 indicating 49.7% **2-PROP** in the mixture.

5.7.6 Figure S5.17 Hirshfeld Analysis with host selected as target.

We studied the packing of all the structures using the programme Crystal Explorer.[12] In each case we targeted the host molecule and analysed the non-bonded interactions, but the only significant differences were those between the cis- versus the trans- host molecules. This was expected and yielded no fresh insights into the mechanism of selectivity.

(a) Structure **5.1**
trans-

		Out (%)		
		C	**H**	**O**
In (%)	**C**	0.2	26.5	0.3
	H	3.3	59.8	5.4
	O	0.2	4.4	0

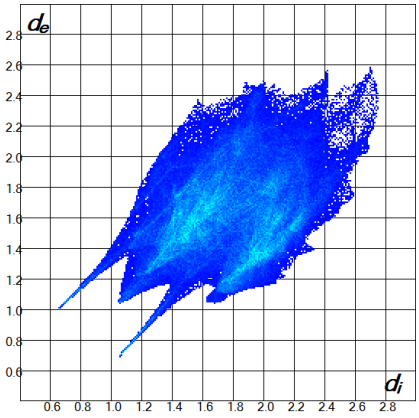

(b) cis α-

		Out (%)			
		C	**H**	**N**	**O**
In (%)	**C**	4.2	22.5	0.6	4.2
	H	19.2	45.1	3.4	19.2
	O	0.2	4.7	0	0.2

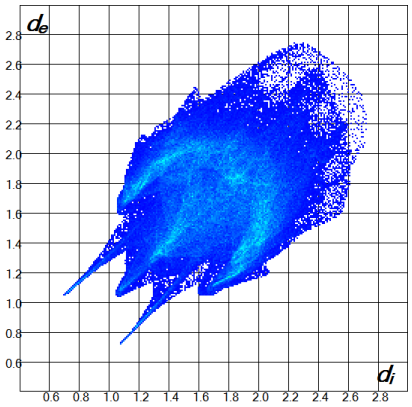

(c) cis β-

		Out (%)			
		C	**H**	**N**	**O**
In (%)	**C**	4.4	22.6	0.2	4.4
	H	20.4	44.1	3.3	20.4
	O	0.3	4.7	0	0.3

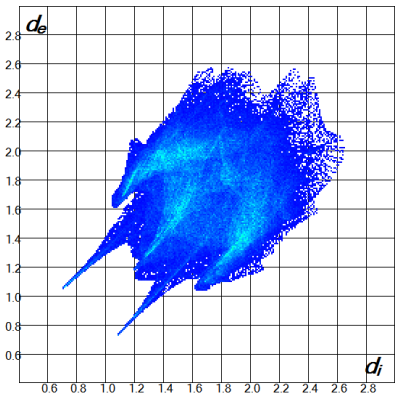

(d) Structure **5.2**
trans-

		Out (%)			
		C	**H**	**N**	**O**
In (%)	**C**	0	26.7	0	0
	H	5.8	59.4	4.0	5.8
	O	0	4.2	0	0

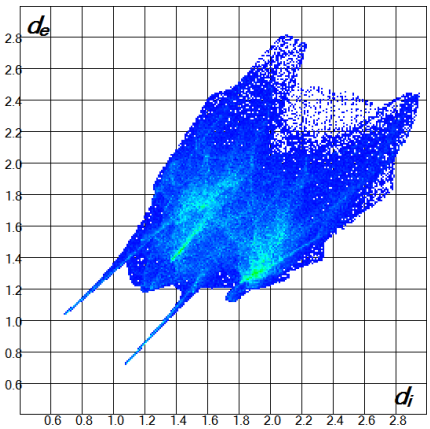

(e) Structure **5.3** (major component of disordered guest selected only)

trans-

		Out (%)			
		C	**H**	**N**	**O**
In (%)	**C**	0.3	26.2	0.3	0.3
	H	5.8	57.3	5.3	5.8
	O	0.2	4.5	0	0.2

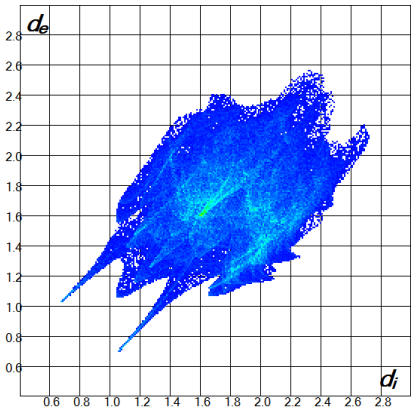

(f) cis-

		Out (%)			
		C	**H**	**N**	**O**
In (%)	**C**	4.1	22.5	0.2	4.1
	H	19.8	45.1	3.4	19.8
	O	0.1	4.8	0	0.1

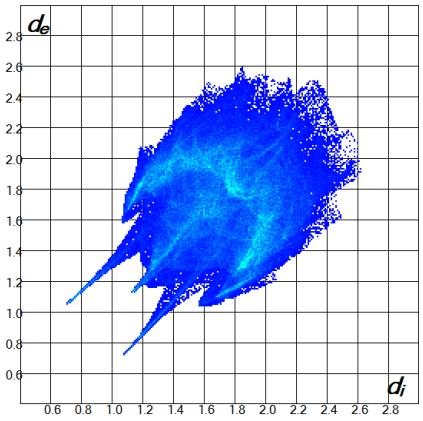

Structure **5.4**

(g) trans-

		Out (%)			
		C	**H**	**N**	**O**
In (%)	**C**	0	26.1	0.5	0
	H	3.1	62.6	3.1	3.1
	O	0	4.6	0	0

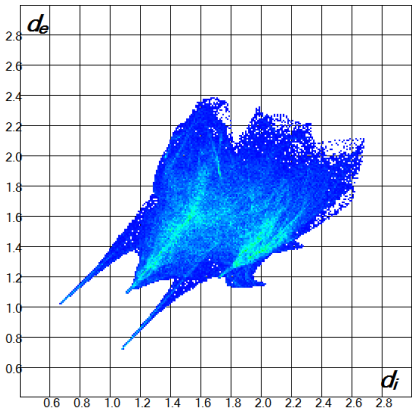

Structure **5.5**

(h) cis- α

		Out (%)			
		C	**H**	**N**	**O**
In (%)	**C**	2.2	24.2	0	0.4
	H	9.4	52.2	4.5	2.0
	O	0	5.0	0	0

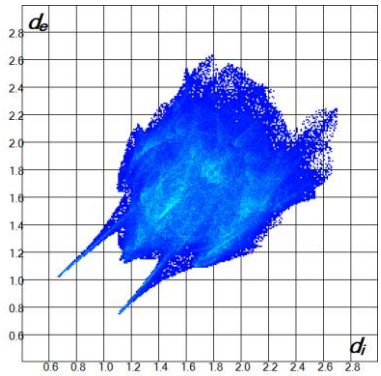

(i) cis- β

		Out (%)			
		C	**H**	**N**	**O**
In (%)	**C**	3.6	18.7	0	4.3
	H	0.1	49.7	4.1	5.6
	O	0	4.8	0	0.2

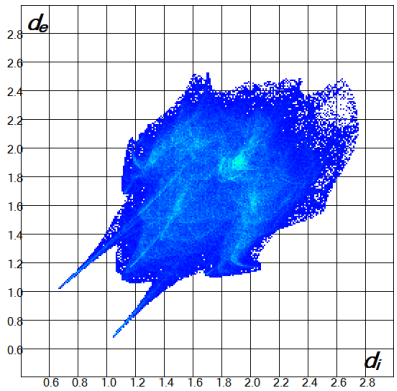

Structure **5.6** (major component of disordered guests selected only)

(j) trans-

		Out (%)			
		C	**H**	**N**	**O**
In (%)	**C**	0	27.5	0	0
	H	5.3	53.5	8.3	5.3
	O	0	5.3	0	0

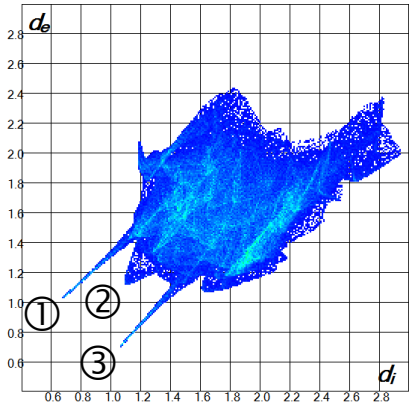

(k) cis-

		Out (%)			
		C	**H**	**N**	**O**
In (%)	**C**	4.4	22.8	0	4.4
	H	17.7	47.0	2.8	17.7
	O	0	5.2	0	0

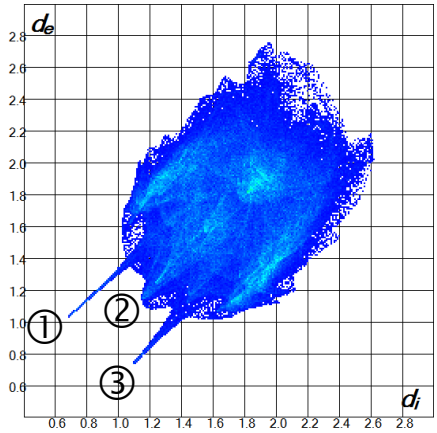

5.7.7 In Situ PXRD Vapour Sorption Experiments.

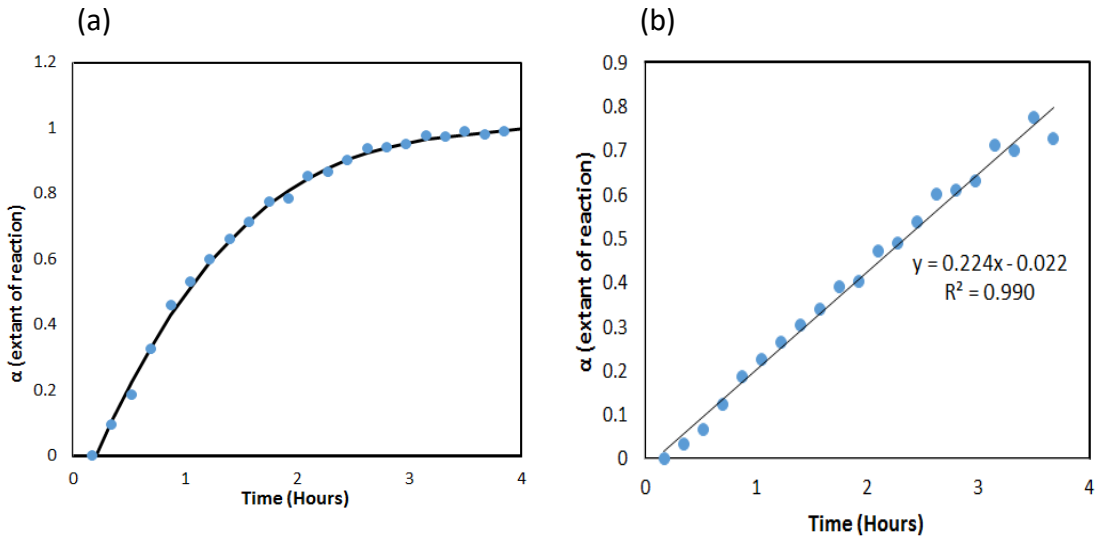

Figure S5.18 Experiment 1 (a) plot of extent of reaction vs time and (b) data fitted to the contracting volume equation: 1 - $(1-\alpha)^{1/3} = k\,t$, yielding a rate constant of 3.7 x 10^{-3} min^{-1}, corresponding to a half-life of 55.4 min.

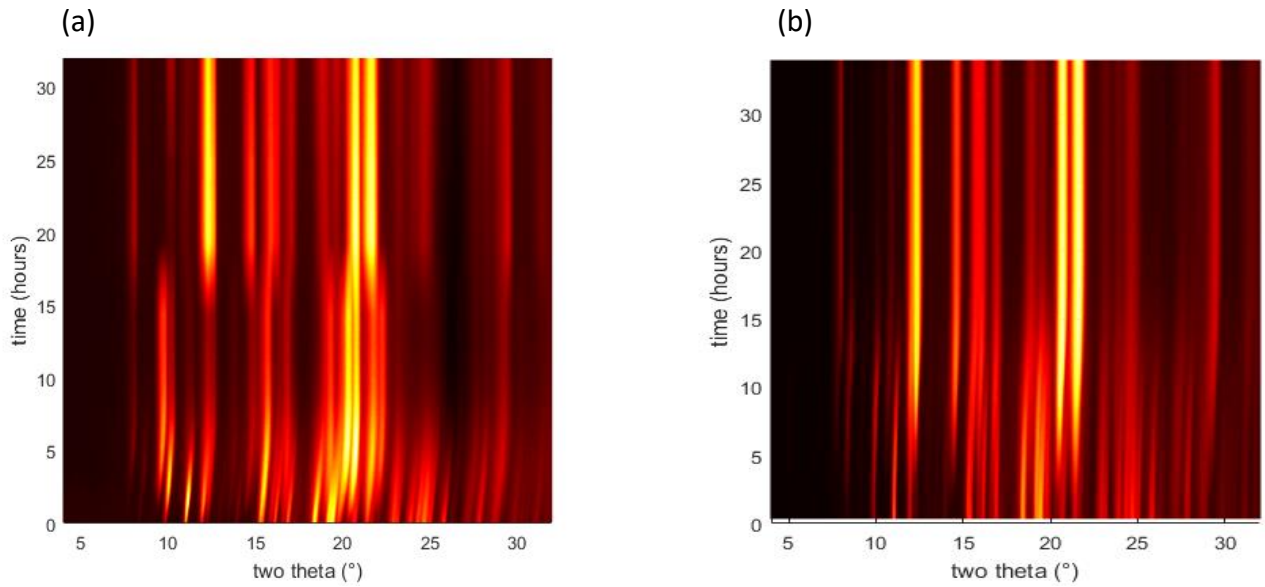

Figure S5.19 (a) Experiment 2: time resolved *in situ* diffractogram for the reaction of apohost with **t-BUT** vapour showing conversion from apohost to phase **III** to phase **II**. This was achieved by adding a smaller amount of guest solvent to grooves. This is analogous to the crystallisation result from the liquid: at the similar temperature of 30 °C, H1 recrystalised from liquid **t-BUT** results in crystalline material of phase **III** (b) Experiment 3: time resolved in situ diffractogram for the reaction of apohost with an equimolar mixture of **2-PROP** and **t-BUT** showing conversion to phase **II** only. Similarly, when H1 is exposed to an equimolar mixture of **2-PROP** and **t-BUT** at 5 °C, crystalline material of phase **II** results, and phase **III** is only achieved at much lower temperatures.

6.7.1 List of Werner clathrates

Table S6.1: A list of Werner clathrates of type $M(NCS)_2(L)_4$ where M is a transition metal; guests in bold are aromatic. They have been grouped by ligand. Structures were sourced from the 2019 version of the Cambridge Structural Database.

No.	M	L	G	REFCODE
1	Ru	pyridine	dichloromethane	AGOHUZ
2	Cu	pyridine	-	AVUJEG
3	Cu	pyridine	-	AVUJEG01
4	Cd	pyridine	-	BEVMEV
5	Ni	pyridine	-	CNSPYN
6	Ni	pyridine	-	CNSPYN01
7	Ni	pyridine	-	CNSPYN02
8	Ni	pyridine	-	CNSPYN03
9	Ni	pyridine	-	CNSPYN04
10	Ni	pyridine	-	CNSPYN05
11	Fe	pyridine	-	FETPYR
12	Fe	pyridine	-	FETPYR01
13	Fe	pyridine	-	FETPYR02
14	Mn	pyridine	-	HIQWOU
15	Mn	pyridine	-	HIQWOU01
16	Co	pyridine	-	ITCPCO
17	Co	pyridine	-	ITCPCO02
18	Zn	pyridine	-	MAHROD
20	Co	pyridine	iodoform	TCPYCO
21	Ni	pyridine	**pyridine**	TEDWUU
22	Ni	pyridine	methanol, **tetraphenylmethane**	TUNROJ
23	Ni	4-methylpyridine	**p-nitrotoluene**	BAMSIR
24	Ni	4-methylpyridine	**m-nitrotoluene**	BAMSOX
25	Ni	4-methylpyridine	**o-nitrotoluene**	BAMSUD
26	Ni	4-methylpyridine	**p-xylene**	BAPZAT
27	Ni	4-methylpyridine	**m-xylene**	BAPZEX
28	Ni	4-methylpyridine	methanol	BAPZIB
29	Ni	4-methylpyridine	**naphthalene**	BEZCAK
30	Ni	4-methylpyridine	**p-cymene**	BUJPEB
31	Co	4-methylpyridine	**p-toluidine**	CECCOC
32	Ni	4-methylpyridine	**p-toluidine**	CECCUI
33	Ni	4-methylpyridine	**1-bromonaphthalene**	CULLOK
34	Ni	4-methylpyridine	**1-bromonaphthalene**	CULLOK10
35	Ni	4-methylpyridine	**azulene**	CULLUQ
36	Ni	4-methylpyridine	**azulene**	CULLUQ01
37	Ni	4-methylpyridine	**benzene**	DALDEA
38	Ni	4-methylpyridine	**benzene**	DALDEA01
39	Cd	4-methylpyridine	**4-methylpyrdine**, water	DEXYIO
40	Cd	4-methylpyridine	**4-methylpyrdine**, water	DEXYIO10
41	Cd	4-methylpyridine	**4-methylpyrdine**, water	DEXYIO11

No.	M	L	G	REFCODE
42	Zn	4-methylpyridine	**4-methylpyrdine**, water	EFESOX
43	Ni	4-methylpyridine	unknown	EMEHUA
44	Mn	4-methylpyridine	unknown	EQEGEN
45	Ni	4-methylpyridine	-	ICMPNI
46	Ni	4-methylpyridine	-	ICMPNI01
47	Ni	4-methylpyridine	-	ICMPNI02
48	Ni	4-methylpyridine	-	ICMPNI03
49	Ni	4-methylpyridine	-	ICMPNI04
50	Ni	4-methylpyridine	-	ICMPNI05
51	Ni	4-methylpyridine	-	ICMPNI06
52	Ni	4-methylpyridine	**o-xylene**	ICNIPX
53	Ni	4-methylpyridine	**o-xylene**	ICNIPX10
54	Ni	4-methylpyridine	**1-methylnaphthalene**	IMPNIN
55	Ni	4-methylpyridine	**1-methylnaphthalene**	IMPNIN10
56	Ni	4-methylpyridine	**2-bromonaphthalene**	IPNBNP
57	Ni	4-methylpyridine	**2-methylnaphthalene**	IPNMNP
58	Cu	4-methylpyridine	**4-methylpyridine**	LITVEP
59	Ni	4-methylpyridine	**p-terphenyl**	MPNITP
60	Ni	4-methylpyridine	**p-xylene**	QQQGKA
61	Ni	4-methylpyridine	furan	RUDWAO
62	Ni	4-methylpyridine	tetrahydrofuran	RUDWES
63	Ni	4-methylpyridine	**benzene**, ethanol	RUDWIW
64	Ni	4-methylpyridine	dichloromethane	RUDWOC
65	Ni	4-methylpyridine	dichloromethane	RUDWUI
66	Ni	4-methylpyridine	methylcellosolve	RUDXAP
67	Co	4-methylpyridine	-	VERNUC
68	Fe	4-methylpyridine	**benzene**	VEVKEM
69	Fe	4-methylpyridine	**m-xylene**	VEVKOW
70	Fe	4-methylpyridine	**p-xylene**	VEVKUC
71	Cu	4-methylpyridine	**4-methylpyridine**, water	VUJBUX
72	Cu	4-methylpyridine	**4-methylpyridine**, water	VUJBUX01
73	Mn	4-methylpyridine	**4-methylpyridine**, water	VUJCAE
74	Fe	4-methylpyridine	**4-methylpyridine**	XIHHAX
75	Fe	4-methylpyridine	**4-methylpyridine**	XIHHAX01
76	Co	4-methylpyridine	**4-methylpyridine**	XIHHEB
77	Co	4-methylpyridine	**4-methylpyridine**	XIHHEB01
78	Zn	4-methylpyridine	**4-methylpyridine**	YORHAO
79	Ni	4-methylpyridine	**p-xylene**	ZZZUXE
80	Ni	4-methylpyridine	**benzene**	ZZZUXK
81	Ni	4-methylpyridine	**benzene**	ZZZUXK01
82	Ni	4-methylpyridine	nitroethane	ZZZUXO
83	Ni	4-methylpyridine	1,4-methanol	ZZZUXQ
84	Ni	4-methylpyridine	**1,4-dichlorobenzene**	ZZZUXS
85	Co	4-methylpyridine	**nitrobenzene**	ZZZUXU
86	Co	4-methylpyridine	nitroethane	ZZZUXY
87	Co	4-methylpyridine	**benzene**	ZZZUYI

No.	M	L	G	REFCODE
88	Ni	4-phenylpyridine	dimethylsulfoxide	CIVJIA
89	Ni	4-phenylpyridine	dimethylsulfoxide	CIVJIA10
90	Ni	4-phenylpyridine	dimethylsulfoxide	CIVJIA20
91	Ni	4-phenylpyridine	**m-xylene**	DUTXAR
92	Ni	4-phenylpyridine	**m-xylene**	DUTXAR10
93	Ni	4-phenylpyridine	**m-xylene**	DUTXAR11
94	Ni	4-phenylpyridine	**m-xylene**	DUTXAR12
95	Ni	4-phenylpyridine	**m-xylene**	DUTXAR13
96	Ni	4-phenylpyridine	**m-xylene**	DUTXAR14
97	Ni	4-phenylpyridine	**4-phenylpyridine**, 2-methoxyethanol	DUTXIZ
98	Ni	4-phenylpyridine	**4-phenylpyridine**, 2-methoxyethanol	DUTXIZ10
99	Ni	4-phenylpyridine	-	FOPREH
100	Ni	4-phenylpyridine	**o-xylene**	FOPRIL
101	Ni	4-phenylpyridine	**p-xylene**, dimethylsulfoxide	FOPRUX
102	Ni	4-phenylpyridine	**4-phenypyridine**, dimethylsulfoxide	SAHHAK
103	Ni	4-phenylpyridine	dimethylsulfoxide, **phenylacetylene**	SAHHIS
104	Ni	4-phenylpyridine	**toluene**	SEZKEP
105	Ni	4-phenylpyridine	**toluene**	SEZKEP01
106	Ni	4-phenylpyridine	**benzene**	SEZKOZ
107	Ni	4-phenylpyridine	**benzene**	SEZKUF
108	Ni	4-phenylpyridine	**benzene**	VANCIW
109	Ni	4-vinylpyridine	-	DOJXOP
110	Ni	4-vinylpyridine	-	DOJXOP01
111	Ni	4-vinylpyridine	**p-xylene**	FINCOU
112	Ni	4-vinylpyridine	**m-xylene**	FINCUA
113	Ni	4-vinylpyridine	**o-xylene**	FINDAH
114	Ni	4-vinylpyridine	chloroform	FOCDEG
115	Co	4-vinylpyridine	-	ICVPCO
116	Co	4-vinylpyridine	-	ICVPCO01
117	Ni	4-vinylpyridine	cyclohexene, tetrahydrofuran	PIZLOZ
118	Ni	4-vinylpyridine	cyclohexene, tetrahydrofuran	PIZLUF
119	Ni	4-vinylpyridine	1,3-cyclohexadiene tetrahydrofuran	PIZMAM
120	Ni	4-vinylpyridine	1,4-cyclohexadiene tetrahydrofuran	PIZMIU
121	Ni	4-vinylpyridine	**benzene**, tetrahydrofuran	PIZMOA
122	Ni	4-vinylpyridine	**benzene**	PIZMUG
123	Ni	4-vinylpyridine	tetrahydrofuran	PIZNAN
124	Ni	4-vinylpyridine	**1h-indene**	QAKCOX
125	Ni	4-vinylpyridine	**naphthalene**	QAKCUD
126	Ni	4-vinylpyridine	**azulene**	QAKDAK
127	Ni	4-vinylpyridine	**fluorene**	QAKDEO

No.	M	L	G	REFCODE
128	Ni	4-vinylpyridine	**fluorene**	QAKDIS
129	Ni	4-vinylpyridine	**phenanthrene, benzene**	QAKDOY
130	Ni	4-vinylpyridine	**phenanthrene**	QAKDUE
131	Ni	4-vinylpyridine	**anthracene**	QAKFAM
132	Ni	4-vinylpyridine	**pyrene**, methanol	QAKFEQ
133	Ni	4-vinylpyridine	tetrachloromethane	VAXVAR
134	Ni	4-vinylpyridine	iodoform	VAXVEV
135	Ni	4-vinylpyridine	iodoform, di-isothiocyanato-tetrahydrofuran-tris(4-vinylpyridine-n)-nickel(ii)	VAXVIZ
136	Ni	4-vinylpyridine	**1,2,4,5-tetrafluoro-3,6-diiodobenzene**	WUXZIA
137	Ni	4-ethylpyridine	**p-xylene**	CIVJOG
138	Ni	4-ethylpyridine	**p-xylene**	CIVJOG01
139	Ni	4-ethylpyridine	**p-xylene**	CIVJOG02
140	Ni	4-ethylpyridine	**m-xylene**	CIVJUM
141	Ni	4-ethylpyridine	**m-xylene**	CIVJUM01
142	Ni	4-ethylpyridine	**m-xylene**	CIVJUM02
143	Fe	4-ethylpyridine	-	FOCXEC
144	Fe	4-ethylpyridine	-	FOCXEC01
145	Mn	4-ethylpyridine	-	FOCXOM
146	Mn	4-ethylpyridine	-	FOCXOM01
147	Ni	4-ethylpyridine	-	GAJWOD
148	Ni	4-ethylpyridine	-	GAJWOD01
149	Ni	4-ethylpyridine	carbon tetrachloride	GAJWUJ
150	Ni	4-ethylpyridine	carbon tetrachloride	GAJXAQ
151	Ni	4-ethylpyridine	**o-xylene**	GAJXOE
152	Ni	4-ethylpyridine	**o-xylene**	GAJXOE01
153	Ni	4-ethylpyridine	carbon disulphide	GAJXUK
154	Ni	4-ethylpyridine	carbon disulphide	GAJXUK01
155	Ni	4-ethylpyridine	**p-dichlorobenzene**	LIDZON
156	Ni	4-ethylpyridine	**p-dichlorobenzene**	LIDZUT
157	Cd	4-ethylpyridine	-	PEQNAC
158	Co	4-ethylpyridine	-	PIRROZ
159	Co	4-ethylpyridine	-	PIRROZ01
160	Ni	4-ethylpyridine	**1-methylnaphthalene**	SOGWEQ
161	Zn	isoquinoline	-	EFOXII
162	Cd	isoquinoline	-	EFOXUU
163	Ni	isoquinoline	**p-xylene**	JOZZUV
164	Ni	isoquinoline	**m-xylene**	JUBBAL
165	Ni	isoquinoline	**o-xylene**	JUBQII
166	Ni	isoquinoline	dichloromethane	YAWSIZ
167	Ni	4-methylpyridine, 4-phenylpyridine	2-methoxyethanol	BUJPAX
168	Ni	4-methylpyridine, 4-phenylpyridine	acetylacetone	VEJHAT

No.	M	L	G	REFCODE
169	Ni	4-methylpyridine, 4-phenylpyridine	1-chlorobutane	VEJHEX
170	Ni	3-methylpyridine	chloroform	CIVJEW
171	Ni	3-methylpyridine	chloroform	CIVJEW10
172	Co	3-methylpyridine	-	EYAROM
173	Co	3-methylpyridine	-	EYAROM01
174	Ni	3-methylpyridine	carbon tetrachloride	JICMIR
175	Ni	3-methylpyridine	dibromo-dichloromethane	LAYLAY
176	Ni	3-methylpyridine	2,2-dichloropropane	LAYLEC
177	Ni	3-methylpyridine	2,2-dichloromethane	LAYLIG
177	Ni	3-methylpyridine	chloroform	LAYLOM
178	Ni	3-methylpyridine	dichloromethane	LAYLUS
179	Ni	isoquinoline, 4-phenylpyridine	**p-xylene**	ETOFEA
180	Ni	isoquinoline, 4-phenylpyridine	**m-xylene**	ETOFIE
181	Ni	isoquinoline, 4-phenylpyridine	**o-xylene**	ETOFOK
182	Co	4-acetylpyridine	-	EDAQUV
183	Ni	4-acetylpyridine	**p-dichlorobenzene**	LIFBAD
184	Ni	4-acetylpyridine	-	OGOREJ
185	Fe	4,4'-ethene-1,2-diyldipyridine	**4,4'-ethene-1,2-diyldipyridine**, ethanol	FESVIJ01
186	Fe	4,4'-ethene-1,2-diyldipyridine	**4,4'-ethene-1,2-diyldipyridine**, ethanol	FESVIJ
187	Co	4,4'-ethene-1,2-diyldipyridine	**4,4'-ethene-1,2-diyldipyridine**	UWACAX
188	Co	trans-4,4'-azopyridine	ethanol, water	AKONIX
189	Fe	trans-4,4'-azopyridine	ethanol	GUTDOO
190	Fe	trans-4,4'-azopyridine	ethanol	GUTDOO01
191	Co	trans-4,4'-azopyridine	ethanol	REBZIH
192	Ni	trans-4,4'-azopyridine	-	XESBED
193	Ni	trans-4,4'-azopyridine	ethanol	XETNUG
194	Ni	trans-4,4'-azopyridine	methanol	XETPAO
195	Fe	4,4’-ethylenedipyridine	acetone	DORCIX
196	Fe	4,4’-ethylenedipyridine	acetone	DORCIX01
197	Fe	4,4’-ethylenedipyridine	acetone	DORCIX03
198	Co	2,4,6-tris(4-pyridyl)-1,3,5-triazine	**4-hydroxydiphenylamine**	FALBAX
199	Co	2,4,6-tris(4-pyridyl)-1,3,5-triazine	unknown	PUZLOM
200	Co	2,4,6-tris(4-pyridyl)-1,3,5-triazine	tetrathiafulvalene	PUZLUS
201	Co	2,4,6-tris(4-pyridyl)-1,3,5-triazine	**diphenylamine**	PUZMAZ
202	Co	(pyridin-4-yl)methanol	-	GEHPER
203	Co	(pyridin-4-yl)methanol	water	GEHPIV
204	Ni	(pyridin-4-yl)methanol	-	HUGWAJ

No.	M	L	G	REFCODE
205	Ni	(pyridin-4-yl)methanol	unkown	HUGWEN
206	Ni	2-cyano-n-((pyridin-4-yl)methyl)acetamide	water	CAXWEG
207	Fe	1,2-bis(4-pyridyl)ethane-N,N'	acetone	DORCIX
208	Fe	1,2-bis(4-pyridyl)ethane-N,N'	acetone	DORCIX01
209	Fe	1,2-bis(4-pyridyl)ethane-N,N'	acetone	DORCIX03
210	Co	1-methyl-1-(3-pyridyl)-2-(4-pyridyl)ethene	methanol, nitromethane	EBOFEH
211	Co	μ2-4'-(4-(nonyloxy)phenyl)-4,2':6',4''-terpyridine	chloroform, methanol	EMEJUD
212	Ni	2-methylfuro(3,2-c)pyridine	water	YAWSOF
213	Ni	2,3-dimethylfuro(3,2-c)pyridine	water	ETOGID
214	Co	4-(n-t-butyl-n-oxylamino)pyridine-n'	dichloromethane	HENQOH
215	Co	μ2-1-methyl-1-(3-pyridyl)-2-(4-pyrimidyl)ethene	methanol, nitromethane	ILALOW
216	Co	μ2-1-methyl-1-(3-pyridyl)-2-(4-pyrimidyl)ethene	methanol, nitromethane	ILALOW01
217	Fe	μ2-N,N'-bis(pyridin-4-ylmethylene)ethane-1,2-diamine	water	ITIJEB
218	Co	μ2-N,N'-bis(pyridin-4-ylmethylene)ethane-1,2-diamine	ethanol	LUVZOR
219	Fe, Cu	μ4-hydrogen tris(3-(4-pyridyl)pyrazolyl)borato)-dodecakis(acetonitrile)	triperchlorate, acetonitrile, water	MOXLAN
220	Fe, Cu	μ4-hydrogen tris(3-(4-pyridyl)pyrazolyl)borato)-dodecakis(acetonitrile)	triperchlorate, acetonitrile, water	MOXLAN01
221	Co	3-cyanopyridine	1,4-dioxane	OBONOK
222	Ni	3-cyanopyridine	-	UDABAC
223	Ni	3-cyanopyridine	ethanol	UDABEG
224	Ni	3-cyanopyridine	dichloromethane	UDABIK
225	Co	(isonicotinamide)-bis(isothiocyanate)	**isonicotinamide**, ethanol	OQAFET
226	Ni	4-aminopyridine-N	-	QILBAO
227	Ni	4-aminopyridine-N	acetone, ethanol	QILBES
228	Ni	4-aminopyridine-N	dimethylsulfoxide	QILBEW
229	Co	μ3-2,4,6-tris(3-pyridyl)-1,3,5-triazine	**thiophene**	LAFQOA
230	Co	μ3-2,4,6-tris(3-pyridyl)-1,3,5-triazine	furan	LAFQUG
231	Co	μ3-2,4,6-tris(3-pyridyl)-1,3,5-triazine	2,3-dihydrofuran	LAFRAN

No.	M	L	G	REFCODE
232	Co	μ3-2,4,6-tris(3-pyridyl)-1,3,5-triazine	**diphenyl ether**	LAFRER
233	Co	μ3-2,4,6-tris(3-pyridyl)-1,3,5-triazine	cyclopentadiene, tricyclo[5.2.1.02,6]deca-3,8-diene	LAFRIV
234	Co	μ3-2,4,6-tris(3-pyridyl)-1,3,5-triazine	cyclopentadiene, tricyclo[5.2.1.02,6]deca-3,8-diene	LAFROB
235	Co	μ3-2,4,6-tris(3-pyridyl)-1,3,5-triazine	methylisothiocyanate	LAXJAX
236	Co	m3-2,4,6-tris(3-pyridyl)-1,3,5-triazine	cyclopentane	RIFSOQ
237	Co	μ3-2,4,6-tris(3-pyridyl)-1,3,5-triazine	t-butyl acrylate	RIVDIL
238	Fe	bis(μ2-n,n'-bis(4-pyridylmethylene)-1,5-naphthalenediamine)-bis(m2-4,4'-bipyridine	chloroform, water	TALREF
239	Fe	μ2-4-pyridinecarbaldehyde 4'-(2,2':6',2''-terpyridyl)hydrazone-n,n',n'',n'''	ethanol, water, isothiocyanate	TOPLIU
240	Fe	4-(4-(3,3,4,4,5,5-hexafluoro-2-(2-methyl-5-phenylthiophen-3-yl)cyclopent-1-enyl)-5-methylthiophen-2-yl)pyridine	dichloromethane, water	UFEBUD
241	Ni	benzofuro(3,2-c)pyridine	water	YAWSEV
242	Co	μ2-4'-(4-methoxyphenyl)-4,2':6',4''-terpyridine	chloroform, methanol, water	ZUNJOJ
243	Co	μ-1-(4-pyridyl)butane-1,3-dionato	dichloromethane, dichoride	QELXIR
244	Co	pyridine-4-carbothioamide	water	QEMXIS
245	Co	pyridine-4-carbothioamide	methanol	SEMWUF
246	Co	4-(n-(4-methoxyphenyl)-N-oxylamino)pyridine	diethylether	MOBGOA
247	Co	4-(N-(2,4,6-tris(t-butyl)phenyl)-N-oxylamino)pyridine	diethylether	MOMGUG
248	Co	4'-pyridyl)pyridin-4-one-N,O	methanol, water, isothiocyanato	NERNIH
249	Fe	μ2-4,4'-bipyridine	chloroform	QAQTOT

6.7.2 TGA, DSC, and PXRD traces of structures 6.1–6.6 and the apohost H3.

All DSC traces presented are exothermic up.
TGA mass loss percentages were calculated using the following molar mass (g/mol) values:

NCS: 58.08
Ni: 58.69
Methylnaphthalene (MN): 142.20
4-phenylpyridine (4-PhPy):155.20
Monomer host: 795.64 [Ni + 2 (NCS) + 4(4-phenylpyrine)]
Dimer host: 1280.88 [2(Ni) + 4(NCS) + 6(4-phenylpyridne)]

As an example, for structure **I**: the first mass loss % totals 63.8% and we surmise this is due to the loss of two 4-PhPy ligands and four 1-MN molecules.

$$\text{calculated mass loss} = \frac{(2\times\text{molar mass 4-PhPy})+(4\times\text{molar mass MN})}{\text{molar mass of monomer host}+(4\times\text{molar mass MN})}\times 100$$

$$= \frac{(2\times 155.20)+(4\times 142.20)}{795.64+(4\times 142.20)}\times 100$$

$$= 64.4\%$$

Similarly, we can calculate that two 4-PhPy ligands amount to 22.7% of the total mass in compound **6.1**. In each of the compounds **6.1**-**6.6** and the apohost, the portion of the compound that remains at 400 °C is $Ni(NCS)_2$, for structure **6.1** this amounts to 12.8% of the total compound mass.

Powder X-ray Diffraction (PXRD) data were collected by mounting powders on a flat zero-background sample holder on a Bruker D8 Advance diffractometer with copper radiation (Cu Kα, λ = 1.5406 Å) at 30 kV and 40 mA. Each sample was scanned between 4 and 40° 2θ with a step size of 0.025°. Powders were mounted on a flat zero-background sample holder.

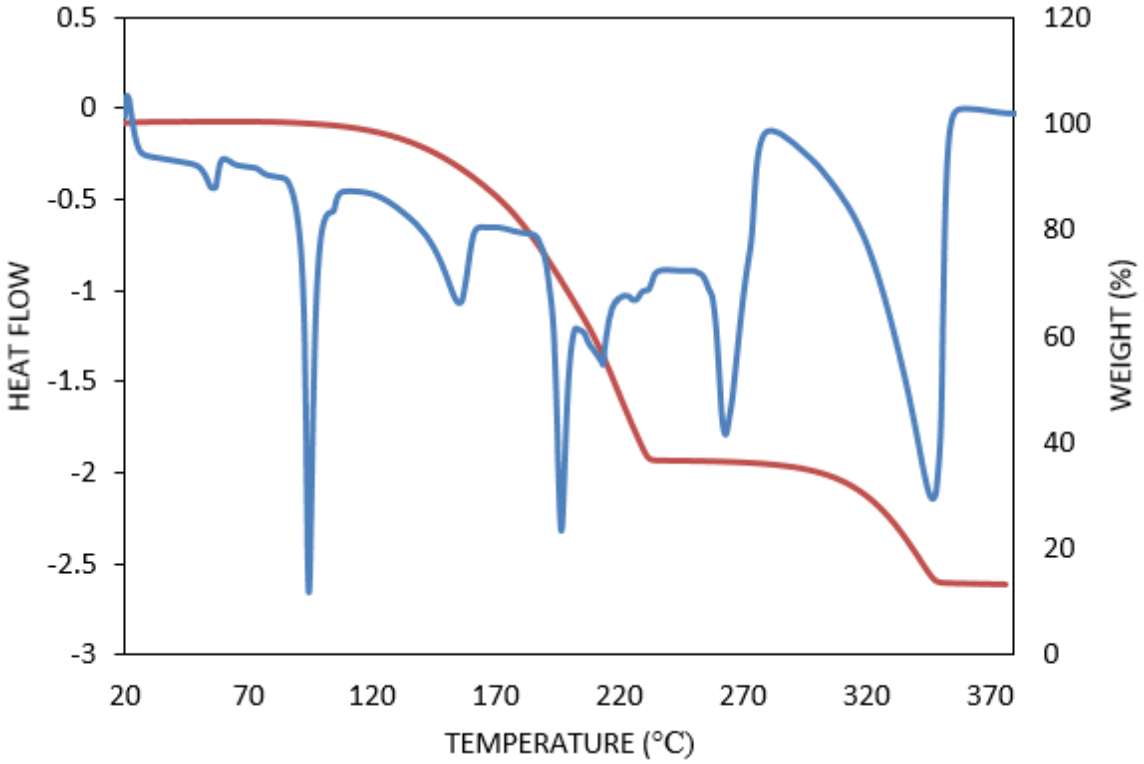

Figure S6.1. DSC (blue) and TGA (red) traces of structure **6.1**, collected at 30 °C/min. The DSC displays multiple endothermic peaks: 56, 94, 155, 196, 213, 263, and 347 °C. The TGA displays two broad mass losses of 63.8% and 23.2%. The first likely corresponds to the loss of the two 4-PhPy ligands and all four **1-MN** guest molecules (calc = 64.4%), the second mass loss is attributed due to the remaining two 4-PhPy ligands (calc = 22.7%).

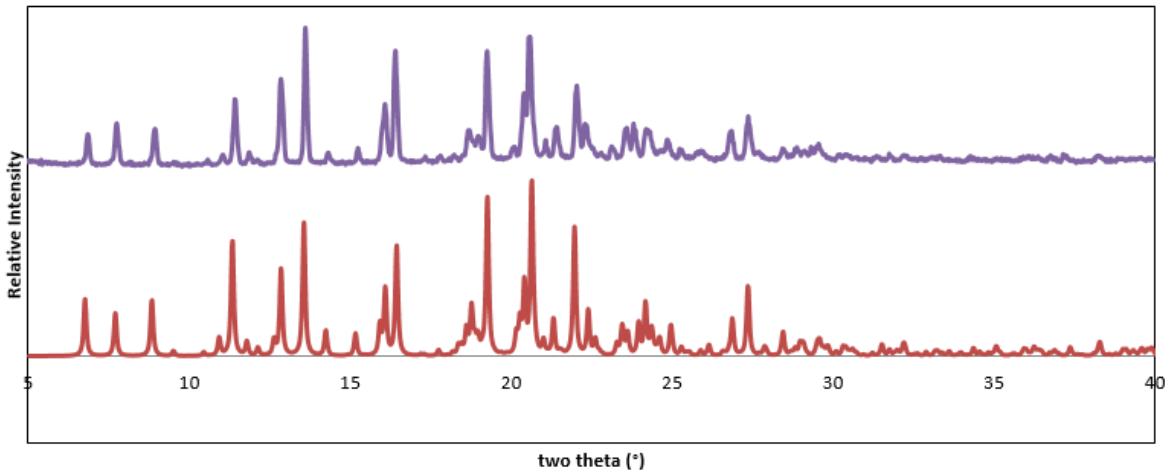

Figure S6.2. Calculated PXRD trace (red) and experimental (purple) for structure **6.1**.

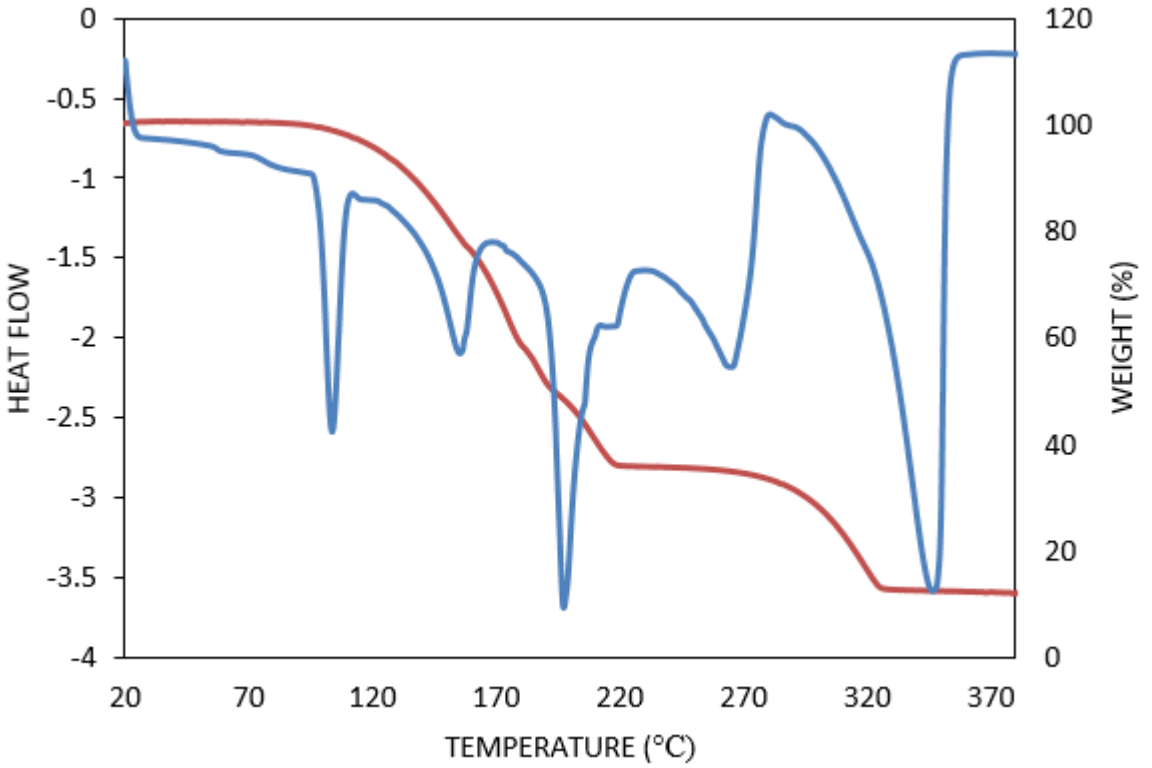

Figure S6.3. DSC (blue) and TGA (red) traces of structure **6.2**, collected at 30 °C/min. The DSC displays multiple endothermic peaks: 104, 156, 197, 219, 267, and 347 °C The TGA displays an initial bumpy mass loss totalling 64.6%, attributed to the loss of two 4-PhPy ligands and four **1-MN** molecules (calc = 64.4%). The second mass loss totals 23.3% and could be due to the remaining 4-PhPy ligands (calc = 22.7%).

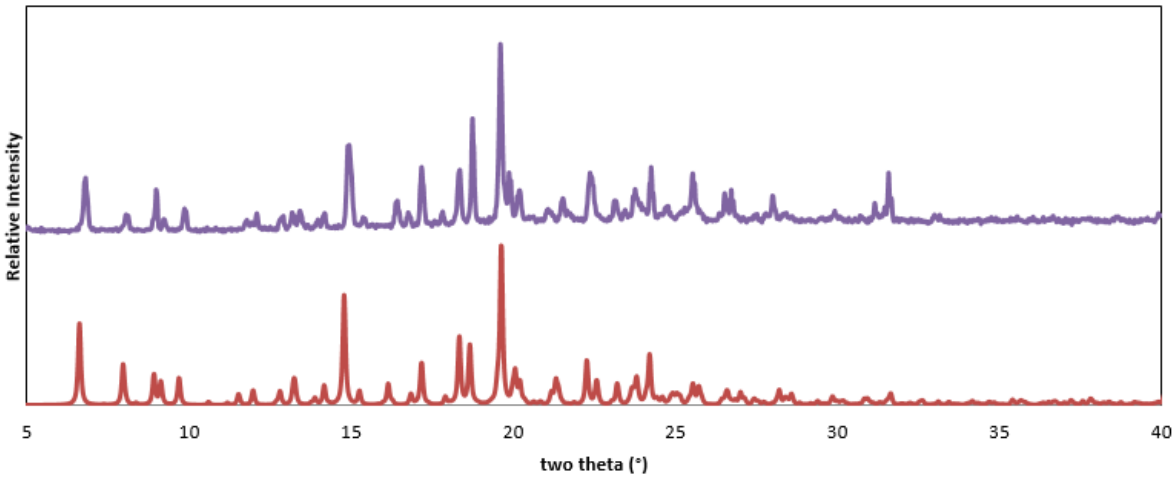

Figure S6.4. Calculated PXRD trace (red) and experimental (purple) for structure **6.2**.

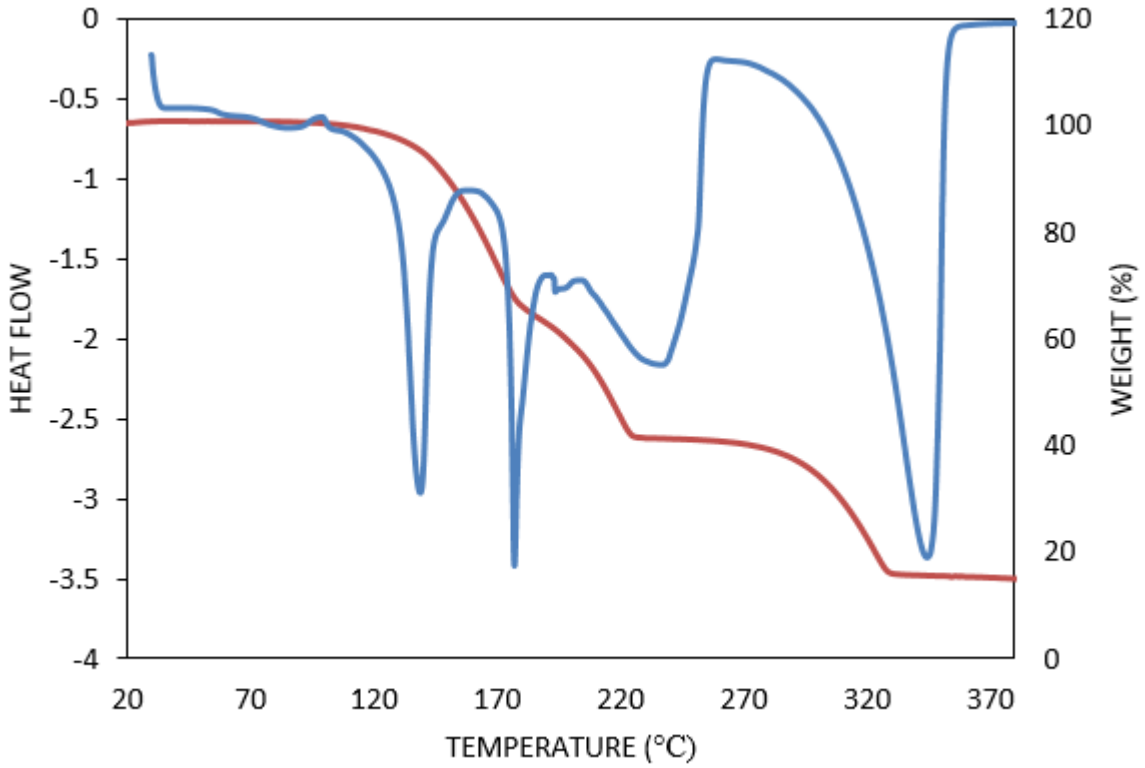

Figure S6.5. DSC (blue) and TGA (red) traces of structure **6.3**, collected at 30 °C/min. The DSC displays multiple endothermic peaks: 139, 177, 193, 239, and 345 °C. The TGA displays an initial bumpy mass loss totalling 59.3%, attributed to the loss of two 4-PhPy ligands and three **2-MN** molecules (calc = 60.3%). The second mass loss totals 25.8% and we attribute this to the loss of the two remaining 4-PhPy ligands (calc = 25.4%).

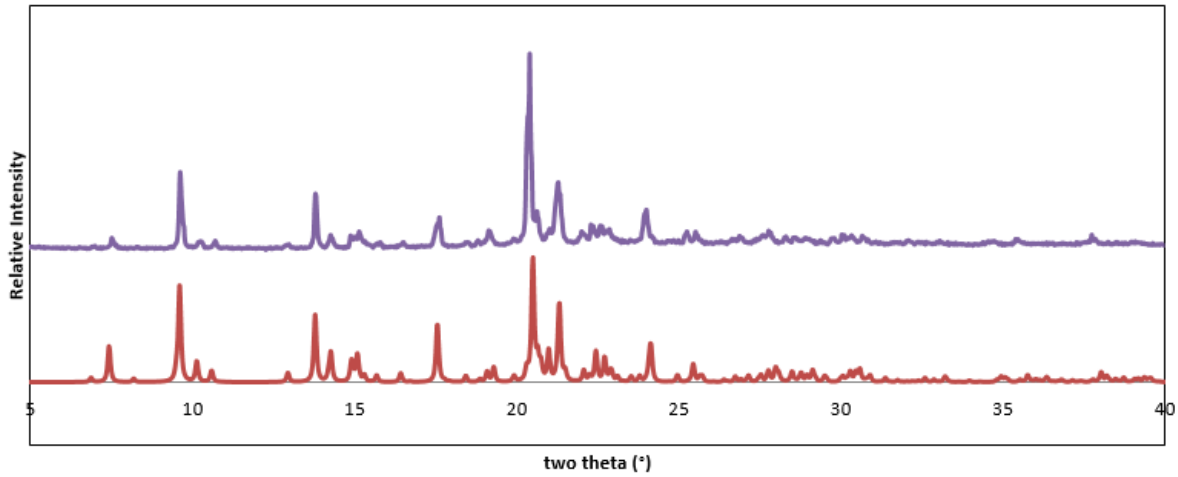

Figure S6.6. Calculated PXRD trace (red) and experimental (purple) for structure **6.3**.

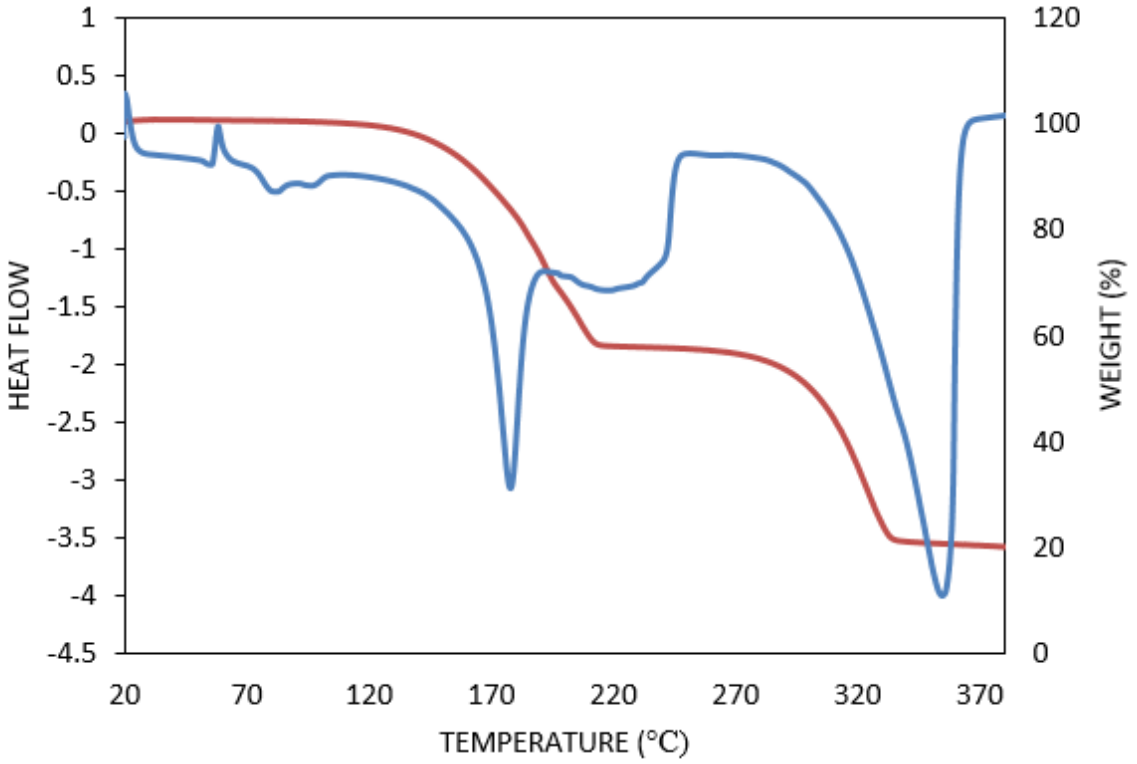

Figure S6.7. DSC (blue) and TGA (red) traces of structure **6.4**, collected at 30 °C/min. The DSC displays multiple endothermic peaks (°C): 80 (broad), 176, 226 (broad), 353 °C, and an exothermic peak at 57 °C. The TGA displays an initial large mass loss totalling 42.9%, attributed to the loss of two 4-PhPy ligands and three **2-MN** molecules (calc = 43.2%). The second mass loss totals 36.8% and we attribute this to the loss of the four remaining 4-PhPy ligands (calc = 36.4%).

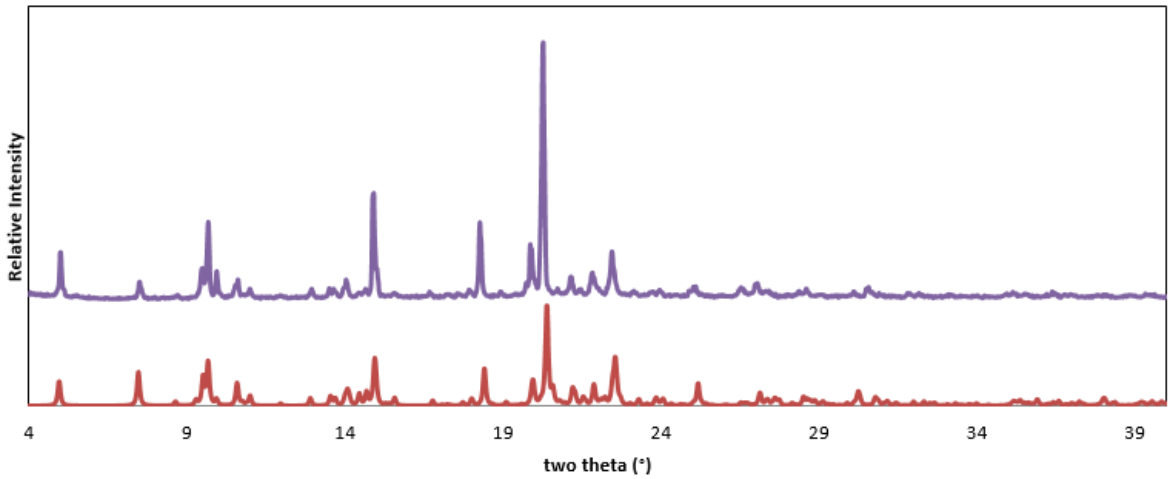

Figure S6.8. Calculated PXRD trace (red) and experimental (purple) for structure **6.4**, the experimental trace suffered from preferred orientation.

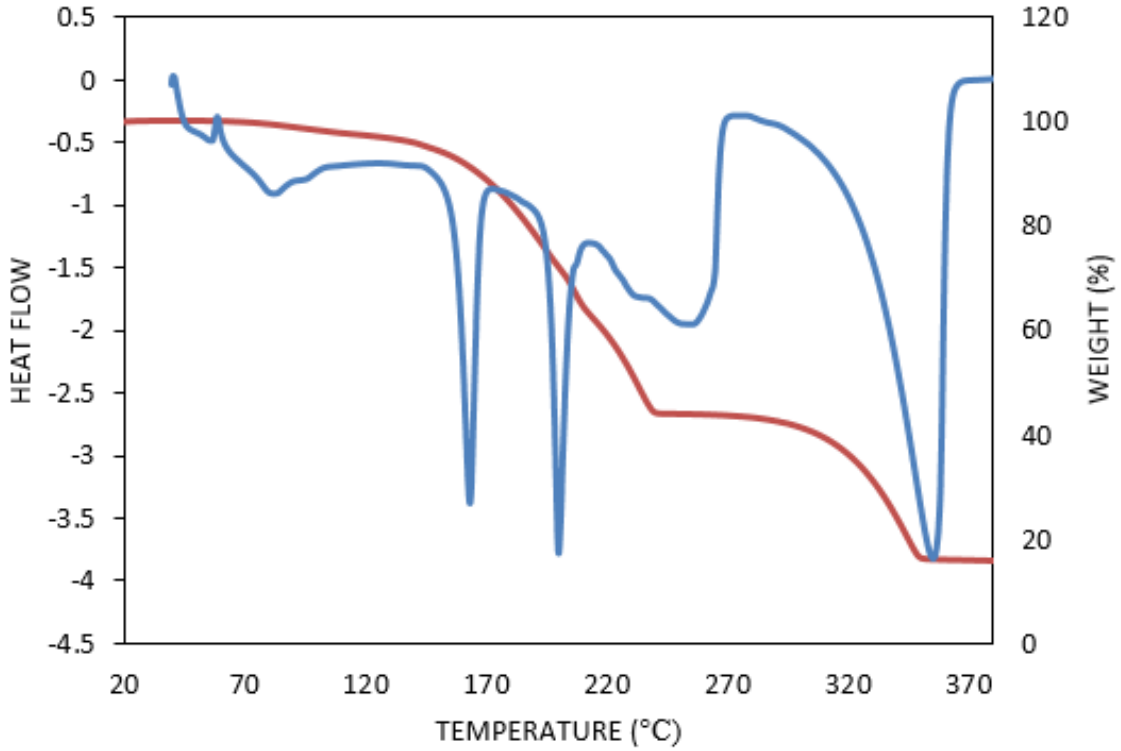

Figure S6.9. DSC (blue) and TGA (red) traces of structure **6.5**, collected at 30 °C/min. The DSC displays multiple endothermic peaks (°C): 86, 163, 200, 254 (broad), and 356 °C. The TGA displays a small, broad initial large mass loss totalling 2.6%, attributed to the loss of one MeOH molecule (calc = 2.9%). The second, large mass loss totals 53.7% and is attributed to the loss of two 4-PhPy ligands and two methylnaphthalene molecules (calc = 53.4%). The third mass loss totals 27.8% and we attribute this to the loss of the two remaining 4-PhPy ligands (calc = 28.7%).

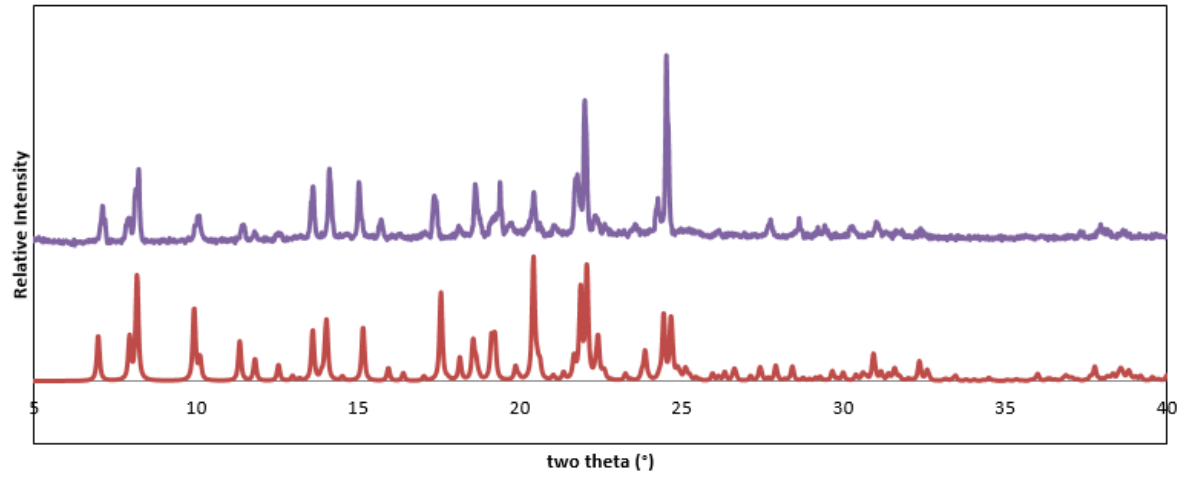

Figure S6.10. Calculated PXRD trace (red) and experimental (purple) for structure **6.5** collected 4 days after competition experiment was initiated. The NMR result was 87% **1-MN** : 13% **2-MN**.

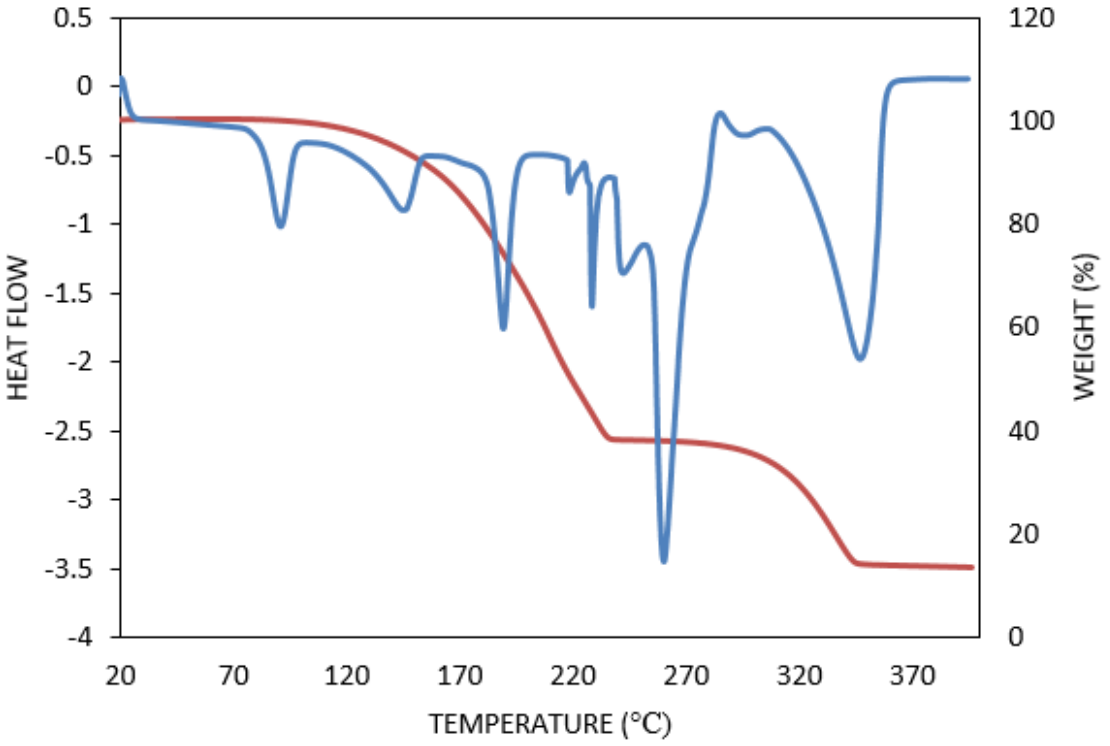

Figure S6.11. DSC (blue) and TGA (red) traces of bulk crystals from competition experiment taken 20 days after experiment began and collected at 30 °C/min. The DSC is complex, and the endothermic peaks occur at 91, 146, 190, 219, 229, 242, 260, 295, and 347 °C. The first, large mass loss totals 62.2% and is attributed to the loss of two 4-PhPy ligands and either three methylnaphthalene molecules (calc = 60.3%) or four methylnaphthalene molecules (calc = 64.4%). The second mass loss totals 24.5% and we attribute this to the loss of the two remaining 4-PhPy ligands (calc = 25.4% for 3 guest molecules or 22.7% for 4 guest molecules).

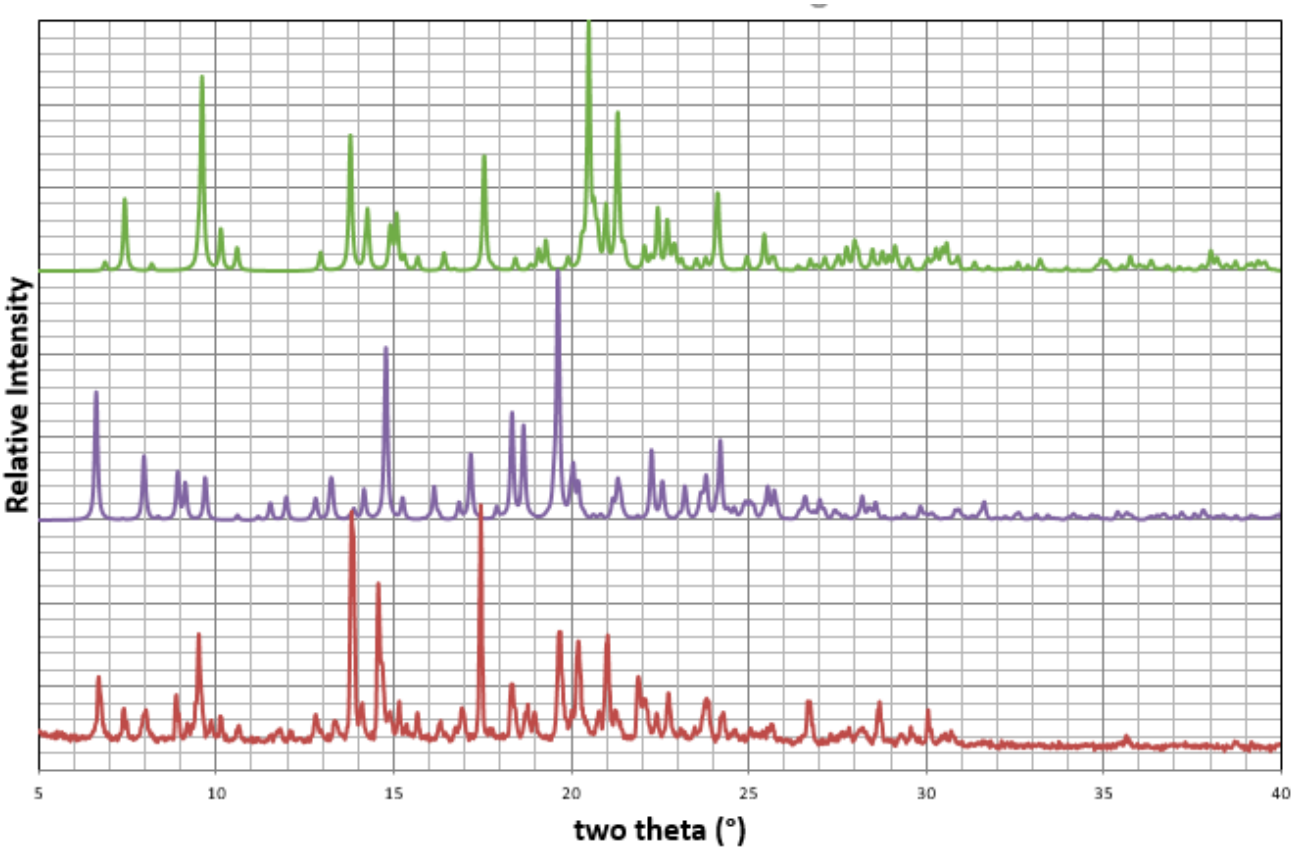

Figure S6.12. The experimental (red) PXRD trace was collected 20 days after the competition experiment was initiated; the NMR result yielded 54% **1-MN**: 45% **2-MN**. This is compared to the calculated PXRD traces of structure II, a 1-MN clathrate (purple trace), and structure **6.3**, a **2-MN** clathrate (green trace). A random crystal was selected from the bulk and the structure collected and named **6.6**, which is very similar to **6.3** (see section 4).

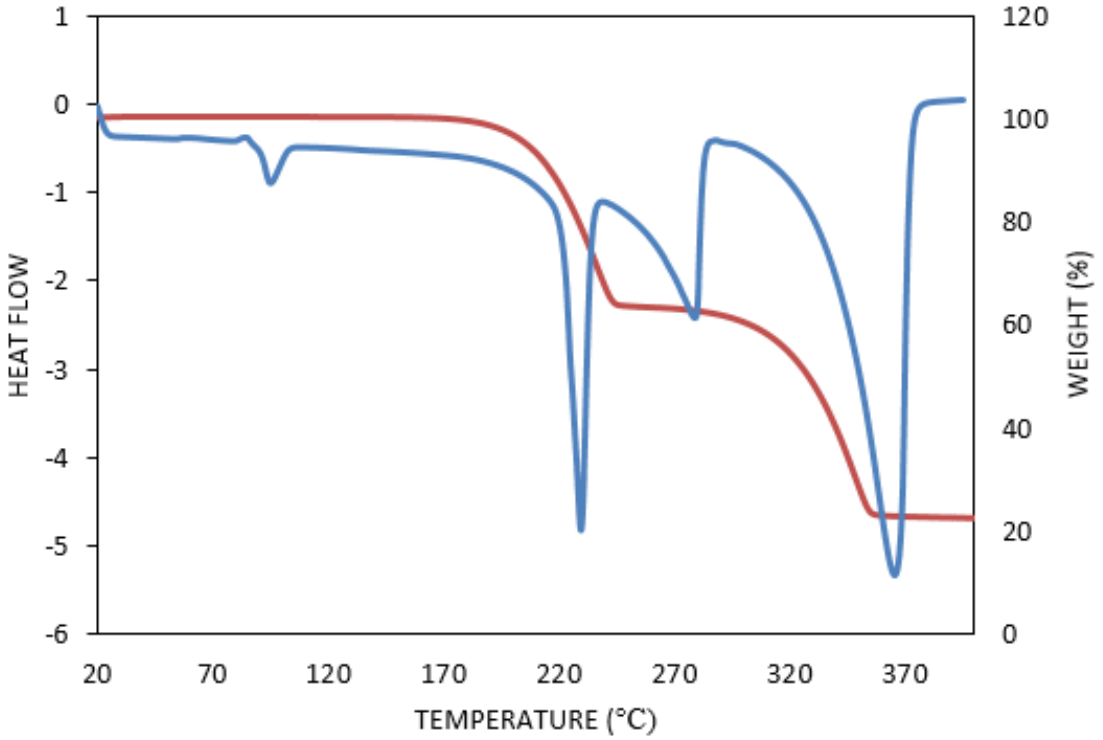

Figure S6.13. DSC (blue) and TGA (red) traces of apohost, recrystallized from MeOH and airdried, collected at 30 °C/min. The DSC displays multiple endothermic peaks (°C): 95, 229, 278, 366. The TGA displays two mass loss events, the first mass loss totals 37.4% and the second 39.8%. The calculated mass loss % values for two 4-PhPy ligands is 39.0%.

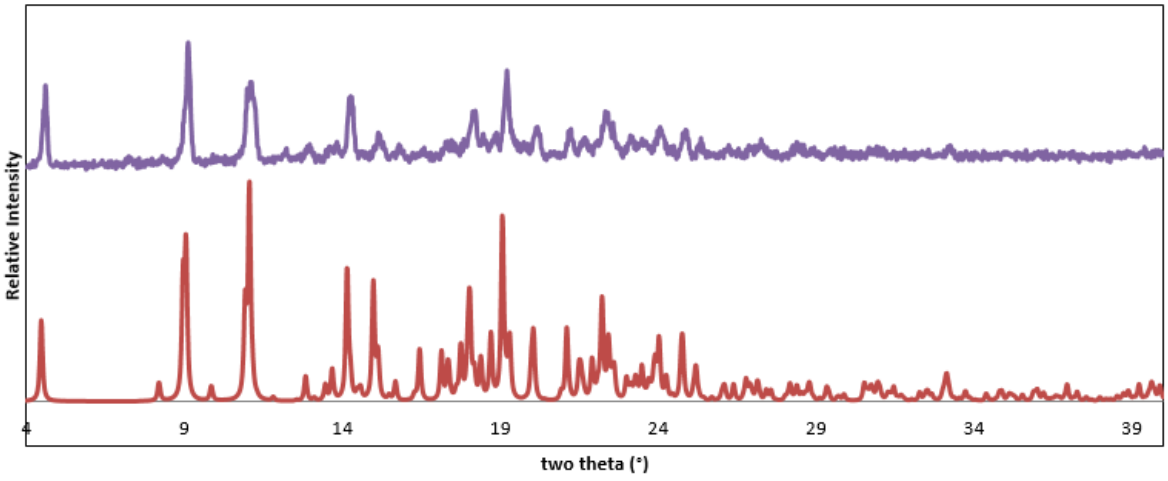

Figure S14. Calculated PXRD trace (red) of the apohost (FOPREH) and experimental (purple) for apohost synthesized in house and recrystallized from methanol.

6.7.3 ^{1}H NMR results from competition experiments.

All ^{1}H NMR spectra were collected using $CDCl_3$ as the solvent, and the $CHCl_3$ peak (7.26 ppm) was used to reference the spectra.

The CH_3 singlet of the methylnaphthalene guests was integrated to compare the relative proportions of 1- and 2-methylnapthalene in crystals derived from competition experiments. The CH_3 singlet of 1-methylnapthalene occurs more downfield (2.45 ppm) compared to that of 2-methylnaphthalene (2.35 ppm).

Samples are prepared by removing crystals from mother liquor, then drying on filter paper. Crystals are crushed and dissolved in $CDCl_3$. The host is unstable in chloroform, and after a short while a light green powder precipitates. The sample is filtered into NMR tubes using a 0.45 µm nylon filter attached to a 5 ml syringe and needle.

The NMR spectra from competition experiments contain signals from the host, methylnapthalenes, and various impurities. The CH_3 singlets of 1- and 2-methylnaphthalene shift downfield to 2.70 ppm and 2.52 ppm respectively. Peaks present in the spectra arise due to 'grease' (CH_3, m, 0.86 ppm; CH_2, broad s, 1.26 ppm), silicon grease (CH_3, s, 0.07 ppm), and water, the peak of which is deshielded (broad s, 1.70 ppm) (Table 1, *J. Org. Chem.* 1997, 62, 21, 7512-7515). In some cases, glycerol (CH_2, m 3.52 ppm; CH_2, m, 3.64 ppm, m CH 3.85 ppm) was observed in the spectra, the introduction of which we attribute to the filtration step via a wet filter.

The relative amount of 1- and 2-methylnaphthalne present in the NMR spectra (and thus in the crystals resulting from competition experiments) is calculated by integrating their CH_3 singlets and obtaining the percentage. For example, in Figure S6.20 the CH_3 singlet for **1-MN** is calibrated to integrate for 1.00 and the CH_3 singlet for **2-MN** integrates for 0.15.

$$\%\ \textbf{1-MN} = \frac{1.00}{1.00 + 0.15} \times 100$$

$$= 86.96\%$$

$$\approx 87\ \%$$

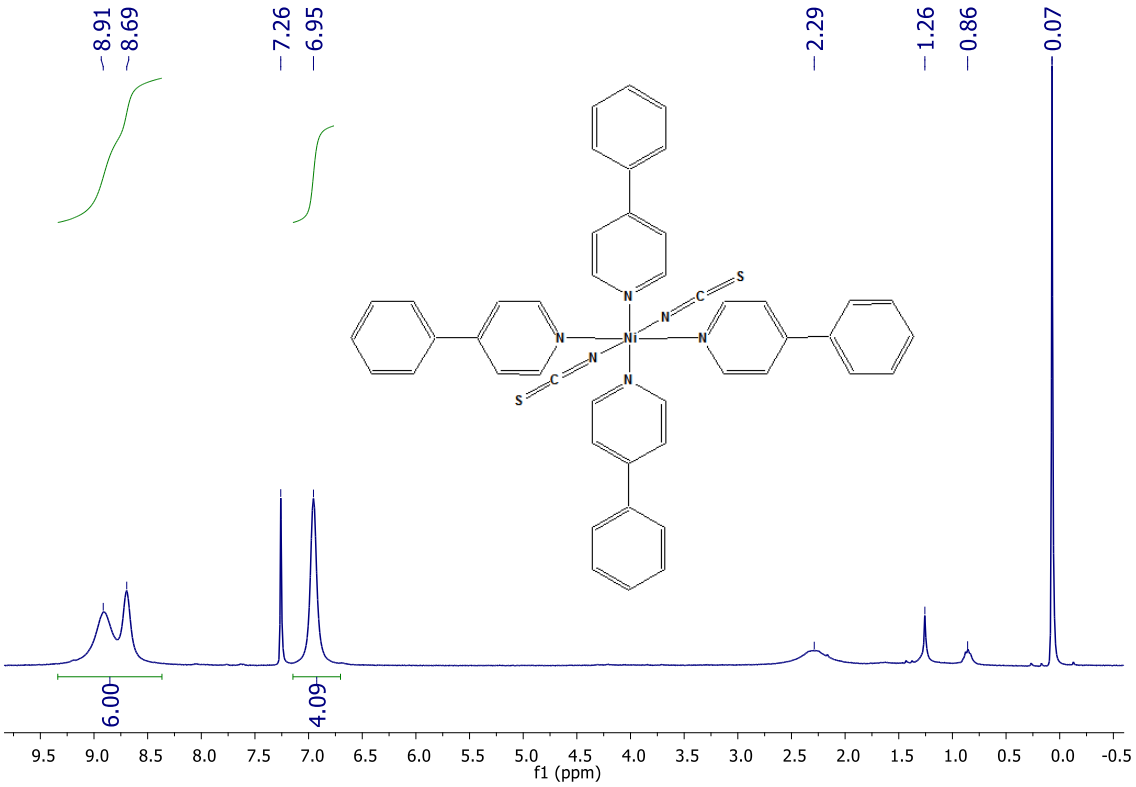

Figure S6.15. ^{1}H NMR of host **H3**, $Ni(NCS)_2(4\text{-phenylpyridine})_4$, post filtering from a $CDCl_3$ solution.

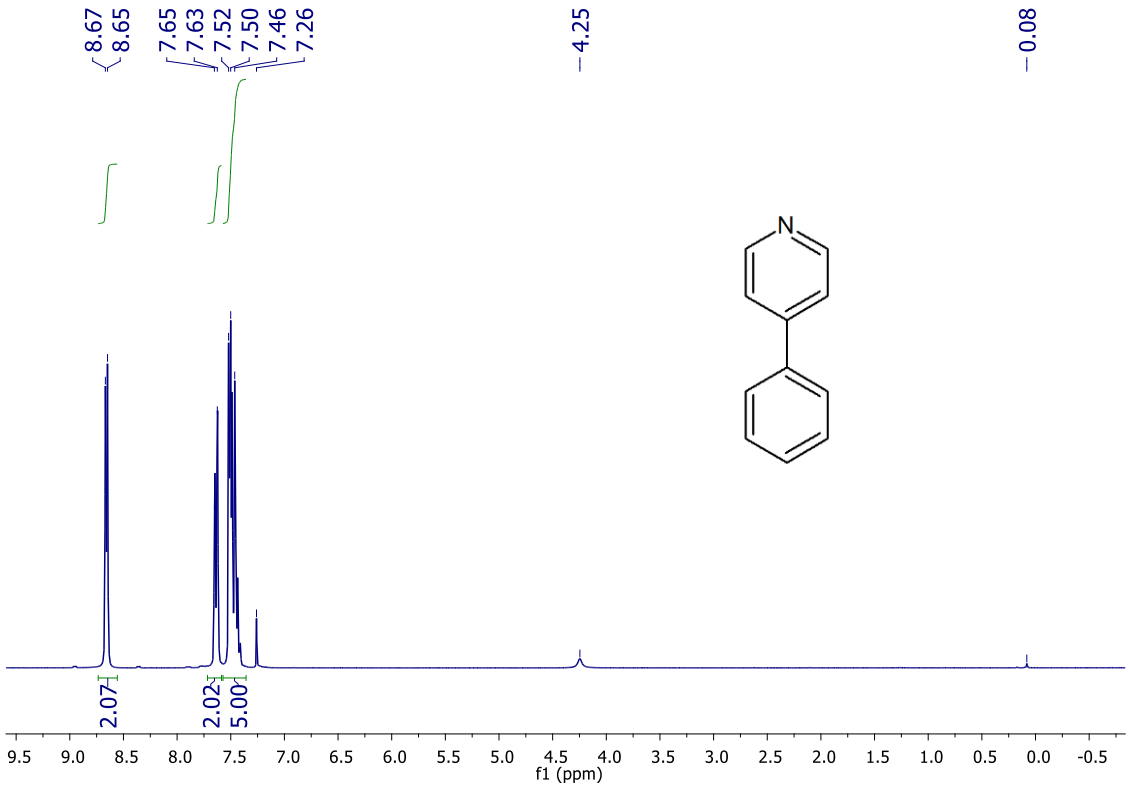

Figure S6.16. ^{1}H NMR of 4-phenylpyridine in $CDCl_3$.

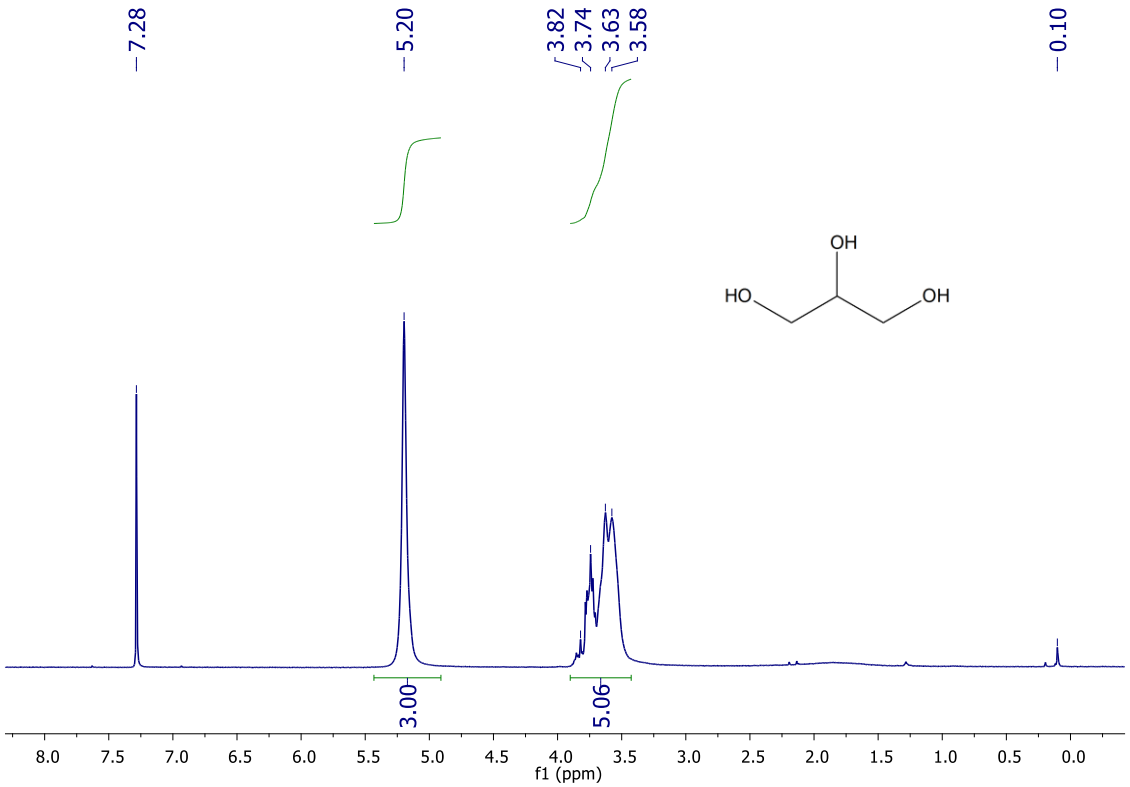

Figure S6.17. ^{1}H NMR of glycerol in $CDCl_3$.

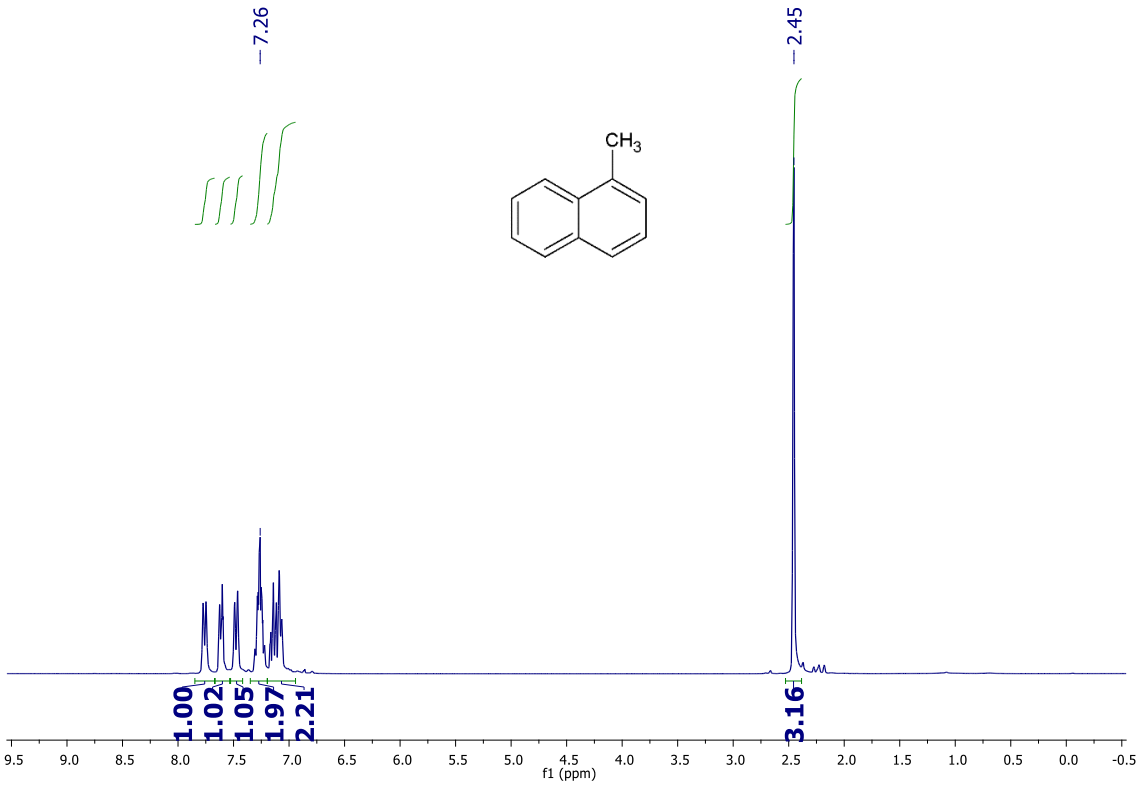

Figure S6.18. ^{1}H NMR of 1-methylnaphthalene in $CDCl_3$ with CH_3 peak at 2.45 ppm.

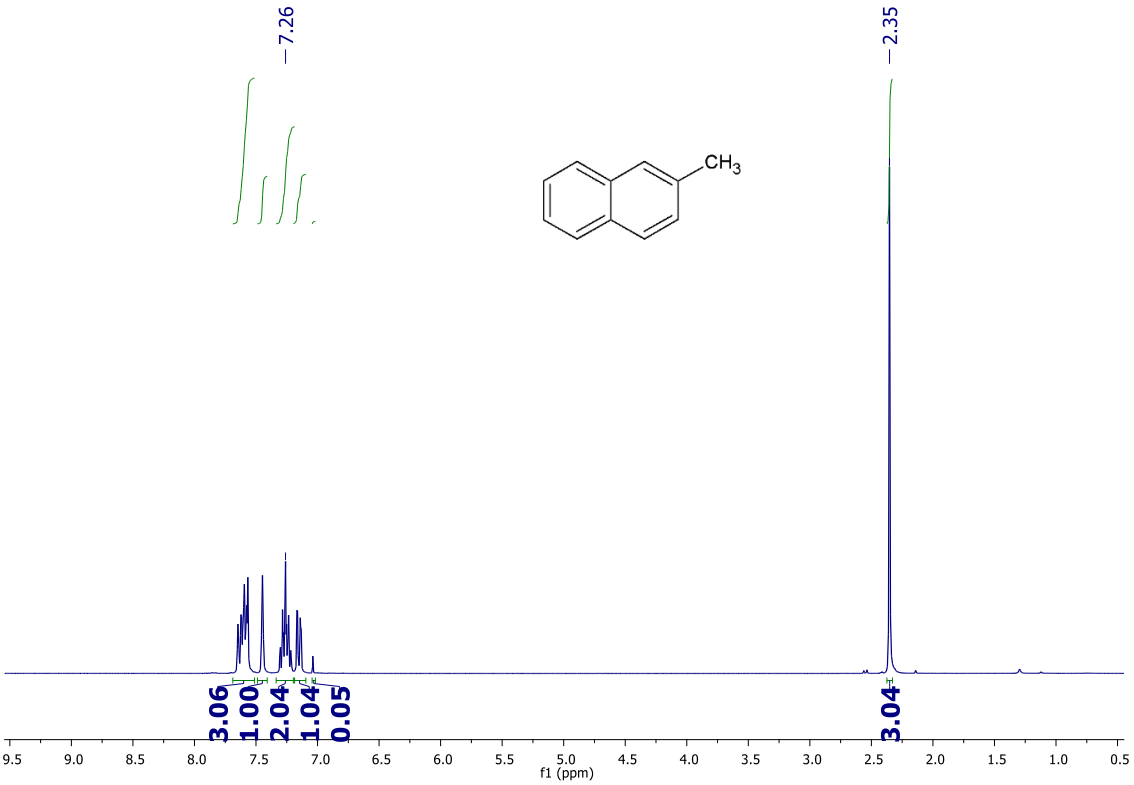

Figure S6.19. ^{1}H NMR of 2-methylnaphthalene with CH_3 peak at 2.35 ppm.

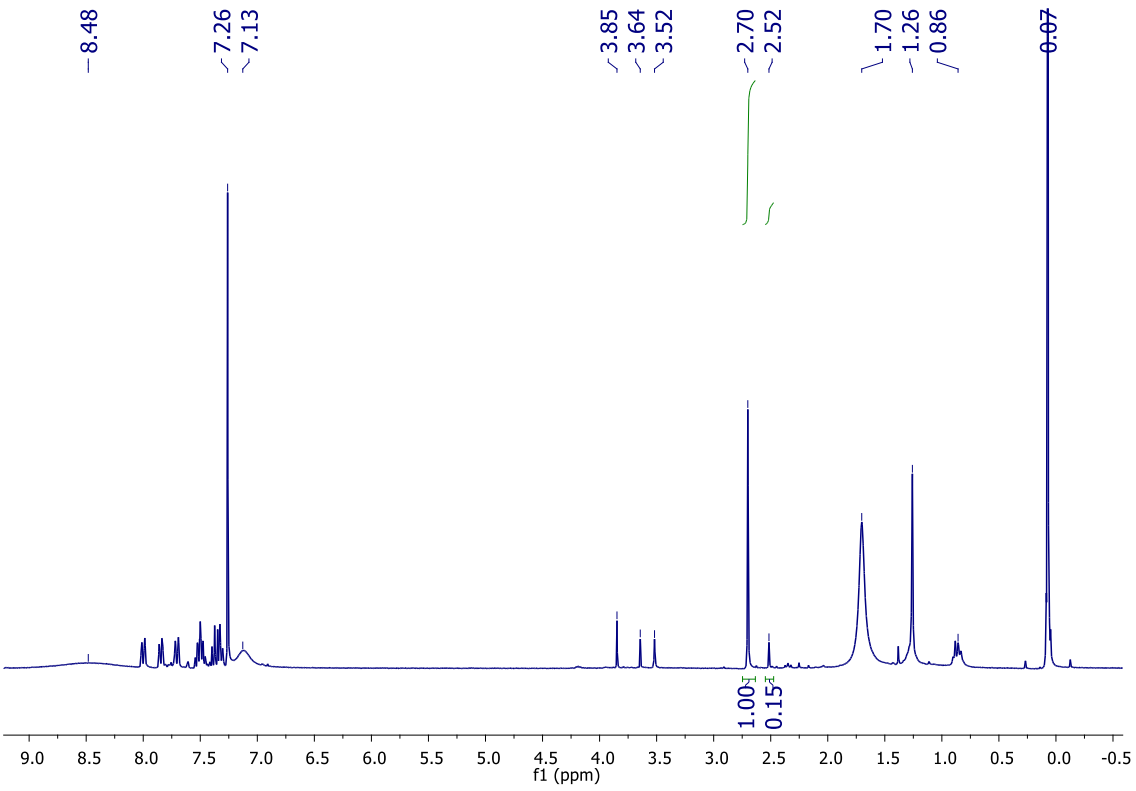

Figure S6.20. ^{1}H NMR from competition experiment after 4 days, final concentration of **1-MN** : **2-MN** = 87 : 13.

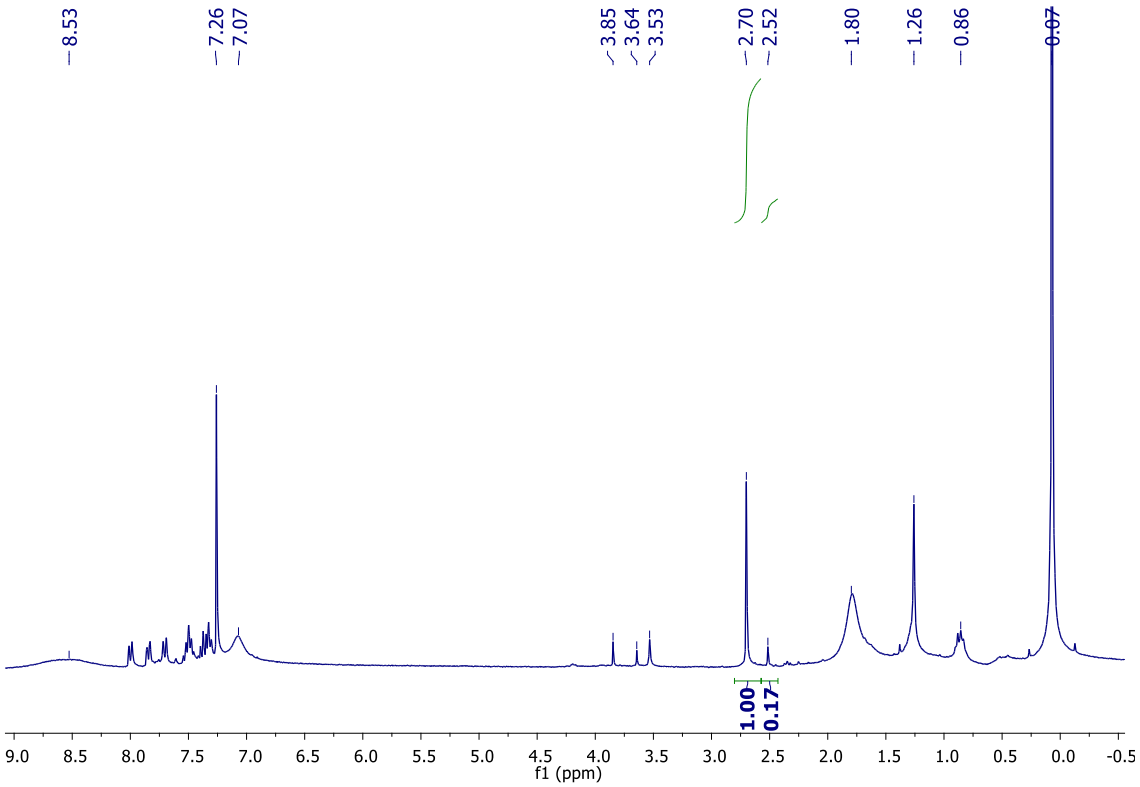

Figure S6.21. ^{1}H NMR from competition experiment after 8 days, final concentration of **1-MN** : **2-MN** = 85 : 15.

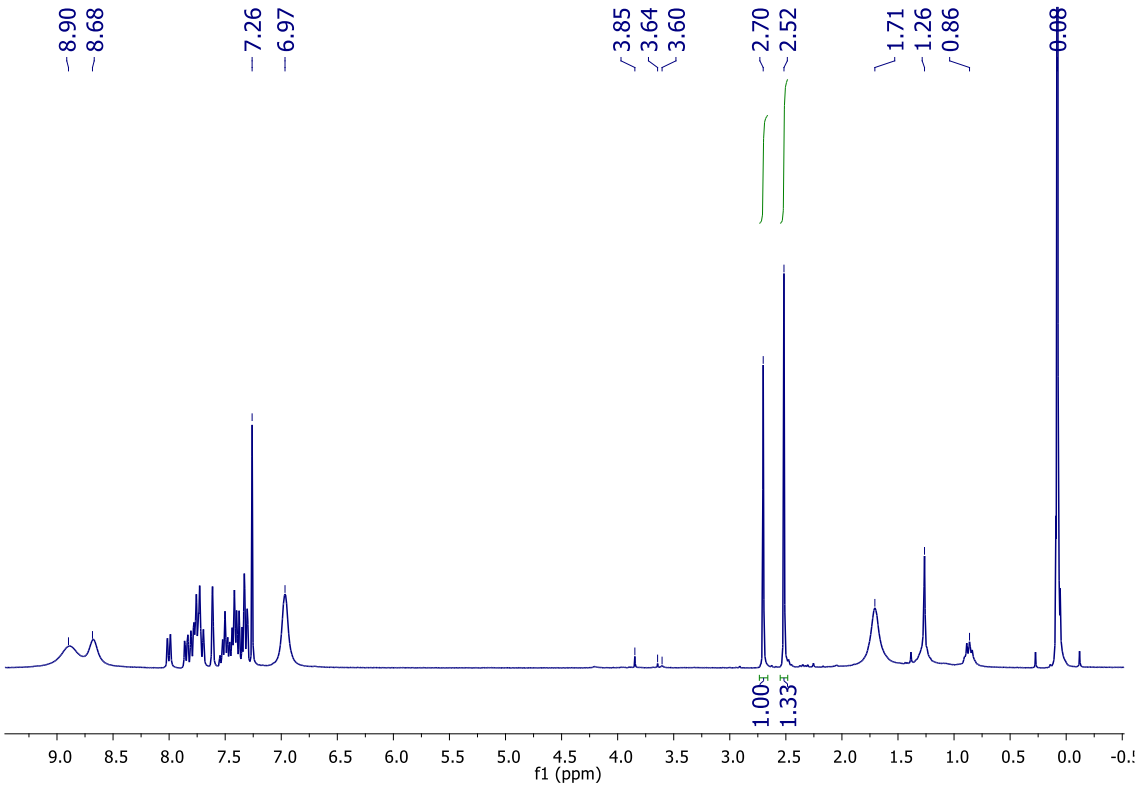

Figure S6.22. ^{1}H NMR from competition experiment after 11 days, final concentration of **1-MN** : **2-MN** = 43 : 57.

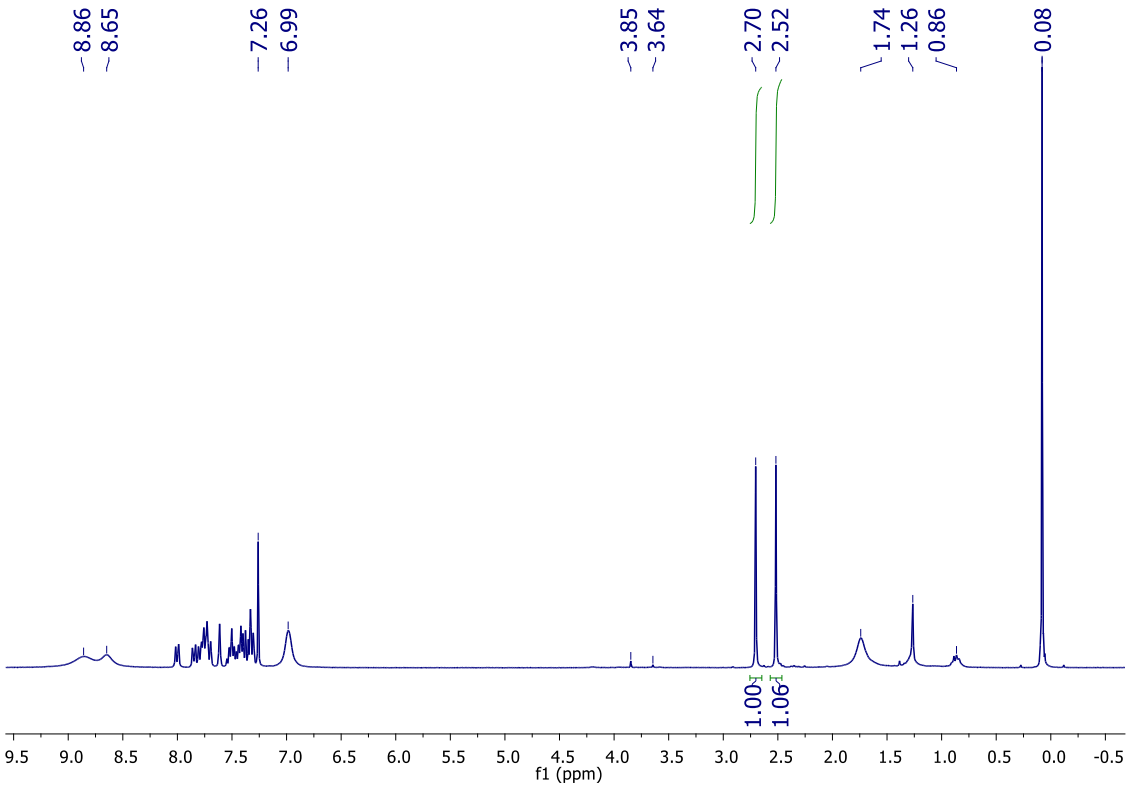

Figure S6.23. ^{1}H NMR from competition experiment after 13 days, final concentration of **1-MN** : **2-MN** = 49 : 51.

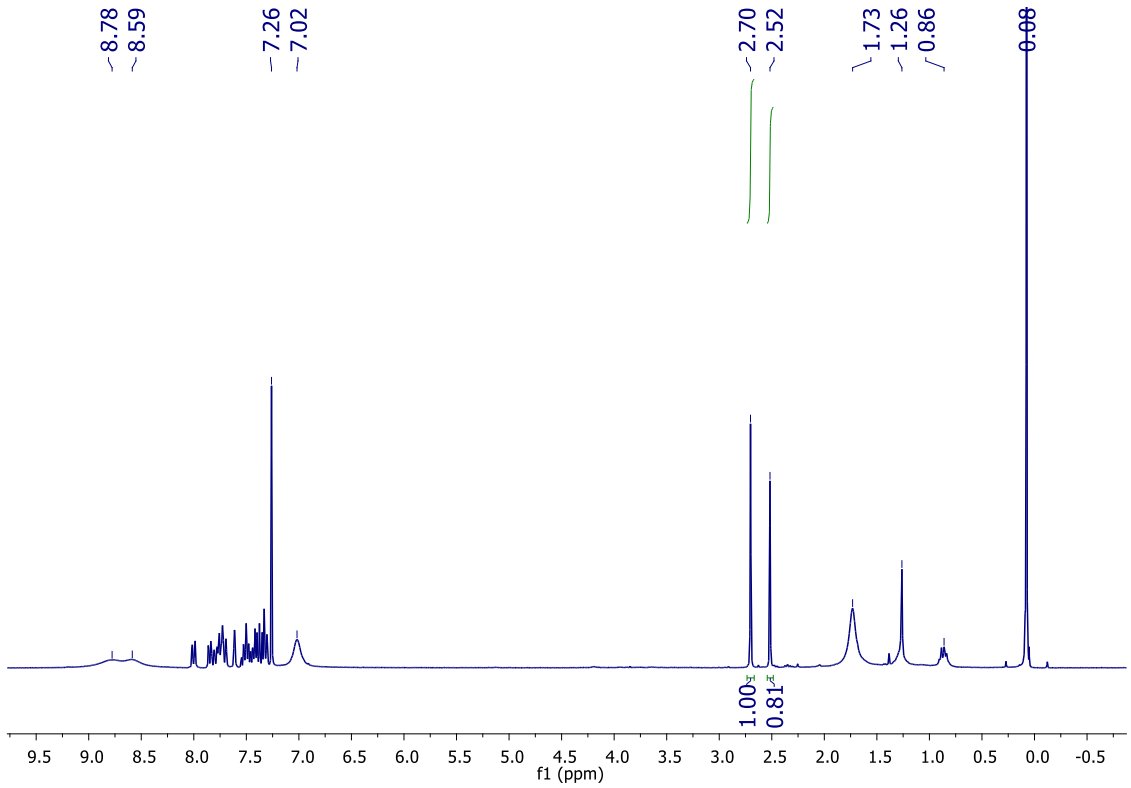

Figure S6.24. ^{1}H NMR from competition experiment after 14 days, final concentration of **1-MN** : **2-MN** = 55 : 45.

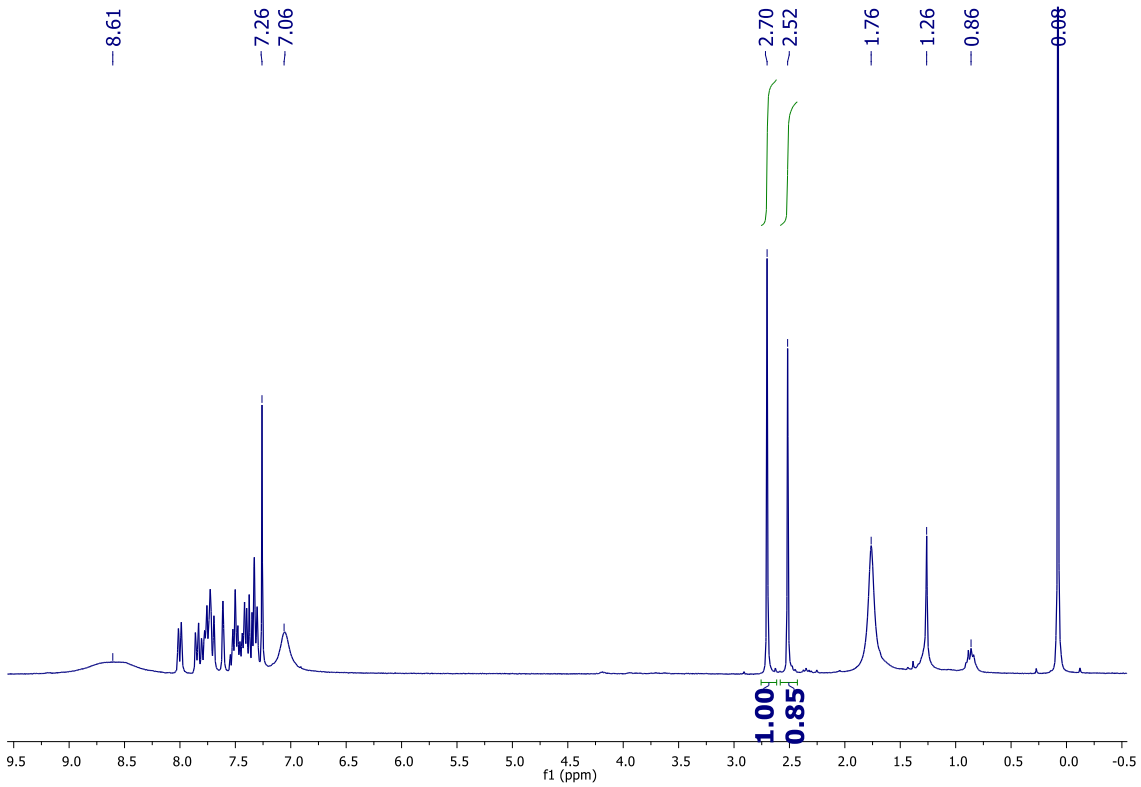

Figure S6.25. ^{1}H NMR from competition experiment after 20 days, final concentration of **1-MN** : **2-MN** = 54 : 46.

Table S6.2: Summary of ^{1}H NMR results

Days after competition experiment initiated	% **1-MN** measured in crystals
4	87
8	85
11	43
13	49
14	55
20	54

6.7.4 Comparison of polymorphs 6.1 and 6.2.

A) Atom-labelled host molecules

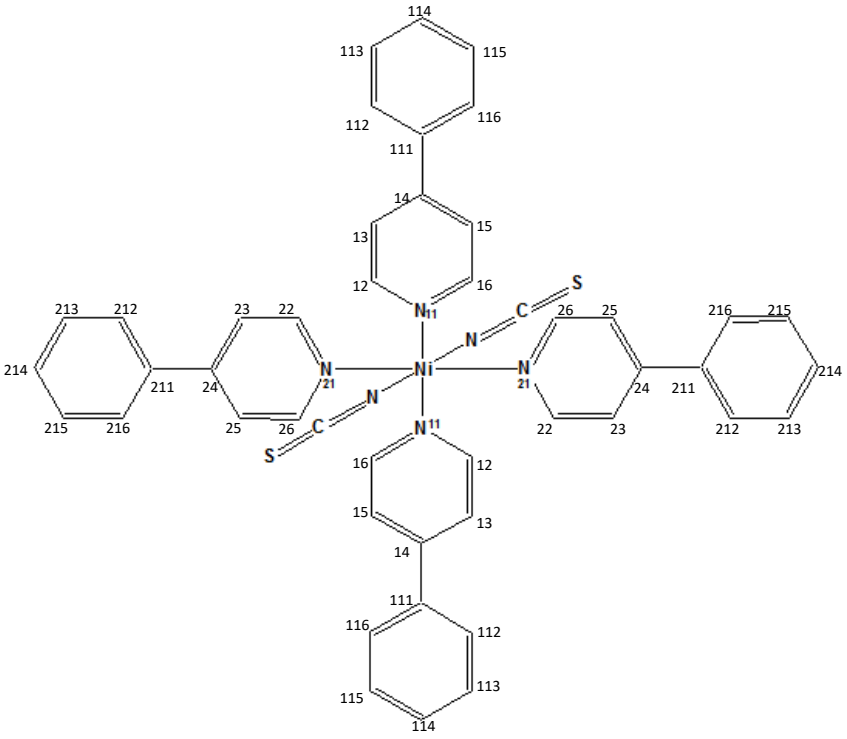

Figure S6.26. Host molecule of structure **6.1** with some atom labels; the Ni ion is located on a centre of inversion.

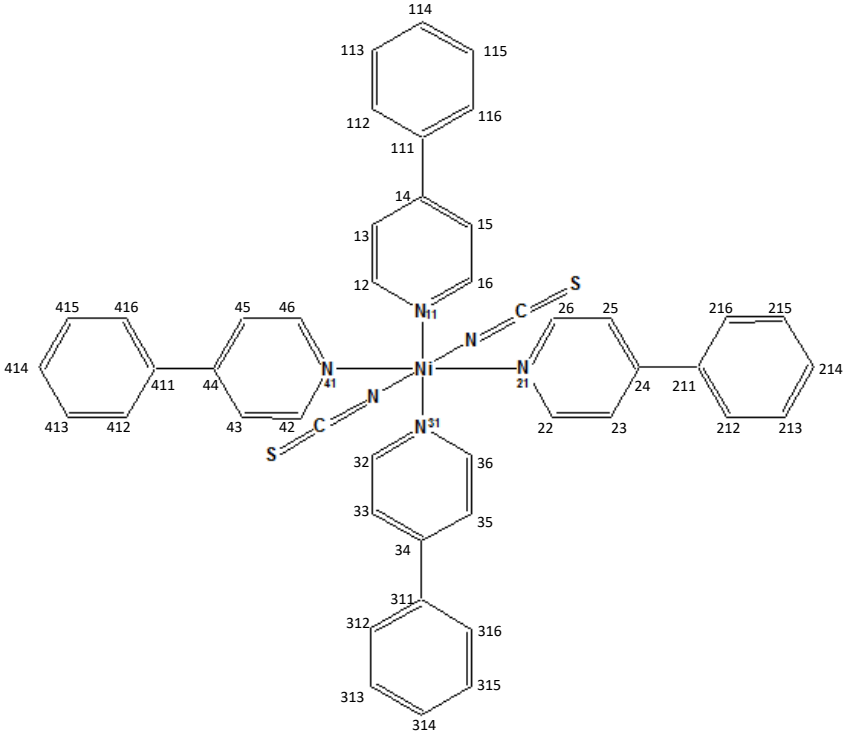

Figure S6.27. Host molecule of structure **6.2** with some atom labels.

B) Overlay of host molecules in structures **6.1** (blue) and **6.2** (purple)

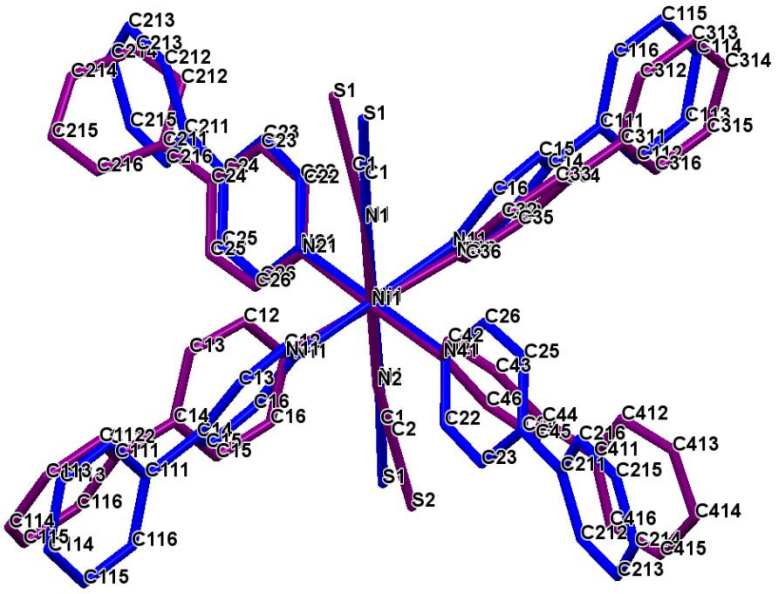

Figure S28. Overlay of structure **6.1** (blue) and structure **6.2** (purple) using Mercury's 'Automatic Molecule Overlay'. The guest molecules were deleted, and the hydrogen atoms are omitted for clarity. Note the labelling for both structures are identical for the N11 and N21 ligands, but is necessarily different for N31 in **6.2**, corresponding to N11[a] in **6.1**, and N41 in **6.2** - corresponding to N21[a] in **6.1**, where [a] is 1-x, 2-y, 1-z and refers to the symmetry generated atoms of the apohost in **6.1**.

C) **Table S6.3**: Relevant bond lengths for structures **6.1** and **6.2**

Structure 6.1		**Structure 6.2**	
Atom labels	Distance (Å)	Distance (Å)	Atom labels
Ni1-N1	2.050(2)	2.055(2)	Ni1-N1
Ni1-N1[a]	2.050(2)	2.051(2)	Ni1-N2
Ni1- N11	2.156(2)	2.152(2)	Ni1- N11
Ni1-N21	2.159(2)	2.122(2)	Ni1-N21
Ni1-N11[a]	2.156(2)	2.124(2)	Ni1-N31
Ni1-N21[a]	2.160(2)	2.130(2)	Ni1-N41

[a]1-x, 2-y, 1-z

D) **Table S6.4**: N-Ni-N bond angles for structures **6.1** and **6.2**

6.1		**6.2**	
Atom labels	Angle (°)	Angle (°)	Atom labels
N11 Ni N21	85.4(1)	91.0(1)	N11 Ni N21
N21 Ni N11[a]	94.6(1)	89.3(1)	N21 Ni N31
N11[a] Ni N21[a]	85.4(1)	89.1(1)	N31 Ni N41
N21 [a] Ni N11	94.6(1)	90.6(1)	N41 Ni N11
N1 Ni N11	89.9(1)	90.5(1)	N1 Ni N11
N1 Ni N21	90.0(1)	89.1(1)	N1 Ni N21
N1 Ni N11[a]	90.2(1)	89.0(1)	N1 Ni N31
N1 Ni N21[a]	90.0(1)	90.7(1)	N1 Ni N41
N1[a] Ni N11	90.2(1)	90.8(1)	N2 Ni N11
N1[a] Ni N21	90.0(1)	89.3(1)	N2 Ni N21
N1[a] Ni N11[a]	89.9(1)	89.7(1)	N2 Ni N31
N1[a] Ni N21[a]	90.0(1)	90.8(1)	N2 Ni N41

[a]1-x, 2-y, 1-z

E) **Table S6.5**: torsion angles T1–T8 for structures **6.1** and **6.2**

	Structure 6.1		**Structure 6.2**	
Torsion	Atom labels	Angle (°)	Angle (°)	Atom labels
T1	N1-Ni1-N11-C12	-28.2(1)	13.6(2)	N1-Ni1-N11-C12
T2	C13-C14-C111-C112	35.7(4)	-36.1(5)	C13-C14-C111-C112
T3	N1-Ni1-N21-C22	33.5(1)	35.7(2)	N1-Ni1-N21-C22
T4	C23-C24-C211-C212	-24.9(1)	29.8(5)	C23-C24-C211-C212
T5	N1[a] -Ni1-N11[a] -C12[a]	28.2(1)	35.8(2)	N2-Ni1-N31-C36
T6	C13[a] -C14[a] -C111[a] -C112[a]	-35.7(4)	-36.0(5)	C35-C34-C311-C316
T7	N1[a] -Ni1-N21[a] -C22[a]	-33.5(1)	22.1(2)	N2-Ni1-N41-C46
T8	C23[a] -C24[a] -C211[a] -C216[a]	24.9(1)	-38.4(5)	C45-C44-C411-C416

[a]1-x, 2-y, 1-z

Figure **S6.29**. Comparison of torsion angles T1-T8 of **6.1** (blue) and **6.2** (purple)

F) 2D fingerprint plots of Hirshfeld surfaces of structures **6.1** and **6.2**

In each case the host molecule was selected as the target and the Hirshfeld surface[E1] generated about the molecule.
Relevant Bondi[E2] van der Waals radii: H: 1.20 Å, C: 1.70 Å, S: 1.80 Å

References
E1 CrystalExplorer (Version 17.5), S. K. Wolff, D. J. Grimwood, J. J. McKinnon, M. J. Turner, D. Jayatilaka, M. A. Spackman, University of Western Australia, 2012
E2 A. Bondi, van der Waals Volumes and Radii, *J. Phys. Chem.*, 1964, **68**, 441–451

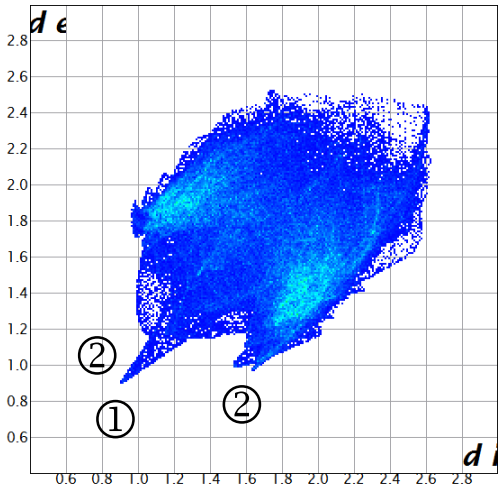

Figure S6.30. Fingerprint plot of structure I. The spike labelled (1) indicates close H···H contacts and the wings labelled (2) indicate S···H and C···H interactions.

Table S6.6. Close contacts (less than the sum of the van der Waals radii less 5%) to the host in structure I. Note that the Ni atom of the host lies on a centre of inversion, so that for each interaction recorded in the table below there is a corresponding interaction.

Atom labels	Distance (Å)	Sum of Bondi van der Waals Radii less 5% (Å)	Host component	Interaction
H116···H6B[a]	2.08	2.09	Phenyl ring 1	Minor guest 1
C116···H1B[b]	2.69	2.76	Phenyl ring 1	Minor guest1
H113···C1C	2.72	2.76	Phenyl ring 1	Minor guest 2
H114···C5B[c]	2.72	2.76	Phenyl ring 1	Minor guest 1
C212···H1C[c]	2.72	2.76	Phenyl ring 2	Minor guest 2
S1···H15[d]	2.81	2.85	NCS	Host pyridyl ring 1
H15···S1[d]	2.81	2.85	Pyridyl ring 1	NCS
S1···H11A[a]	2.75	2.85	NCS	Major guest 1

[a] 1+x, y, z
[b] 1+x, 1.5-y, z-0.5
[c] 1-x, 1-y, 1-z
[d] 2-x, 2-y, 1-z

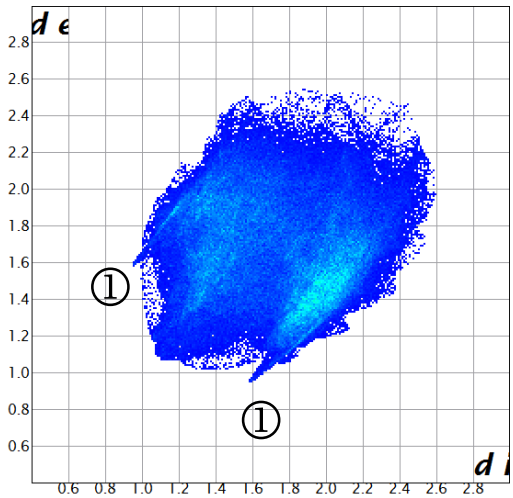

Figure S6.31. Fingerprint plot of structure **6.2**. The wings labelled (1) refer to close S···H and C···H contacts

Table S6.7. Close contacts (less than the sum of the van der Waals radii less 5%) to the host in structure **6.2**

Atom labels	Distance (Å)	Sum of Bondi van der Waals Radii less 5% (Å)	Host component	Interaction
C112···H3E[a]	2.71	2.76	Phenyl ring 1	Minor guest 3
S1···H412[b]	2.66	2.85	NCS	Host phenyl ring 4
H412···S1[b]	2.66	2.85	Phenyl ring 4	NCS

[a] x, 1+y, z

[b] 1-x, 2-y, -z

6.7.5 Comparison of structures 6.3 and 6.6.

A) Overlay of host molecule in structures **6.3** (orange) and **6.6** (green).

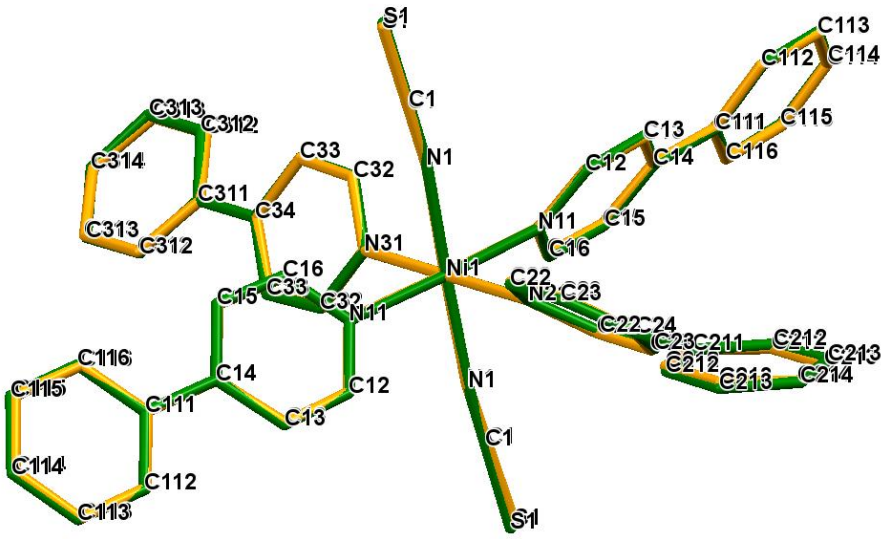

Figure S6.32. Overlay of host molecule in **6.3** (orange) and **6.6** (green) using Mercury's 'Automatic Molecule Overlay'. The guest molecules were deleted, and the hydrogen atoms are omitted for clarity.

B) Packing diagrams of structures **6.3** and **6.6**

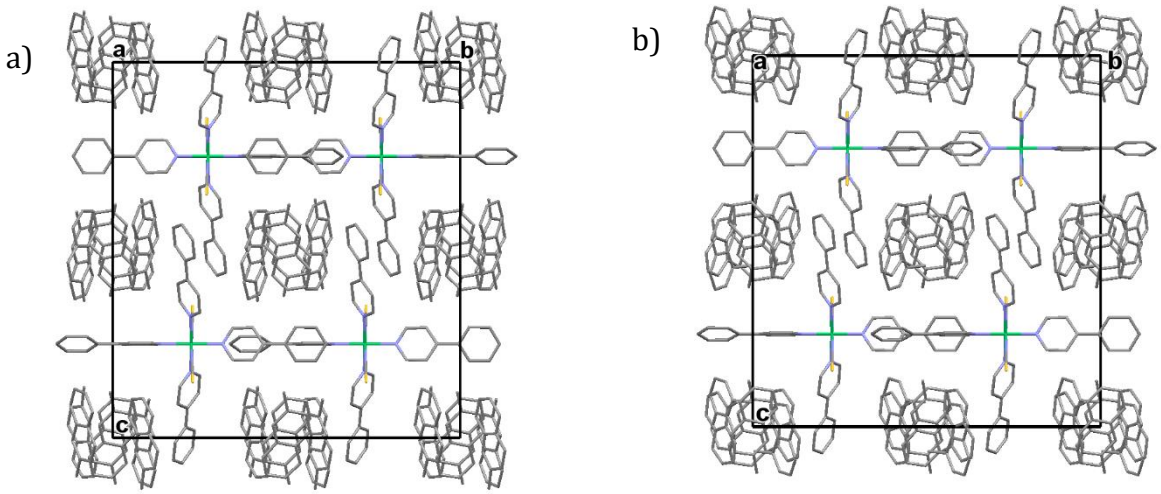

Figure S6.33. packing of a) structure **6.3** and b) structure **6.6**. Hydrogen atoms have been omitted for clarity.

C) Comparison of calculated PXRD traces of **6.3** and **6.6**

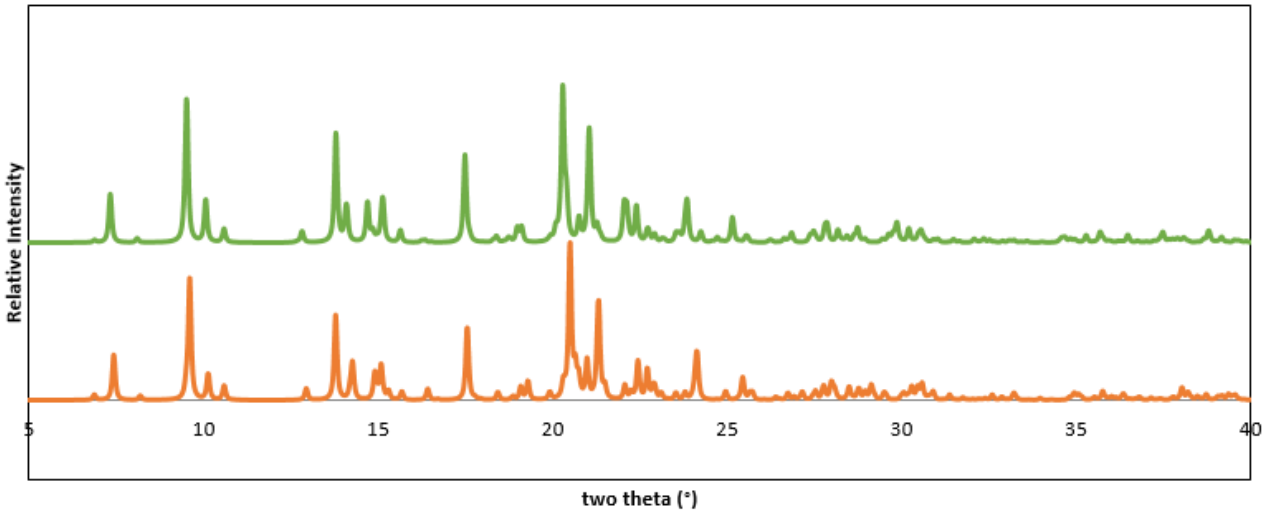

Figure S6.34. Calculated PXRD traces of structure **6.3** (orange) and **6.6** (green).

D) **Table S6.8**: torsion angles T1-T8 for structure **6.3** and **6.6**

	Structure 6.3		**Structure 6.6**	
Torsion	Atom labels	Angle (°)	Angle (°)	Atom labels
T1	N1-Ni1-N11-C12	39.30	38.27	N1-Ni1-N11-C12
T2	C13-C14-C111-C112	-3.58	-2.16	C13-C14-C111-C112
T3	N1-Ni1-N21-C22	45.30	46.59	N1-Ni1-N21-C22
T4	C23-C24-C211-C212	30.34	32.10	C23-C24-C211-C212
T5	N1-Ni1-N11-C12	39.30	38.27	N1-Ni1-N11-C12
T6	C13-C14-C111-C112	-3.58	-2.16	C13-C14-C111-C112
T7	N1-Ni1-N31-C32	29.96	31.13	N1-Ni1-N31-C32
T8	C33-C34-C311-C312	22.43	17.32	C33-C34-C311-C312

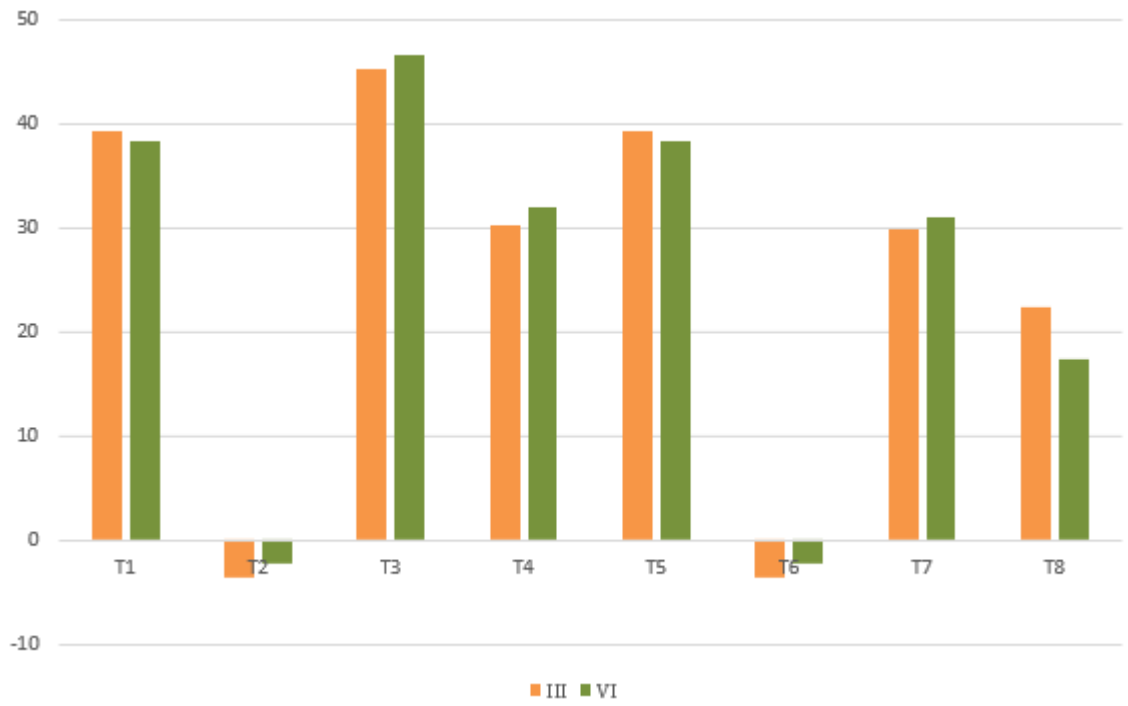

Figure S6.35. Comparison of torsion angles T1-T8 of **6.3** (orange) and **6.6** (green), showing that torsion angles for **6.3** and **6.6** are very similar.

6.7.6 Structure 6.5: H•2(1-MN)•1(MeOH).

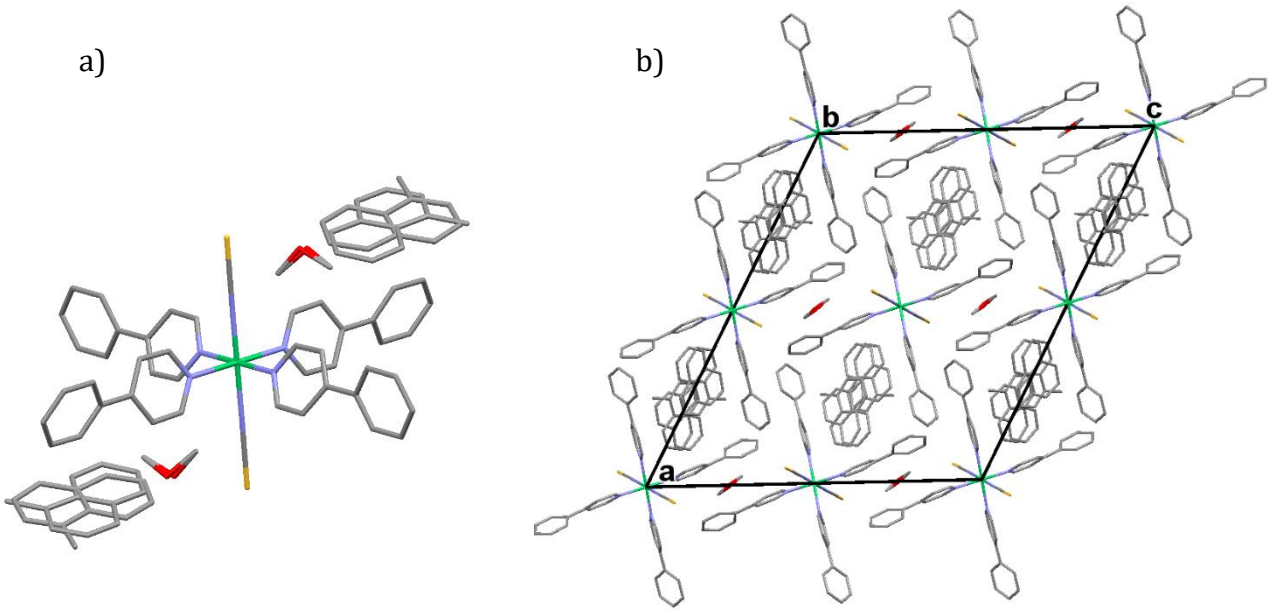

Figure S6.36. a) Asymmetric unit of structure **6.5** grown to show the full host, two disordered naphthalene guest molecules and one disordered methanol molecule (located about the diad), and b) packing diagram of structure **6.5**, the naphthalene molecules are in channels parallel to [010]. Hydrogen atoms have been removed for clarity.

7.7.1 Channels in H•2(DMSO) structure.

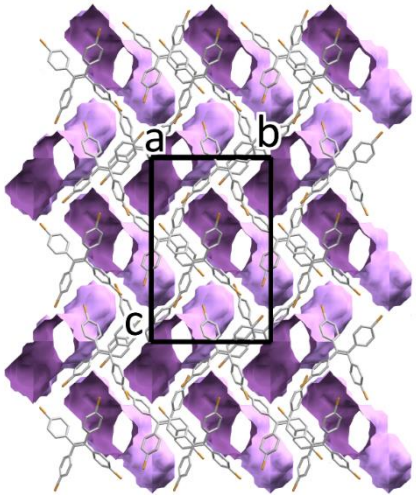

Figure S7.1. Void spaces of **H•2(DMSO)** structure viewed down [100] shows jagged channels running along this direction.

7.7.2 Torsion angles of Host in inclusion compounds.

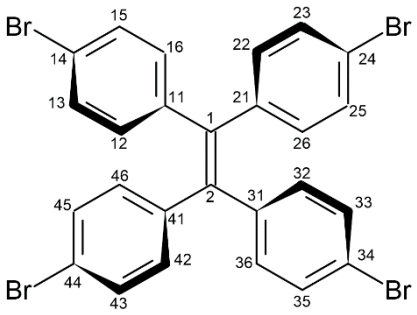

Figure S7.2. The host (H) tetrakis(*p*-bromophenyl)ethylene (left) takes on a propeller conformation, similar to the blades of a European post mill[F1] (right).

WinGX[F2] and Platon[F3 – F6] were used to calculate torsion angles. The symmetry operator labelled "a" corresponds to 1 – x, y, ½ – z.

Table S7.1. Torsion angles of host molecules in inclusion compounds

H•DIOX 1		**H•DIOX 2**	
Atom labels	Angle (°)	Angle (°)	Atom labels
C1-C2-C11-C12	46.8(5)	41.0(3)	C1[a] -C1-C11-C12
C1-C2-C21-C22	46.8(6)	53.4(3)	C1[a] -C1-C21-C22
C2-C1-C31-C32	51.2(6)	41.0(3)	C1-C1[a] -C11[a] -C12[a]
C2-C1-C41-C42	52.3(6)	53.4(3)	C1-C1[a] -C21[a] -C21[a]

H•PENT		**H•CYNO**	
Atom labels	Angle (°)	Angle (°)	Atom labels
C1A-C2A-C11A-C12A	55.3(7)	43.5(2)	C1[a] -C1-C11-C12
C1A-C2A-C21A-C22A	55.2(7)	50.7(2)	C1[a] -C1-C21-C22
C2A-C1A-C31A-C32A	50.0(7)	43.5(2)	C1-C1[a] -C11[a] -C12[a]
C2A-C1A-C41A-C42A	43.8(7)	50.7(2)	C1-C1[a] -C21[a] -C21[a]
C1B-C2B-C11B-C12B	61.8(7)		
C1B-C2B-C21B-C22B	56.2(7)		
C2B-C1B-C31B-C32B	51.7(7)		
C2B-C1B-C21B-C22B	47.2(8)		

H•2(DMSO)		**H•2(ACE)** (XALBUH)[F11]	
Atom labels	Angle (°)	Angle (°)	Atom labels
C1-C2-C11-C12	47.4	45.1	C1-C2-C3-C8
C1-C2-C21-C22	46.9	52.1	C1-C2-C9-C10
C2-C1-C31-C32	47.7	46.5	C2-C1-C21-C26
C2-C1-C41-C42	54.6	55.8	C2-C1-C15-C16

H•2(THF) (XALCAO)[F11]	
Angle (°)	Atom labels
50.5	C1-C2-C3-C4
44.1	C1-C2-C9-C10
46.3	C2-C1-C21-C26
62.5	C2-C1-C15-C16

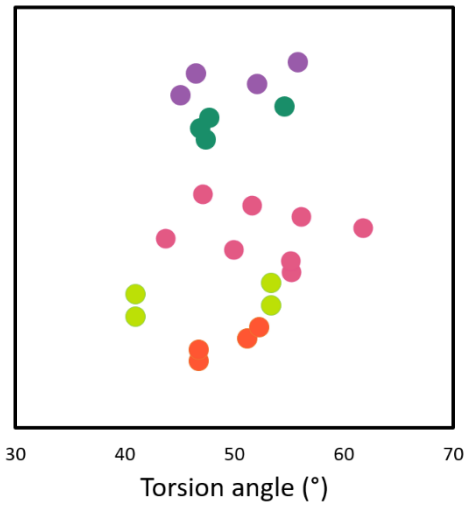

Figure S7.3. Narrow range of torsion angles of the host in inclusion compounds. Orange (**H•DIOX 1**), light green (**H•DIOX 2**), pink (**H•PENT**), dark green (**CYNO**)**,** purple (**DMSO**)**.**

7.7.3 DSC comparison between H•DIOX 1 and H•DIOX 2.

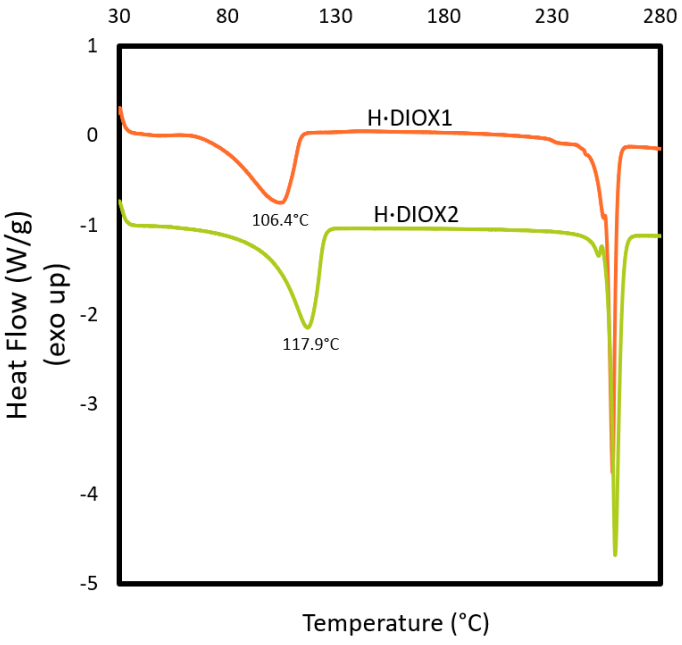

Figure S7.4. Comparison of DSC traces of **H•DIOX 1** (orange) and **H•DIOX 2** (green), recorded at a heating rate of 20 °C/min. Endothermic peaks due to dioxane desorption occur at 106 °C for **H•DIOX 1** and 118°C for **H•DIOX 2**. The endotherms at 258 °C are due to the host melting.

7.7.4 Br···Br contacts in Inclusion compounds.

We used the Bondi[F7] van der Waals radii (Br = 1.85 Å) to record Br···Br distances less than the sum of the vDW radii +1% (3.788 Å) for interactions of type I, IIa and IIb (see scheme S7.1). We note that in most cases the angles θ1/θ2 for type II interactions deviated from the ideal values of 90°/180°.

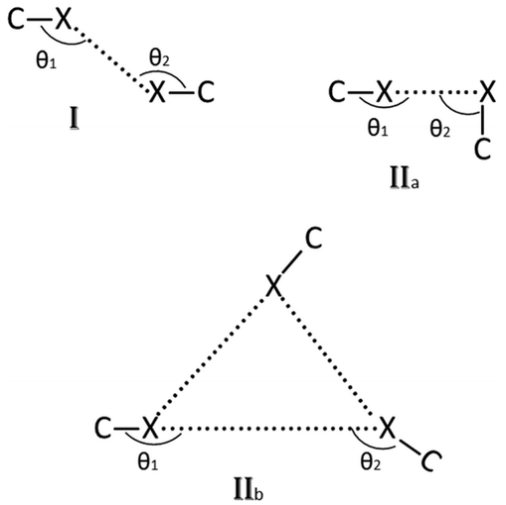

Scheme S7.1. Type I interactions are of the van der Waals type. Type II_a and II_b interactions are mainly electrostatic and considered attractive. [F8 – F10]

Table S7.2. Br ···Br contacts in inclusion compounds

H•PENT (2 hosts in ASU)

Br	Br	Distance (Å)	θ_1°/θ_2°	Type
2A	4A[j]	3.595(1)	164/164	I trans
4A	2A[l]	3.595(1)	164/164	I trans
3A	2B[k]	3.723(1)	119/148	II a
2B	3A[n]	3.723(1)	119/148	II a
2A	1B	3.724(1)	69/167	II a
1B	2A	3.724(1)	69/167	II a
4A	3B[k]	3.736(1)	91/166	II a
3B	4A[n]	3.736(1)	91/166	II a
2B	4B[l]	3.788(1)	150/152	I trans
4B	2B	3.788(1)	150/152	I trans

H•2(DMSO)

Br	Br	Distance (Å)	θ_1°/θ_2°	Type
1	2	3.785	113/129	II b
2	1	3.785	113/129	II b

H•DIOX 1

Br	Br	Distance (Å)	$\theta_1°/\theta_2°$	Type
1	3[b]	3.677(1)	143/145	I trans
3	1[e]	3.677(1)	143/145	I trans
1	4[c]	3.691(1)	109/142	I cis
4	1[d]	3.691(1)	109/142	I cis

H•DIOX 2

Br	Br	Distance (Å)	$\theta_1°/\theta_2°$	Type
1	1[f]	3.487(1)	151/151	I trans
1[a]	1[g]	3.487(1)	151/151	I trans

H•CYNO

Br	Br	Distance (Å)	$\theta_1°/\theta_2°$	Type
1	1[a]	3.541(1)	154/154	I trans
1[a]	1[g]	3.541(1)	154/154	I trans
2[a]	1[i]	3.768(1)	76/158	II a
1	2[h]	3.768(1)	76/158	II a
2	1[h]	3.768(1)	76/158	II a
1[a]	2[i]	3.768(1)	76/158	II a

Table S7.3. Table of symmetry operators

label	Symmetry operator	Symmetry operator	label
a	1 – x, y, ½ – z	³⁄₂ – x, ½ – y, 1 – z	h
b	x, y – 1, z	x – ½, ½ – y, z – ½	i
c	1 – x, y – ½, ³⁄₂ – z	x – 1, y, z	j
d	1 – x, ½ + y, ³⁄₂ – z	1 – x, y – ½, 1 – z	k
e	x, 1 + y, z	1 + x, y, z	l
f	1 – x, y, ³⁄₂ – z	x, y, 1 + z	m
g	x, y, z – 1	1 – x, ½ + y,1 – z	n

7.7.5 Void spaces of dioxane polymorphs.

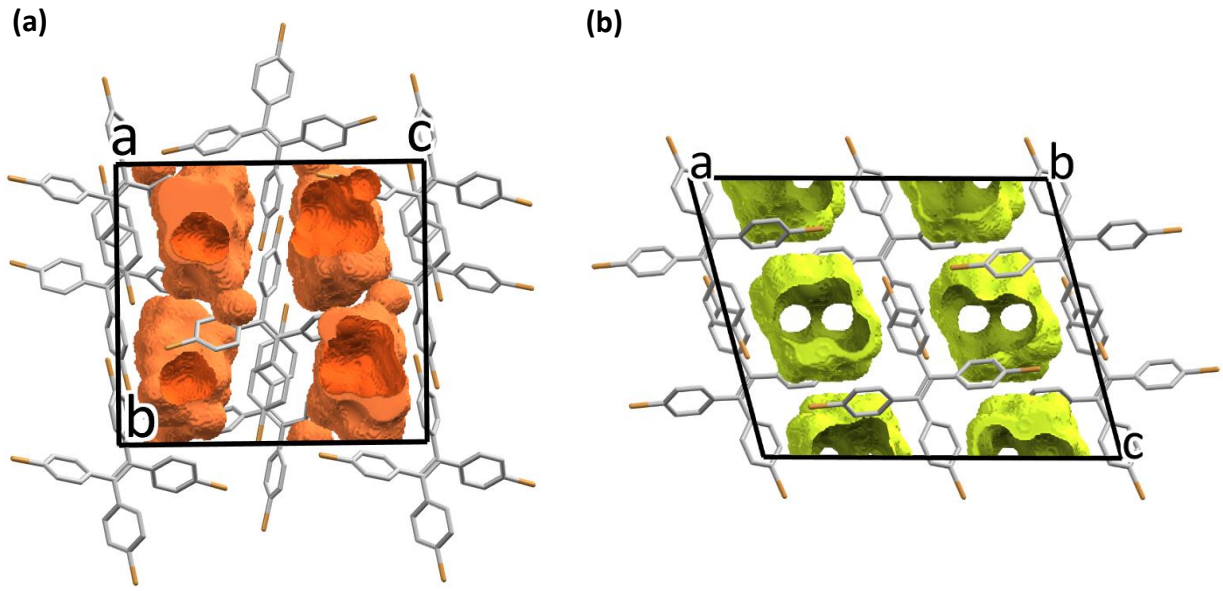

Figure S7.5. Void spaces displayed of a) **H•DIOX 1** and b) **H•DIOX2** using the Mercury settings of: probe radius = 1 Å and grid spacing = 0.1 Å.

7.7.6 Hirshfeld fingerprint plots of H•DIOX 2 major and minor guest components

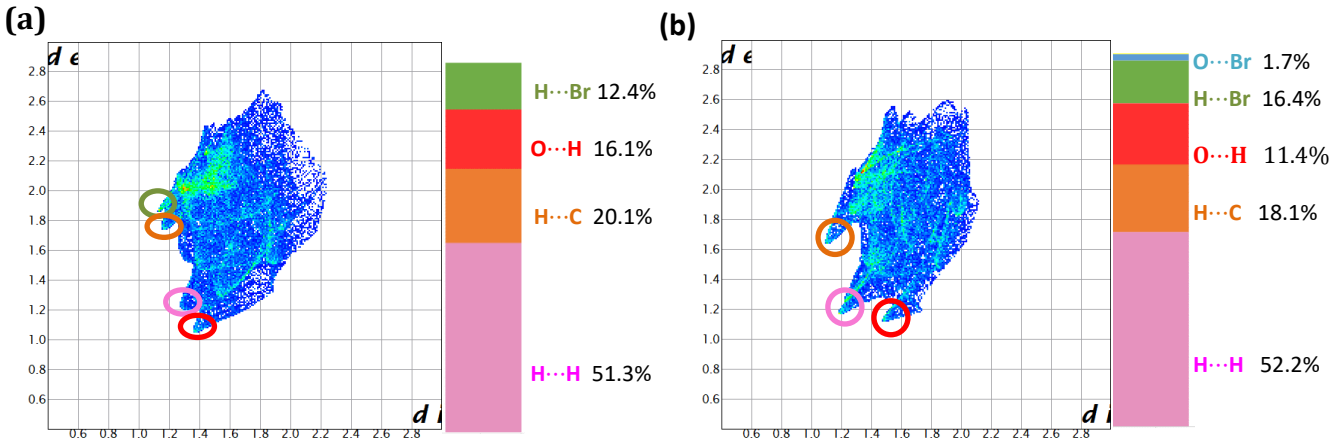

Figure S7.6. Hirshfeld fingerprint plots with dioxane selected as target in (a) **H•DIOX 2** major component (63%) and (b) **H•DIOX 2** minor component (37%). Circled are spikes due to short O···H (red), H···H (pink), H···C (orange), and H···Br (green) interactions. The adjoining bar graphs display the percentage breakdown of the types of non-bonded interactions.

7.7.7 Thermal data and PXRD traces for:

(a) H•CYNO.

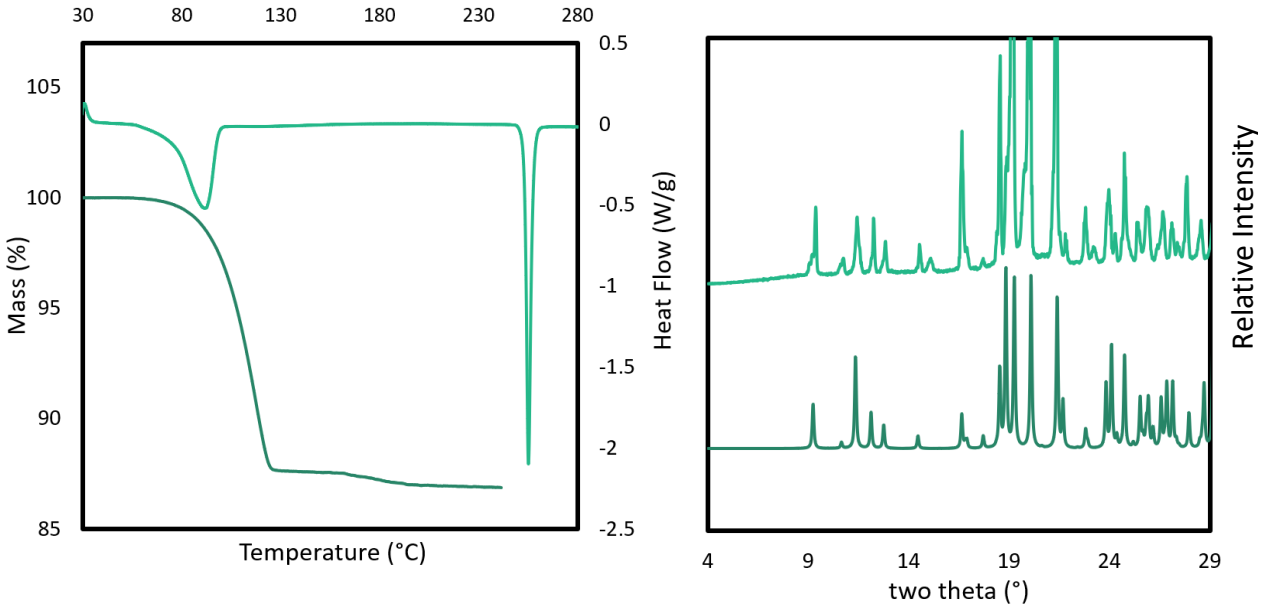

Figure S7.7. **H•CYNO** a) TGA and DSC trace recorded at 20 °C /min, and b) Calculated (bottom) and experimental (top) PXRD traces.

(b) H•PENT.

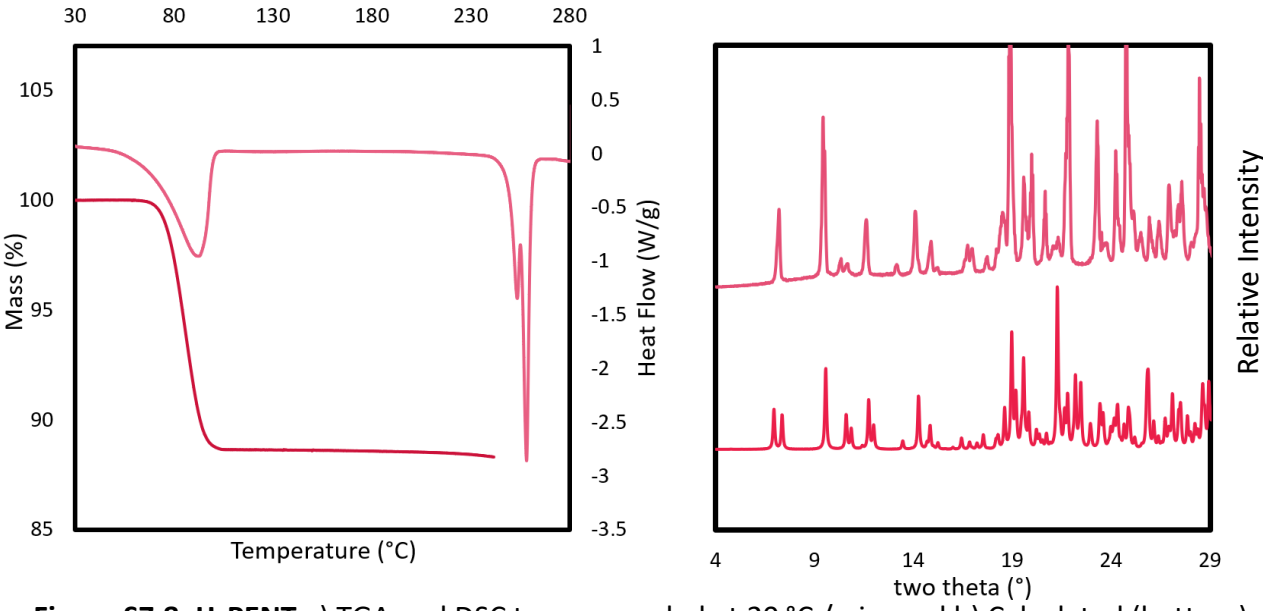

Figure S7.8. H•PENT a) TGA and DSC trace recorded at 20 °C /min, and b) Calculated (bottom) and experimental (top) PXRD traces.

(c) H•2(DMSO).

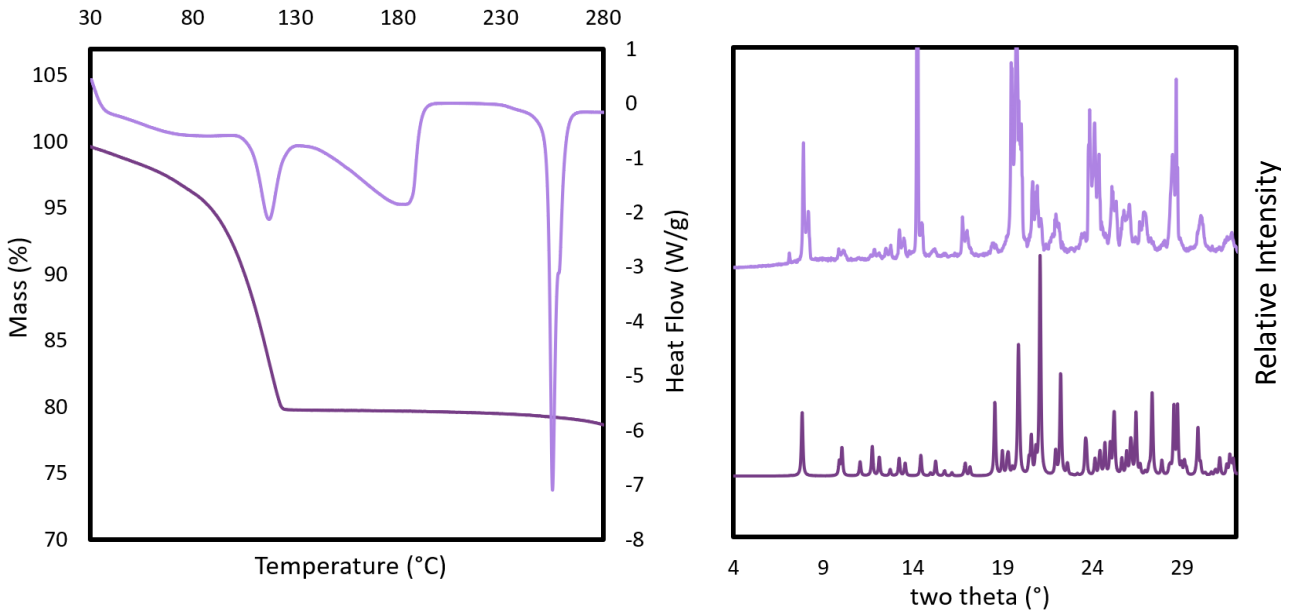

Figure S7.9. **H•2(DMSO)** a) TGA and DSC trace recorded at 20 °C /min, and b) Calculated (bottom) and experimental (top) PXRD traces.

(d) H•2(ACE).

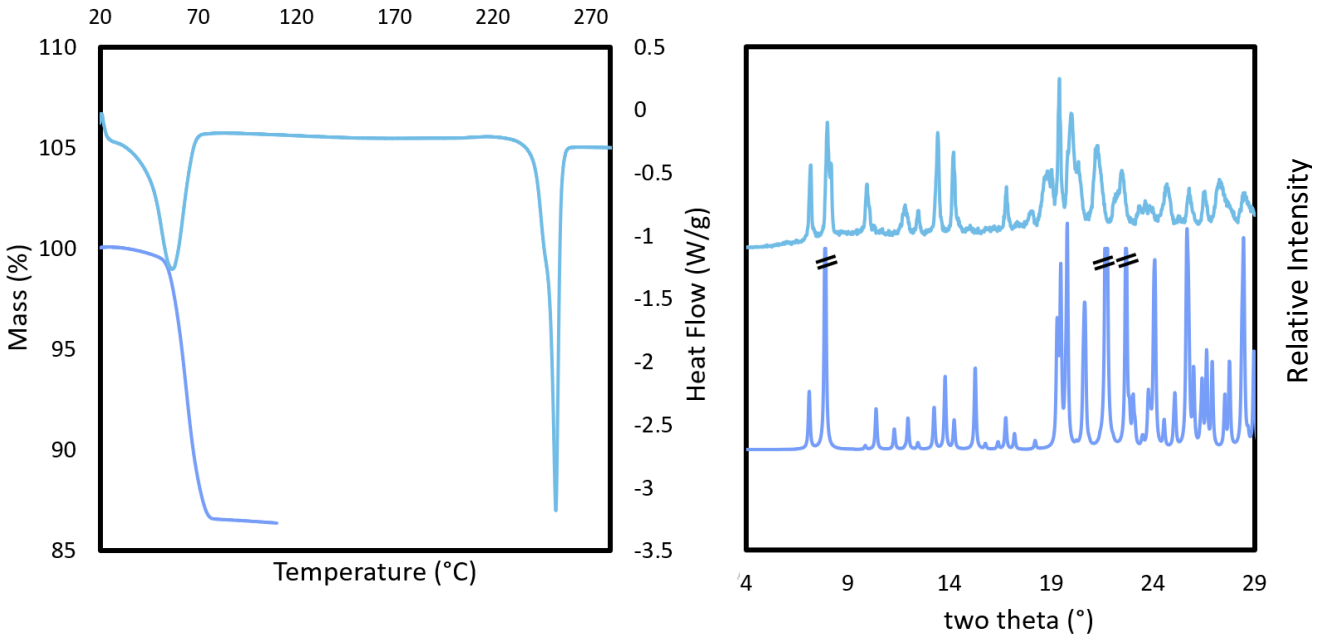

Figure S7.10. **H•2(ACE)** a) TGA and DSC trace recorded at 20 °C /min, and b) Calculated of CIF refcode XALBUH (bottom) and experimental (top) PXRD traces.

7.7.8 Summary of thermal data of relevant inclusion compounds.

Table S7.4. TG and DSC data of relevant inclusion compounds.

Inclusion compound	T_{boil} of guest (°C)	DSC T_{peak} of guest desorption (°C)	DSC T_{peak}-T_{boil} (°C)	DSC T_{peak} of host melt (°C)	TG calculated mass loss (%)	TG experimental mass loss (%)
H•2(DMSO)	189	109, 126 (broad), 161 (broad)	–80	256, 258	20.9	19.4
H•CYNO	156	94	–62	255	13.1	13.2
H•PENT	102	93	–9	256, 258	11.4	11.7
H•2(ACE)	56	57	+1	252	13.6	15.2
H•DIOX 1	101	105	+4	258	11.7	12.0
H•DIOX 2	101	117	+16	259	11.7	12.0

7.7.9 Comparison of calculated PXRD patterns.

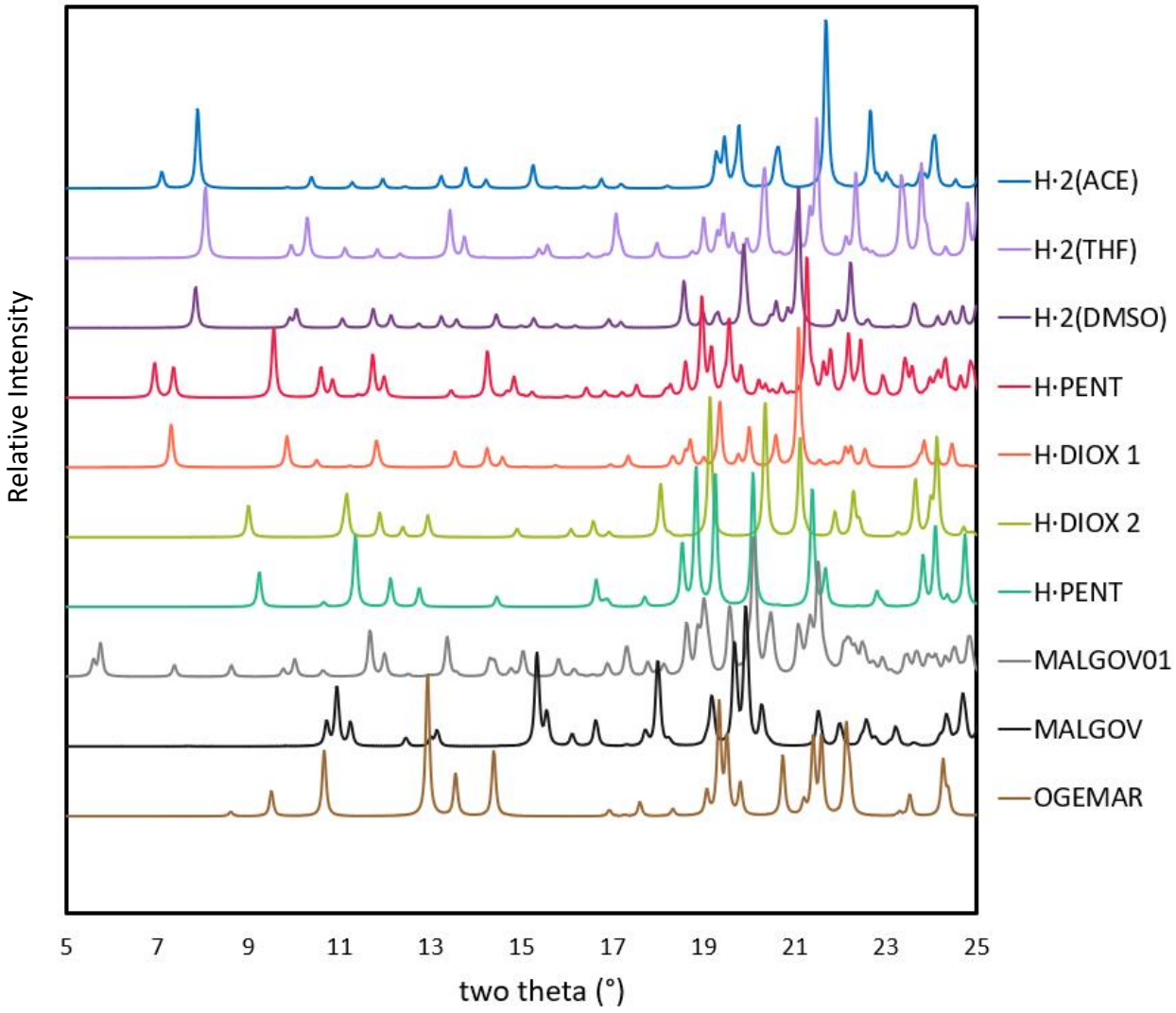

Figure S7.11. Comparison of calculated PXRD traces of relevant inclusion compounds, the two apohost structures (CIF refcode MALGOV[F11] and MALGOV01[F9]) and the starting material tetraphenylethylene (CIF refcode OGEMAR[F12]).

7.7.10 Guest exchange H•CYNO to H•DIOX 2.

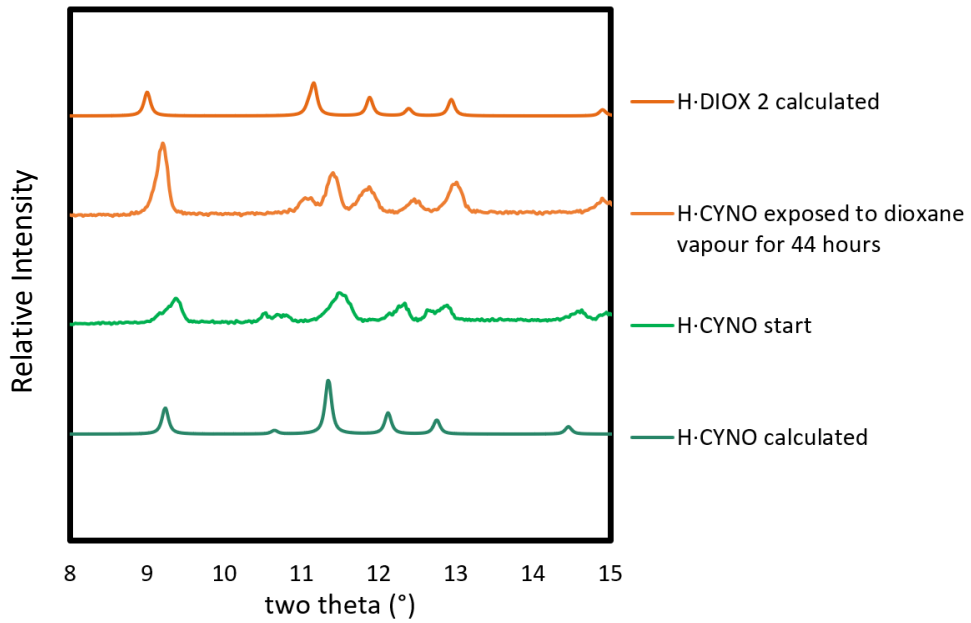

Figure S7.12. **H•CYNO** powder was exposed to dioxane vapour for 44 hours

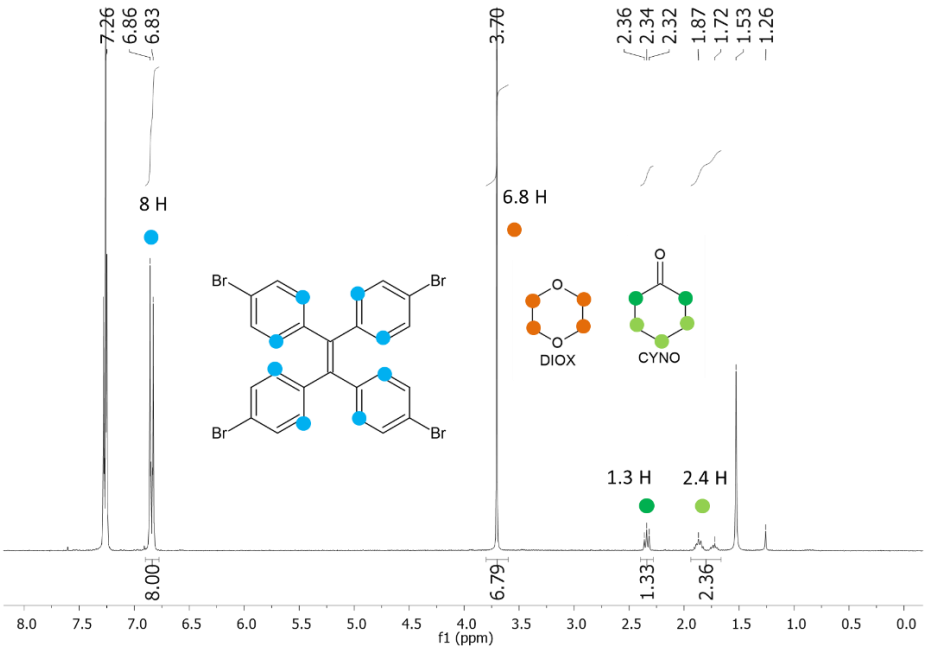

Figure S7.13. **H•CYNO** powder was exposed to DIOX vapour for 44 hours in a two-vial experiment, after which the ^{1}H NMR spectrum of the powder was recorded in $CDCl_3$ (referenced $CHCl_3$ at δ = 7.26 ppm). The doublet at δ = 6.83-6.86 ppm is due to 8 x C-H aromatic host protons and is calibrated to 8, representing one host molecule. The overall ratio of products is 1 host: 0.85 dioxane : 0.36 cyclohexanone.The singlet at δ = 3.70 ppm corresponds to the 4 x CH_2 protons of DIOX, however the peak integrates for 6.8 H - giving 0.85 DIOX molecules per host. Approximately 0.36 molecules of CYNO per host remain: δ = 2.32-2.36 ppm corresponds to 2 x CH_2 protons of CYNO, and integrates for 1.3 H. Similarly, δ = 1.72-1.87 corresponds to 3 x CH_2 protons of CYNO, but integrates for only 2.4 H. The peak at δ = 1.53 ppm is water in the $CDCl_3$, and the singlet at δ = 1.26 ppm is uncertain, but possibly results from greasy rubber caps leaching into solution.

7.7.11 Guest exchange H•PENT to H•DIOX 1.

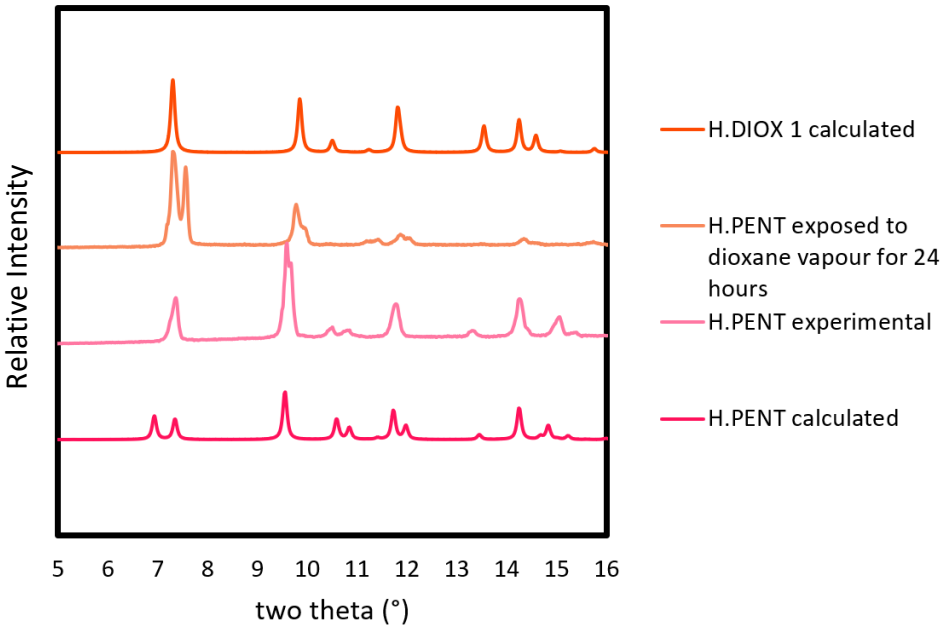

Figure S7.14. **H•PENT** powder was exposed to dioxane vapour for 24 hours in a two-vial experiment.

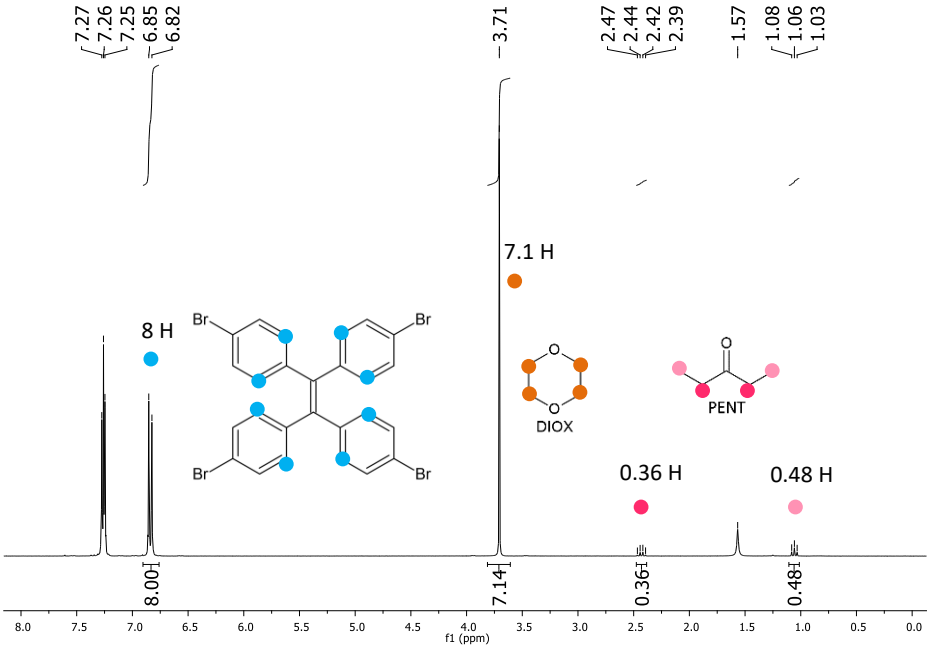

Figure S7.15. **H•PENT** powder was exposed to DIOX vapour for 24 hours in a two-vial experiment, after which the ^{1}H NMR spectrum of the powder was recorded in $CDCl_3$ (referenced $CHCl_3$ at δ = 7.26 ppm). The overall ratio of products is 1 host: 0.89 dioxane : 0.08 3-pentanone.The doublet at δ = 6.82 - 6.85 ppm is due to 8 x C-H aromatic host protons, and is calibrated to 8, representing one host molecule. The singlet at δ = 3.71 ppm corresponds to the 4 x CH_2 protons of DIOX, however the peak integrates for 7.1 - giving 0.89 DIOX molecules per host. Approximately 0.08 PENT molecules per host are still present: δ = 1.03 - 1.08 ppm corresponds to 2 x CH_3 protons and δ = 2.39 - 2.47 ppm corresponds to 2 x CH_2 protons. The peak at δ = 1.57 ppm is water in the $CDCl_3$.

7.7.12 Guest exchange H•2(DMSO) to H•DIOX 1.

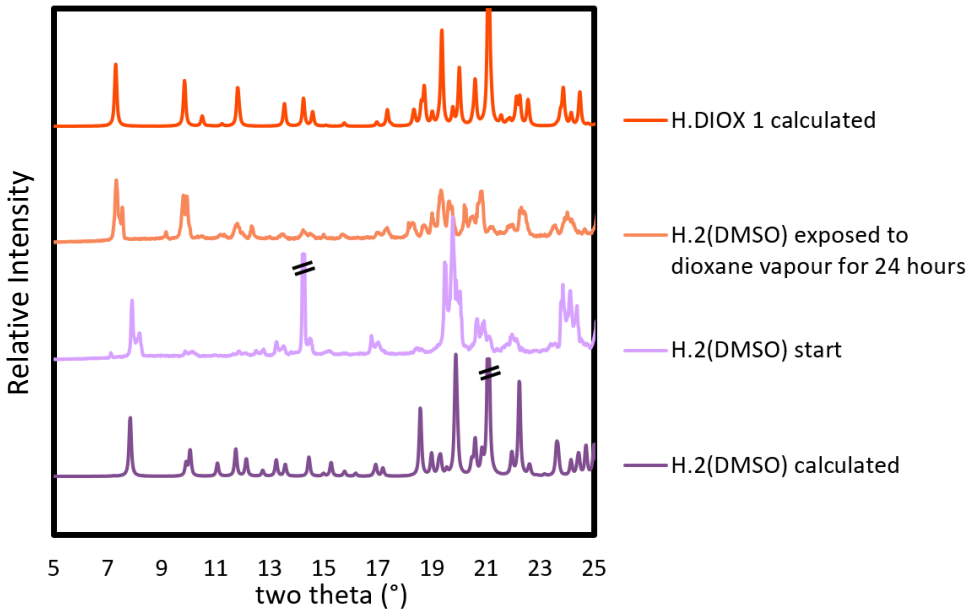

Figure S7.16. **H•2(DMSO)** powder was exposed to dioxane vapour for 24 hours in a two-vial experiment.

7.7.13 Guest exchange MALGOV01 to H•DIOX 1.

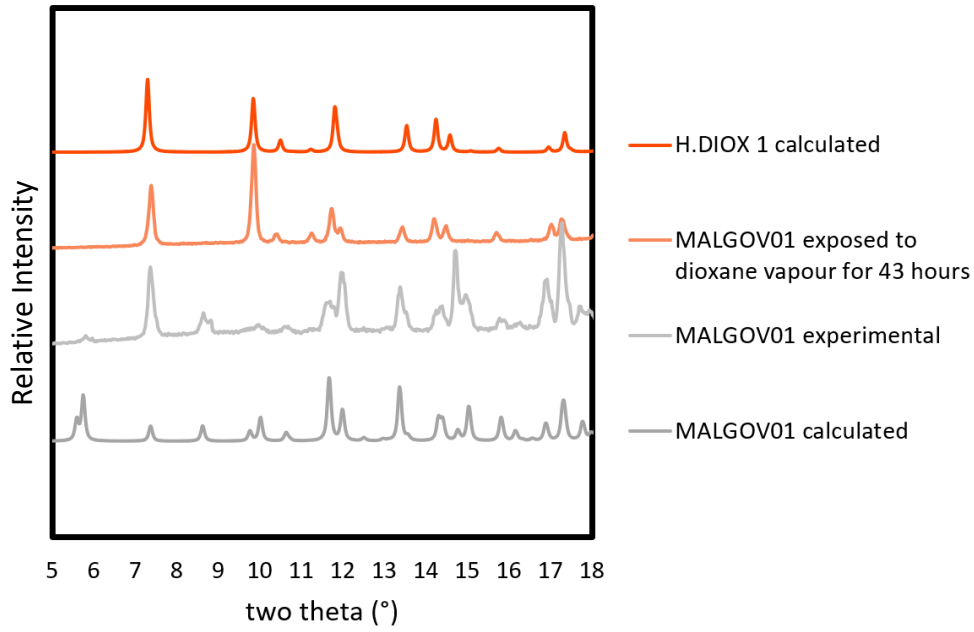

Figure S7.17. **MALGOV01** powder was exposed to dioxane vapour for 43 hours in a two-vial experiment.

7.7.14 Guest exchange MALGOV01 to H•CYNO.

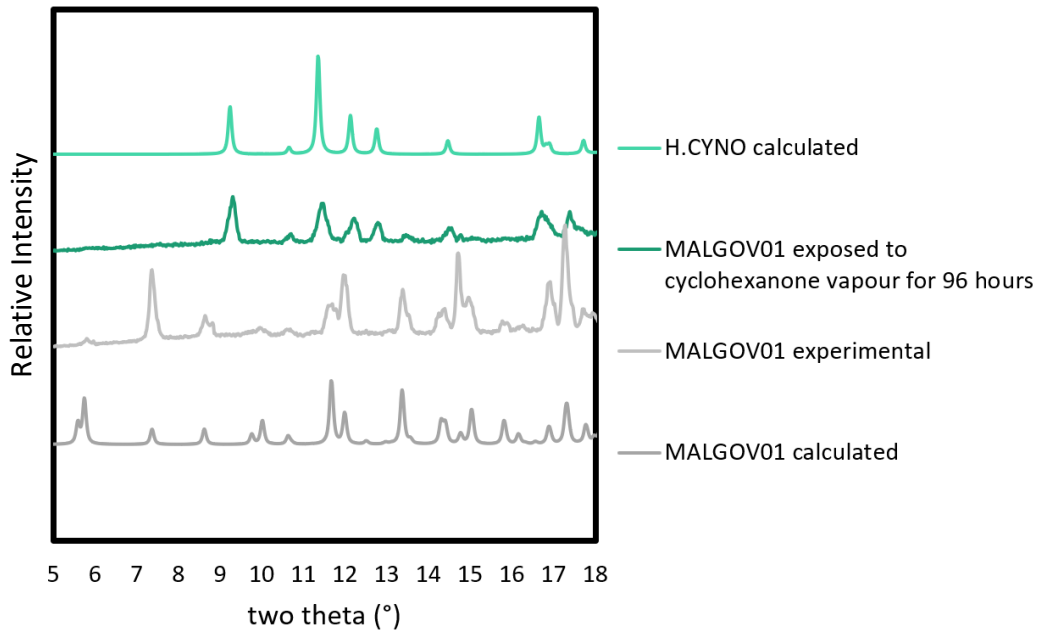

Figure S7.18. **MALGOV01** powder was exposed to cyclohexanone vapour for 96 hours in a two-vial experiment.

7.7.15 Guest exchange MALGOV01 to H•PENT.

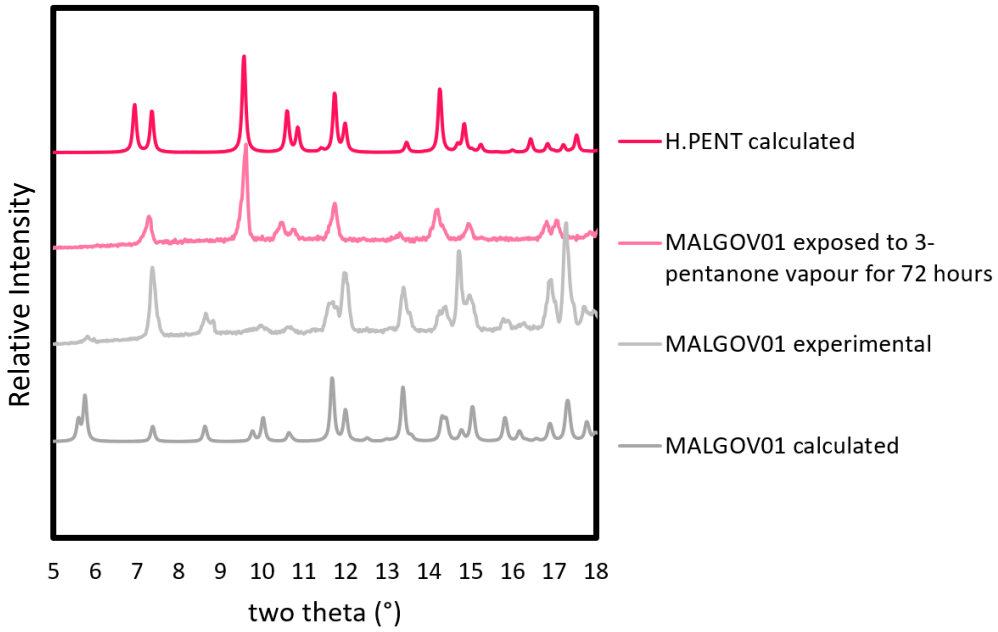

Figure S7.19. **MALGOV01** powder was exposed to 3-pentanone vapour for 72 hours in a two-vial experiment.

7.7.16 Guest exchange MALGOV01 to H·2(ACE).

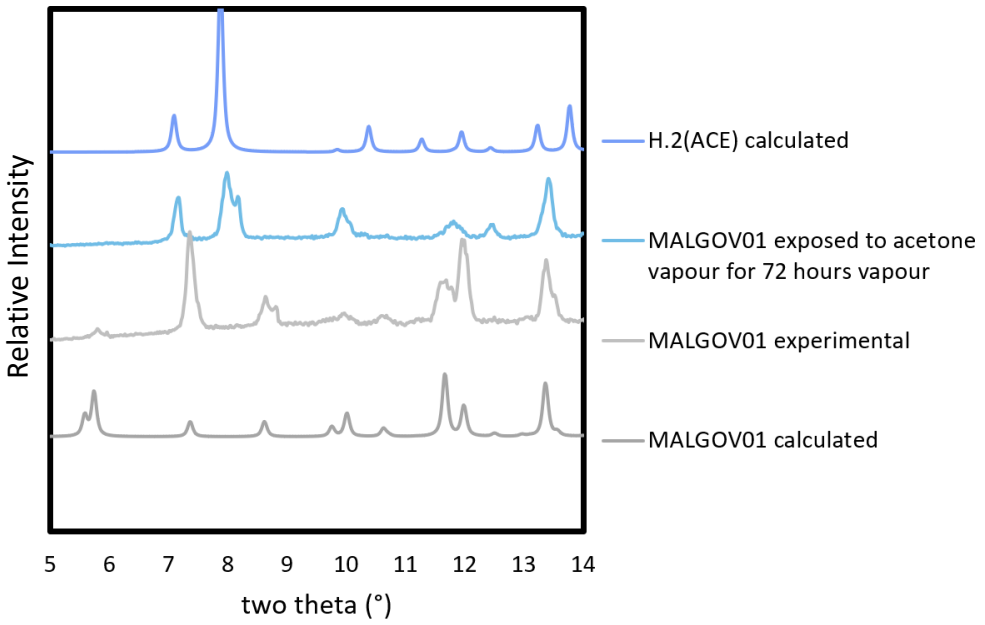

Figure S7.20. **MALGOV01** powder was exposed to acetone vapour for 72 hours in a two-vial experiment.

7.7.17 References.

F1 Sushisen1111, "Trelleborg Old Windmill", CC BY-SA 4.0 via Wikimedia Commons. Accessed 4 August 2021

F2 L. J. Farrugia, WinGX and ORTEP for Windows: an update, *J. Appl. Cryst*, 2012, **45**, 849–854.

F3 A. L. Spek, Single-crystal structure validation with the program PLATON, *J. Appl. Cryst.*, 2003, **36**, 7–13.

F4 A. L. Spek, Structure validation in chemical crystallography, *Acta Cryst. D*, 2009, **65**, 148–155.

F5 A. L. Spek, What makes a crystal structure report valid?, *Inorg. Chim. Acta*, 2018, **470**, 232–237.

F6 A. L. Spek, checkCIF validation ALERTS: what they mean and how to respond, *Acta Cryst. E*, 2020, **76**, 1–11.

F7 A. Bondi, van der Waals Volumes and Radii, *J. Phys. Chem.*, 1964, **68**, 441–451.

F8 T. T. T. Bui, S. Dahaoui, C. Lecomte, G. R. Desiraju and E. Espinosa, The Nature of Halogen···Halogen Interactions: A Model Derived from Experimental Charge-Density Analysis, *Angew. Chem. Int. Ed.*, 2009, **48**, 3838–3841.

F9 F. M. Amombo Noa, S. A. Bourne and L. R. Nassimbeni, Halogen Bonding in Host–Guest Compounds: Structures and Kinetics of Enclathration and Desolvation, *Cryst. Growth Des.*, 2015, **15**, 3271–3279.

F10 M. A. A. Ibrahim and N. A. M. Moussa, Unconventional Type III Halogen···Halogen Interactions: A Quantum Mechanical Elucidation of σ-Hole···σ-Hole and Di-σ-Hole Interactions, *ACS Omega*, 2020, **5**, 21824–21835.

F11 K. Tanaka, D. Fujimoto, T. Oeser, H. Irngartinger and F. Toda, Chiral inclusion crystallization of tetra(p-bromophenyl)ethylene by exposure to the vapor of achiral guest molecules: a novel racemic-to-chiral transformation through gas–solid reaction, *Chem. Commun.*, 2000, 413–414.

F12 D. Li, R. Hu, D. Guo, Q. Zang, J. Li, Y. Wang, Y.-S. Zheng, B. Z. Tang and H. Zhang, Diagnostic Absolute Configuration Determination of Tetraphenylethene Core-Based Chiral Aggregation-Induced Emission Compounds: Particular Fingerprint Bands in Comprehensive Chiroptical Spectroscopy, *J. Phys. Chem. C*, 2017, **121**, 20947–20954.